Vol. 158, No. 2, April 15, 1984

ISSN 0003-2670

ANALYTICA CHIMICA ACTA

International journal devoted to all branches of analytical chemistry

EDITORS

A. M. G. MACDONALD (Birmingham, Great Britain)
HARRY L. PARDUE (West Lafayette, IN, U.S.A.)
ALAN TOWNSHEND (Hull, Great Britain)
J. T. CLERC (Bern, Switzerland)

Editorial Advisers

F. C. Adams, Antwerp
H. Bergamin F°, Piracicaba
G. den Boef, Amsterdam
A. M. Bond, Waurn Ponds
D. Dyrssen, Göteborg
J. W. Frazer, Livermore, CA
S. Gomišček, Ljubljana
S. R. Heller, Bethesda, MD
G. M. Hieftje, Bloomington, IN
J. Hoste, Ghent
A. Hulanicki, Warsaw
G. Johansson, Lund
D. C. Johnson, Ames, IA
P. C. Jurs, University Park, PA
D. E. Leyden, Fort Collins, CO
F. E. Lytle, West Lafayette, IN
H. Malissa, Vienna
D. L. Massart, Brussels
A. Mizuike, Nagoya
E. Pungor, Budapest
W. C. Purdy, Montreal
J. P. Riley, Liverpool
J. Růžička, Copenhagen
D. E. Ryan, Halifax, N.S.
S. Sasaki, Toyohashi
J. Savory, Charlottesville, VA
W. D. Shults, Oak Ridge, TN
H. C. Smit, Amsterdam
W. I. Stephen, Birmingham
G. Tölg, Schwäbisch Gmünd, B.R.D.
B. Trémillon, Paris
W. E. van der Linden, Enschede
A. Walsh, Melbourne
H. Weisz, Freiburg i. Br.
P. W. West, Baton Rouge, LA
T. S. West, Aberdeen
J. B. Willis, Melbourne
E. Ziegler, Mülheim
Yu. A. Zolotov, Moscow

ELSEVIER

ANALYTICA CHIMICA ACTA

International journal devoted to all branches of analytical chemistry
Revue internationale consacrée à tous les domaines de la chimie analytique
Internationale Zeitschrift für alle Gebiete der analytischen Chemie

PUBLICATION SCHEDULE FOR 1984

	J	F	M	A	M	J	J	A	S	O	N	D
Analytica Chimica Acta	156	157/1	157/2	158/1 158/2	159	160	161	162	163	164	165	166

Scope. *Analytica Chimica Acta* publishes original papers, short communications, and reviews dealing with eve aspect of modern chemical analysis, both fundamental and applied.

Submission of Papers. Manuscripts (three copies) should be submitted as designated below for rapid and efficie handling:

Papers from the Americas to: Professor Harry L. Pardue, Department of Chemistry, Purdue University, West Lafayet IN 47907, U.S.A.

Papers from all other countries to: Dr. A. M. G. Macdonald, Department of Chemistry, The University, P.O. Box 36 Birmingham B15 2TT, England. Papers dealing particularly with computer techniques to: Professor J. T. Cle Universität Bern, Pharmazeutisches Institut, Baltzerstrasse 5, CH-3012 Bern, Switzerland.

Submission of an article is understood to imply that the article is original and unpublished and is not being consider for publication elsewhere. Upon acceptance of an article by the journal, authors will be asked to transfer the copyrig of the article to the publisher. This transfer will ensure the widest possible dissemination of information.

Information for Authors. Papers in English, French and German are published. There are no page charg Manuscripts should conform in layout and style to the papers published in this Volume. Authors should cons Vol. 150/2 for detailed information. Reprints of this information are available from the Editors or from: Elsevier Editor Services Ltd., Mayfield House, 256 Banbury Road, Oxford OX2 7DH (Great Britain).

Reprints. Fifty reprints will be supplied free of charge. Additional reprints (minimum 100) can be ordered. An ord form containing price quotations will be sent to the authors together with the proofs of their article.

Advertisements. Advertisement rates are available from the publisher.

Subscriptions. Subscriptions should be sent to: Elsevier Science Publishers B.V., Journals Department, P.O. B 211, 1000 AE Amsterdam, The Netherlands. Tel: 5803 911, Telex: 18582.

Publication. *Analytica Chimica Acta* appears in 11 volumes in 1984. The subscription for 1984 (Vols. 156–166) Dfl. 2145.00 plus Dfl. 231.00 (p.p.h.) (total approx. U.S. $950.40). All earlier volumes (Vols. 1–155) except Vols. and 28 are available at Dfl. 200.00 (U.S. $80.00), plus Dfl. 15.00 (U.S. $6.00) p.p.h., per volume.

Our p.p.h. (postage, packing and handling) charge includes surface delivery of all issues, except to subscribers Australia, Brazil, Canada, China, Hong Kong, India, Israel, Japan, Malaysia, New Zealand, Pakistan, Singapore, Sou Africa, South Korea, Taiwan and the U.S.A., Canada and India who receive all issues by air delivery (S.A.L. — Surfa Air Lifted) at no extra cost. For the rest of the world, airmail and S.A.L. charges are available upon request.

Claims for issues not received should be made within three months of publication of the issues. If not they cannot honoured free of charge.

For further information, or a free sample copy of this or any other Elsevier Science Publishers journal, readers in t U.S.A. and Canada can contact the following address: Elsevier Science Publishing Co., Inc., Journal Informati Center, 52 Vanderbilt Avenue, New York, NY 10017, U.S.A., Tel: (212) 867-9040.

Analytica Chimica Acta, 158 (1984) 147—156
Elsevier Science Publishers B.V., Amsterdam — Printed in The Netherlands

PRECONCENTRATION AND MATRIX ISOLATION OF HEAVY METALS THROUGH A TWO-STAGE SOLVENT EXTRACTION IN A FLOW SYSTEM

MATS BENGTSSON and GILLIS JOHANSSON*

Department of Analytical Chemistry, University of Lund, P.O. Box 740, S-220 07 Lund (Sweden)

(Received 11th October 1983)

SUMMARY

Metal ions (Cd, Cu, Pb, Co and Ni) in trace amounts were isolated from sample matrices and concentrated by extraction in a flow system. The sample flow was first mixed with buffer and reagent (carbamates) and the combined aqueous flow was next segmented with trichlorotrifluoroethane (Freon 113). The metal complexes were extracted into the organic phase in a 2-m long coil which was followed by a separator with a teflon membrane. The organic phase passed on to a second segmentor where an acidic, aqueous mercury(II) solution was added. Back-extraction to the aqueous solution took place in a 1-m long coil. The Freon was removed in a second membrane separator and the aqueous phase was collected and analyzed by graphite-furnace atomic absorption spectrometer. The enrichment factors were of the order of 15—20 and the recoveries were 90—100% from the sub-μg l^{-1} level up to 20—50 μg l^{-1}. The recoveries decreased at concentrations above 50 μg l^{-1}, presumably because of slow dissolution of precipitated complexes in the sample solutions. The observed recoveries for copper were generally somewhat lower, being in the range 80—90%.

Solvent extraction is quite often used in sample treatments preceding measurements by atomic absorption spectrometry (a.a.s.) either in order to remove the metal ions from interfering matrix components or in order to preconcentrate them. The extraction procedure may become very time-consuming because of the cleaning of glassware and clean working areas may be necessary in order to prevent significant contamination. More automated methods would therefore be very useful, in particular when the metal levels are very low. The need became apparent during a project involving analysis of uncontaminated inland waters. The sensitivity of the graphite-furnace a.a.s. method was often insufficient when samples were injected directly.

Nord and Karlberg [1] have described a flow extraction system which was interfaced with flame a.a.s. A fraction of the organic phase (MIBK) was collected and aspirated periodically into the flame. A main advantage of the approach is that a closed system is used so that atmospheric contamination is excluded during part of the procedure. Furthermore, fewer surfaces need cleaning and the method is automated. It was decided, therefore, to modify the method to suit the graphite-furnace technique.

0003-2670/84/$03.00 © 1984 Elsevier Science Publishers B.V.

A double extraction method, developed at the University of Gothenburg [2, 3], is attractive, in particular for work with the graphite furnace, because the final extract is an aqueous solution. High enrichment factors can be achieved because of the low mutual solubility of the organic solvent (Freon) and water. Adaptation of this extraction system to the flow extraction method described by Nord and Karlberg seemed promising for a start. This paper describes the components as well as the further modifications which were found to be necessary.

EXPERIMENTAL

Apparatus

A flow-extraction system was set up, with an 8-channel peristaltic pump (Gilson Medical Electronics model HP8) with Tygon pump tubings (Fig. 1). The various parts were connected with teflon tubings and Altex screw fittings. The inlet was selected by a four-way pneumatically operated valve (Cheminert) and the stream was mixed with buffer and reagent solution in W-formed mixing points made of Kel-F. Freon was delivered through a displacement bottle and segmented with the aqueous stream in a segmentor (described in Results and Discussion). The first extraction took place in teflon tubing (0.9 mm i.d., length 2 m) wound in a coil with a diameter of 16 mm. The back-extraction coil (0.5 mm i.d., length 1 m) was wound with the same diameter. The phase separators were machined from perspex blocks by cutting two U-formed grooves (0.25 mm deep, 1.5 mm wide) on the

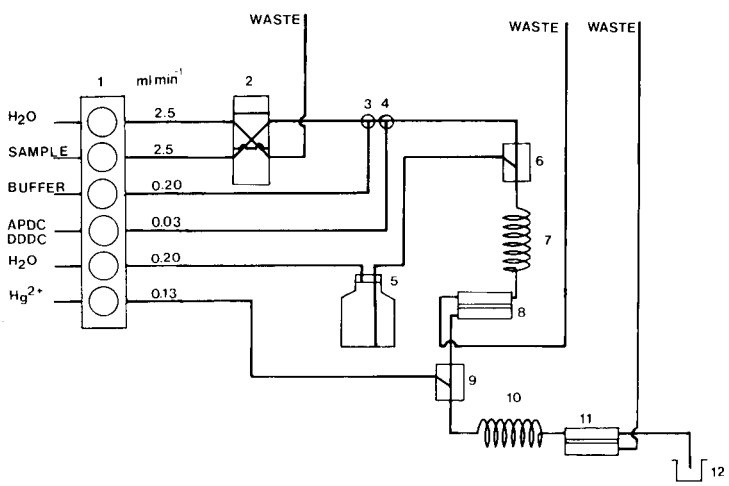

Fig. 1. Schematic diagram of the flow extraction system. (1) Peristaltic pump; (2) 4-way valve for selection of the water or sample channel; (3) buffer mixing point; (4) reagent mixing point; (5) displacement bottle for Freon delivery; (6) segmentor; (7) first-stage extraction coil; (8) membrane separator; (9) segmentor; (10) second-stage extraction coil; (11) membrane separator; (12) cup for sample collection.

opposite faces of the two blocks. A porous teflon membrane (Millipore type FA, 1.0 μm) was clamped tightly and evenly between the planar surfaces of the blocks by 12 screws. An O-ring, encircling the grooves outside the membrane, made an additional seal to prevent solvent seepage. The total groove length was 75 mm for the first separator and 35 mm for the second.

The operation of the flow extraction system can be seen in Fig. 1. The selection between sample and water is made by valve 2. Assuming that the valve is in the position for sample introduction, it can be seen that the sample will be mixed with buffer and reagent in the mixing points (3 and 4, respectively). The combined aqueous flow is then interspaced with Freon segments in 6 and the metal complexes will be extracted into the organic phase during the passage through coil 7. A slight overpressure in the waste channel for the aqueous phase causes the Freon to pass through the teflon membrane in the separator 8. The overpressure is adjusted by a needle valve (not shown) in the waste channel. The organic phase, which now contains the metal complexes, continues into the next segmentor, 9, where it is interspaced with an aqueous solution containing excess of mercury(II). The mercury ions form very strong carbamate complexes and the other ions are therefore displaced and back-extracted into the aqueous phase in coil 10. The two phases are separated in 11, but now the organic phase is discarded while the aqueous phase is collected in plastic cups for subsequent measurements.

When a sample is introduced into the extraction system, the output concentration at 12 will start to rise after some delay until it reaches a steady-state level. The collection of a sample was normally started at the beginning of the plateau, i.e., after 3.5 min (with the flow rates shown in Fig. 1), and continued for 2 min until about 0.2 ml had been collected. The metals were determined with an atomic absorption spectrometer (Varian AA6 and a CRA-90 graphite furnace provided with an auto-injector ASD-53 and a temperature control unit).

Chemicals

Freon-113 (trichlorotrifluoroethane; Merck AG) was used without further purification. The water was purified by reverse osmosis, ion exchange, carbon absorption and filtration in a commercial still (Millipore). The chelating reagent, which consisted of 1% (w/v) ammonium pyrrolidine-1-dithiocarbamate (APDC) and 1% (w/v) diethylammonium-*N*,*N*-diethyldithiocarbamate (DDDC), was purified by filtration and repeated extractions with Freon. The buffer, 0.5 M ammonium citrate, pH 6.0, was purified by repeated extractions with carbamates and Freon. Redistilled mercury was dissolved in concentrated nitric acid (Merck, Suprapur) and the solution was diluted so that it contained 100 mg l^{-1} Hg(II) in 0.5 M nitric acid.

RESULTS AND DISCUSSION

Segment formation

A glass surface will be wetted by the aqueous phase and a teflon surface by the Freon phase. A teflon coil was therefore used so that the water segments would flow in a solvent medium which covered the walls and formed the spacers between the different water droplets (see Fig. 2A). Each aqueous segment is mixed through internal flows, which may be enhanced by winding the tubing in the form of a coil. The solvent film is of utmost importance for the rate of extraction and thus for the efficiency of the system [4, 5]. This statement is supported by observations in this work; Nord and Karlberg [6] have also found that the extraction efficiency decreases drastically if the organic droplets become too small to touch the walls.

Different segmentors have been described in the literature [7, 8] but none was well suited to cope with the large ratios of aqueous to organic flows which are needed in the present application. In both the Technicon A8 and the Nord—Karlberg [8] segmentor, the dead volume at the confluence point is excessive when the organic flow is much smaller than the aqueous flow. It was found that a relatively large Freon droplet would cling to the entrance and cause undue dispersion. The segmentation became irregular at high phase ratios and even with a careful adjustment occasional droplets of larger size would be dislodged. The segmentation was mainly studied by

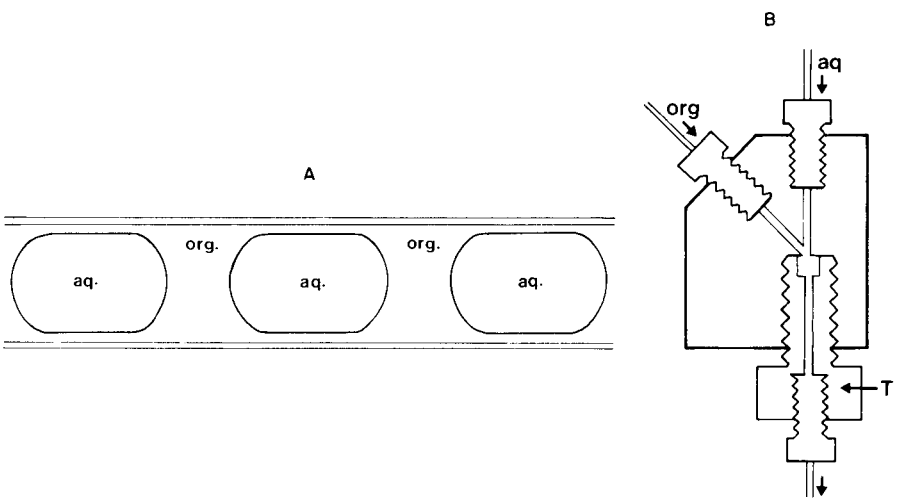

Fig. 2. Schematic representations. A, The segment flow in a teflon tube; the lengths of the aqueous and organic segments were 15 and 1 mm, respectively, in the first-stage extraction and 1 and 1.5 mm, respectively, in the second-stage extraction. B, The Segmentor; the segments form in a chamber (2.0 mm i.d., 7.0 mm long) in the teflon screw T. The i.d. of the exit bore was 0.9 mm and 0.5 mm in the first- and second-stage segmentors, respectively.

using coloured additives and the indicators may affect the behaviour of the segmentors somewhat.

The segmentor used in this work is shown in Fig. 2B. The organic segments form on the hydrophobic surface of a teflon screw which is screwed into a perspex block containing connectors for the aqueous and the organic solvent lines. The segmentation is usually regular and it is not changed when the segmentor is turned by 180°. Adsorbed solids may, however, cause irregularities in the segment formation and make the segmentation position-dependent. The behaviour of the segmentor is improved if flow pulsations are decreased and a damping coil (0.3 mm i.d., 2 m long; not shown in Fig. 1) was therefore inserted in the organic solvent line after the displacement bottle (5 in Fig. 1).

The construction of a segmentor is now more or less empirical and small changes may result in rather large differences in behaviour. A previous model had a continuously adjustable length of mixing chamber and at certain settings it could produce segments of widely different sizes. When the flow rate was increased at such a setting, the mixing chamber tended to switch to modes with segments of half or a third of the previous size. A large hysteresis was observed when the flow rate was decreased. The conclusion is that the dimensions of the mixing chamber may be critical and the optimum may possibly be different for different solvents.

The enrichment factor, which equals the ratio of the flows of the sample and the back-extraction reagent, cannot be much higher than twenty with the described arrangement. The length of the organic segments cannot be reduced below a certain limit or instabilities may occur through coalescence of adjacent aqueous segments. The lower limit was estimated to be 1.5 times the internal diameter of the tubing. A smaller diameter of the tubing in the first extraction step will require a higher pump pressure than that which can be reached with peristaltic pumps. Normal h.p.l.c. pumps are out of question because of metal contamination. The ratio of the organic to aqueous solvent flows in the second extraction step was selected to be about 1.5 in order to reduce the time necessary for collection of a representative fraction. This ratio could, of course, be increased after development of another interfacing technique to the graphite furnace.

Phase separation

Immiscible flowing phases can be separated either with a T-piece separator or with a membrane separator [9]. It is normally necessary to adjust the separator so that one stream contains one phase only while the other stream contains the other phase as well as small amounts of the first phase and possible emulsions. Freon-113 separates exceptionally well from water and it is almost impossible to produce stable emulsions, so that a total separation of the phases should be feasible. Freon-113 passes easily through porous teflon and even teflon plumbing tape may serve as a membrane if an over-pressure is applied in the aqueous output line. The Millipore filters finally

selected had larger mechanical strength and required less over-pressure than the teflon tape. With a sufficient overpressure, the separation became visibly complete, i.e., no Freon droplets could be seen in a test-tube or beaker containing the collected aqueous phase. Large irregularities in the segment formation may, however, result in occasional organic droplets in the aqueous stream. A separator with a 160-mm long groove was originally used but no advantages were noted compared with the shorter separator described under Experimental. The smaller size was therefore selected because of its smaller dispersion.

Back-extraction

The procedure of the manual method [2, 3] was first adopted for the back-extraction in the flow system. A flow of concentrated nitric acid was mixed with the Freon stream in an auxiliary confluence point. The carbamates were decomposed in a reaction coil which had to be fairly long (2.5 m, 0.5 mm i.d.). Water was then added in a segmentor followed by the back-extraction coil and the phase separator. Several disadvantages of the arrangement were apparent: the dispersion and the pressure drop were both excessively large because of the reaction coil. The metal contents of the aqueous segments were highly variable, which made it necessary to collect a large final volume to average out the fluctuations. Furthermore, the lifetime of the Viton pump tubings used for nitric acid was very short.

A much simpler back-extraction procedure was achieved when mercury(II) was added to the segmenting aqueous buffer as shown in Fig. 1. Mercury(II) replaces the other metal ions bound in complexes in the organic phase because of its higher binding constant. The other ions are then rapidly transferred to the aqueous phase [10]. The concentration of mercury(II) should be in excess compared to the sum of all other extractable ions. The iron(III) concentration may reach tens of milligrams per liter in the organic phase and a mercury(II) concentration of 100 mg l^{-1} was therefore selected; 10 mg l^{-1} was sufficient if the metal content of the water sample was low.

The mercury is normally lost during drying and ashing in the graphite furnace except when metals like cadmium are present, in which case a certain fraction remains in the tube even if the ashing time is increased. This conclusion is based on measurements with a mercury hollow-cathode lamp. The level of interference from mercury depends on the acid concentration of the sample and no interferences remain at a 0.5 M nitric acid concentration, except for cadmium in much-used graphite tubes. Even that interference can be removed if new tubes are used for the cadmium measurements. The nitric acid removed the interfering effects but did not change the amount of mercury remaining in the tube.

The segmentation in the back-extraction step was less critical because the organic and aqueous segments were of about the same size. The segmentor and the coil were of the same design as that reported above for the first stage, except that the perspex was replaced by Kel-F for increased resistance

to acids. Because both flows are low in this stage, there will be ample time for phase separation and a separator half as large as that in the first stage was found to be sufficient.

Concentration-time profiles

Some technical problems were caused by the alternating arrival of organic or aqueous solvent plugs to the separators. Depending on whether one or the other phase was entering there was an increase in the flow rate of the aqueous or the nonaqueous output channel. The pulsations were increased if the segmentation was irregular. The segmentation in the two extraction stages are not in step and an aqueous segment in the last stage may thus contain metals from a smaller or larger part of the sample stream. The net result is that the metal concentration in successive aqueous segments in the last stage may show small fluctuations up and down. The present procedure for sample collection will, however, average out any fluctuations. The sample sizes, which could have been much smaller from this point of view, were selected to reduce evaporation losses before the a.a.s. measurements. An averaging method of sampling was also used by Nord and Karlberg [1].

The concentration-time profiles are affected by dispersion in both the continuous and the segmented parts of the system, as well as by mixing in the separators. Figure 3 shows the rise in concentration in response to an input step function, i.e., the input was switched from water to a copper standard solution. The output was collected in cups, which were changed every 30 s, giving fractions with a volume of about 65 μl. It can be seen that a steady state is reached 3.5 min after sample introduction. The return to the baseline (not shown) shows the same time course, except that some tailing is apparent just before the baseline is reached. The tailing occurs mainly at high metal concentrations and is probably due to adsorption of solid metal complexes on the walls of the tubings. It may add another two minutes to the time necessary for a complete wash-out. The curve in Fig. 3 shows that the response can be described by a delay as well as a dispersion mechanism

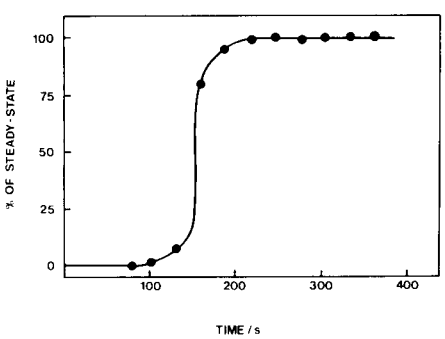

Fig. 3. Concentration-time profile in response to an input step function. The sample solution was 4.0×10^{-8} M Cu^{2+} standard.

(the time of transition from a low to a high state), both being of a similar size. A slow chemical step (dissolution) may also affect a step in the other direction.

The described double-extraction system can be run either in a flow injection or in a steady-state mode. In the flow-injection mode, a fixed sample volume can be introduced through a loop; for practical purposes, the sample should have a volume of at least a few ml in order to utilize the advantages of the enrichment fully. Because the graphite-furnace technique is non-continuous and rather large fractions have to be collected as mentioned above, it becomes difficult to evaluate the peak height precisely. A single fraction containing the rising as well as the descending parts of the profile has therefore to be collected for the a.a.s. measurement. The average concentration during this time is less than the peak concentration so that some sensitivity will be lost. With the other mode, which was used in this work, the sample is pumped into the extraction manifold for a sufficiently long time to reach a steady state at the output. A fraction, the volume of which is unimportant, is collected for the a.a.s. measurement. The next sample may be drawn into the pump directly or a wash-out with water may be interspaced. The steady-state method is more convenient and reliable and it is actually faster than the flow-injection method because of the added dispersion in the sample loop with the latter technique.

Extraction of synthetic samples

The overall extraction recovery was determined for samples consisting of acidified mixed standard solutions (Table 1). The enrichment factors (which were calculated from the flow rates) times the sample concentrations give the calculated output concentrations. The ratios between the measured and the calculated concentrations give the recoveries. Each value in Table 1 is a

TABLE 1

Overall recoveries for metals at different concentration levels

Metal ($\mu g\ l^{-1}$)	Recovery (%)					
	Cd	Cu	Pb	Co	Ni	Fe
0.02	117	—	—	—	—	—
0.2	98	82	97	92	—	—
0.5	—	—	—	—	106	37
2.0	97	88	99	89	96	41
20.0	93	85	95	94	100	40
50.0	—	86	92	82	97	—
100.0	94	60	102	47	82	23
R.s.d. (%)	3	3	3	3	5	4
Flow ratio	21.6	23.4	20.3	20.7	16.8	17.9

mean of three extractions and each a.a.s. determination was made in duplicate. The pooled overall standard deviation (at >20× the detection limit) was 3% except for nickel for which it was 5%. The flow rate ratios alone had a standard deviation of 2.5% for short-time variations.

The recoveries for Cd, Pb, Co and Ni were 90—100% and for copper 80—90% (Table 1). High levels of metal result in decreasing recoveries, especially for Cu, Co and possibly Ni. Precipitates form in the aqueous phase when the sample and the reagent are mixed and a heavier precipitate becomes more difficult to dissolve during extraction. Table 2 shows that a lower flow rate had no significant influence on the recovery, which is in accord with the earlier assumption [3] that the extraction kinetics is fast. The slow step is probably the mass transfer from the surface of the precipitate particle to the Freon phase boundary and its rate should increase if the mixing in the aqueous segments could be increased, e.g., by decreasing the diameter of the extraction coil. Slow dissolution of particles and decreased recoveries were also observed with the manual method, but the recoveries could be increased by increasing the shaking times [3, 10]. The recoveries decreased somewhat when the extraction coil was shortened. It was not possible to increase the length or decrease the internal diameter of the tubings because of the limited pressure range of the pump.

The iron levels of lake waters are frequently quite high so that the solubility product in the organic phase may be exceeded. Precipitates of metal complexes will then form at the interface between the phases if a direct extraction is tried. The pH and citric acid concentration were therefore adjusted to increase the complex-forming capacity of the aqueous phase. Table 1 shows that these attempts were partly successful; only 40% of the iron was carried into the Freon phase. The method could then cope with most of the fresh-water samples analyzed in this laboratory (iron should be less than 1.5—2 mg l^{-1}).

The recovery of spikes added to sea water was reported to be 90—100% [2], except for cadmium for which it was 80%. An a.a.s. matrix interference, which should be absent with the proposed back-extraction method, was later found to explain the low cadmium recovery [3].

TABLE 2

Recoveries for cadmium and copper at two different flow rates with a flow ratio of 17.8

Flow rates (ml min^{-1})		Recovery (%)		
Sample	Back-extraction reagent	Cd (0.2 $\mu g\ l^{-1}$)	Cu (2.0 $\mu g\ l^{-1}$)	Cu (50 $\mu g\ l^{-1}$)
2.5	0.14	93	94	86
1.16	0.062	93	95	86

CONCLUSIONS

The reported data show that the flow extraction method works well for extraction ratios of 15—20. The second extraction step adds little to the enrichment but it simplifies the a.a.s. measurements significantly. The number of samples which can be processed per hour may not be much higher than with a manual method but the auxiliary work, e.g., the cleaning of glassware, is decreased substantially. The flow method puts less strict requirements on the cleanliness of the working area because contamination is small within the closed system. The flow method consumes smaller amounts of reagents and solvents than those which are practical with a manual method.

Some improvements, in particular concerning the interfacing of the flow extractor with the graphite furnace sampler, are obviously needed in order to take full advantage of the flow concept. Further development, e.g., on-line purification of buffers, may make the method still more attractive. In fact, zinc extracts well but it was not included in this study because of high blanks. On-line purification may also make it possible to use high-pressure pumps and so to work with higher pressure drops over the first extraction coil. Work on some of these improvements is under way and a more careful validation of the method, also covering real samples, has therefore been postponed.

Financial support for this work was obtained from the Swedish Environment Protection Board. The authors thank Dr. A. Torstensson for comments on the manuscript.

REFERENCES

1 L. Nord and B. Karlberg, Anal. Chim. Acta, 125 (1981) 199.
2 L. G. Danielsson, B. Magnusson and S. Westerlund, Anal. Chim. Acta, 98 (1978) 47.
3 B. Magnusson and S. Westerlund, Anal. Chim. Acta, 131 (1981) 63.
4 T. M. Rossi, D. C. Shelly and I. M. Warner, Anal. Chem., 54 (1982) 2056.
5 T. Imasaka, T. Harada and N. Ishibashi, Anal. Chim. Acta, 129 (1981) 195.
6 L. Nord and B. Karlberg, Anal. Chim. Acta, 145 (1983) 151.
7 J. Kawase, Anal. Chem. 52 (1980) 2124.
8 L. Nord and B. Karlberg, Anal. Chim. Acta, 98 (1978) 1.
9 L. Nord and B. Karlberg, Anal. Chim. Acta, 118 (1980) 285.
10 J. M. Lo, J. C. Yu, F. I. Hutchinson and C. M. Wal, Anal. Chem. 54 (1982) 2536.

Analytica Chimica Acta, 158 (1984) 157—167
Elsevier Science Publishers B.V., Amsterdam — Printed in The Netherlands

DETERMINATION OF IODINE VALUE OF FATTY ACIDS BY A FLOW-INJECTION METHOD

CHENG-CHIH LEE[a] and BRUCE D. POLLARD*
Marquette University, Department of Chemistry, Milwaukee, WI 53233 (U.S.A.)
(Received 8th August 1983)

SUMMARY

An automated method for determining the iodine value for various industrial fatty acids is described. The method is based on flow-injection techniques and the chemistry is a modified version of the standard Wij's solution method. The system is fully computerized with an AIM-65 microcomputer. Two detection systems, u.v.-visible absorbance and potentiometric sensing, are compared. Results comparable to the conventional method are obtained. Continuous-run sample throughput rates of 12 h^{-1} are realistic.

Iodine value or number is a measure of the unsaturation in organic compounds. The iodine value is defined as the number of grams of I_2 absorbed (added across the multiple bonds) in a 100-g sample. This value has been used in the fats and oils industry for many years as an important indicator of physical properties, such as melting point, hardness, gumming, and drying power [1]. For example, the iodine value is an indicator of the difference between a liquid salad oil and a solid shortening (fat); shortenings are hydrogenated.

Classical titration methods have been used to determine iodine values for many years. In these methods, a reagent containing excess of iodine is added to a sample and allowed to react. Then the excess of iodine is titrated with standardized potassium thiosulfate as in classical iodimetry. Initially, an alcoholic solution of iodine with mercury(II) chloride was used as the iodinating reagent, but it has long been replaced by the Wij's solution, consisting of iodine monochloride in glacial acetic acid. The Wij's solution has the advantages of being stable for months and of reducing the reaction period from several hours to 30 min. Methods that use the Wij's solution have been adopted by the Fat Analysis Committee of the Oil Chemists' Society and the Association of Official Analytical Chemists [2]. Typical working time for a single determination is about 25 min (weighing, mixing, titrating and calculating) or 55 min total (including reaction time). These times include an allotment for titrant and reagent standardization. Although accuracy and

[a]Present address: Cooperative C.L. Enterprise Co., 9th Floor, 67 Sung Kiang Rd., Taipei, Taiwan.

0003-2670/84/$03.00 © 1984 Elsevier Science Publishers B.V.

reproducibility are typically quite good, the long time does not lend itself to on-line process control or quality control of high sample volumes. No automated method for iodine values seems to have been reported and the need for one should be great.

In developing an automated method for iodine values (IV), various chemical approaches were considered. Agreement with the existing method was best assured by utilizing the same chemistry for the new method as that used in the manual method. A preliminary study of the kinetics of the Wij's solution reaction with oleic acid (IV = 90), by monitoring the decrease in iodine monochloride absorbance using u.v.-visible spectrophotometry at 360 nm, revealed that the reaction was 90% complete in 3 min. Although this rate could differ for various fatty acids, a first assumption was made that the difference would not be large. Based on this assumption, a kinetic fixed-time method based on iodine monochloride in glacial acetic acid solvent was developed.

A flow method was chosen to automate the procedure. Either segmented or unsegmented (flow-injection) approaches would have been suitable choices. The flow-injection approach was chosen because of equipment availability and relative simplicity. Flow-injection techniques [3] have been successfully applied to many methods similar to this one. For this method, a continuous flow of 0.045 M iodine monochloride in anhydrous acetic acid was pumped through a reaction coil and into an ICl-sensitive detector. Periodically, a fatty acid sample was injected and mixed with the flowing carrier. As the sample plug flowed through the tube, iodine monochloride from the carrier was absorbed across the double bond(s) of the fatty acid. This resulted in a decrease in iodine monochloride concentration as sensed by the detector when the mixture finally passed through it. The amount of iodine monochloride absorbed was proportional to the concentration of double bonds in the sample, the carrier reagent flow rate, the reaction rate and the reaction coil length. If a fixed amount of sample was injected, the detector response was related to the theoretical iodine value.

The performance of two detection methods was evaluated and compared. In one method, a u.v.-visible absorption detector set to 360 nm monitored the absorbance of iodine monochloride in the flowing stream. When iodine monochloride reacted with fatty acid in an injected sample, the decreasing absorbance resulted in an inverted peak. Examples are shown in Fig. 1. The second detection method involved an iodine-sensitive electrode system which also responded to iodine monochloride. A special flow cell was constructed and when samples were pumped through it, a response similar to that of the u.v. absorption detector, but in a positive millivolt direction, was observed.

Development of the new method proceeded in logical steps: choice of chemistry, set-up of apparatus, preliminary testing, optimization, and final evaluation. Through all of these steps, the performance criteria were accuracy, reproducibility, calibration range and linearity, simplicity, and analysis time. The use of a computer facilitated acquisition of standard deviations, linear regression statistics, and percent deviations from expected values.

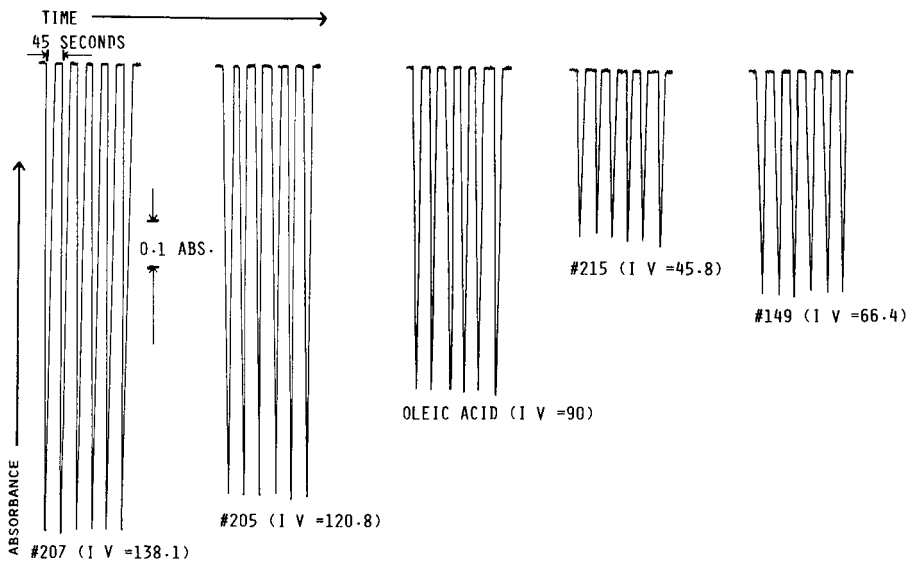

Fig. 1. The u.v. absorbance detector response for various samples.

EXPERIMENTAL

Samples and reagents

The fatty acids used as standards and unknowns are listed in Table 1. The pure compounds were obtained commercially as noted. The mixtures were industrial samples donated by Procter and Gamble Co., Industrial Chemicals Div. and are samples quantified by their laboratory on a routine basis. For all samples, conventional iodine values and the deviation from theoretical value for pure acids or Procter and Gamble accepted test values for mixtures are reported in Table 1. Reagent-grade (ACS) iodine monochloride (Eastman, Rochester, NY) and reagent-grade anhydrous acetic acid (DuPont, Wilmington, DE) were used. The carrier/reagent solution was prepared by adding 25.0 g of iodine monochloride to 78.2 ml of anhydrous acetic acid, mixing well, and filtering through Whatman No. 41H filter paper into a clean dry dark glass bottle. Pouring 52.5 ml of this solution into a standard five-pound bottle of anhydrous acetic acid and mixing resulted in the approximately 0.045 M iodine monochloride reagent. Although the concentration was not critical, it could be determined exactly by classical iodimetry. Fatty acid samples were prepared by adding a 0.750-g portion (melted and weighed exactly) to about 30 ml of anhydrous acetic acid in a 100-ml volumetric flask, stirring, and after complete dissolution, diluting to the mark with anhydrous acetic acid. All solutions were carefully sealed and vented to prevent evaporation of the solvent during use.

TABLE 1

Fatty acid samples and standards

Fatty Acid	Content	Iodine value		Deviation from accepted (%)
		Accepted	By Wij's method[a]	
Erucic Acid	99% Erucic acid	75.0[b]	75.1 ± 0.9	0.1
Oleic Acid	99% Oleic acid	90.0[b]	90 ± 1	0
Linoleic Acid	99% Linoleic acid	181.0[b]	180 ± 2	0.6
065	Coconut oil-derived fatty acid	6.3[c]	6.3 ± 0.4	0
169	Coconut and tallow-derived, mostly oleic acid	41.0[c]	40 ± 1	−2.4
193	Tallow-derived	41.9[c]	44.1 ± 0.7	+5.0
215	Tallow-derived	45.8[c]	46.4 ± 0.8	+1.3
192	Tallow-derived	55.0[c]	55.0 ± 0.8	0
149	Tallow-derived	66.4[c]	65.5 ± 0.4	−1.4
205	Soybean-derived[d]	120.8[c]	119.2 ± 0.6	−1.3
207	Soybean-derived	138.1[c]	137.4 ± 0.5	−0.5
211	Linseed oil-derived[e]	194.0[c]	194 ± 1	0

[a]Average of 3 results with standard deviation. [b]Theoretical value. [c]Value obtained by Procter and Gamble testing. [d]45% linoleic, 27% oleic, 6% linolenic acid. [e]52% linolenic, 16% oleic, 20% linoleic, 12% stearic acid.

Equipment

An SHS-200 Flow Injection Analyzer (FIAtron, Milwaukee, WI) was used. It consisted of a microprocessor-controlled peristaltic pump and injection valve system. It pumped the carrier reagent and sample streams into the automatically-timed injection valves and into a reaction coil. The injection mode was chosen such that the sample was butt-mixed with the carrier for a known injection time. In some tests, a carousel-type autosampler which could be controlled by the SHS 200 was attached to provide automatic introduction of samples, standards, and blanks. Standard 0.13-mm and 0.16-mm (inside diameter) PVC pump tubes (Fischer Scientific, Pittsburgh, PA) were used in the pump manifold and 0.5-mm (inside diameter) teflon tubing (FIAtron) was used for the reaction coil and interconnections. A Thelco constant-temperature bath (Precision Scientific, Chicago, IL) was used to fix the reaction coil temperature.

A model IC-UV u.v.-visible column monitor (Gilson Medical Electronics, Madison, WI), consisting of a deuterium-arc light source, monochromator, 50-μl flow cell with 3-mm light path, phototube detector, log amplifier and servochart recorder, was used as the absorbance detector. An Orion model 97-70 iodine electrode (Orion Research, Cambridge, MA) coupled with an Orion model 702 digital pH/millivolt meter was used as the potentiometric detection system. A special flow-through cell (Fig. 2) was constructed

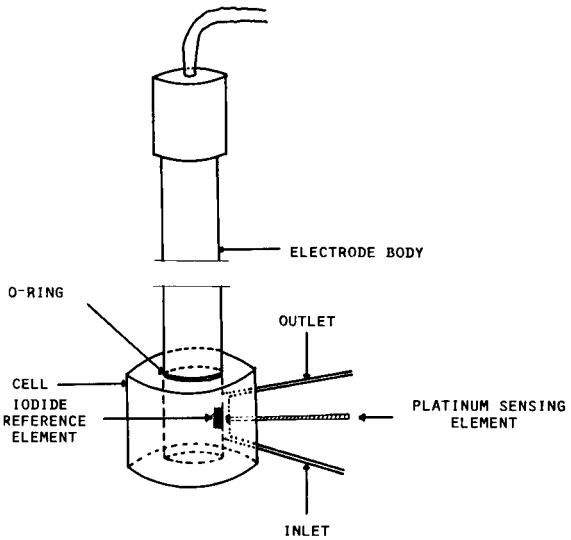

Fig. 2. Flow-through cell for the potentiometric detector.

of teflon. Instead of using the platinum electrode at the end of the iodine electrode, a separate platinum wire was used. The dead volume was found to be about 200 μl.

The complete system was computerized using a Rockwell AIM-65 microcomputer (Anaheim, CA) as shown in Fig. 3. Switching between detectors was achieved by simply switching tubings at the reaction coil outlet. Digital signals were obtained from the millivolt meter binary-coded decimal output and sent in parallel fashion to the versatile interface adapter chip located on the AIM circuit board. A special signal-conditioning amplifier which filtered and shifted the baseline of the absorbance monitor output was required to match the input characteristics of the millivolt meter. A strip-chart recorder was attached to verify the computer results until the programming was reliable.

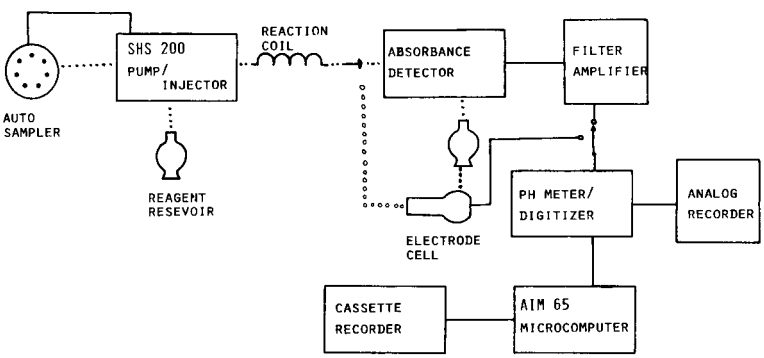

Fig. 3. Flow injection system showing both detection systems.

TABLE 2

Optimized parameters

Parameters	Optimal value	Maximum	Minimum
Temperature (°C)	25	55	20
Reaction coil length (m)	6	12	1
Flow rate (ml min^{-1})	1.6	0.1	5
Injection time (s)	20[a]	5	60
	50[b]		
Injection rate (h^{-1})	80[a]	200	10
	30[b]		
ICl concentration (M)	0.045	0.10	0.010
Baseline (A)	~2.0[a]		
(mV)	~−100[b]		

[a]Absorbance detector, IV range 40—120. [b]Potentiometric detector, IV range 6—200.

(0.03 M—0.001 M) to the iodine monochloride carrier. Evaluation was based on their catalytic activity as measured by increases in slopes of calibration plots and on their performance as indicated by the usual figures of merit. Because no statistical differences in the calibration slope were observed, it was concluded that catalysis was not present under the range of conditions used. A constant baseline shift took place when a potential catalyst was present. This indicated some reaction between the iodine monochloride reagent and the potential catalyst. A precipitate from such a reaction between mercury(II) acetate and the iodine monochloride was recovered and identified as HgI_2. It was finally decided that a catalyst would not be used, nor was it needed for this automated method.

After optimization, evaluation of the overall method and of the two detection methods was accomplished through a double blind test of accuracy. Samples were provided by Procter and Gamble; the accepted iodine values for these samples were transmitted in a separate envelope and opened after the samples had been processed by the flow-injection method. A theoretical unknown, erucic acid (IV = 75), was included. Calibration stability and sample throughput were tested on the system with the autosampler attached. This test consisted of a calibration and then continual determination of unknowns for up to four hours.

RESULTS

Ultraviolet absorbance detector

Results for the iodine values with an absorbance detector are listed in Table 3 with typical calibration plots in Fig. 5. Data for both absorbance peak height and absorbance peak area are included. For both measures, the calibration was linear up to values of 138 with intercepts statistically near zero. The non-linear response at higher iodine values was due to the choice

TABLE 3

Results obtained by the flow-injection method with u.v.-visible detection (360 nm)

Calibration

	Peak height	Peak area
Slope ± *s*	−0.0094 ± 0.0005 ΔA IV^{-1}	−0.118 ± 0.014 ΔA s IV^{-1}
Intercept ± *s*	−0.0011 ± 0.0004 ΔA	−0.028 ± 0.013 ΔA s
Standard error of estimate	0.008 ΔA	0.2 ΔA s
Corr. coeff.	0.996	0.98
%RSD of slope	5	12

Double blind test

Iodine value							
Unknown	Expected	Found[a]	%RSD	%Dev.	Found[b]	%RSD	%Dev.
193	41.9	41.0	3.1	−2.0	51.7	8.5	+23
215	45.8	46.4	2.0	+1.3	52.4	4.5	+14
192	55.0	53.7	4.0	−2.4	56.9	5.4	+3.5
Erucic	75.0	76.3	1.0	+1.7	64.5	8.1	−14
205	120.8	119.0	1.0	−1.5	112.0	6.0	−10

[a]From peak height. [b]From peak area.

of sample size and reagent concentration. The line could be extended by adjusting these parameters but this caused nonlinearity at low iodine values demonstrating the limiting range of linearity to cover about ΔIV = 100. For the peak-height measure, the correlation coefficient, 0.996, and the percent relative standard deviation (%RSD) of the slope, 5.3%, were better than those for peak area; this indicated that peak height was the better measure.

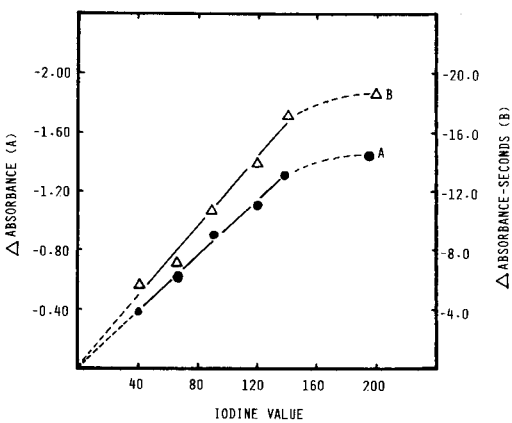

Fig. 5. Calibration plots for the u.v. absorbance detector. A is peak height and B is peak area. Regression data are in Table 3. Error limits are represented by point size.

In the double blind test of accuracy, peak height was better than peak area. Percent deviations from expected values of peak height were always within the corresponding %RSD. For peak areas, %RSD were as high as 8.3% and percent deviations from actual values sometimes exceeded the %RSD by 3-fold (sample 193). Multiple runs showed peak area results to be erratic but peak height results to be dependable. When the peak height measure was used for the fully automated test, the calibration remained stable enough to give results that agreed within 5% throughout the four-hour time period.

Potentiometric detection

Based on the Nernst equation, a logarithmic relation between iodine value and potential change was expected for the iodine electrode-based detector. As illustrated by the plot of potential change vs. ln[IV] in Fig. 6, this was not the case. Instead, a linear relationship between iodine value and both peak height and peak area was found as shown in the calibration plots (Fig. 7). Presumably, this was because convolution of the logarithmic Nernstian electrode concentration function with some intrinsic exponential function resulted in a linear one. Whether the exponential function was due to the electrode time response, cell dead volume, or the peak shape is under investigation.

Linearity was observed for the total range (IV = 6—194) for peak height and peak area. Table 4 shows statistical data for the two calibration lines to be very similar; the intercepts are near zero. The slightly smaller %RSD of the slope for the peak area measure, 2.5%, than for the peak height measure, 4.2%, indicates a generally tighter fit for the standards when peak area is used. In the double blind study, %RSD for all determinations using both

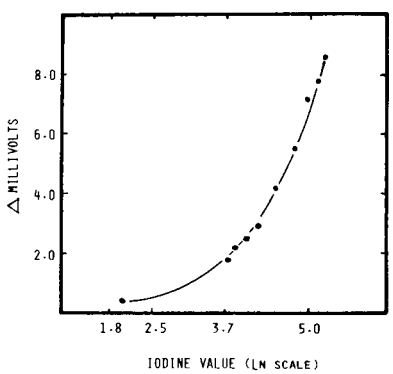

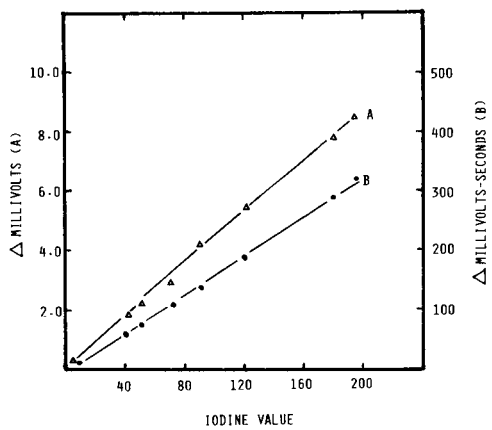

Fig. 6. Electrode response (peak height) vs. natural logarithm of the iodine value.

Fig. 7. Linear coordinate calibration plot for iodine value using the electrode system. A is peak height and B is peak area. Regression data are in Table 4. Error limits are represented by point size.

TABLE 4

Results obtained by the flow-injection method with potentiometric detection

Calibration

	Peak height	Peak area
Slope ± *s*	0.044 ± 0.02 ΔmV IV^{-1}	1.65 ± 0.04 ΔmV s IV^{-1}
Intercept ± *s*	0.092 ± 0.005 ΔmV	−0.23 ± 0.01 ΔmV s
Standard error of estimate	0.003 ΔmV	0.09 ΔmV s
Corr. coeff.	0.996	0.998
%RSD of slope	4.2	2.5

Double blind test

Iodine value							
Unknown	Expected	Found[a]	%RSD	%Dev.	Found[b]	%RSD	%Dev.
193	41.9	42.8	0.29	+2.1	41.9	0.58	0
215	45.8	46.2	0.34	+0.9	46.2	0.83	+0.9
192	55.0	53.8	0.27	−2.1	54.2	0.95	−1.4
Erucic	75.0	72.9	0.23	−2.8	71.3	0.35	−5.0
205	120.8	128.4	0.08	+6.3	123.1	0.32	+1.9
Linoleic	181.0	180.8	0.53	−0.1	180.7	0.67	−0.2

[a]From peak height. [b]From peak area.

measures were very good, always being less than 1%. Accuracy was better when peak area rather than peak height was used although it was reasonable in both cases; for peak areas only erucic acid was considered poorly determined with −5.0% deviation from the true value. In the long-term automated stability test, there was a cyclical drift in the peak area calibration slope of about 5% having a period of about 1 h, but within that tolerance, the method was accurate to the specified reproducibility over the 4-h test period. Although a substantial drift in the electrode asymmetry potential was present, it did not affect the results because the computer was programmed to subtract a recently updated baseline measure.

DISCUSSION

In general, the results for both detection systems show that the method is accurate and reproducible. For the u.v.-visible detector, peak heights gave substantially better results than peak area. If the signals used to obtain these measures were random-noise limited, the reverse should have been true [6]. After evaluation of possible causes, the errors in peak areas were attributed to detector electronics noise, present only at high absorbance, causing poor start/stop detection in the integration algorithm. Using a start pulse from the injection system or better detector electronics should correct the problem.

Results for replicate samples showed that deviations in accuracy could be explained by variation in sample preparation (melting, weighing, etc.).

Compared to the conventional Wij's method, as evaluated in this laboratory (Table 1), the automated method has about the same reproducibility but somewhat poorer accuracy. Possible explanations include variation in sample preparation, as discussed above, or differing reaction rates for the various fatty acids, because the assumption was made that all fatty acids react at about the same rate. Because the deviations from expected values were not systematic, sample preparation was considered the cause. In cases for which higher accuracy is required, an automated sample preparation system such as the one described by Owens and Eckstein [7] or multiple samples should result in accuracy equal to that of the conventional method. In terms of time and materials, the automated method is about five times faster than the conventional one and requires about one-tenth the reagents; no exact standardization of the iodine monochloride reagent is required because a calibration curve is made for each set of unknowns. The automated method is suitable for process control applications. While careful attention would be required in designing a representative sampling device, comparison of the sample stream with a pair of standards (bracketing the iodine value of the sample) could result in a continuous readout for on-line monitoring of mixing or hydrogenation operations.

The authors thank Dr. Alan Ullman and his employer, Procter and Gamble Company, for providing the industrial samples and for comparison data.

REFERENCES

1 D. Swern (Ed.), Bailey's Industrial Oil and Fat Products, Vol. 1, 4th edn., Wiley, New York, NY, 1979.
2 W. Horwitz (Ed.), Official Methods of Analysis of the Association of Analytical Chemists, 11th edn., A.O.A.C. Press, Washington, DC 1970, p. 444.
3 J. Růžička and E. H. Hansen, Anal. Chim. Acta, 78 (1975) 145; Flow Injection Analysis, Wiley, New York, NY, 1981.
4 H. D. Hoffman and G. C. Green, Oil Soap (Chicago), 16 (1939) 236.
5 Nisshin Oil Mills, Japanese Kokai Tokyo Koho, 22 (1981) 957.
6 B. D. Pollard, A. H. Ullman and J. D. Winefordner, Anal. Chem., 53 (1981) 330.
7 G. D. Owens and R. J. Eckstein, Anal. Chem., 54 (1982) 2347.

Analytica Chimica Acta, 158 (1984) 169—177
Elsevier Science Publishers B.V., Amsterdam — Printed in The Netherlands

HIGH-PERFORMANCE LIQUID CHROMATOGRAPHY OF NITROPHENOLS WITH A SWEPT-POTENTIAL ELECTROCHEMICAL DETECTOR

JOYCE J. SCANLON, PATRICIA A. FLAQUER, GEORGE W. ROBINSON, GERALD E. O'BRIEN and PETER E. STURROCK*

School of Chemistry, Georgia Institute of Technology, Atlanta, GA 30332 (U.S.A.)

(Received 1st August 1983)

SUMMARY

The advantages of a swept-potential electrochemical detector are demonstrated by application to the high-performance liquid chromatography (h.p.l.c.) of nitrophenols. The primary advantage of the detector is that an additional dimension of information is obtained which can be used to help identify a chromatographic peak and help to resolve overlapping peaks. The detector retains the selectivity of a differential-pulse detector and yet is general enough to minimize the time for development of new procedures and to detect true unknowns. The h.p.l.c. of nitrophenols was studied on C-18 reverse-phase columns, with methanol-acetate buffer mobile phases. Selectivity factors of the mononitrophenols are independent of the composition of the mobile phase from pH 3.25 to 6.00 and from 40 to 55% methanol. The selectivity factors of dinitrophenols are highly dependent on pH. Limits of detection depend on many parameters but are approximately 1 ng injected for the nitrophenols.

This paper is the first in a series to discuss the design and applications of a swept-potential electrochemical detector for high-performance liquid chromatography (h.p.l.c.). The relative advantages of the detector will be illustrated by application to nitrophenols. Future papers will discuss the detailed design and performance of the instrument as well as applications to other types of compounds.

The basic concept of a swept-potential detector using square-wave voltammetry have been discussed by Samuelsson et al. [1] and reviewed by Bratin and Kissinger [2]. Different approaches to swept-potential detectors were reported by Wang et al. [3], Stastny et al. [4], Last [5], and Caudill et al. [6]. The primary advantage of the swept-potential detector is that an additional dimension of information is obtained. The current response as a function of potential can be used to help identify a component and to help resolve two components not completely separated on the column. In addition, the potential for maximum current response is crossed for all components within the potential range of the sweep, thus decreasing the time required to optimize a procedure and allowing the determination of multiple components in one chromatogram, each at its optimum potential. If, as in the

0003-2670/84/$03.00 © 1984 Elsevier Science Publishers B.V.

present case, the data are stored in a computer file, chromatograms can be displayed for any desired potential within the sweep range, or chromatograms for the summations between desired potentials can be displayed. Thus, this detector retains the selectivity of a differential-pulse detector and at the same time is general enough to evaluate true unknowns.

Nitrophenols were selected as the first class of compounds for application of the swept-potential detector for several reasons. First, several nitrophenols are on the list of priority pollutants of the United States Environmental Protection Agency. Second, while the performance of the electrochemical detector was being improved and evaluated, it was desirable to work with a class of compounds which can be detected with a u.v. detector. Third, the literature on electrochemistry of nitrophenols is extensive. Finally, nitrophenols are detected by electrochemical reduction reactions while the majority of previous work with electrochemical detectors has been with oxidation reactions. Applications to reduction reactions are generally considered to be more difficult than to oxidation reactions because of higher background currents from the reduction of hydrogen ions and oxygen. Thus, successful application to reductions would serve as a rigorous test of the detector system.

EXPERIMENTAL

Apparatus

The chromatographic instrumentation was locally assembled from components and designed for isocratic elution. Initially the pump on the instrument was a Haskel pneumatic amplifier pump (No. 26740) as modified by DuPont for their Model 830 chromatograph. Later determinations were made with a Spectra-Physics 8770 pump, which was found to be sufficiently pulse-free for the electrochemical detector. Columns (4.6 × 250 mm) were locally packed with RSIL C18 HL (10 μm) for reverse-phase separations and were preceded by a guard column (4.6 × 50 mm) containing pellicular C-18 resin (Alltech 9260). Valco injectors (either 6-port or 10-port), driven by air actuators, were fitted with 10-μl sample loops. The system was all stainless steel from the solvent reservoir to the detector inlet with 1/8-in. tubing (2.16-mm i.d.) connecting the solvent reservoir to the pump and 1/16-in. tubing (0.25-mm i.d.) was used in the rest of the system. The column effluent was attached to a u.v. detector (Chromatronix model 220), for monitoring at 254 nm, or to the electrochemical detector.

The electrochemical detector was designed and assembled in this laboratory. It consists of a computer-controlled potentiostat and a modified PARC 310 electrode stand and flow cell. The computer system consists of a Z80A processor with 64 kbyte of RAM and dual 5.25-in. floppy-disk drives. The graphics terminal also includes a Z80A and 64-kbyte RAM. The graphics are bit-mapped with 640 points horizontally and 480 points vertically Any alphanumerics or graphics can be dumped to the IDS Prism 80 dot-matrix

printer. The instrument-control and data-acquisition programs are written in assembly language while the data-processing programs are written in BASIC or FORTRAN IV.

All parameters for the detector are selected from a choice displayed on the CRT and are down-loaded from the computer to the potentiostat in digital format. The potentiostat contains a current-interrupt circuit, by use of which the IR drop of the cell can be measured, and a positive-feedback circuit for IR compensation. A direct current offset can be adjusted automatically to give a net current of zero at the start of the voltammetric sweep. These two features are important in a practical instrument and are lacking in the swept-potential detectors previously described [1, 3—6]. During an experiment, a 3-D plot of the data is displayed, as it is acquired, on the upper two-thirds of the CRT while the selected parameters are displayed on the lower third of the CRT. After the experiment, any desired voltammogram or chromatogram can be extracted from the data file, displayed on the CRT, and hard copies made on the printer. Details of the instrument will be provided to interested readers.

Reagents

The nitrophenols used were commercial products that were not purified further. The dinitrophenols contained 15—50% "moisture" as indicated on their labels. Samples were prepared on a weight basis in methanol with concentrations calculated on the basis of an estimated dry weight. Acetate buffers of the desired pH values were prepared by mixing sodium acetate and anhydrous acetic acid with water so that the final concentration of acetate was 0.20 molar. These buffers were filtered through a 0.45-μm nylon filter under vacuum. Mobile phases were made by mixing the acetate buffers with methanol on a volume basis. The methanol (Burdick and Jackson, h.p.l.c. grade) was used unfiltered.

Procedures

Each of the nitrophenols was chromatographed, individually and in mixtures, with a number of mobile phases which differed in the pH of the acetate buffers and in percentage of methanol. Plots of retention time vs. pH or percent methanol were constructed for each compound. Square-wave voltammetry at various values of pH and percent methanol was applied to each nitrophenol, and the limits of favorable electrochemical response were thereby determined.

For use with the u.v. detector, the mobile phase was equilibrated with air. When the electrochemical detector was used, the mobile phase was purged vigorously with helium for at least 30 min before the pump was started, and purging was continued for a further 30 min with mobile phase flowing through the column. Oxygen was not removed from the injected samples because the system clearly separated oxygen from the nitrophenols. The outer cell of the PARC 310 was filled with mobile phase and purged with nitrogen.

Although the u.v. cell could have been placed in the effluent stream before the electrochemical cell, this arrangement was not done because of band broadening in the u.v. cell. Also, the u.v. cell allowed enough oxygen to enter the effluent stream that the background currents in the electrochemical cell were excessive. The reverse sequence of the cells is not possible.

At the start of each day, the capillary was removed from the electrode stand, flushed with water and methanol, and then air-dried by use of a vacuum pump. After re-installation, a vacuum pump was attached to the capillary tip to remove any air entrapped in the valve system. Large mercury drops were dispensed continuously as the vacuum pump was disconnected from the capillary tip. If excessive capillary noise was noted, the capillary was replaced with a new or resiliconized capillary. The saturated KCl solution in the Ag/AgCl reference electrode was also replaced daily.

RESULTS AND DISCUSSION

Aromatic nitro compounds are excellent electron acceptors. The electrode reactions are irreversible, however, and result in broad voltammetric peaks. Mononitrophenols give a single peak, whereas the simple dinitrophenols produce two peaks, the first being generally sharper and higher than the second. Figure 1 depicts typical voltammograms and shows that the second peak for 2,6-dinitrophenol is only a shoulder on the first peak. Table 1 summarizes experimental peak potentials for the compounds studied here. Peak potentials are functions of pH and percent methanol, but response is

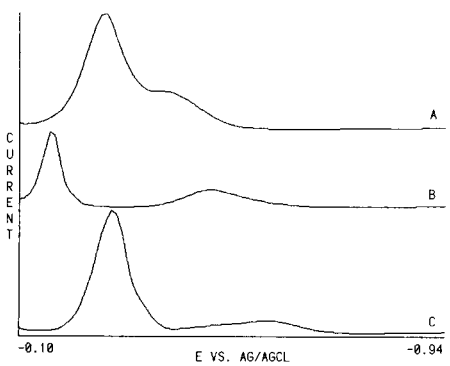

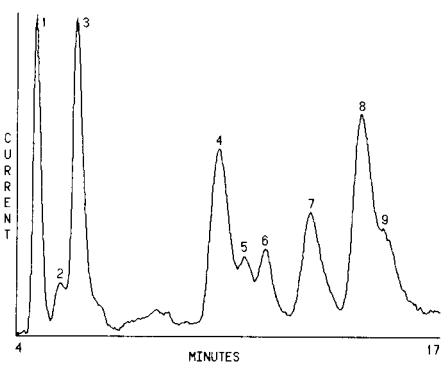

Fig. 1. Square-wave voltammograms: (A) 2,6-dinitrophenol, (B) 2,5-dinitrophenol, (C) 2,4-dinitrophenol. Data taken with 30-Hz square wave in a flow stream as in Table 1.

Fig. 2. Chromatogram of a mixture of nitrophenols. Peaks: (1) 2,6-dinitrophenol (75 ng); (2) unknown impurity; (3) 2,4-dinitrophenol (128 ng); (4) *p*-nitrophenol (150 ng) and 2,3-dinitrophenol (120 ng); (5) *m*-nitrophenol (150 ng); (6) 2,5-dinitrophenol (98 ng); (7) 3,4-dinitrophenol (128 ng); (8) 2,4-dinitro-*o*-cresol; (9) *o*-nitrophenol (150 ng). Currents summed over potential range of —0.06 to —0.61 V vs. Ag/AgCl. Mobile-phase flow rate 1.2 ml min^{-1}. See text for other conditions.

TABLE 1

Voltammetric peak potentials

Compound	Peak potentials[a] (V)		Compound	Peak potentials[a] (V)	
p-nitrophenol	—	−0.58	2,5-Dinitrophenol	−0.15	−0.45
m-nitrophenol	—	−0.45	2,6-Dinitrophenol	−0.24	−0.34
o-nitrophenol	—	−0.40	3,4-Dinitrophenol	−0.24	−0.52
2,3-Dinitrophenol	−0.25	−0.40	2,4-Dinitro-*o*-cresol	−0.24	−0.47
2,4-Dinitrophenol	−0.25	−0.48			

[a]Potentials were measured versus Ag/AgCl in equal volumes of methanol and 0.20 M acetate buffer. Final pH was 5.4.

generally acceptable in the pH range 3—6 and in the methanol range 40—55%.

Initial experiments were done with a mobile phase consisting of equal volumes of methanol and 0.20 M acetate buffer of pH 4.5. The pH value measured in the mixed mobile phase was 5.4. Under these conditions, the sequence of elution was 2,6-, 2,4-, and 2,3-dinitrophenol followed by the overlapping peaks for *p*-nitrophenol, *m*-nitrophenol, 2,5-dinitrophenol, and 3,4-dinitrophenol. As expected from its internal hydrogen bonding, *o*-nitrophenol was the last to elute. The elution sequence for the dinitrophenols corresponds to the decreasing acid dissociation constants. The same relationship holds between *p*-nitrophenol and *m*-nitrophenol.

Varying the percent methanol expands or contracts the chromatograms along the time axis. Increasing the percent methanol decreases capacity factors (k'), whereas decreasing the percent methanol increases capacity factors, but the decreased peak heights lower sensitivity. For our locally packed columns, 45% methanol was judged to be optimum, although, with more efficient columns, a higher percentage of methanol in the mobile phase might be preferable.

Selectivity factors among the mononitrophenols are independent of methanol concentration from 40 to 55% and pH from 3.25 to 6.00. This effect seems reasonable because the thermodynamic pK values range from 7.15 to 8.4, and therefore no significant change in ionization would occur in these experiments. However, the thermodynamic pK values for the dinitrophenols range from 3.71 to 5.42, and these compounds showed large changes in selectivity factors as the mobile-phase pH was changed. Table 2 summarizes these observations; the selectivity factors given were calculated by dividing k' for each compound by k' for *p*-nitrophenol. The results of Mourey and Siggia [8] are consistent with an extension of Table 2 to the more acidic conditions that they used. However, the elution sequence reported by Roseboom et al. [9] with somewhat different conditions are not consistent with our results.

TABLE 2

Selectivity factors for nitrophenols (see text)

pH	CH_3OH (%)	*m*-	*o*-	2,6-	2,4-	2,3-	2,5-	3,4-
3.25	45	1.12	1.74	0.72	1.17	1.21	1.44	1.56
3.70	45	1.12	1.68	0.58	1.05	1.18	1.40	1.52
4.20	45	1.14	1.75	0.39	0.74	1.19	1.38	1.54
4.72	45	1.14	1.77	0.30	0.51	1.10	1.28	1.47
5.12	40	1.14	1.74	0.30	0.43	1.02	1.16	1.42
5.20	40	1.15	1.73	0.31	0.40	1.01	1.09	1.40
5.22	45	1.15	1.76	0.29	0.37	0.92	1.06	1.25
5.30	45	1.13	1.75	0.28	0.37	0.85	1.03	1.18
5.45	50	1.13	1.73	0.27	0.34	0.76	0.98	1.05
5.50	45	1.13	1.72	0.27	0.33	0.73	0.92	1.08
5.55	55	1.10	1.74	0.26	0.32	0.68	0.93	0.93
6.00	45	1.17	1.75	0.29	0.31	0.55	0.69	0.72
pK_a [7]		8.40	7.23	3.71	4.11	—	5.22	5.42

From the above information, a pH for the mobile phase can be selected that minimizes overlap between the chromatographic peaks. Among the mononitrophenols, no two compounds have overlapping chromatographic peaks. Among the dinitrophenols, the greatest overlap is between 2,5- and 3,4-dinitrophenol, but this overlap presents no problem for the electrochemical detector because the first reduction peaks of these two compounds occur at different potentials. The real problem develops when the chromatographic peaks for *p*-nitrophenol or *m*-nitrophenol overlap with a dinitrophenol. Then the dinitrophenol can be determined from its first reduction peak, but the mononitrophenol cannot be determined without complex data analysis.

Table 1 indicates that minimal interference on the potential axis occurs between *p*-nitrophenol and the second peak of 2,3-dinitrophenol. Therefore the pH of the mobile phase was selected so that these two compounds would coelute. A final pH of 4.9 was selected. Under these conditions, some overlap still occurs between *m*-nitrophenol and 2,5-dinitrophenol and between *p*-nitrophenol and 2,4-dinitro-*o*-cresol. However, each of these peaks can be seen in Fig. 2.

Figure 3 shows the output of the swept-potential electrochemical detector. The figure contains data without baseline subtraction,which can easily be done via the the computer system. The detector was operated with a 30-Hz square wave and the potential was swept from —0.18 to —0.66 V vs. Ag/AgCl in steps of —10 mV. The pulse size was —50 mV. Voltammograms were recorded every 2.5 s. The PARC 310 was used with large-sized drops which were replaced before each voltammogram. Figure 2 was obtained by summing all current values from the start of each voltammetric sweep to the

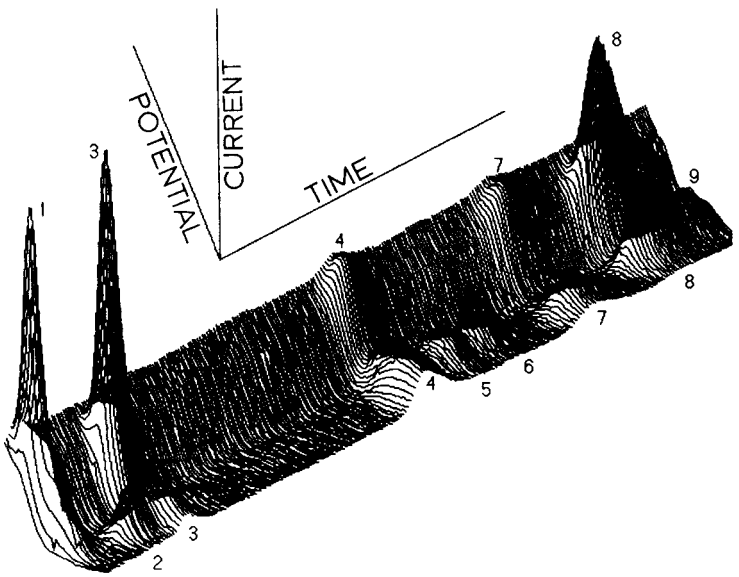

Fig. 3. 3-D chromatogram. Data are from the same experiment as Fig. 2. The time axis shows retention time from 4.4 to 15.6 min. See text for other conditions.

stated potential. It should approximate the results obtained with a d.c. electrochemical detector held at the stated potential and should also be similar to the result with a u.v. detector, although the relative peak heights would be different.

Figure 4 contains four chromatograms taken from the data file used for Figs. 2 and 3. Any one of the chromatograms of Fig. 4 consists of the current data for the same potential step of each voltammogram. Any potential, within the range swept, could have been used, and the four selected are only examples to point out salient features. Figure 4A is the chromatogram for —0.25 V and shows peaks for five dinitrophenols with no interference. The only dinitrophenol not included in this chromatogram is 2,5-dinitrophenol which has reduction peaks on each side of the potential selected here (see Fig. 1). At a less negative potential, 2,5-dinitrophenol is the only nitrophenol in the chromatogram. Figure 4B is the chromatogram for —0.39 V and shows a well-developed peak for orthonitrophenol. In addition, peaks for *m*-nitrophenol and the second peak for 2,5-dinitrophenol are evident. Figure 4C is for —0.48 V. Here, the peak for *o*-nitrophenol is only a shoulder on the peak for 2,4-dinitro-*o*-cresol, as it is in Fig. 2. The peaks for *m*-nitrophenol and 2,5-dinitrophenol are now well developed. In addition, a peak for an unknown impurity appears between those for 2,6- and 2,4-dinitrophenol. This peak can also be seen in Figs. 2 and 3. This unknown peak would not have been detected by a differential-pulse detector unless the potential was

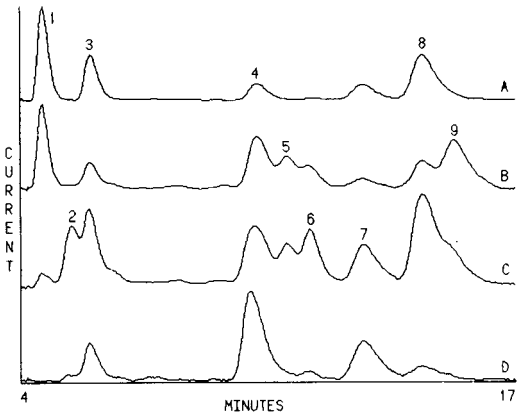

Fig. 4. Chromatograms at constant base potentials. Data are from the same experiment as Figs. 2 and 3. See text for explanation of A—D.

set near —0.48 V. A d.c. amperometric detector would not have detected the unknown unless its potential was more negative than approximately —0.45 V.

Figure 4D is for —0.61 V. The important peak here is for *p*-nitrophenol. Careful examination of Fig. 4 shows that this peak has shifted throughout the series 4A to 4D. In Fig. 4A, the peak represented pure 2,3-dinitrophenol. In the intermediate chromatograms, the peak represents a mixture of *p*-nitrophenol and 2,3-dinitrophenol. The compound nature of the peak can be seen in Fig. 3. Thus, the attempt to adjust the pH so that these two compounds would coelute was close but not perfect. Under these conditions, the *p*-nitrophenol elutes approximately 12 s before 2,3-dinitrophenol, consistent with the selectivity factors of Table 1.

It is obvious that the resolution between some of the peaks is not adequate for precise, straightforward quantitation. Several solutions are possible. In addition to using a column with greater resolution, it is possible to scale and subtract one curve from another. This process can be done on either a chromatogram as in Fig. 4 or a voltammogram as in Fig. 1. A future paper will deal with the mathematical deconvolution of such peaks. If the problem is simply to quantify one specific compound, the selectivity factors in Table 2 can be used to select a different pH for another experimental run. For example, *p*-nitrophenol can be separated from 2,3-dinitrophenol by changing the mobile phase to pH 6 or 3.25.

Square-wave voltammetry and the closely related technique of differential-pulse voltammetry are known to give linear response to changes in concentration over several orders of magnitude. Thus, the primary limit to linearity might come from chromatographic factors rather than from the detector. Although no careful study was done over an extended range of amount injected, peak height was linear with concentration until peak broadening became evident.

The sensitivity and limit of detection depend on several factors. Because the voltammetric peaks of the mononitrophenols are much lower than the first peaks of the dinitrophenols, the mononitrophenols have poorer sensitivities and limits of detection. Column resolution and retention time have obvious effects on peak heights. Flow rate is also important. The results of Samuelsson and Osteryoung [10] that the sensitivity increases with flow rate in this flow cell were confirmed. Sensitivity also increases with increasing size of the mercury drop. From the data for Fig. 3, the limit of detection for 2,6-dinitrophenol can be estimated to be slightly below 1 ng. An earlier experiment, with a smaller amount injected and different instrument settings, indicated a limit of detection of approximately 0.25 ng. Thus, the limits of detection are not as favorable as with a d.c. amperometric detector.

While the application of the swept-potential electrochemical detector discussed here is for h.p.l.c. in the reductive mode, the detector should be well suited to the oxidative mode with a wall-jet detector cell [11]. It might be necessary to include a pulse, before each voltammetric sweep, to some extreme potential to remove any reaction products from the electrode surface as suggested by Fleet and Little [11]. The detector should also find application to flow-injection systems and ion chromatography.

This work was supported by Cooperative Agreement CR-808565 between the School of Chemistry of the Georgia Institute of Technology and the Analytical Chemistry Branch of the Environmental Research Laboratory, U.S. Environmental Protection Agency.

REFERENCES

1 R. Samuelsson, J. O'Dea and J. Osteryoung, Anal. Chem., 52 (1980) 2215.
2 K. Bratin and P. T. Kissinger, J. Liq. Chromatogr., 4 (1981) 321.
3 J. Wang, E. Ouziel, Ch. Yarnitzky and M. Ariel, Anal. Chim. Acta, 102 (1978) 99.
4 M. Stastny, R. Volf, H. Benadikova and I. Vit, J. Chromatogr. Sci., 21 (1983) 18.
5 T. A. Last, Anal. Chem., 55 (1983) 1509.
6 W. L. Caudill, A. G. Ewing, S. Jones and R. M. Wightman, Anal. Chem., 55 (1983) 1877.
7 L. Meites (Ed.), Handbook of Analytical Chemistry, 1st edn., McGraw-Hill, New York, NY, 1963, pp. 1—23, 25.
8 T. H. Mourey and S. Siggia, Anal. Chem., 51 (1979) 763.
9 H. Roseboom, C. J. Berkhoff, J. Wammes and R. C. C. Wegman, J. Chromatogr., 208 (1981) 331.
10 R. Samuelsson and J. Osteryoung, Anal. Chim. Acta, 123 (1981) 97.
11 B. Fleet and C. J. Little, J. Chromatogr. Sci., 12 (1974) 747.

Analytica Chimica Acta, 158 (1984) 179—197
Elsevier Science Publishers B.V., Amsterdam — Printed in The Netherlands

THE DETERMINATION OF THALLIUM IN ROCKS AND BIOLOGICAL MATERIALS AT ng g^{-1} LEVELS BY DIFFERENTIAL-PULSE ANODIC STRIPPING VOLTAMMETRY AND ELECTROTHERMAL ATOMIC ABSORPTION SPECTROMETRY

I. LIEM, G. KAISER and M. SAGER[a]

Max-Planck-Institut für Metallforschung, Institut für Werkstoffwissenschaften, Laboratorium für Reinststoffe, 7070 Schwäbisch Gmünd, Katharinenstr. 17 und Stuttgart, Seestraße 92 (Federal Republic of Germany)

G. TÖLG*

Institut für Spektrochemie und Angewandte Spektroskopie, Bunsen-Kirchhoff-Str. 11, 4600 Dortmund (Federal Republic of Germany)

(Received 11th October 1983)

SUMMARY

Thallium is volatilized from biological materials and rocks after admixture with silicic acid and cellulose/magnesium chloride, respectively, by combustion in oxygen in a quartz apparatus, and from rocks after admixture with magnesium chloride by fusion at 1250°C in a quartz tube drawn to a capillary at one end and sealed at the other end. The condensed thallium is dissolved in a small volume of acid which is used directly to determine thallium by differential-pulse anodic stripping voltammetry. The detection limit of the overall procedure was found to be 1 ng g^{-1} (deposition time 10 min). The results are in satisfactory agreement with those obtained by electrothermal atomic absorption spectrometry after extraction.

Thallium is not a ubiquitous trace element. In the earth's crust average figures range between 0.3 and 0.5 $\mu g\ g^{-1}$ [1—3]. Although it is very toxic (MAC 0.1 mg m^{-3}) [4] it was not considered a potential environmental pollutant. Very few cases of poisoning from industrial exposure are known, probably because chronic thallium poisoning mimics many diseases and thallotoxicosis has not been recognized, but accidental poisoning caused by contact with thallium-containing materials or their careless handling occurs more frequently [5].

Thallium occurs in small concentrations in sulphide ores (Fe, Pb, Zn), which are used for the production of sulphuric acid. In the roasting process, thallium may arrive in the flue dust or in the lead chamber slime or it may remain in the pyrites cinder (0.03—0.05% Tl) which is used in the cement industry [6]. Thallium has received much attention as an environmental contaminant ever since high thallium contents were found in cement powders

[a]Present address: Bundesversuchs- und Forschungsanstalt Arsenal, Wien, Austria.

0003-2670/84/$03.00 © 1984 Elsevier Science Publishers B.V.

discharged from stacks and emissions from brickworks which contaminated adjacent farmland [7].

In order to be able to monitor for normal and aberrant thallium concentrations in pertinent matrices, analytical procedures with the known figures of merit required in extreme trace analysis [8] are in high demand. At present, several very sensitive methods for determining thallium partly down to the sub-ng g^{-1} range in pure solutions are available (Table 1). The analysis of actual samples is, however, beset with problems deriving from concomitant

TABLE 1

Detection limits of some methods for the determination of thallium

Method	Detection limit	Remarks	Ref.
Spectrometry	10 ng ml^{-1}	Rhodamine B	9
	4 ng ml^{-1}	Brillant green	10
Flame a.a.s.			
Aspiration	0.4 μg ml^{-1}	Minerals	11
	2 μg ml^{-1}	Human tissues	12
Injection tech.	0.3 μg ml^{-1}		13
Loop technique	1 ng ml^{-1}	Pure solutions	14
Electrothermal a.a.s.			
Wall atomization	2 ng ml^{-1}	Pure solutions	15
	7 ng ml^{-1}	Extract. of Tl from soils zirconium-coated graphite tubes	16
	10 ng ml^{-1}	Separation of Tl from cement on activ. carbon	11
Platform atomization	0.15 ng ml^{-1}	Pure solutions, drying 130°C; charring 400°C; atomization 1500°C (max. power)	17
Emission spectrometry			
I.c.p. (Ar/Ar)	7 ng ml^{-1}		18
M.i.p. (HCl/Ar)	0.1 ng		19
(Ar)	30 ng ml^{-1}	Pure solutions	20
Atomic fluorescence spectrometry	0.5 pg ml^{-1}	Vitreous carbon atomizer, laser excitation, deionized water	21
Neutron activation analysis	0.5 ng ml^{-1}	Urine (coprecip. with Bi_2S_3 prior to irradiation)	22
$^{203}Tl(n, 2n)^{202}Tl$			
$Tl(n, xn)^{200}Tl$	0.1 μg		23
Isotope dilution	1—10 fg	Rocks, orchard leaves	24
Mass spectrometry	16 ng	Pure solutions	25
Anodic stripping voltammetry			
HMDE	0.5 ng ml^{-1}	Natural waters	26
MFE	0.01 ng ml^{-1}		

elements or reagents used for decomposition, so that the detection limit of the method of choice deteriorates substantially or the method becomes inapplicable, as has been found, e.g., in Pt-loop flame atomic absorption spectrometry (a.a.s.) [11] and electrothermal a.a.s. [27—30]. In inductively-coupled plasma emission spectrometry, even traces of iron interfere, whereas in voltammetric methods, an incomplete decomposition of the sample (organic residues) make the determination of thallium impossible [31, 32].

While several authors have dealt with the determination of thallium in waters [26, 31] and rocks [11, 32—39], analytical data for biomaterials are scarce [12, 38], because tedious destruction methods are necessary for these materials and the levels of thallium are very low.

In almost all cases on record, thallium is separated from the matrix (normally, minerals and rocks) to avoid cross-interferences by concomitants in the measurement step. The solid sample is either broken down in acids prior to liquid-liquid extraction [33, 35, 36] or ion-exchange [33], or thallium is separated from the matrix by volatilization [32, 34, 37, 39]. More details on separation methods are available [15].

Only in a few cases can the decomposition solution be used directly for the measurement procedure; e.g., the digestates of human liver and kidney after low-temperature ashing and enzymatic degradation in connection with flame a.a.s., or pressurized decomposition in a Parr bomb at 170°C with nitric acid in connection with differential-pulse anodic stripping voltammetry (d.p.a.s.v.) [40]. According to published evidence [41—44], however, it is impossible to use a decomposition solution which still contains organic residues for voltammetric measurements. A pressurized decomposition of biomaterials at 170°C does not mineralize the substance completely unless the solution is fumed twice with perchloric acid. Problems have also been reported in the direct use of acid digestates of hair in connection with electrothermal a.a.s. [45]. The present work was aimed at the determination of trace levels of thallium in environmental solid samples by using decomposition methods in which thallium is volatilized, in order to avoid various interferences, thus dispensing with the need for a lengthy separation step; d.p.a.s.v. and electrothermal a.a.s. were used for the final measurements, because their sensitivity is ample to meet the low detection limit required.

Decomposition methods

Ignition tube technique under static conditions. Volatilization tube techniques compare favourably with wet decomposition methods because they are less time-consuming and provide a simultaneous separation of some potential interferents. As thallium is a relatively volatile element (b.p. 1457°C) and forms a range of fugacious compounds, e.g., $TlNO_3$ (430°C), TlCl (720°C), TlBr (815°C), a volatilization technique is advantageous.

The classical ignition tube technique where a quartz tube is sealed at one end and extended to a capillary at the other end has already proved to be especially suitable for the evolution of Se, Te and Bi from rocks after

admixture with appropriate additives [46]. In the same way, thallium can be released from rocks at 1250°C after the sample has been blended with magnesium chloride dihydrate in the ratio 1:1. The quartz tube is placed upright in a muffle furnace with the capillary protruding from the oven. In the decomposition, the magnesium salt decomposes to MgO, H_2O and HCl, the hydrogen chloride being a carrier gas for the thallium(I) chloride that probably forms. The evolved thallium condenses in the cold capillary which is cut from the quartz tube after decomposition. The condensate is dissolved in 0.5 ml of a 5 M HBr—1 M HF mixture or in hydrochloric acid (37%) by allowing the acid to stand for 20 min. Addition of the hydrofluoric to the hydrobromic acid has proved to shorten the dissolution time because thallium is tenaciously adsorbed on quartz. The d.p.a.s.v. technique lends itself best to the final measurement, but it has one serious drawback. Drying of the commercially available magnesium chloride hexahydrate at 180°C results in the dihydrate. A higher temperature causes degradation. In the decomposition process, water covolatilizes, condenses in the capillary, and dissolves part of the thallium. Therefore, if extreme care is not taken, there is a possibility of losing thallium with condensed water when the capillary is cut. The sample weight of 0.3 g is sufficient to detect the concentration of thallium in nearly all rocks.

Combustion under quasi-static conditions. The volatility of thallium and its compounds was utilized long ago by Geilman [32] who volatilized the element at 1100°C from various materials in a quartz tube placed in a tube furnace. This technique is now a standard method for the analysis of minerals, rocks and metals [34, 37, 39]. For biological solid samples, however, this technique is inferior to a combustion method (Trace-O-Mat) in which the sample is placed on a sample holder after pelletting and is burnt in pure oxygen within a few seconds while the apparatus is intensively cooled with liquid nitrogen [47]. During the combustion, thallium volatilizes and condenses on a cold finger whence it is dissolved by refluxing with acids within 40 min. This principle has been successfully applied in the analysis of rocks and biomaterials for thallium [48] in connection with liquid-liquid extraction and spectrophotometry [9]. With this procedure, however, thallium could not be detected in all materials based on a sample weight of $\leqslant 1$ g. Therefore the combustion method was matched to d.p.a.s.v. and electrothermal a.a.s. to permit its detection in all pertinent materials. In d.p.a.s.v., the best results as regards sensitivity and diminution of interferences were obtained by using 5.5 M sulphuric acid as the refluxing acid, whereas with the electrothermal a.a.s. both nitric and sulphuric acid served the purpose well because thallium has to be separated from the decomposition solution in any case, to obviate interferences from halides that covolatilize in the combustion technique.

Methods for the final measurement

Among many sensitive methods for quantifying thallium (Table 1), anodic stripping voltammetry (a.s.v.) and atomic absorption spectrometry

(a.a.s.) appear to be suitable because they provide a high degree of sensitivity and reliability while being rapid, easy to handle and relatively cheap. There are, however, some decisive differences between the two methods with respect to thallium.

Flame atomic absorption spectrometry. The direct use of a sample or a decomposition solution has not been reported. In the conventional aspiration mode (air-acetylene flame), detection limits of 0.01 $\mu g\ ml^{-1}$ [49] and 0.07 $\mu g\ ml^{-1}$ [50] were achieved after thallium had been complexed in the sample digest of minerals with ammonium pyrrolidinecarbodithioate and thus extracted into 4-methylpentan-2-one; the limit was 0.1 $\mu g\ g^{-1}$ with diethyldithiocarbamate extraction [35]. The organic solvent can be nebulized directly, which enhances the sensitivity compared to aqueous solutions [35]. With a sample weight of 10 g, a detection limit of 0.06 $\mu g\ g^{-1}$ for foodstuffs (e.g., spinach, bovine liver and kale) was achieved [38]. In one instance the HCl/HNO_3 liver digest was evaporated to a constant volume and diluted with water prior to aspiration. Background problems have however been reported on [51]. The sensitivity can be enhanced with the injection [13] or the Pt-loop technique, the latter yielding a detection limit of 1 $ng\ ml^{-1}$ if thallium is present in isolated form [14]. The presence of salts causes the detection limit to deteriorate severely [11].

Electrothermal atomic absorption spectrometry. The sensitive determination of thallium in pure solutions is far from being a problem. Detection limits of 1 $ng\ ml^{-1}$ with wall atomization (Perkin-Elmer spectrometer type 430, HGA-76B) [15], and 0.16 $ng\ ml^{-1}$ (Perkin-Elmer spectrometer type 5000, HGA-500) [17] with the stabilized-temperature platform furnace atomization [52]. The latter technique, where fast heating rates are applied, was found to be superior to wall atomization [53]. Also in electrothermal a.a.s. the analysis of real samples is marred by many acids, e.g., hydrochloric and perchloric acids [27, 28] and metals, e.g., Fe, Co, Ni, Zn, even in the $\mu g\ ml^{-1}$ range depending on the ramp parameters [27, 29]. In 0.5 M sulphuric acid, the depression of the signal was found to decrease in the sequence Cu > Fe > Na > Co, whereas zinc did not affect the signal. Heavy depressions also occur in the presence of boric acid. Vanadium, Nb and La increase the signal slightly.

In order to avoid lengthy separation methods, special ramp programs have been proposed, or additives used, e.g., tartaric or sulphuric acid to reduce interferences [29] which allow the direct analysis of metal chips [54—56] with a detection limit of 0.03 $\mu g\ g^{-1}$ [56]. However, metal residues remain in the furnace and bias the sensitivity depending on the type of furnace and number of firings [56]. A detection limit of 0.2 $\mu g\ g^{-1}$ can be achieved if the metal chips are dissolved in acid, the solution is evaporated with sulphuric acid, and tartaric acid is added [29]. The direct analysis of rocks (detection limit 1 ng) using an exactly adjusted temperature program [57], and of sewage sludge after homogenization and application of the standard additions method [58], has been proposed.

In most cases, a separation, e.g., by volatilization [37, 59], extraction [35, 36], which may include sophisticated separation schemes [60] or sorption on charcoal after complexation [11], has been employed to obviate multiple interferences.

The situation is still worse in the analysis of biomaterials in which high concentrations of trace elements and salts (e.g., halides) can occur. Thallium(I) halides, oxide and nitrate volatilize from the carbon rod even at about 600°C, depending on the matrix. The halides do not undergo degradation in the atomization step [61—63] and that accounts for the severe signal depressions in the presence of halides. Addition of lithium nitrate has been reported to help the situation [64] but at the expense of a poorer detection limit; this has been confirmed here. Interferences by NaCl, $FeCl_3$ and $MgCl_2$ cannot be avoided by applying this technique. Fuming off the halides with sulphuric acid [29] has proved to be effective. Addition of ammonium salts to volatilize ammonium chloride [65] or phosphate [66] does not improve the situation. The latter remedy helps by allowing an increase in the charring temperature to 800°C, but this causes fuming and thus decreases the signal-to-noise ratio. Without a separation of the interferents, measurement of thallium in 0.25 M H_2SO_4 seems to be most favourable. These investigations refer to wall atomization. For the stabilized-temperature platform technique, the situation might be more favourable [52].

In practical analysis, calibration must be done with samples matched to the sample to be analyzed as far as possible. Moreover, the analytical data must be checked for accuracy with the method of standard additions. In routine analysis where simple and rapid procedures are required, the process of levelling interferences is considered a remedy. Thus, e.g., in 0.25 M H_2SO_4 at a molar chloride excess of 2000—50 000, the signal depression amounts to 10% and upon addition of sodium dihydrogenphosphate or diammonium hydrogenphosphate, the signal was constant for $\leqslant$10 000-fold amounts of, e.g., NaCl, $FeCl_3$, $CuCl_2$. The advantage of a shorter analysis time in this process has to be paid for by the poorer detection limit and sensitivity.

From what has so far been said on electrothermal a.a.s., it can be seen that a separation of thallium from the matrix is usually indispensable. Liquid-liquid extraction is favoured by using various complexing agents and extractants, as has been reviewed elsewhere [15]. A separation of thallium by volatilization from orchard leaves and Bowen's kale in a quartz tube at 1000°C in an oxygen carrier gas stream has been reported to be successful [59].

In the present work, electrothermal a.a.s. is applied in the analysis of rocks and biomaterials after combustion and wet decomposition of the sample and separation of thallium(III) bromide by extraction into diisopropyl ether and elimination of the bromide by fuming off the solution with nitric or sulphuric acid.

Differential-pulse anodic stripping voltammetry (d.p.a.s.v.). Voltammetric

methods compare favourably with a.a.s. because they can be applied to a wider measurement range, they are less prone to the effects of high salt concentrations (e.g., halides) and larger sample aliquots can be used. Besides these advantages, the apparatus costs are much lower. A detailed compilation of the various voltammetric methods of determining thallium is available [67].

Direct current polarography (d.c.p.), alternating current voltammetry (a.c.v.) and differential pulse voltammetry (d.p.v.) are favoured, with the a.c. and d.p. modes showing the highest sensitivity [68]. Statements whether the hanging mercury drop electrode (HMDE) or the mercury film electrode (MFE) yields better sensitivity are in conflict [26, 68]. A detection limit of about 0.01 ng ml^{-1} can be achieved with a MFE [26].

Metal ion interferences from, e.g., Cd, Sn, Sb, Pb, are encountered in the determination of thallium, as the reversible redox system Tl^+/Tl is very close to the potentials of these elements [69, 70]. Variation of the electrolysis potential helps to avoid some of these problems [68]. With a MFE plated in situ, the thallium and lead peaks which overlap at a HMDE can be resolved [71], and with a mercury-plated copper disk electrode as little as 90 pg ml^{-1} can be determined along with lead and cadmium [72]. In the presence of tartrate and polyethylene glycol 4000, thallium can be determined along with Pb and Cd at a HMDE [73], and a computer program has been used to resolve the Tl and Pb peaks [74]. At a mercury-plated glassy carbon electrode, thallium can be determined directly in urine acidified with perchloric acid to 0.1 M, down to 0.2 ng ml^{-1} [75].

For accurate determinations of thallium at extremely low levels, it should be separated from complex materials [33, 68]. A separation often involves a preconcentration, so that very low detection limits can be achieved. Thus, e.g., as little as 3 pg ml^{-1} can be determined in water by using an ion-exchange resin (Bio-Rad Ag1-X8) [76].

Separation of interferences by electrodeless deposition on gallium. By partial dissolution of elemental gallium, it is possible to preconcentrate traces of elements which are electrochemically nobler than gallium [77]. Tests were made here to establish if the reverse process, the cementation of metal ions on gallium from the decomposition solution, could be applied to remove these elements which interfere in d.p.a.s.v. Although thallium has a more positive standard potential than gallium (−0.336 V and −0.52 V, respectively), it is not deposited. Cementation proceeds in sulphuric acid or hydrochloric acid medium. The depletion of some metal ions both from 4 M H_2SO_4 and 1 M HCl is shown in Table 2. In nitric acid solutions (>0.8 M), passivation of gallium hampers the cementation of a number of elements. For the cementation process, gallium (m.p. 29.8°C) is heated in a drying oven to about 50°C. With an Eppendorf pipette, a drop (0.1—0.15 g) is added to the analyte (10-ml quartz beaker) which is heated to 50°C for 1 h while stirring with a magnetic bar.

TABLE 2

Tolerable quantities of metal ions in the sample solution without and with their prior separation by electrodeless deposition on gallium from acidic solutions (>1 M in H_2SO_4 or HCl) in the determination of 20 ng of thallium (deposition potential −0.75 V vs. SCE, deposition time 2 min, pH 7)

Metal ion	Tolerable amount (μg)		Metal ion	Tolerable amount (μg)	
	Without separation	With separation		Without separation	With separation
Cu(II)	0.5	>1000	V(V)	500	500
Hg(II)	100	>1000	Ag(I)	500	>500
Bi(III)	80	>1000	Au(III)	>500	>500
Cd(II)	50	50	As(V), Co(II),	>1000	>1000
Ti(IV)	20	20	Mn(II), Mo(VI),		
Sb(IV)	100	200	Ni(II), Pb(II),		
Se(V)	100	150	Sn(IV), Zn(II),		
In(III)	500	500	Ga(III)		
Fe(III)	500	>1000			

Optimization of the voltammetric determination

Supporting electrolyte. A number of interferences by metal ions can be reduced or eliminated with (ethylenedinitrilo)tetraacetic acid, disodium salt (EDTA). Complex formation is strongly pH-dependent (Table 3). The lead peak overlaps exactly with the thallium peak at pH ≤5.5 for a deposition potential of −0.6 V vs. SCE and cadmium appears at −0.5 V if their concentrations are above certain borderline concentrations (Table 4). A drawback to the use of EDTA lies in a shift of the peak potentials of the complexes of, e.g., Cu, Mo, Sb and Bi to more negative values which accounts for possible interferences [80]. At pH 7—8, the limiting concentrations of most of the potential interferences can be increased substantially (Table 2), but only at the cost of a shorter potential range which makes evaluation of the voltammograms difficult (Fig. 1).

In order to avoid precipitation of EDTA on addition of acidic decomposition solutions, buffer substances are needed, e.g., acetate, tartrate or citrate [26, 68, 81]. The EDTA precipitates in acidic solutions containing only 0.1 M citrate, but not in solutions that are 1 M in citrate. Moreover, the

TABLE 3

Optimal pH values for the complex formation of metal interferences with EDTA [78, 79]

Metal ion	pH	Metal ion	pH	Metal ion	pH
Ti(IV)	5.5	Cd(II)	7.8	As(III)	5.6
V(IV)	5.9	Hg(II)	4.2	Sb(III)	3.0
Fe(III)	2.8	Sn(II)	4.0	Bi(III)	1.9
Cu(II)	5.9	Pb(II)	6.4		

TABLE 4

Influence of the pH value of the electrolysis solution on metal ion interferences in the determination of 5 ng of thallium (deposition time 5 min)

Interference	Tolerable amount (μg)		Interference	Tolerable amount (μg)	
	pH 5	pH 7		pH 5	pH 7
Se	1[a]		Pb	4[a]	
	5[b]	100[b]		0.3[b]	1000[b]
Cd	40[a]		Bi	18[a]	
	30[b]	50[b]		15[b]	100[b]
Hg	350[a]				
	350[b]	100[b]			

[a] Deposition potential, −0.6 V. [b] Deposition potential, −0.75 V vs. SCE.

presence of citrate during the neutralization of the decomposition solution with ammonia, avoids the precipitation of metal hydroxides which redissolve only very slowly. A supporting electrolyte consisting of 0.02 M EDTA and 1 M citrate has a sufficient buffer and complexing capacity and was used throughout the investigations.

Deposition potential. A deposition potential of −0.75 V vs. SCE proved suitable as regards sensitivity, metal ion interferences and baseline current. At this potential and at pH 5, only 0.3 μg of lead can be tolerated whereas at pH 7, the limiting concentration is 1 mg (Tables 2, 4). Interference by lead can, however, be avoided by shifting the potential to −0.6 V [68] at the expense of a decrease in sensitivity of about 20%.

The interferences listed in Table 4 are confined to those elements which covolatilize in the combustion technique (Trace-O-Mat) and thus are liable to pose problems if present in higher concentrations.

Dependence of the signal on pH of sample solution and deposition potential. The stripping peak currents depend strongly on the pH of the sample solution and on the deposition potential. At pH 5 and a deposition potential of −0.75 V, the voltammograms can be evaluated perfectly and the thallium peak is about 50% higher than at pH 7, but an 8-fold amount of lead with respect to thallium has the same response. The elimination of the lead interference by a change of the deposition to −0.6 V (Fig. 2) has to be paid for by a 20% decrease in sensitivity. In practical analysis, a compromise has to be reached between deposition potential and pH of the sample solution.

EXPERIMENTAL

Instrumentation

Decomposition. For the combustion, a Trace-O-Mat [47] and a pelleting press were used (H. Kürner, Rosenheim, FRG). For the pressurized decom-

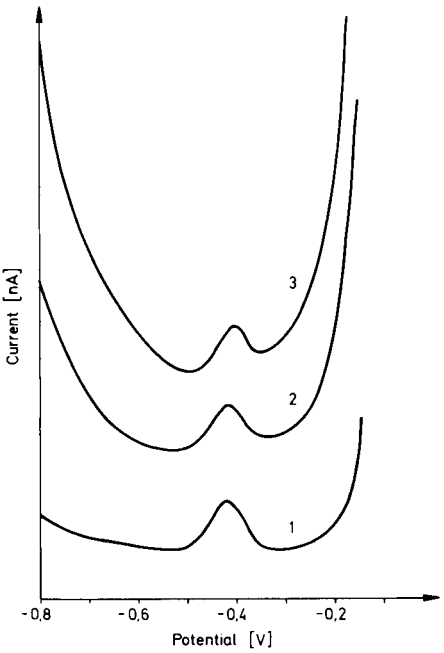

Fig. 1. Dependence of the baseline current on the pH of the electrolysis solution (10 ng Tl, EDTA/Na citrate electrolyte, deposition potential —0.75 V vs. SCE, deposition time 3 min). Curves: (1) pH 5; (2) pH 7; (3) pH 8.

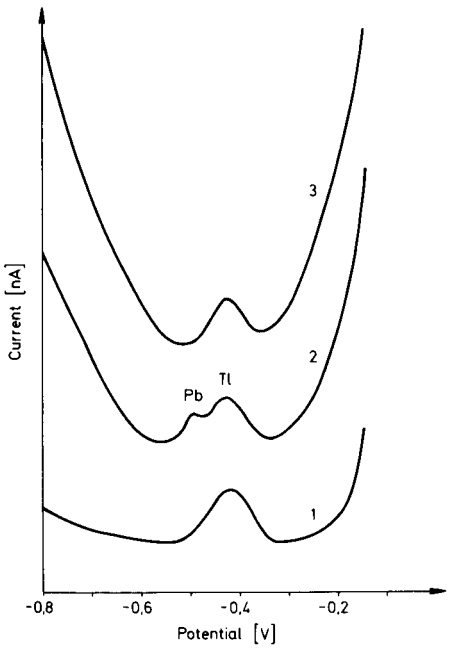

Fig. 2. Dependence of the Tl and Pb stripping peak currents on the pH of the electrolysis solution (10 ng Tl, 5 μg Pb, deposition potential —0.75 V vs. SCE, deposition time 3 min). Curves: (1) pH 5 (Tl an Pb overlap); (2) pH 6 (Tl and Pb resolved); (3) pH 7 (Pb eliminated).

position a commercially available device with electronic temperature setting [82] was used (H. Kürner, Rosenheim, FRG). For the ignition tube technique, quartz glass tubes (15 mm o.d., 12 mm i.d.; Heraeus Schott Quarzschmelze) and a muffle furnace (type TIK/R 11/12, maximum temperature 1300°C; Heraeus, Hanau, FRG) were used.

Voltammetry. A Metrohm Polarecord E-506 was used with a VA Controller E-608 and a stand E-648. The electrode system consisted of a HMDE as working electrode, a Pt-counter electrode and a SCE as reference electrode (sat. KCl). The polarographic cell (Metrohm) had a capability of 5 ml.

The mode was differential-pulse voltammetry (pulse amplitude 50 mV, drop time 0.4 s, ΔU + 2 V) with an electrolyte volume of 4—5 ml, an electrolysis time of 1—12 min depending on the thallium concentration, and a deposition potential between —0.6 V and —0.75 V vs. SCE with magnetic stirring. The mercury drop size corresponded to 3 divisions on the electrode scale; the quiescent period after electrolysis was 10 s. The peak potential (E_p) under these conditions was —0.43 V vs. SCE.

Interferences were studied with an Amel multipolarograph type 471. The electrode system and the cell were the same as mentioned above. Sweep rate was 20 mV s^{-1}, voltage range 100 mV cm^{-1}, pulse frequency 4 Hz.

Atomic absorption spectrometry. The Perkin-Elmer spectrometer (type 430) used was equipped with deuterium background correction and a hollow cathode lamp operated at 10 mA. The thallium resonance line at 276.8 nm was employed, the spectral band width was set to 0.7 nm, and the absorbance was traced with a recorder (Perkin-Elmer 56).

Reagents

All reagents were of analytical grade (Merck) and all gases from Messer Griesheim (Düsseldorf, FRG) if not stated otherwise.

For combustion in the Trace-O-Mat, the oxygen was 99.995% pure. The additions were silicic acid (Riedel de Haen Seelze-Hannover, FRG) previously heated to 1000°C, cellulose, and magnesium chloride hexahydrate previously dried at 150°C for 2 h. For refluxing, 5 M sulphuric acid was used.

For the ignition tube technique, magnesium chloride dried at 150°C for 2 h was used as additive. The dissolving acids were a mixture at 5 M hydrobromic acid and 1 M hydrofluoric acid or hydrochloric acid (37%).

The wet decomposition in a closed or an open system required hydrochloric (37%), nitric (65%) and hydrofluoric (40%) acids purified by sub-boiling-point distillation, as well as perchloric acid (70%) and boric acid.

For the d.p.a.s.v., the supporting electrolyte was prepared by dissolving 29.4 g of trisodium citrate dihydrate and 0.745 g of EDTA (disodium salt) in water and dilution to 100 ml, giving a final concentration of 1 M citrate and 0.02 M EDTA. Adjustment of the pH was done with diluted ammonia liquor.

For the extraction, HBr, KBr, Br_2 and diisopropyl ether were used. Stock solutions for thallium(I) were prepared from Titrisol ampoules (1 g l^{-1}) by dilution to a final concentration of 1 μg ml^{-1}. More diluted solutions were prepared freshly before use. All other metal ion solutions were also prepared from Titrisol ampoules. The gallium needed for the electrodeless deposition was 99.999% pure (Alusuisse Switzerland). Doubly-distilled water from a quartz still was used in all cases.

Procedure

Decomposition. The combustion [48] and the pressurized decomposition [82] have been described in detail in previous papers. The decomposition in an open system, applied to rock samples, was done in platinum crucibles. The sample (0.05—0.3 g) was wetted with about 0.1 ml of water, and 0.3 ml of perchloric acid and 1 ml of hydrofluoric acid were added. The solution was evaporated to dryness. The evaporation step was repeated twice after addition of 0.1 ml of perchloric acid and 0.3 ml of hydrofluoric acid each time. After the last evaporation step, the crucible was heated to about

220°C for 15 min. To the residue 2 ml of hydrochloric acid and about 30 mg of boric acid were added and the mixture was gently heated until a clear solution resulted.

In the ignition tube technique, a quartz tube 10 cm in length was sealed off at one end, and ⩽3 g of the sample and the same quantity of magnesium chloride dihydrate were added. Sample and additive were thoroughly mixed. The tube was extended to a capillary of at least 15 cm in length and placed in the cold muffle furnace. The temperature was first set to 350°C for 1 h to evaporate most of the water. After 1 h the temperature was raised to 1250°C and maintained for 5 h. Subsequently, the tube was removed from the oven, and the capillary was closed with a small rubber stopper and cut about 1 cm above the taper of the tube. By means of an Eppendorf pipette, 0.5 ml of hydrochloric acid (37%), was injected into the capillary and left to stand for 20 min. The capillary was then rinsed with 0.5 ml of water and 2 ml of electrolyte with the aid of a syringe which fitted in a hole of the rubber stopper. The solution was used directly for d.p.a.s.v.

Separation methods

Electrodeless deposition on gallium. The sulphuric or hydrochloric decomposition solution which should be ⩾1 M in acid was placed in a 10-ml quartz beaker and a drop of gallium (0.1—0.15 g) was added. The solution was stirred for 1 h at 50°C with a magnetic bar and then transferred to the polarographic cell leaving the gallium in the beaker, which was rinsed with 1 ml of supporting electrolyte. The pH of the solution was adjusted to 7 with ammonia solution. If the concentrations of the interference stated above were below borderline a lower pH value could be used.

Liquid-liquid extraction. An aliquot of the decomposition solution was transferred to a quartz test tube to which 1 ml of potassium bromide solution (30% w/v) was added. The acidity of the solution should be 1—1.5 M. With the standard additions method, 30 μl of bromine was added to oxidize Tl(I) to Tl(III). The mixture was extracted with three 1-ml portions of diisopropyl ether. The collected organic phases were evaporated to complete dryness and the residue was dissolved with 0.2 ml of 5 M sulphuric acid. After addition of 1.8 ml of water and 2 ml of supporting electrolyte (pH 5), the solution was transferred to the polarographic cell. Figure 3 shows the voltammograms obtained in the analysis of a rock sample directly in the decomposition solution and after extraction of thallium. For the measurements by a.a.s., bromide was eliminated by fuming the solution with 0.3 ml of nitric acid (65%); the residue was taken up with 1 ml of water.

Final measurements

D.p.a.s.v. The solution was deaerated by argon for 10 min while stirring. During the remaining procedure, argon was passed over the solution. A mercury drop was extruded from the electrode (3 scale divisions) and the solution was electrolysed for 1—12 min at a potential of —0.75 V vs. SCE.

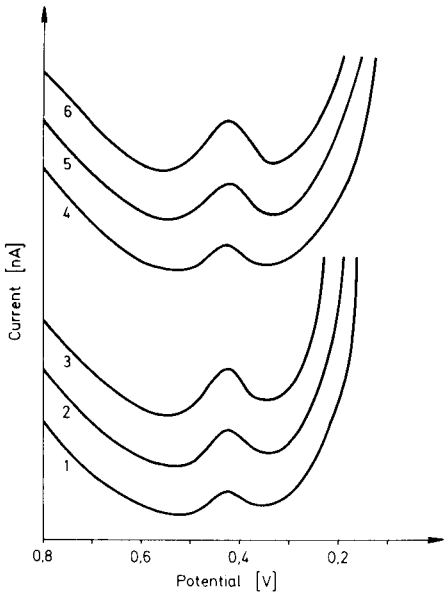

Fig. 3. Determination of Tl in Albtalgranite by d.p.a.s.v. (deposition potential —0.75 V vs. SCE, deposition time 2 min). Curves: (1) decomposition solution; (2) spiked with 4 ng Tl; (3) spiked with 8 ng Tl; (4) Tl extracted from decomposition solution; (5) spiked with 4 ng Tl; (6) spiked with 8 ng Tl.

In the presence of more than 4 μg of lead, a potential of —0.6 V vs. SCE was applied. After 10 s of quiescence, the stripping process was started to a final potential of —0.15 V vs. SCE. For calibration, at least 4 standard additions were made by dispensing measured volumes into the polarographic cell (the same amount of thallium was added each time).

A.a.s. The measurements were done by the standard additions method; 10-μl portions were injected into the furnace and argon served as purge gas. The controller of the furnace was operated under the conditions listed in Table 5.

Recommended procedure

The sample ($\leqslant$0.6 g) was mixed with magnesium chloride dihydrate (7:3) and cellulose (1:3) in the case of rocks, and with silicic acid (9:1) in the case of biological materials. The mixture was pelletted and the pellet wrapped in a thin cellulose tissue which was squeezed on top of the pellet to form a match cord which allowed the pellet to be ignited easily in the Trace-O-Mat [48]. After combustion, the thallium was dissolved from the cold areas by refluxing with 5 M sulphuric acid for 30 min. The apparatus was rinsed through the condenser with about 3 ml of water and the solution was made up to 5 ml or to 10 ml with water depending on the expected thallium concentration in the sample. An aliquot part of the solution was transferred directly to the polarographic cell, 2 ml of supporting electrolyte

TABLE 5

Operating parameters in electrothermal a.a.s.

	Temperature (°C)	Time (s)	Heating rate
Drying	125	20	2
Ashing	600	20	2
Atomization	2300	10	1
High-temperature treatment	2600	3	0

were added and the solution was diluted with twice-distilled water to a final volume of 4 ml; the pH was adjusted with ammonia liquor (ca. 0.6 ml) to 5 if the lead content of the sample was $\leqslant 2\ \mu g\ g^{-1}$. With higher lead levels, the pH had to be adjusted to 7. This solution was electrolysed as described above. Figure 4 shows a flow diagram of the procedure.

RESULTS AND DISCUSSION

In order to provide for a simple, economic and reliable procedure for the determination of trace amounts of thallium in environmental samples, available decomposition and separation methods were tested for their suitability as part of a multistage combined procedure in connection with d.p.a.s.v. and electrothermal a.a.s. which have reported detection limits of 4×10^{-10} M [72] and 0.15 ng ml^{-1} [17], respectively, under ideal conditions. In pursuing this goal, decompositions by combustion, fusion and wet digestion and

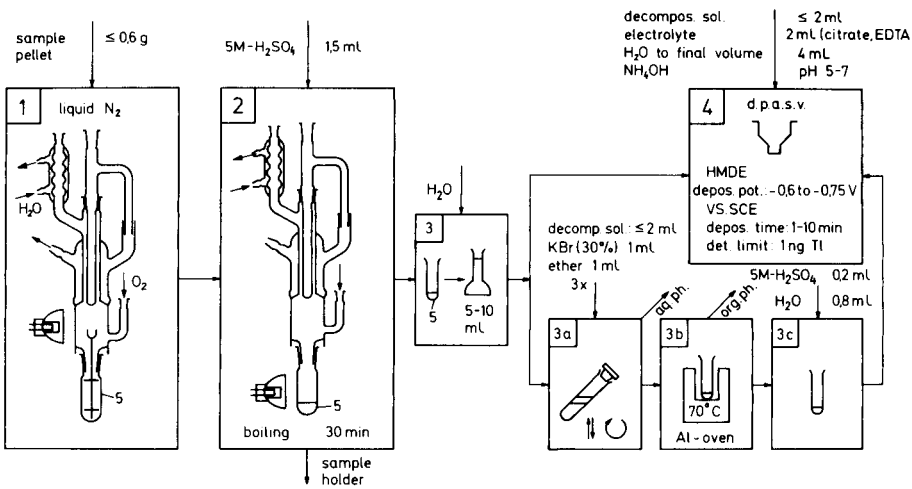

Fig. 4. Flow diagram for the determination of Tl by d.p.a.s.v. after decomposition of the sample in the Trace-O-Mat.

separations by volatilization, electrodeless deposition on gallium and liquid-liquid extraction were examined.

In all decomposition solutions, thallium was not present in an isolated form but along with numerous metal ions. In the volatilization techniques, there is covolatilization of fugacious elements (e.g., Hg) or metal halides (e.g., of Cd, Bi, Pb, Se) or oxides (e.g., SeO_2). These elements interfere with d.p.a.s.v. whereas the halides cause serious signal depressions in electrothermal a.a.s. A separation of these interferents is, therefore, imperative if they are present in moderately high concentrations (Tables 2, 4).

The electrodeless deposition of metal ions on gallium is a simple technique with which a large number of elements that interfere in d.p.a.s.v. can substantially be removed from the solution. It is, however, of little avail in combination with volatilization techniques, as those elements that covolatilize are not or only incompletely deposited (Table 2). Selenium and antimony are only partly, and cadmium and titanium are not, removed from the solution. Titanium, however, is not volatilized in the volatilization techniques described in this paper and can be neglected. With concentrations of these elements in a matrix exceeding the quantities given in Table 2, another or additional separation methods are needed.

The borderline concentrations given for the electrodeless deposition on gallium were established with the individual elements. In the presence of several metal ions, there may be synergic effects which reduce the tolerable concentrations of these elements considerably. Thus, for instance, the detection of 20 ng of thallium is impossible in the presence of $\geqslant 5$ μg each of Cu, As, Se, Cd, Sb, Hg and Bi, even though this quantity is far below the threshold limit values established on individual elements. A separation of these interfering ions from the decomposition solution is therefore imperative. The electroless deposition was successfully applied after a pressurized decomposition and spiking the digestate with 20 ng of thallium and 5 μg each of Cu, Hg, Bi, Se, Pb (Table 6).

Volatilization techniques provide considerable advantage over wet decompositions in that many metal interferences can be eliminated because sparingly volatile metal compounds remain in the residue. The indisputably cheap ignition-tube technique is subject to some difficulties. First, the extension of quartz tubes to capillaries requires manipulative skill, as does the dissolution of the condensed thallium from the capillaries. These manipulations render the technique laborious although 8 decompositions can be done simultaneously with the furnace available. Moreover, this technique is not suitable for biomaterials. The time needed for 8 tubes is about 6 h. For these reasons, the combustion technique which is easier to handle was selected and matched with d.p.a.s.v. which was preferred to electrothermal a.a.s. on account of its lower vulnerability to halides. In the combustion technique, a number of metal oxides (e.g., Cu, Fe, Ti, Cr oxides) remain with the slug on the sample holder while Se, Cd, Hg, Pb and Bi covolatilize and interfere with the voltammetric determination if present in quantities of

TABLE 6

Thallium concentrations (ng g^{-1}) in rocks and biomaterials

Matrix	D.p.a.s.v.					Electrothermal a.a.s.		
	Combustion		Wet decomp. Pt-crucible Extract.	Pressure decomp. treatment with $HClO_4$		Ignition tube	Combustion Extract.	Wet decomp. Pt-crucible Extract.
	Direct	Extract.		Extract.	Dep. on Ga			
Granite USGS-G2	750	730	740			930	720	760
Andesite USGS-AGV1	270	260	280			380	280	270
Granodiorite USGS-GSP 1	930	910		920				
Albtalgranite DFG-KA 1	1050		1100	1030			1150	1100
Dazite KA-2	130	120	130	125	125	110	135	120
Tomato leaves NBS 1573	24	20						
Pine needles NBS 1575	27	30		31	28		29	
Orchard leaves NBS 1571	32	34					36	
Rice flour NBS 1568	<2	<2			<2[a]		<2	
Wheat flour NBS 1567	2	3		3	<3[a]			
Bovine liver NBS 1577	<2	<2		2				

[a]Spiked with 10 ng Tl and 2 μg each of Cu, As, Se, Cd, Sb, Hg, Bi.

$\geqslant$100, 50, 350, 1000 and 80 μg, respectively. As the sample weight is 0.5 g and only an aliquot of the digestate is used the threshold limit concentrations are at least 4 times higher. It is rare for the concentrations in biological samples to be such that the combustion technique cannot be matched directly to d.p.a.s.v.

The stated limiting concentrations were ascertained with a sample solution adjusted to pH 7. This is a compromise figure as regards baseline current and tolerable amount of interferences. At pH 5, the resolution of the thallium peak is much better than at pH 7 [7] but the borderline concentrations of the above-mentioned interferences become worse (Table 4). If the concentrations of these elements are expected to be below these levels, it is recommended to work at pH 5 for a better evaluation.

In order to check the results obtained by d.p.a.s.v., electrothermal a.a.s. after wet decomposition in a platinum crucible or in a closed system under pressure and after the combustion technique was examined for some materials. A direct determination of thallium in the sample digestate proved to be impossible on account of the severe signal depressions resulting mainly from the presence of halides. Liquid-liquid extraction of thallium(III) bromide was therefore employed to get rid of interferences, and bromide

was eliminated by fuming the solution with nitric acid. With these procedures, thallium was determined in several environmental materials. The results are in good agreement (Table 6). The standard deviation varies considerably from matrix to matrix. For pine needles and tomato leaves, the standard deviation of the overall procedure (combustion and d.p.a.s.v.) lay in the range 11—13% (n = 10), whereas for orchard leaves (s_r = 25%), and particularly for rocks the results showed a wider scatter. This may be due to inhomogeneous distribution of thallium within the samples, particularly rocks, for which the standard deviation often amounted to 30%, when small samples (0.05—0.2 g) were taken.

We are grateful to Mr. L. Kotz for his help in the a.a.s. measurements.

REFERENCES

1 C. A. R. De Albuquerque and D. M. Shaw, in K. H. Wedepohl (Ed.), Thallium, in Handbook of Geochemistry, Springer, Berlin, 1974.
2 H. Heinrichs, B. Schulz-Dobrick and K. H. Wedepohl, Geochim. Cosmochim. Acta, 43 (1979) 1303.
3 V. M. Goldschmidt, Geochemistry, Oxford University Press, London, 1954.
4 Deutsche Forschungsgemeinschaft, Maximale Arbeitsplatzkonzentrationen. Senatskommision zur Prüfing gesundheitsschädlicher Arbeitsstoffe, H. Boldt, Boppard, F.R.G., 1982.
5 W. Wirth and Ch. Gloxhuber, Toxikologie, 3. Aufl., Georg Thieme, Stuttgart, 1981, p. 128.
6 R. T. Holt and W. Wallace, Int. Metals Rev., 21 (1976) 1.
7 M. J. Brumsack, Environ. Geol., 2 (1977) 33.
8 G. Tölg, Pure Appl. Chem., 55 (1983) 1989.
9 M. Sager and G. Tölg, Mikrochim. Acta, (II) (1982) 231.
10 Z. Marczenko, H. Kalowska and M. Mojski, Talanta, 21 (1974) 93.
11 H. Berndt, J. Messerschmidt, F. Alt and D. Sommer, Fresenius Z. Anal. Chem., 306 (1981) 385.
12 R. C. Carpenter, Anal. Chim. Acta, 125 (1981) 209.
13 H. Berndt and W. Slavin, At. Absorpt. Newsl., 17 (1978) 109.
14 H. Berndt and J. Messerschmidt, Spectrochim. Acta, Part B, 36 (1981) 809.
15 M. Sager and G. Tölg, Analytiker Taschenbuch, Bd. 4, Springer, Berlin, in press.
16 W. Schmidt and V. Dietl, Fresenius Z. Anal. Chem., 315 (1983) 690.
17 L. Kotz, Max-Planck-Institut für Metallforschung, Institut für Werkstoffwissenschaften, Schwäbisch Gmünd, F.R.G., unpublished work.
18 M. A. Floyd, V. A. Fassel, R. K. Winge, J. M, Katzenberger and A. P. D. Silva, Anal. Chem., 52 (1980) 431.
19 R. K. Skogerboe, D. L. Dick, D. Pavlica and F. E. Lichte, Anal. Chem., 47 (1975) 568.
20 D. Kollotzek, P. Tschöpel and G. Tölg, Spectrochim. Acta, in press.
21 J. P. Hohimer and P. J. Hargis, Jr., Anal. Chim. Acta, 97 (1978) 43.
22 I. M. Cohen, S. M. Resnizky and G. B. Baró, J. Radioanal. Chem., 72 (1982) 451.
23 P. P. Parekh and H. L. Finston, J. Radioanal. Chem., 72 (1982) 365.
24 M. Murozumi, S. Nakamura and T. Igarashi, Nippon Kagaku Kaishi, 11 (1978) 1515.
25 K. G. Heumann, P. Kastenmayer and H. Zeininger, Fresenius Z. Anal. Chem., 306 (1981) 173.
26 J. E. Bonelli, H. E. Taylor and R. K. Skogerboe, Anal. Chim. Acta, 118 (1980) 243.

27 G. G. Welcher, O. H. Kriege and J. Y. Marks, Anal. Chem., 46 (1974) 1227.
28 C. W. Fuller, Anal. Chim. Acta, 81 (1976) 199.
29 K. Osamu, K. Takeshi and S. Emiko, Fresenius Z. Anal. Chem., 297 (1979) 398.
30 K. H. Sauer and S. Eckhard, Mikrochim. Acta, Suppl., 9 (1981) 87.
31 M. T. D. Dellefield, At. Spectrosc., 3 (1982) 165.
32 W. Geilmann, Fresenius Z. Anal. Chem., 160 (1958) 410.
33 G. Calderoni and T. Ferri, Talanta, 29 (1982) 371.
34 H. Heinrichs, Fresenius Z. Anal. Chem., 294 (1979) 345.
35 R. Keil, Fresenius Z. Anal. Chem., 309 (1981) 181.
36 C. M. Elson and C. A. R. Albuquerque, Anal. Chim. Acta, 134 (1982) 393.
37 J. Erzinger and H. Puchelt, Erzmetall, 35 (1982) 173.
38 W. H. Evans, P. J. Brooke and B. E. Lucas, Anal. Chim. Acta, 148 (1983) 203.
39 W. Geilmann and K. H. Neeb, Fresenius Z. Anal. Chem., 165 (1959) 251.
40 J. T. Kinard, Anal. Lett., 10 (1977) 1147.
41 H. Eschnauer and R. Neeb, Z. Lebensm.-Untersuch., 112 (1960) 275.
42 S. Gomišček, V. Hudnik and V. Veber, Developments in Toxicology and Environmental Science. Vol. 1. Clinical Chemistry and Chemical Toxicology of Metals, Elsevier, Amsterdam, 1977, p. 319.
43 M. Stoeppler, K. P. Müller and F. Backhaus, Fresenius Z. Anal. Chem., 297 (1979) 107.
44 L. Kotz, G. Henze, G. Kaiser, S. Pahlke, V. Veber and G. Tölg, Talanta, 26 (1979) 681.
45 J. F. Chapman and B. E. Leadbeatter, Anal. Lett., 13 (1980) 439.
46 G. Tölg, Pure Appl. Chem., 50 (1978) 1075.
47 G. Knapp, S. Raptis, G. Kaiser, G. Tölg, P. Schramel and B. Schreiber, Fresenius Z. Anal. Chem., 308 (1981) 97.
48 H. B. Han, G. Kaiser and G. Tölg, Anal. Chim. Acta, 134 (1982) 3.
49 J. M. Iskowitz, J. J. Lee, H. Zeitlin and Q. Fernando, Mar. Min., 3 (1982) 285.
50 Ch. Wachter and W. Weisweiler, Mikrochim. Acta, (I) (1982) 307.
51 Ch. R. Johnson, Anal. Chim. Acta, 81 (1976) 69.
52 W. Slavin, D. C. Manning and G. R. Carnrick, At. Spectrosc., 2 (1981) 137.
53 W. Slavin and D. C. Manning, Spectrochim. Acta, Part B, 35 (1980) 701.
54 E. Norval and W. H. Gries, Anal. Chim. Acta, 83 (1976) 393.
55 A. A. Baker, J. B. Headridge and R. A. Nicholson, Anal. Chim. Acta, 113 (1980) 47.
56 J. Y. Marks, G. G. Welcher and R. J. Spellmann, Appl. Spectrosc., 31 (1977) 9.
57 F. J. Langmyhr, J. R. Stubergh, Y. Thomassen, J. E. Hanssen and J. Dolezal, Anal. Chim. Acta, 71 (1974) 35.
58 S. Kempton, Sterrit R. M. and J. N. Lester, Talanta, 26 (1979) 929.
59 H. Heinrichs and H. Keltsch, Anal. Chem., 54 (1982) 1211.
60 N. T. Voskresenskaya, N. F. Pchelintseva and T. I. Tsekhonya, Zh. Anal. Khim., 36 (1981) 667.
61 K. Dittrich and P. Meistner, Anal. Chim. Acta, 121 (1980) 205.
62 K. Dittrich, Anal. Chim. Acta, 115 (1980) 189.
63 K. Dittrich and S. Schneider, Anal. Chim. Acta, 115 (1980) 201.
64 B. V. Lvov, L. A. Pelieva and A. I. Sharnopol'skii, Zh. Prikl. Spektrosk., 28 (1978) 19.
65 T. R. Dulski and R. R. Bixler, Anal. Chim. Acta, 91 (1977) 199.
66 S. Callio, At. Spectrosc., 1 (1980) 80.
67 R. Neeb, Inverse Polarographie und Voltammetrie, Verlag Chemie, Weinheim, 1969.
68 V. Gemmer-Colos, I. Kiehnast, J. Trenner and R. Neeb, Fresenius Z. Anal. Chem., 306 (1981) 149.
69 I. Šinko and S. Gomišček, Mikrochim. Acta, (I) (1972) 163.
70 A. J. Bard, Encyclopedia of Electrochemistry of the Elements, Vol. 14, M. Dekker, New York, NY, 1975.

71 J. Dieker and W. E. van der Linden, Fresenius Z. Anal. Chem., 274 (1975) 97.
72 J. P. Roux, O. Vittori and M. Porthault, Analusis, 8 (1975) 411.
73 Z. Lukaszewski, M. K. Pawlak and A. Ciszewski, Talanta, 27 (1980) 181.
74 D. P. Blinkley and R. E. Dessy, Anal. Chem., 52 (1980) 1335.
75 A. R. Curtis, J. Assoc. Off. Anal. Chem., 57 (1974) 1366.
76 G. E. Batley and T. M. Florence, J. Electroanal. Chem., 61 (1975) 205.
77 E. Jackwerth and J. Messerschmidt, Anal. Chim. Acta, 87 (1976) 341.
78 R. Pribil, Komplexometrie, VEB Verlag für Grundstoffindustrie, Leipzig, 1963.
79 G. Anderegg, Critical Survey of Stability Constants of EDTA complexes, IUPAC Chem. Data Ser. No. 14, Pergamon Press, Oxford, 1975.
80 R. Pribil, Analytical Applications of EDTA and Related Compounds, Pergamon Press, 1972.
81 R. G. Dhaneshwar and L. R. Zarapkar, Analyst, 105 (1980) 386.
82 L. Kotz, G. Kaiser, P. Tschöpel and G. Tölg, Fresenius Z. Anal. Chem., 260 (1972) 207.

Analytica Chimica Acta, 158 (1984) 199—206
Elsevier Science Publishers B.V., Amsterdam — Printed in The Netherlands

A COMPARATIVE STUDY OF THE DETERMINATION OF PHOSPHORUS BY ELECTROTHERMAL ATOMIC ABSORPTION SPECTROMETRY AND SOLUTION SPECTROPHOTOMETRY

SHAO-WEN LIN[a] and KAARE JULSHAMN*

Institute of Nutrition, Directorate of Fisheries, P.O. Box 4285, 5013 Bergen-Nygaardstangen (Norway)

(Received 22nd September 1983)

SUMMARY

Graphite-furnace atomic absorption spectrometry (a.a.s.) and a spectrophotometric AutoAnalyzer method for phosphorus based on molybdovanadophosphate formation are compared. Only slight improvements in accuracy and reproducibility were obtained when SiC- or ZrC-coated graphite tubes replaced uncoated tubes. Perchloric acid enhanced the phosphorus signal in a.a.s. The digestion system was found to be critical for the AutoAnalyzer method. Digestion with nitric/perchloric acids gave higher recoveries than a micro-Kjeldahl digestion for most of the biological samples studied. Better accuracy was obtained by the a.a.s. method, whereas the AutoAnalyzer method was more reproducible. The methods were applied to NBS Oyster Tissue and Spinach, and fish samples.

Phosphorus is of interest as a major element essential to all living organisms. Together with calcium, phosphorus constitutes most of the material in bones, and is also present in lipids and other compounds. The requirement for this element is assumed to be covered when intakes of calcium and protein are sufficient. Phosphorus depresses the retention of trace elements in animals [1, 2]. In fish nutrition studies, the serum phosphorus content of mature brown trout has been used as an indirect determination of serum phospholipids [3].

Many procedures are sufficiently sensitive for the determination of phosphorus in biological samples because the phosphorus content is high. There is a need, however, for such phosphorus determinations to have increased reproducibility, reliability and recovery. In the present study, a comparison has been made between graphite-furnace atomic absorption spectrometry (a.a.s.) and a spectrophotometric method based on yellow molybdovanadophosphate formation, which is frequently applied in the analysis of oils [4] and biological samples [5]. The sensitivity for phosphorus determinations by electrothermal a.a.s. is poor compared to that for most other elements because of the unresolved doublet chosen. Better sensitivity has been ob-

[a] Present address: Wuxi Institute of Light Industry, Wuxi, People's Republic of China.

0003-2670/84/$03.00 © 1984 Elsevier Science Publishers B.V.

tained by paying attention to the temperature [6], thermal stabilization by lanthanum [7] and impregnation of the graphite tubes [8].

EXPERIMENTAL

Apparatus

Atomic absorption measurements were made with a Perkin-Elmer model 5000 spectrometer, equipped with a HGA-76 graphite furnace, a phosphorus electrodeless-discharge lamp with a 213.6-nm resonance line and a deuterium background corrector. Sample solutions (20 μl) were introduced into the furnace by means of a Perkin-Elmer AS-1 automatic sample injection system. The signals were recorded on a Perkin-Elmer 56 chart recorder. Argon of 99.9% purity was used to sheath the graphite tubes. Conventional and coated graphite tubes were used, and cleaned by heating (see the coating procedures below). A Tecator AB digestion system 400 thermostatted heating block was used for the nitrogen digestion. For the colorimetric analysis and standard Technicon AutoAnalyzer equipment was used. The solution absorbance was read on a Gilford 300N spectrophotometer of 430 nm in a Model 3019 debubbler flow through cuvette.

Reagents

All acids were of Suprapur quality; hydrogen peroxide (30%) was of reagent-grade quality (all from Merck). Distilled deionized water was used throughout. A commercially available 1 mg ml^{-1} standard solution of phosphorus was applied. Lanthanum solutions were prepared from La_2O_3 (99.99%, Fluka). A 10% (w/v) solution of lanthanum was prepared by dissolving 29.32 g of the reagent in 50 ml of concentrated nitric acid and diluting to 250 ml with water. For the spectrophotometric method, 20 g of ammonium molybdate (Merck) was dissolved in 150 ml of water, heated and cooled; 1 g of ammonium vanadate (Merck) was dissolved in 150 ml of boiling water and cooled, and 24 ml of a 1:1 (v/v) nitric/perchloric acid mixture was added. The solution was again cooled. The molybdate solution was slowly added to the latter solution with constant stirring and made up to 1 l with water.

Digestion procedures

Procedure A. To 50—200 mg of freeze-dried samples or a blank were added 2 ml of a (1 + 1) conc. nitric/perchloric acid mixture in 20-ml capped Sovirel bottles. The bottles were capped, and the acids allowed to predigest the samples overnight. The bottles were sealed and heated in a household pressure boiler at 110°C for 2 h. The solutions were transferred to 10-ml volumetric flasks and made up to volume with water [9, 10]. Prior to phosphorus determination, appropriate dilutions were made with a 1% (v/v) solution of the (1 + 1) nitric/perchloric acid mixture as described above.

Procedure B. Freeze-dried samples (200 mg) were digested by the micro-

Kjeldahl technique [11]. The samples were weighed into 75-ml digestion tubes, 3 ml of concentrated sulphuric acid (Merck, p.a.) was added and the tubes were heated in a thermostated heating block. At 200°C, 1.5 g of potassium sulphate and 7.5 mg of selenium were added in the form of one tablet of Kjeltab Auto (Tecator). The temperature was further raised to 375°C for 1 h. After dilution to 75 ml with water, appropriate aliquots were taken for the measurement of phosphorus (working range 0.25—3 mg l^{-1}).

Coating procedures

Conventional Perkin-Elmer tubes were either soaked overnight in a coating solution of 1% (w/v) zirconyl chloride in ethanol or placed in pure silicon tetrachloride [12]. Prior to further treatment, the silicon tetrachloride-soaked tubes were hydrolyzed in distilled water. The soaked tubes were either placed in an ultrasonic bath for 20 min, whereby the pores were degassed and filled with the coating material, or they were kept in a vacuum desiccator under reduced pressure for 10 min, the pressure restored for 5 min, and this procedure repeated three times [8, 13]. The tubes were dried in an oven at 105°C for 2 h, and mounted in the graphite furnace. For the zirconium-treated tubes the temperature was increased gradually up to 1500°C (over 120 s), and thereafter held at 2650°C for 5 s. This procedure was repeated three times. The silicon-treated tubes were gradually heated to 500°C, held there for 10 s, held at 1500°C for 20 s and at 2650°C for 5 s. This cycle was repeated twice.

Procedures for final measurement

Graphite-furnace a.a.s. Appropriate aliquots of the digests together with 1% (v/v) nitric/perchloric acid mixture were added to each cup, giving a concentration in the sample solution of 1—2 μg ml^{-1}. Three cups of each digest were used in the AS-1 injection system. Two of the three cups were fortified with appropriate amounts of phosphorus for the standard addition procedure. The instrumental parameters are summarized in Table 1.

Spectrophotometry [5]. Standard Technicon AutoAnalyzer equipment was used with a 430-nm interference filter. A series of standard phosphorus

TABLE 1

Instrumental conditions for the determination of phosphorus in biological samples by graphite-furnace a.a.s.[a]

Instrument settings		*Temperature program*	
Wavelength	213.5/213.6 nm	Dry	120°C, 20 s hold.
Slit	0.7 nm	Char	120—600°C in 45 s,
Lamp power	9 W		600—1400°C immediately,
Read time	6.0 s		1400°C for 30 s.
Inert gas	Argon (99.9%), 240 ml min^{-1}	Atomize	1400—2650°C, ramp time 0 s; 5-s hold at
Background corrector	On		2650°C. Gas stop.

[a]Sample volume, 20 μl.

solutions was prepared from the stock solutions of (1 + 1) 2.6 M nitric/perchloric acid. The concentration range covered the values expected in the samples being assayed. A series used to provide calibration results was placed at the beginning and the end of the sample series. The phosphorus contents of the samples were calculated from the calibration graph established after linear regression evaluation.

RESULTS AND DISCUSSION

Temperature optimization

The instrumental parameters outlined in Table 1 were generally used. In initial tests, 20 μl of 5 mg l^{-1} phosphorus standard in 1% acid mixture and the same volume of a nitric/perchloric acid digest of NBS oyster tissue were introduced into silicon carbide-coated tubes in the furnace. The solution of the decomposed oyster tissue sample was diluted with 1% acid mixture to give a response similar to that of 5 mg P l^{-1}. Omitting the ramp charring gave inferior reproducibility. An atomization temperature of less than 2650°C lowered the response substantially (Fig. 1). An atomization time of less than 5 s gave a memory effect from previous measurements. Maximum power heating was not available for this graphite furnace. It is noteworthy that a 40% decrease in the response from sample digests and a 10% decrease in the response from simple solutions were obtained when ramp atomization was used, instead of the high-speed increase of temperature.

Figure 1 shows the responses obtained for digested oyster tissue and simple solutions when the charring temperature was increased from 400°C to 1600°C, with silicon carbide-coated tubes. The best precision was found at 1400°C, but not the greatest sensitivity.

Various types of graphite tubes were studied; they were untreated, silicon-treated and zirconium-treated, prepared by vacuum or ultrasonic treatment as described above. No significant difference between vacuum and ultrasonic treatment was observed with regard to sensitivity or reproducibility. In further work, ultrasonic treatment was used. The calibration graphs (Fig. 2) were linear up to about 10 mg l^{-1} for 20-μl samples. The sensitivity with the zirconium carbide-coated tube was 10—15% higher, and with the silicon carbide-coated tube 8—10% higher than that obtained with uncoated tubes. The lifetime of the tubes did not seem to be improved by coating the tubes. A decrease of 30% in the absorbance signal was obtained after about 70 injections of a 5 mg P l^{-1} standard in 20% (v/v) nitric/perchloric acid mixture, whereas about 400 injections were possible with the 0.1% acid mixture. Small variations in sensitivity between different conventional tubes were not observed in the present study.

Matrix effects

The suppressive effect of perchloric acid on the absorbance of trace elements in electrothermal a.a.s. is well established [14, 15]. The mechanism

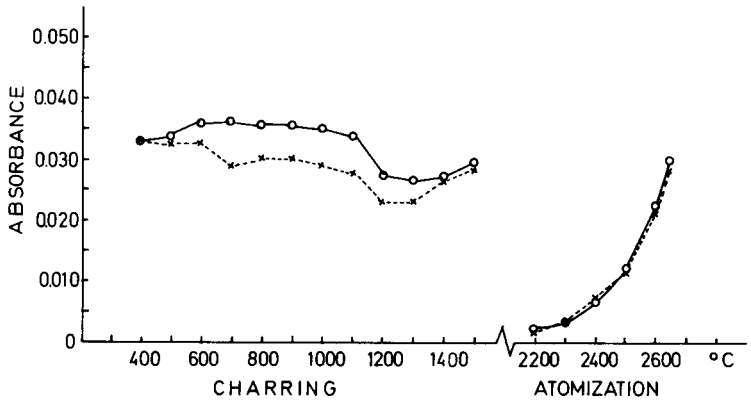

Fig. 1. Effect of charring and atomization temperatures on the phosphorus peak height responses for: (○) digested oyster sample; (×) 5 mg P l^{-1} solution (conditions as in Table 1, silicon carbide-coated tube).

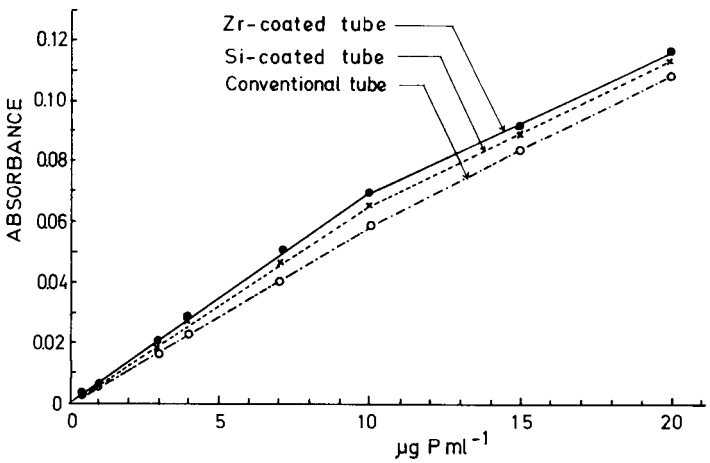

Fig. 2. Calibration graphs for phosphorus obtained by using different graphite tubes (conditions as in Table 1).

of its effect on the determination of aluminium and other elements has been studied by Koirtyohann et al. [16] and Slavin et al. [17]. Table 2 shows that the signal for phosphorus increased and reached a maximum at 1% (v/v) perchloric acid. The most efficient atomization of phosphorus was obtained from a matrix initially of lanthanum nitrate. The sensitivity was three times greater than that obtained with 1% nitric acid, and double that with 1% perchloric acid. Zirconium carbide-coated tubes gave only minor differences in response compared to the uncoated tubes. However, the coated tubes gave a more stable and substantially lower blank response.

TABLE 2

Effect of matrix on phosphorus absorbance (20 μl of a solution containing 10 μg P ml^{-1}; conditions as in Table 1; values are absorbance × 10^{-3})

Matrix	Tube	Concentration (%, v/v)						
		0.01	0.05	0.1	0.5	1.0	5.0	10
HCl	Uncoated ZrC	17	19	19	20	19	20	20
		18	18	20	21	21	20	20
H_2SO_4	Uncoated ZrC	14	18	18	18	20	16	15
		15	16	14	15	16	13	12
HNO_3	Uncoated ZrC	18	18	19	20	22	20	18
		17	18	18	19	21	20	18
HNO_3:H_2O (1 + 1)	Uncoated ZrC	17	17	18	19	18	18	17
		19	20	19	19	20	19	17
$HClO_4$	Uncoated ZrC	20	20	21	27	30	26	22
		21	21	24	28	32	28	26
$HClO_4$:HNO_3 (1 + 1)	Uncoated ZrC	18	20	21	26	28	26	21
		20	22	23	28	31	29	26
$La(NO_3)_3$[a]	Uncoated ZrC	22	23	23	35	44	61	52

[a](w/v).

Recovery, reproducibility and accuracy

Recoveries were based on standard addition experiments in which the calibration graphs were obtained for samples spiked before and after digestion with nitric/perchloric acid. The completely overlapping graphs indicated a recovery of 100%. Such recovery tests were carried out for the a.a.s. procedure with the three types of tubes studied. Six sets of experiments were done for each tube. The results showed recoveries of 99 ± 6% for the uncoated tubes, 96 ± 4% for silicon carbide-coated tubes and 102 ± 3% for zirconium carbide-coated tubes.

The reproducibility of the a.a.s. system for the different tubes was studied by measuring the same digest of NBS Spinach (SRM 1570) ten times, which gave relative standard deviations of 8.1, 3.6 and 5.2% for uncoated, silicon carbide-coated and zirconium carbide-coated tubes, respectively. The overall reproducibilities of Procedure A are given in Table 3. The relative standard deviation of the procedure with uncoated tubes was about 10%, whereas better reproducibility (about 5%) was found for the carbide-coated tubes.

To evaluate the accuracy of the method, solutions of NBS reference materials (obtained by Procedure A and a standard addition procedure) were analyzed in the different tubes. The results given in Table 3 show only minor effects of the surface treatment of the graphite tubes. All tubes gave very good accuracies. The results obtained for phosphorus in the oyster tissue tended towards higher values with the uncoated tubes than with those having a coated surface. The values of phosphorus obtained with coated tubes are in consistent agreement with recently reported values [18]. More accurate

TABLE 3

Phosphorus (g kg^{-1}, dry weight) determined in NBS samples by digestion procedure A, with standard addition at levels of 2 and 4 mg l^{-1} and a.a.s. with different tubes (Values in parentheses were obtained by using a calibration graph)

Sample	Phosphorus found (g kg^{-1})[a]			NBS values
	Uncoated	SiC-coated	ZrC-coated	
Spinach (SRM 1570)[b]	5.5 ± 0.5 (5.9 ± 0.3)	5.6 ± 0.3 (6.3 ± 0.3)	5.5 ± 0.3 —	5.5 ± 0.2[c]
Oyster tissue (SRM 1566)[b]	8.1 ± 0.9 (8.3 ± 0.5)	7.7 ± 0.4 (8.1 ± 0.4)	7.8 ± 0.5 —	8.1[d]

[a]Mean ± standard deviation of single result (n = 10 for standard addition, n = 4 for calibration graph). [b]Dried as specified by NBS. [c]Certified value with 95% confidence limit. [d]Uncertified value.

determinations are likely to be obtained by a standard addition procedure compared to that of a calibration graph; this is also shown in Table 3. No significant differences were found between uncoated and coated tubes.

Spectrophotometric method

The data recorded in Table 4 relate to the Kjeldahl digestion (Procedure B) and the nitric/perchloric acid digestion (Procedure A). Evidently a significant proportion of the total phosphorus was often unavailable for spectrophotometric measurement when Procedure B was used. The recovery could be improved by about 8% by boiling the diluted Kjeldahl digests prior to the measurements, but the results were still significantly low. The accuracy of the phosphorus determination in the NBS samples obtained by Procedure A and a spectrophotometric finish showed that the results for Spinach were within the certified values, whereas the value for Oyster Tissue was lower

TABLE 4

Comparative results for phosphorus (g kg^{-1} dry weight) by using a $HNO_3/HClO_4$ digestion procedure (A) and a Kjeldahl digestion procedure (B), with a spectrophotometric finish

Sample	Phosphorus found (g kg^{-1})	
	Procedure B[a]	Procedure A[a]
Spinach (SRM 1570)[b]	4.53 ± 0.12	5.60 ± 0.10
Oyster tissue (SRM 1566)[b]	6.42 ± 0.15	6.53 ± 0.12
Fish product no. 1	5.83 ± 0.13	6.16 ± 0.11
Fish product no. 2	3.20 ± 0.08	4.87 ± 0.08
Fish product no. 3	3.18 ± 0.08	4.99 ± 0.08
Fish product no. 4	3.98 ± 0.07	6.36 ± 0.10
Fish product no. 5	4.56 ± 0.10	6.88 ± 0.14

[a]Mean standard deviation of single result (n = 4). [b]For certified values, see Table 3.

than that given by NBS, or that obtained by a.a.s. (Table 3). There was good correlation between results obtained on fish products with the spectrophotometric and a.a.s. methods ($Y = -0.45 + 1.08$, $r = 0.982$). The spectrophotometric method gave better reproducibility, but the total phosphorus contents of all samples were more accurately determined by electrothermal a.a.s.

We thank the Norwegian Agency for International Development (NORAD) for the award of a Research Fellowship to Mr. Shao-Wen Lin, and Dr. L. R. Njaa for his help with the spectrophotometric analyses.

REFERENCES

1 C. A. Cabell and I. P. Earle, Am. J. Sci., 24 (1965) 800.
2 E. T. Monsen and J. D. Cook, Am. J. Clin. Nutr., 29 (1976) 1142.
3 T. H. McCartney, Fish. Res. Bull. N.Y., 30 (1967) 1.
4 A. Prévot and M. Gente-Jauniaux, At. Absorpt. Newsl., 17 (1978) 1.
5 J. V. O'Neill and R. A. Webb, J. Sci. Food Agric., 21 (1970) 217.
6 J.-Å Persson and W. Frech, Anal. Chim. Acta, 119 (1980) 75.
7 R. D. Ediger, At. Absorpt. Newsl., 15 (1976) 145.
8 I. Havezov, E. Russeva and N. Jordanov, Fresenius Z. Anal. Chem., 296 (1979) 125.
9 K. Julshamn and O. R. Brækkan, At. Absorpt. Newsl., 13 (1975) 49.
10 K. Julshamn, Fiskeri dir. Skr., Ser. Ernæring, 1 (1981) 161.
11 L. R. Njaa, Fiskeri dir. Skr., Ser. Teknol. Unders., 4 (1963) 5.
12 A. Driedger and W. R. Seitz, Anal. Chem., 51 (1979) 1197.
13 T. M. Vickrey, G. V. Harrison and G. J. Ramelow, At. Spectrosc., 1 (1980) 116.
14 K. Julshamn, At. Absorption Newsl., 16 (1977) 149.
15 A. Pilate, P. Geladi and F. Adams, Talanta, 24 (1977) 512.
16 S. R. Koirtyohann, E. D. Glass and F. E. Lichte, Appl. Spectrosc., 35 (1981) 22.
17 W. Slavin, G. R. Carnick and D. C. Manning, Anal. Chim. Acta, 138 (1982) 103.
18 F. J. Langmyhr and I. M. Dahl, Anal. Chim. Acta, 131 (1981) 303.

Analytica Chimica Acta, 158 (1984) 207—215
Elsevier Science Publishers B.V., Amsterdam — Printed in The Netherlands

DIFFERENTIAL PRECONCENTRATION OF ARSENIC(III) AND ARSENIC(V) WITH THIONALIDE LOADED ON SILICA GEL

KIKUO TERADA*, KEN MATSUMOTO and TOHRU INABA

Department of Chemistry, Faculty of Science, Kanazawa University, Kanazawa, Ishikawa 920 (Japan)

(Received 11th July 1983)

SUMMARY

2-Mercapto-*N*-2-naphthylacetamide (thionalide) on silica gel is used for differential preconcentration of $\mu g\ l^{-1}$ levels of arsenic(III) and arsenic(V) from aqueous solution. In batch experiments, arsenic(III) was quantitatively retained on the gel from solutions of pH 6.5—8.5, but arsenic(V) and organic arsenic compounds were not retained. The chelating capacity of the gel was 5.6 $\mu mol\ g^{-1}$ As(III) at pH 7.0. Arsenic retained on the column was completely eluted with 25 ml of 0.01 M sodium borate in 0.01 M sodium hydroxide containing 10 mg l^{-1} iodine (pH 10). The arsenic was determined by silver diethyldithiocarbamate spectrophotometry. Arsenic(V) was subsequently determined after reduction to arsenic(III) with sulphite and iodide. Arsenic(III) and arsenic(V) in sea water are shown to be < 0.12 and 1.6 $\mu g\ l^{-1}$, respectively.

Determination of traces of arsenic in natural waters has become of interest with reference to environmental pollution which might have arisen from wide usage of the element in agriculture and industry. During the past ten years, numerous papers have been published on the determination of arsenic species at the trace level. Among the methods, atomic absorption spectrometry involving the conversion of arsenic species to arsine by reduction, and introduction into an argon-hydrogen flame, has become of interest because the hydride-generation separation technique affords several useful methods for determining different arsenic species [1]. For example, at pH 4.5, arsenic(III) but not arsenic(V) is converted to arsine. Liquid-liquid extraction with ammonium pyrrolidinedithiocarbamate (APDC) also separates arsenic(III) from arsenic(V) [2].

Although these methods are useful for speciation of arsenic, simple, rapid and selective preconcentration procedures for the various arsenic species are still required. Portman and Riley [3] have used 2-mercapto-*N*-2-naphthylacetamide (thionalide) as a coprecipitation agent for collection of arsenic from sea water. Thionalide forms water-insoluble precipitates with most of the divalent metals from dilute mineral acid solutions [4—7]. Furthermore, thionalide can form a complex with arsenic(III), but not with arsenic(V). Nakatani [8] has reported the separation of arsenic(III) from arsenic(V) by extraction of its thionalide complex into ether. Recently, Terada et al. [9]

have reported a preconcentration procedure for palladium in natural waters involving thionalide loaded on silica gel. This paper describes the use of this reagent, impregnated on silica gel, for the differential preconcentration of arsenic(III) and arsenic(V) from natural water samples.

EXPERIMENTAL

Reagents

Thionalide and acetone were analytical-reagent grade. Standard solutions of arsenic(III) and arsenic(V) were prepared as follows. Analytical-reagent grade arsenic(III) oxide was dried at 110°C for 4 h; 0.32999 g was dissolved in 50 ml of 5% sodium hydroxide and the solution was neutralized with hydrochloric acid and diluted with deionized water to 250 ml. The standard solution of arsenic(V) was prepared by heating the neutral arsenic(III) solution, prior to dilution, with a small amount of 1% potassium permanganate solution. Dimethylarsonic acid and phenylarsonic acid were dissolved in 1 M hydrochloric acid to make 1000 mg l^{-1} solutions of each.

The absorption solution for arsine was freshly prepared by dissolving 0.2 g of cinchonine and 0.5 g of silver diethyldithiocarbamate in chloroform with continuous magnetic stirring, and dilution to 200 ml with chloroform. A 5-g portion of sodium tetrahydroborate was dissolved in 100 ml of 0.2% (w/v) sodium hydroxide solution. For buffering, the aqueous solution was adjusted with 0.2 M potassium chloride and 0.2 M hydrochloric acid for pH 1—2, 0.2 M potassium hydrogenphthalate and 0.2 M hydrochloric acid for pH 3, 0.2 M sodium acetate and 0.2 M acetic acid for pH 4, 0.2 M potassium hydrogenphthalate and 0.2 M sodium hydroxide for pH 5, 0.2 M potassium dihydrogenphosphate and 0.2 M sodium hydroxide for pH 6—8 and 0.2 M boric acid with potassium chloride and 0.2 M sodium hydroxide for pH 9.

Silica gel (chromatographic grade, Wakogel C-100) was sieved through a stainless steel sieve (60—80 mesh), soaked with twice its volume of (1 + 1) hydrochloric acid for 1 day at 90°C, and washed with deionized water until free from chloride. The gel was soaked with twice its volume of (1 + 2) nitric acid for 1 day at 90°C, washed with deionized water, dried at 120°C for 3 days and stored in a polyethylene bottle.

Preparation of thionalide-silica gel. About 120 g of silica gel (60—80 mesh) was stirred with 200 ml of redistilled acetone containing 6 g of thionalide. After 16 h the impregnated silica gel was dried at room temperature under reduced pressure for 22 h to expel acetone. The dry material was washed repeatedly with deionized water until the washings were clear. Finally, the product was dried at room temperature under reduced pressure for 24 h and stored in a darkened teflon bottle in a refrigerator.

Apparatus

The equipment for arsine generation is shown in Fig. 1.

A Hitachi-Horiba pH meter (M-5) was used to check the pH of the aqueous

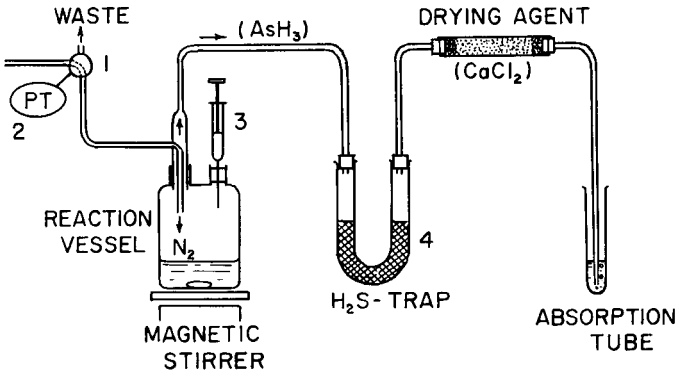

Fig. 1. Apparatus for arsine generation. (1) Solenoid valve to control nitrogen supply; (2) program timer (PT); (3) injector for $NaBH_4$; (4) lead acetate-impregnated gauze.

solutions. An Iwaki VS electric shaker operating at 340 strokes min^{-1} was used for the batch experiments and a Toyo SF-160K fraction collector was used for the column experiments. Other equipment included a Hitachi 239 digital spectrophotometer and Hitachi 170-50 atomic absorption spectrometer fitted with a GA-2 atomizer. Arsine generation was done in a Hitachi arsenic analyzer unit (508-0045). The columns were glass tubes (10 mm i.d., 140 mm long) with a coarse sintered-glass disc and stopcock at the bottom.

Procedures

Batch experiments. To a 50-ml glass centrifuge tube were added 5 ml of 10 mg l^{-1} arsenic solution, 15 ml of buffer solution and 0.5 g of thionalide-silica gel, and the contents were shaken for 30 min at room temperature. After the gel had settled, the supernatant liquid was filtered through dry Toyo No. 5C filter paper. Arsenic was determined in aliquots of the filtrate by a modified silver diethyldithiocarbamate spectrophotometric method after hydride generation. A 10-ml aliquot of the filtrate was transferred to the reaction vessel (100-ml capacity) of the arsenic analyzer unit, 0.3 ml of (1 + 1) hydrochloric acid and 3 ml of 5% (w/v) sodium tetrahydroborate solution were put into the vessel, and nitrogen was passed through the solution to expel the generated arsine into the absorption tube, via a hydrogen sulphide trap containing lead acetate-impregnated cotton (Fig. 1). The arsine was absorbed in a cinchonine-silver diethyldithiocarbamate solution in chloroform (instead of the conventional pyridine solution of silver diethyldithiocarbamate); 10 min was required for complete transfer of arsine to the absorption solution. The calibration graph obeyed Beer's law for 0—3 mg l^{-1} arsenic. The pH of each solution was also measured.

Column method. A glass column was filled with 1 g of thionalide-silica gel to a height of 1.5 cm, and a small disc of Toyo No. 5C filter paper was placed on top so that the gel was not disturbed during sample passage. A

20-ml portion of a 1 mg l^{-1} arsenic(III) or arsenic(V) solution was adjusted to a suitable pH (ca. 7.0), and percolated through the column at 2.5 ml min^{-1}. The effluent was collected in a 25-ml volumetric flask, diluted to the mark and retained for arsenic determination. The column was washed with 20 ml of distilled water and arsenic was eluted with 25 ml of the eluting solution (0.01 M sodium borate in 0.01 M sodium hydroxide solution containing 10 mg l^{-1} iodine and adjusted to pH 10) at 0.5 ml min^{-1}. The whole of the effluent was used for arsenic determination as described above.

Reduction of arsenic(V) with iodide and ascorbic acid. To a 50-ml Erlenmeyer flask were added 2 ml of 10 mg l^{-1} arsenic(V) solution and ca. 10 ml of the reducing solution (40 g of potassium iodide and 25 g of ascorbic acid in 250 ml of water), and the mixture was made 0.6 M in hydrochloric acid and allowed to stand for 30 min. The pH was adjusted to 8 with 9 M ammonia solution, using phenolphthalein as indicator, and made up to 25 ml. A 20-ml aliquot of the solution was shaken with 0.5 g of thionalide-silica gel for 30 min, and the recovery of arsenic was calculated.

Reduction of arsenic(V) with sulphite-iodide. To 25 ml of the solution containing arsenic(V), >8 ml of 5% sodium sulphite solution and >1 ml of 0.1% potassium iodide solution were added. After standing for 30 min, >1 ml of 1% sodium thiosulphate solution was added and the pH was adjusted to 8. If an appreciable turbidity appeared on addition of thiosulphate, 2 ml of formic acid was added to mask free sulphur which interfered positively with the subsequent spectrophotometric determination of arsenic.

Separation of arsenic(III) and arsenic(V). A sample solution containing arsenic(III) and arsenic(V) (ca. 20 μg of total arsenic) was adjusted to pH 7.0 and passed through a column containing 1.5 g of thionalide-silica gel at 2.5 ml min^{-1}. The effluent was collected in a 100-ml Erlenmeyer flask. The column was washed with deionized water (ca. 10 ml) and the washings were collected in the flask. Arsenic(III) retained on the column was eluted with 25 ml of 0.01 M sodium borate in 0.01 M sodium hydroxide containing 10 mg l^{-1} iodine and adjusted to pH 10, at 0.5 ml min^{-1}. The effluent was collected in the reaction vessel of the arsenic analyzer unit, and the pH was adjusted to 1 by adding 0.6 ml of (1 + 1) hydrochloric acid. The vessel was connected to the unit, and 3 ml of 5% (w/v) sodium tetrahydroborate solution was added; 5 ml of absorption solution was added to the absorber. Nitrogen was passed for 10 min, after which the absorption solution was diluted to exactly 5 ml by adding a small amount of chloroform. The absorbance was measured at 510 nm in a 1-cm cell with the absorption solution as reference. The first effluent containing arsenic(V) was subjected to the sulphite reducing procedure. It was passed through another thionalide-silica gel column at 2.5 ml min^{-1}, and the elution and determination of arsenic were done as described above.

RESULTS AND DISCUSSION

The amount of thionalide loaded on silica gel was the same as described previously [9]. The complexing capacity of the thionalide-silica gel for arsenic(III) was measured by the batch method using 25 ml of a 10 mg l^{-1} solution. At pH 7, the capacity of the gel was found to be 5.6 μmol g^{-1} (420 μg g^{-1}). This indicates that each arsenic(III) ion reacts with 4.7 molecules of thionalide. Therefore, some thionalide in the gel does not react with arsenic(III). This is probably due to the porous structure of the silica gel surface. Perhaps, when thionalide at the mouth of the pore is bonded to arsenic, further reaction with inner-pore sites is precluded [10, 11]. The dry material gradually changed colour to pale yellow and its capacity was halved after three months exposure to air. Therefore, it is desirable to store the material under nitrogen in the refrigerator (4°C).

Effect of pH and shaking time on retention of arsenic

The recoveries of arsenic(III) and arsenic(V) from an aqueous solution at various pH values were examined by the batch method. The results are shown in Fig. 2. Arsenic(III) was quantitatively retained at pH 6.5—8.5. Arsenic(V) was not retained at any pH. These results indicate that there is a possibility of separating arsenic(III) from arsenic(V) by a single passage of the sample solution through the thionalide-silica gel column.

The removal of arsenic(III) by the gel from aqueous solution at pH 7 was examined after various shaking times. The results showed that the arsenic was completely removed within 30 s, and was constant for at least 20-min shaking.

Retention of arsenic on the column

The operating capacity of the complexing material was expected to be related to the concentration of arsenic and the flow rate of the water sample. First, a sample solution containing 1 mg l^{-1} arsenic(III) at pH 7.0 was passed through the column at various flow rates. As shown in Fig. 3, arsenic(III) was quantitatively retained on the column at flow rates $\leqslant$3.0 ml min^{-1}.

Arsenic(V) was not retained on the complexing material at any pH. There-

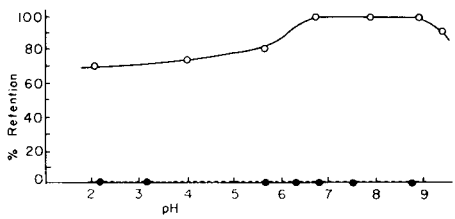

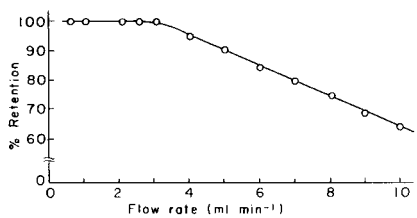

Fig. 2. Effect of pH on retention of: (○) arsenic(III); (●) arsenic(V).

Fig. 3. Relationship between flow rate and retention of arsenic(III) (1 mg l^{-1}) on a thionalide-silica gel column (1 g).

fore, the reduction of this species to arsenic(III), and its subsequent concentration by the thionalide-silica gel, were examined. Because the equilibrium between arsenic(III) and arsenic(V) can be represented as follows [12]

$$AsO_4^{3-} + 2H^+ + 2e^- \rightleftharpoons AsO_3^{3-} + H_2O \quad (E_0 = 0.56\ V)$$

the reduction of arsenic(V) proceeds in acidic solution. As reductants, ascorbic acid [3], ascorbic acid and potassium iodide [13] and ascorbic acid, potassium iodide and sodium thiosulphate [2] were examined.

Ascorbic acid alone gave only 25—30% recovery of arsenic. Ascorbic acid and potassium iodide gave 35.3% recovery (mean of 3 measurements). Iodine oxidizes arsenic(III) to arsenic(V) at pH >6 [12]. Thus, after adjustment of pH 8, reoxidation of much of the arsenic will be expected. It appears that the presence of ascorbic acid does not prevent reoxidation.

Kamada [2] has used sodium thiosulphate for removal of iodine. In the present study, after reduction of arsenic(V) with the iodide and ascorbic acid, various amounts of thiosulphate were added to the solution prior to the adjustment of pH in order to remove iodine. However, the recoveries varied widely, from 45 to 72%; it was assumed that ascorbic acid interfered with retention of arsenic(III) on the thionalide-silica gel. Thus, the retention experiments were conducted after adding the iodide-ascorbic acid mixture to arsenic(III) solutions. Again, although no iodine was present, the average recovery (triplicate determinations) was only 35.7%.

Other reducing mixture systems, therefore, were examined. A mixture of sodium sulphite and potassium iodide was found to be best. As shown in Table 1, this reducing mixture provided almost complete retention of arsenic. It was also confirmed that formic acid did not interfere with arsine generation.

Differential preconcentration of arsenic(III) and arsenic(V)

Based on the results described above, a procedure for differential preconcentration of arsenic(III) and arsenic(V) with the thionalide-silica gel column

TABLE 1

Preconcentration of arsenic(V) after reduction[a]

As(V) ($\mu g\ l^{-1}$)	Sample volume (ml)	Recovery (%)
50	200	94
40	250	94
20	500	94
10	2000	93

[a] 15 ml of 5% sodium sulphite and 2 ml of 0.1% potassium iodide were added; later 2 ml of 1% sodium thiosulphate was added. 2.5 g of thionalide-silica gel was used. Flow rate 2.5 ml min^{-1}.

was established. The results are shown in Table 2. When 1-l samples of arsenic concentrations lower than those in the table were passed through the column, a flow rate lower than 2.5 ml min^{-1} was required to obtain >95% retention. The same or larger amounts of sample may be treated more rapidly if a wider column is used with a larger amount of the complexing material.

Elution of arsenic

Several reagents, such as hydrochloric acid, thiourea and bismuthiol-II with hydrochloric acid, were investigated for the elution of arsenic. However, none of these reagents was effective. According to Charlot [12], in solutions above pH 8 arsenic(III) can readily be oxidized with iodine. Therefore, it was expected that when a solution of high pH containing iodine was poured into the column retaining arsenic(III), this species would be converted to arsenic(V) and liberated from the column. Among the solutions tested, 0.01 M sodium borate in 0.01 M sodium hydroxide solution or 0.01 M sodium hydrogencarbonate solution each containing 10 mg l^{-1} iodine and adjusted to pH 10 with ammonia water was found to be most suitable for the elution of arsenic. As shown in Fig. 4, 20 μg of arsenic could be completely eluted with 25 ml of the former eluting solution. A more concentrated eluant was less effective. It was also found that this solution did not interfere with the subsequent arsine generation for the determination of the element. Sodium hydrogencarbonate solution containing iodine was similarly effective, but this solution generated small bubbles in the column. Similar alkaline solution containing no iodine gave <2% arsenic elution.

Retention behaviour of organic arsenic species

Dimethylarsonic acid (DMA) and phenylarsonic acid (PAA) were investigated. Because of the difficulty of generating arsine from these compounds, arsenic was determined by atomic absorption spectrometry with a graphite-furnace atomizer. However, owing to the low boiling points of these compounds, a considerable amount of arsenic was lost during the ashing step.

TABLE 2

Separation and measurement of arsenic(III) and arsenic(V)

As(III) (μg l^{-1})	As(V) (μg l^{-1})	Sample volume (ml)	Concn. factor[a]	Recovery(%)[b]	
				As(III)	As(V)
20	20	500	20	95	95
12	28	500	20	95	95
10	10	1000	40	94	95
8	12	1000	40	94	95
4	16	1000	40	92	94

[a] 25-ml elution volume. [b] 3 g of thionalide-silica gel, flow rate 2.5 ml min^{-1}.

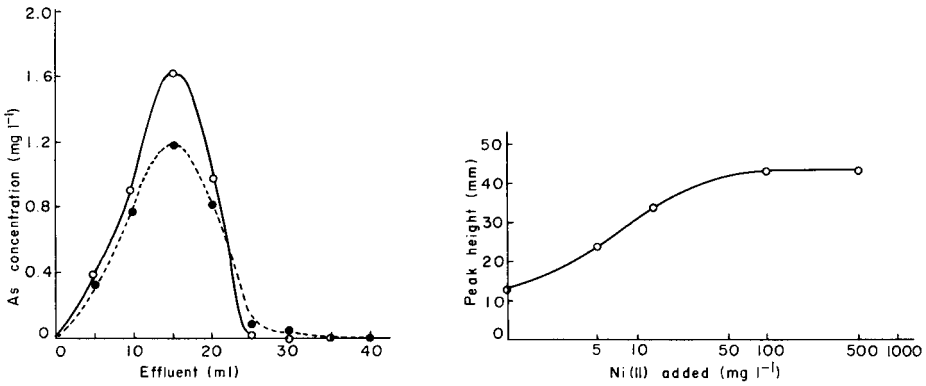

Fig. 4. Elution of arsenic(III) retained on thionalide-silica gel with: (○) 0.01 M sodium borate in 0.01 M sodium hydroxide containing 10 mg l^{-1} iodine, pH 10.0; (●) 0.1 M sodium borate in 0.1 M sodium hydroxide containing 10 mg l^{-1} iodine.

Fig. 5. Effect of concentration of nickel added to the sample on peak height for graphite-furnace atomic absorption spectrometry of DMA.

Therefore, magnesium or nickel ions were added to the sample to form more refractory arsenic compounds. Figure 5 shows the effect of the amount of nickel added to the sample on the peak height obtained for DMA. In the case of PAA a similar result was obtained. The presence of 100 mg l^{-1} nickel ion was sufficient for the determination of organic arsenic compounds. There was no retention of DMA or PAA by the complexing material. Consequently, it is concluded that thionalide-silica gel can serve as a selective collector for arsenic(III).

Effect of various substances on the retention of arsenic

Various metal ions that might react with thionalide [Ag(I), Cd(II), Cu(II), Hg(II), Pd(II), Pt(IV), Rh(III), Sb(III), Bi(III), Tl(I), and Au(III)] were examined for their effect on the retention of arsenic from 500 ml of an aqueous solution and from sea water, which were adjusted to pH 7.0. When these ions were present together in a sample (each at 10 μg l^{-1}), the recovery of 20 μg l^{-1} arsenic(III) was >94% at a flow rate of 2.5 ml min^{-1}. In general, 1 l of sea water contains about 0.3 μmol of heavy metals, which requires only 0.04 g of thionalide-silica gel, and the interference of heavy metal ions will be negligible in practice. With regard to organic materials, their effects also may be neglected, because approximately quantitative recovery of the added arsenic was achieved from sea water collected at Tsukumo Bay, Noto Peninsula, which is more polluted by human activities than open sea water.

Analysis of sea water for arsenic

The present method was applied to a sea-water sample which was collected from 10 m depth about 500 m offshore in Tsukumo Bay, Noto

Peninsula. The water was acidified by adding 2 ml of (1 + 1) sub-boiled hydrochloric acid to every 1 l of sample, filtered through clean absorbent cotton, and passed through the column for preconcentration by a factor of 80. The result obtained was 1.6 $\mu g\ l^{-1}$ for arsenic(V), while no arsenic(III) could be detected. Because the detection limit for spectrophotometry with silver diethyldithiocarbamate is 0.01 mg l^{-1}, the arsenic(III) content in the sample may be estimated as $<0.12\ \mu g\ l^{-1}$.

This work was partly supported by a Grant-in-Aid for Scientific Research from the Ministry of Education, Japan (No. 57340032).

REFERENCES

1 J. Aggett and A. G. Aspell, Analyst (London), 101 (1976) 341.
2 T. Kamada, Talanta, 23 (1976) 835.
3 J. E. Portman and J. P. Riley, Anal. Chim. Acta, 31 (1964) 509.
4 R. Berg and W. Roebling, Z. Angew. Chem., 48 (1935) 430.
5 R. Berg and E. S. Fahrenkamp, Fresenius Z. Anal. Chem., 109 (1937) 305; 112 (1938) 162.
6 H. Kienitz and L. Rombock, Fresenius Z. Anal. Chem., 117 (1939) 241.
7 W. D. Rogers, F. E. Beamish and D. S. Russell, Ind. Eng. Chem., Anal. Ed., 12 (1940) 561.
8 S. Nakatani, Bunseki Kagaku, 12 (1963) 241.
9 K. Terada, K. Matsumoto and Y. Taniguchi, Anal. Chim. Acta, 147 (1983) 411.
10 C. Fulcher, M. A. Crowell, R. Bayliss, K. B. Holland and J. R. Jezorek, Anal. Chim. Acta, 129 (1981) 29.
11 H. Jenett, J. Knecht and G. Stock, Fresenius Z. Anal. Chem., 304 (1980) 362.
12 G. Charlot, Les Reactions Chimiques En Solution, L'Analyse Qualitative Minérale, Transl. K. Sone and M. Tanaka, Japanese edn., Vol. 2, Kyoritsu Shuppan, Tokyo, 1974, p. 413.
13 T. A. Hinners, Analyst (London), 105 (1980) 751.

Analytica Chimica Acta, 158 (1984) 217—233
Elsevier Science Publishers B.V., Amsterdam — Printed in The Netherlands

COMPUTER-AIDED ELUCIDATION OF STRUCTURES BY CARBON-13 NUCLEAR MAGNETIC RESONANCE
The DARC-EPIOS Method: Characterization of Ordered Substructures by Correlating the Chemical Shifts of Their Bonded Carbon Atoms

JACQUES-EMILE DUBOIS*, MICHEL CARABEDIAN and ISHAY DAGANE

Institut de Topologie et de Dynamique des Systèmes de l'Université Paris VII, associé au C.N.R.S., 1, rue Guy de la Brosse, 75005 Paris (France)

(Received 28th February 1983)

SUMMARY

A reference substructure (SS) for which all spectral information (I) associated with each carbon atom is expressed as a function of the molecular environment is proposed. This information is expressed by topological relations, within this substructure, for which the spectral responses of its "bonded atoms" are linearly related to external alkyl effects. A correlation space (SS/I) is built with these topological relations (1—4 per carbon substructure). The resolving capacity of this SS/I space is greatly enhanced by introducing, in addition to all the reference substructures, some functions such as heteroatoms, cyclic structures, and stereochemical situations. The action of these functions is estimated by a statistical study of a large population of compounds from the DARC-PLURIDATA ^{13}C-n.m.r. bank. This work introduces the notion of multiatom-centered substructure/multichemical shift relations, the discriminating ability of which compares very favorably to that of the notion of atom-centered substructure/monochemical shift relations. The generic reference substructure defined as $ELCO_b$ with its multichemical shifts constitutes a simple structural whole which is useful for critical improvement of the experimental reference data (distribution of spectral information and medium effects) and has proved to be excellent for the elucidation of new structures.

The computer-aided elucidation of unknown chemical compounds on the basis of their spectroscopic properties is currently a major topic of interest. The ^{13}C-n.m.r. technique offers a large potential for application in this field, because it provides accurate data about the local environment of each carbon atom of a molecule.

However, the absence of a 1:1 relation between a given chemical shift and a particular substructural environment is a basic difficulty in elucidation [1]. While the complete spectrum of a compound corresponds to a fingerprint of the arrangement of its atoms, each chemical shift, when taken alone, can usually be matched with various substructures [2]. In ^{13}C-n.m.r., the inherent difficulties of structural interpretation, i.e., of matching substructures with the chemical shifts in a spectrum, are largely due to the use of insufficiently discriminating substructure/subspectrum relations. In various

computer-aided elucidation systems [2—8], the user generally resorts to interactive procedures to help restrain the combinatorial task involved in solving a substructure problem. The user's knowledge and intuition account for a good part of the heuristic support of such systems and often compensate for the shortcomings of the still-limited theories on structure/$\delta^{13}C$ relations in n.m.r.

Early models of these structure/chemical shift relations are more geared for the prediction or assignment of chemical shifts rather than for structure elucidation, because they allow one to go from a substructure to a chemical shift rather than in the opposite direction. Later substructure/monochemical shift relations are better suited to elucidation because a set of substructures from a data library can be proposed for a chemical shift. The new substructure/multichemical shift model, described here, makes it possible to scale down the set of proposed substructures by rendering the substructure/subspectrum relation more discriminating. This model, which serves as the basis for the EPIOS (Elucidation by Progressive Intersection of Ordered Substructures) system [9], provides a means of avoiding the generation of candidate structures from a molecular formula by means of an isomer generator and, instead, offers a method of making a fragment grow progressively so that it always matches both the formula and the spectrum under consideration. This is possible because the spectral information concerns not only the central carbon atom of a substructure, but the carbon atoms surrounding it as well.

The definition, generalization and analytical use of substructure/multichemical shift relations drawn from the DARC-PLURIDATA ^{13}C-n.m.r. bank [10, 11], as well as the creation of the substructure/information (SS/I) space used by the EPIOS system, are described herein. (DARC: Description, Acquisition, Retrieval, Computer-aided design.)

THE SEARCH FOR SUBSTRUCTURE/$\delta^{13}C$ RELATIONS

Additive models for predicting $\delta^{13}C$

In ^{13}C-n.m.r., the notion of a substructure centred on a carbon atom is inherent to an evaluation of its chemical shifts. A systematic study of the spectra of families of organic compounds made possible an early assessment of the effects of structural environments on a given carbon atom in a reference fragment [12, 13]. This approach provides precious tools for the assignment or prediction of chemical shifts, but the complex effects of molecular environment generally restrict the range of application of the proposed models to only the structural context of their definition [14—23]. With such models, the chemical shift of an atom is a parametric function of its molecular environment. The form of these relations limits their use in computer-aided elucidation systems to checking the coherence of responses provided by an isomer generator [24—26]. These models are ill-adapted to direct interpretation of the spectrum of an unknown compound, because they

cannot be used to predict substructural environments matching the chemical shifts under consideration [27, 28]. Substructure identification from a spectrum requires the establishment of sufficiently discriminating relations characterizing substructures by their $\delta^{13}C$ behavior.

Substructure/monochemical shift relations

The constitution of libraries associating reference fragments with their chemical shifts [26, 29—31] is an approach more adapted to structural interpretation. By providing the means to identify structural fragments in compounds not belonging to a reference population, this approach, based on substructure/monochemical shift relations, broadens the range where reference data can be used. However, characterizing substructures by their $\delta^{13}C$ behavior confronts the possibilities of a structural interpretation system with the wide diversity of organic compounds and their spectroscopic properties.

The examples in Table 1 illustrate the difficulty of associating a given substructure with a specific $\delta^{13}C$ behavior. Although the substructure under consideration is defined up to the position β to the central atom, the recorded chemical shifts illustrate the diversity of its behavior. Its stability in the very different environments of compounds **I**—**VI** ($\Delta\delta^{13}C$ = 1 ppm) gives no hint of the deviations observed for compounds **VII**—**X** ($\Delta\delta^{13}C$ = 10 ppm). However, for a given reference population of structures, the central atom of substructures containing three or four layers of atoms [2, 6] can be characterized by a narrow range of variation.

Substructure/monochemical shift relations are designed so that an accurate $\delta^{13}C$ value can be associated with the centre of a fragment by considering all substructural information as implicitly characterized by this single value. Because the accuracy of this type of substructure/$\delta^{13}C$ relation is based primarily on the size and specificity of substructures centred around a ^{13}C atom, a description by concentric layers of the structural environments around a ^{13}C atom is obviously interesting for a study of structure/$\delta^{13}C$ relations. This type of description can be enhanced by introducing the notion of order therein. This can be achieved through use of the DARC code [11] which deals advantageously with general problems in chemistry, particularly the analysis of structure/property relations [39]. The HOSE code (Hierarchically-Ordered Spherical Environments) devised by Bremser [4—6] and used in chemical shift prediction or substructure identification is yet another approach to introducing a notion of order. Gray et al. [2] have added stereochemical properties to this type of description, thereby increasing fragment selectivity. However, given the high selectivity of these fragments, it can be hard and risky to use this type of substructure/monochemical shift relation far from the reference population.

Substructure/multichemical shift relations

The EPIOS system is an attempt to reduce the selectivity of reference substructures while improving the discriminating ability of a description

TABLE 1

Chemical shifts of the central atom of γ-substructures. For compounds I—VI, the chemical shift ($\delta^{13}C_{FO}$) varies within a range of 1 ppm whereas for compounds VII—X this chemical shift varies within a range of 9.8 ppm. Chemical shifts are given in parts per million relative to TMS

	Structures	$\delta^{13}C_{FO}$	Ref.
I	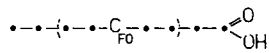	28.1	32
II	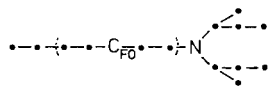	28.2	18
III	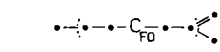	28.1	20
IV	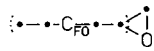	28.4	33
V	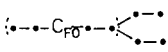	29.1	16
VI	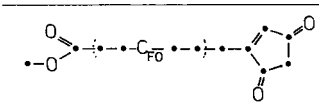	28.8	34
VII	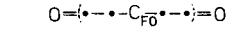	14.6	35
VIII	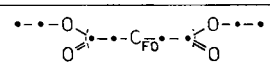	17.2	36
IX	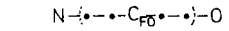	23.2	37
X	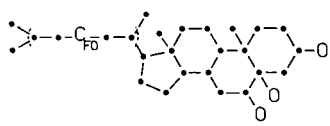	24.4	38

of spectral behavior. An early probe of various possible Environments which are Limited, Concentric and Ordered (ELCO) led to the choice of $ELCO_b$ (constituted by a central carbon atom C_{FO}, its immediate neighbors C_{A_i} ($1 \leqslant i \leqslant 4$) and their related bonds) as an appropriate reference substructure for EPIOS (Fig. 1).

To obtain a discriminating description of the behavior of $ELCO_b$ substructures, the chemical shifts of all their carbon atoms are considered, thereby combining all the spectroscopic information distributed throughout a substructure. In Table 2, the different $ELCO_b$'s corresponding to the γ-substructures can be distinguished from one another on the basis of the chemical shifts of C_{A_1} and C_{A_2} atoms connected to the C_{FO} atoms of these $ELCO_b$'s.

Because of the smallness of an $ELCO_b$, it can be found in a great many

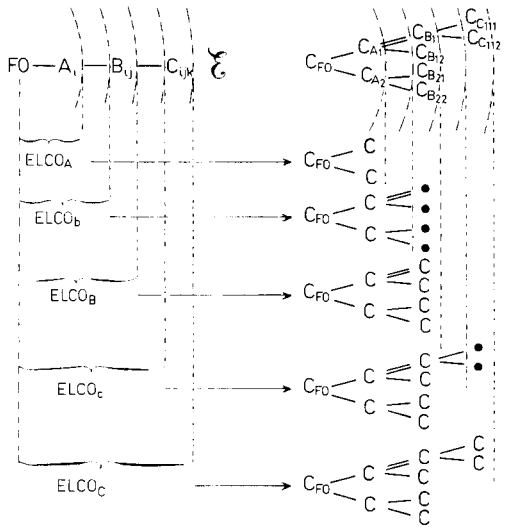

Fig. 1. Reference structure-based generation of Environments which are Limited, Concentric and Ordered (ELCO). The different types of substructures originating from the same atom are hierarchically related and are associated with the chemical shifts observed for each constituent carbon atom.

TABLE 2

Example of various γ-substructures and their corresponding ELCO$_b$ substructures selected for a triplet at 28.1 ppm

	Structures	C_{FO} centered γ substructures	ELCO$_b$	$\delta^{13}C_{FO}$	$\delta^{13}C_{A_1}$	$\delta^{13}C_{A_2}$	Ref.
XI	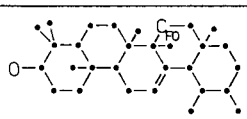	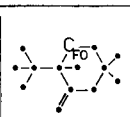	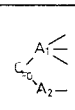	28.1	50.4	31.6	40
XII	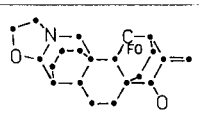	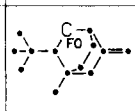	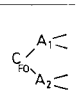	28.1	39.6	36.4	41
XIII	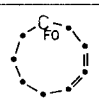			28.1	29.1	25.2	42
XIV				28.1	41.8	24.5	43

reference structures and can be characterized by a large statistical sample of chemical shifts. This characterization of $ELCO_b$'s stems from an analysis of C_{FO} and C_{A_i} chemical shifts as a function of environment effects.

DEFINING SUBSTRUCTURE/MULTICHEMICAL SHIFT RELATIONS

Behavior of $ELCO_b$ atoms C_{FO} and C_{A_i}

By analyzing the influence that variable alkyl environments R (quantified by λ_R) have on the $\delta^{13}C$ chemical shifts of various types of carbon atoms, it has been possible to specify homogeneously the particular behavior of these atoms [44]. For this model, the chemical shift of a ^{13}C-atom considered as the focus of a substructure defined by its immediate neighborhood, A, is expressed as $\delta^{13}C = \omega_c\lambda_R + \eta_c$. The constants ω_c and η_c characterize the substructures and correspond, respectively, to the sensitivity of the ^{13}C-atom and to its chemical shift in the substructure with methyl group substituents ($\lambda_{Me} = 0$). The λ_R parameter, defined from a family of reference alkynes [$\lambda_R = \delta(Me{-}C{\equiv}{}^{13}C{-}R) - \delta(Me{-}C{\equiv}{}^{13}C{-}Me)$], expresses the influence of a variable alkyl environment R (R for a given alkyl group). Here this analysis is extended to the neighboring atoms C_{A_i} of the focus of $ELCO_b$ substructures.

Monoalkyl environment R. The variations in chemical shift for the carbon atoms of three $ELCO_b$ substructures (with a secondary, a tertiary and a quaternary focus) are considered.

$$(C{-}C_{FO}{-}C_{A_1}{-})R \qquad \text{(I)}$$

$$\left(\begin{matrix}C\\ C\end{matrix}\!\!>\!C_{FO}{-}C_{A_1}{-}\right)R \qquad \text{(II)}$$

$$\left(\begin{matrix}C\\ C\end{matrix}\!\!>\!\!\!-C_{FO}{-}C_{A_1}{-}\right)R \qquad \text{(III)}$$

The impact of the effects induced by variable environment R on each of the atoms is different depending on their position in the $ELCO_b$: thus atoms C_{A_1} undergo the direct impact of these effects, whereas focuses C_{FO} undergo the weakened impact (i.e., attenuated by C_{A_1}) of these effects.

Figure 2 illustrates this difference in the perception of the effects of R. Three parallel straight lines with a positive slope represent the variations in the chemical shift of the $^{13}C_{A_1}$ atoms in each of the families. As the environments A of these atoms are identical, the sensitivity of the atoms in response to the variation in R is the same. The contribution of each given group [Et($C{-}C_{FO}{-}$), iso-Pr($\begin{matrix}C\\ C\end{matrix}\!\!>\!C_{FO}{-}$) and tert-Bu($\begin{matrix}C\\ C\end{matrix}\!\!>\!\!\!-C_{FO}{-}$)] to the chemical shift of atom C_{A_1} to which it is bonded is constant for each structural series. These different contributions determine the variation thresholds of $\delta^{13}C_{A_1}$.

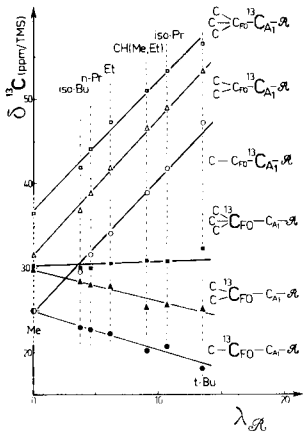

Fig. 2. Correlation of the chemical shifts [16] of atoms C_{FO} and C_{A_1} with parameters λ_R quantifying the influence of monoalkyl environment R: $\lambda_R = \delta(Me{-}C{\equiv}{}^{13}C{-}R) - \delta Me{-}C{\equiv}{}^{13}C{-}Me)$. The behavior of secondary (•), tertiary (▲) and quaternary (■) atoms and that of the corresponding secondary C_{A_1} atoms (○, △, □) are linearly related to the topology of R and specific to each $ELCO_b$.

The negative slope of the straight lines for the secondary and the tertiary focuses is explained by the permanent presence of substituents at the position γ to these atoms. These γ-substituents appear as soon as R takes the value of R = Et, thereby forming with the intermediate atom C_{A_1}, a n-Pr group bonded to the focus C_{FO}. The upfield variation in the chemical shift of these focuses is that usually observed for this type of substitution [15, 19, 45]. Herein, however, this variation contrasts with that recorded for the quaternary focus for which the chemical shift increases with the number of γ-positions occupied. The particular behavior of this atom, previously observed for alkanes [16] and ethers [45], is generally interpreted in terms of steric effects [45, 46].

Dialkyl environment R. To demonstrate the general character of the above-conducted analysis, it is extended to the atoms of an $ELCO_b$ subjected to the influence of a variable external dialkyl environment $R = R_1 + R_2$.

$$R_2(-C_{A_2}-C_{FO}-C_{A_1}-)R_1 \qquad \text{(IV)}$$

Three series of structures are differentiated by the values R_2 = Me, Et and iso-Pr. For each one of these series, the chemical shifts of C_{FO} and C_{A_1} are correlated with the corresponding parameters ($\lambda_R = \lambda_{Me} + \lambda_{R_1}$; $\lambda_R = \lambda_{Et} + \lambda_{R_1}$; $\lambda_R = \lambda_{iso\text{-}Pr} + \lambda_{R_1}$) expressing the variations of R (Fig. 3a–c).

For each family of compounds, two straight lines with opposite slopes represent the respective responses of C_{FO} and C_{A_1}. Each value of R_1 acting on C_{FO} via C_{A_1} provokes an upfield or downfield variation on one of these atoms and the opposite variation on the other. For each type of atom, the value of the slope of the corresponding straight lines (i.e., of their sensitivity)

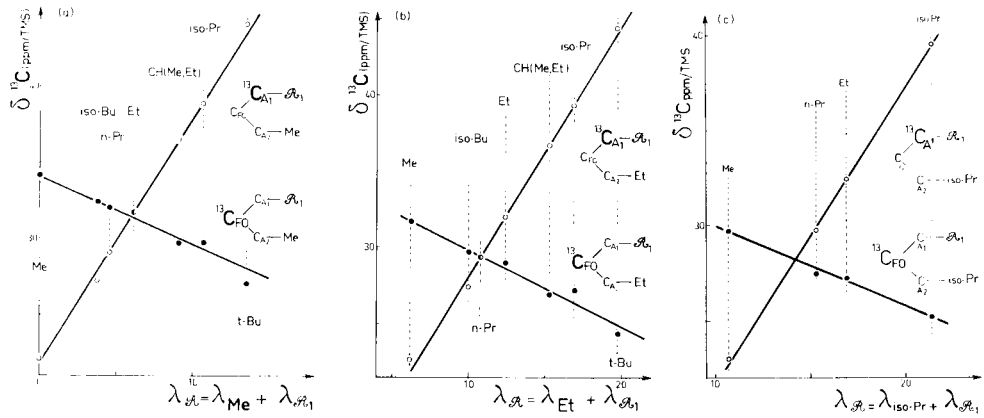

Fig. 3. Correlation of the chemical shifts [16] of atoms C_{FO} and C_{A_1} with parameters λ_R quantifying the influence of variable dialkyl environment, $R = R_1 + R_2$. The different values of R_2 do not affect the sensitivity of the atoms (correlation slope) to the induced perturbations; their contribution to the chemical shift of the atoms, the behavior of which is determined by the topology of the $ELCO_b$, is constant for each series of alkanes. (a) R_2 = Me; (b) R_2 = Et; (c) R_2 = iso-Pr.

is identical for the three series considered. The sensitivities of carbon atoms, thereby revealed through the topological parameter λ_R, are determined by the nature of the $ELCO_b$ and specifically modulate the perturbations exerted by the external environment R.

For the interpretation of the spectrum of an unknown compound, it is clear that relations which separately associate $\delta^{13}C_{FO}$ and $\delta^{13}C_{A_i}$ with their environment R cannot be used directly, because relations in this form require that λ_R be known. However, with such relations, $ELCO_b$ behavior can be characterized in a manner suitable to its identification from chemical shift values. Thus, by passing from external relations $\delta^{13}C_{FO}/\lambda_R$ and $\delta^{13}C_{A_i}/\lambda_R$ to an internal $ELCO_b$ relation $\delta^{13}C_{FO}/\delta^{13}C_{A_i}$ expressing the linear interdependence of neighboring atoms C_{FO} and C_{A_i}, overall $ELCO_b$ behavior can be characterized independently or an assessment of its external environment effects.

Characterization of $ELCO_b$ behavior

Figure 4(a) depicts the straight lines obtained by correlating the chemical shifts of atoms C_{FO} and C_{A_1} determined by the same variation of a monoalkyl environment R on each $ELCO_b$ (I, II, II) cited above. Each value of R determines a particular pair ($\delta^{13}C_{FO}$ and $\delta^{13}C_{A_1}$) for each substructure. The straight lines of the correlation, which associate the chemical shift of neighboring atoms in each $ELCO_b$, express the interdependence of the responses of these atoms to the structural perturbations provoked by the variation of their external environment. This internal relation expresses the behavior of each $ELCO_b$ by a straight line associating the behavior of the atoms. Thus,

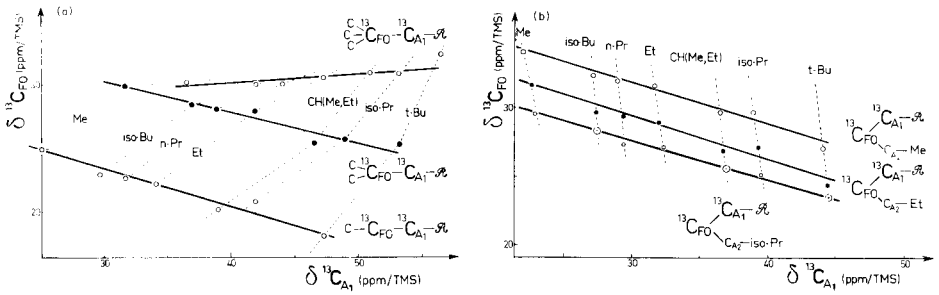

Fig. 4. Networks obtained by correlating the chemical shifts of atoms C_{FO} and C_{A_1}. (a) Monoalkyl environment R: each value of monoalkyl environment R simultaneously determines the chemical shifts of atoms C_{FO} and C_{A_1} for each $ELCO_b$ (I, II, III). (b) Dialkyl environment R: each node corresponds to a given pair, R_1 and R_2 of the external alkyl environment. The set of straight lines forming this network characterizes the $ELCO_b$ considered, independently of an assessment of the influence of external environment R.

one logically finds the particular behavior provoked by the quaternary focus of $ELCO_b$ **III**.

Likewise, the network of straight lines in Fig. 4(b) characterizes the behavior of $ELCO_b$ **IV** when the dialkyl environment R varies. The pairs $\delta^{13}C_{FO}$ and $\delta^{13}C_{A_1}$, determining the nodes of the network, express the response of the atoms to the simultaneous presence of two given alkyl environments R_1 and R_2. Such a network constitutes an accurate quantitative description of the structural effects on the variations in $\delta^{13}C$ and is consequently of obvious interest, not only for the assignment or prediction of chemical shifts, but also for structural interpretation of the spectrum of unknown alkanes.

The definition of $ELCO_b$/multichemical shift relations was made possible by a prior analysis of the alkanes through which the characteristic functions of the $ELCO_b$'s studied were specified. The perturbations induced on these functions by external structural environments & are examined hereafter from a statistical angle. The diversity of these environments, drawn from the DARC-PLURIDATA ^{13}C-n.m.r. bank, leads to generalization of these $ELCO_b$/multichemical shift relations and to an organization of structural and spectral information suited to the EPIOS elucidation system.

GENERATION OF THE DISCRIMINATING SPACE SS/I: $ELCO_b/(\delta^{13}C_{FO}, \delta^{13}C_{A_i})$

With the substructure search program of the DARC system, the set of substructures (ELCO) is extracted from the reference population. These substructures are systematically generated, i.e., each atom is taken successively as a focus in the retrieval stages. Each constituent atom of a structure is designated as a focus of a set of substructures organized concentrically from layer A to layer C. The different types of ELCO containing the same submoiety are hierarchically indexed (Fig. 1). A reference structure is thereby

fragmented into disconnected pairs (ELCO, &) organizing the entire structural environment of each constituent atom of this structure. Thus, the ELCO constitutes a constant moiety for the reference population, and its external environment (&) groups all the structural complements of this substructure. Each ELCO is thus subjected to a set of very diverse structural constraints determined by the values of its external environment, &.

Parallel to this structural fragmentation, the chemical shifts pertaining to each reference structure are associated with the respective atoms of the ELCO. These chemical shifts induced on the carbon atoms of the ELCO by the different values of & constitute the statistical sample used to characterize the behavior of the ELCO.

The distribution (Fig. 5a) obtained by correlation between the chemical

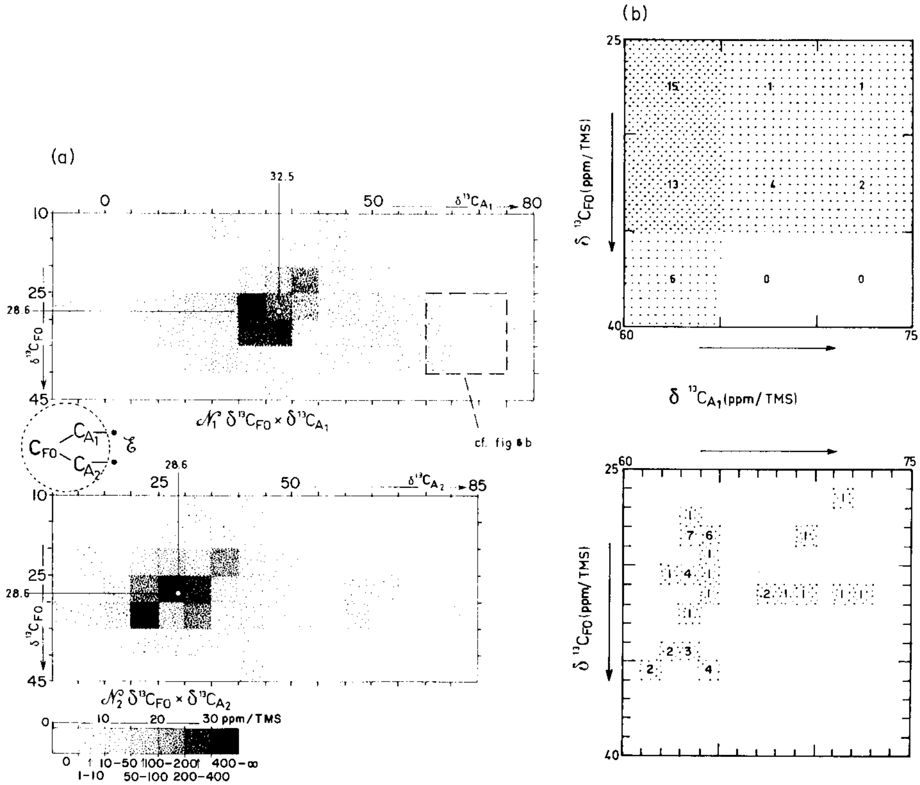

Fig. 5. Statistical distribution of the pairs $\delta^{13}C_{FO} \times \delta^{13}C_{A_i}$. (a) For ELCO$_b$ IV the concentration of points in clusters N_1 and N_2 expresses the occurrence of each elementary unit (side = 5 ppm) and the distribution of the pairs ($\delta^{13}C_{FO} \times \delta^{13}C_{A_i}$) observed for the 2005 structures containing this ELCO$_b$. Both statistical distributions display a high density zone (occurrence >100), around the centroid, corresponding, for N_1, to the limits of the straight line network in Fig. 4(b). (b) The distribution of the points associated with the ELCO$_B$ $C_{FO}\!<\!{}^{C_{A_1}-O}_{C-C}$ shows that the presence of the oxygen atom bonded to C_{A_1}, corresponds to the secondary behavior seen in Fig. 5(a). The description of this distribution is refined by the use of unitary elements of restricted size (side = 1 ppm), better adapted to this type of ELCO$_B$ substructure.

shifts $\delta^{13}C_{FO}$ and $\delta^{13}C_{A_1}$ for $ELCO_b$ IV ($-C_{A_2}-C_{FO}-C_{A_1}-$) groups the responses from the pair $C_{FO}-C_{A_1}$ which were recorded for a set of 2005 reference structures containing $ELCO_b$ IV. The correlation $\delta^{13}C_{FO}/\delta^{13}C_{A_2}$ completes the description of the behavior of the $ELCO_b$ IV from the chemical shifts recorded for all its carbon atoms. The limits and the centroid of these distributions are intrinsically related to the topology of the $ELCO_b$ considered.

Both of these statistical distributions include not only the linear relations established for the alkanes, but also unspecified relations corresponding to a wide variety of molecular environmental effects, of which only $ELCO_b$ chemical shifts are considered. Thus, depending on its topology and its chromaticity (nature of bonds and atoms), an $ELCO_b$ is localized in a five-dimensional substructure/information (SS/I) space determined by the values of $\delta^{13}C_{FO}$ and $\delta^{13}C_{A_i}$ $(1 \leqslant i \leqslant 4)$ (Fig. 6).

The distribution of the points $\delta^{13}C_{FO}/\delta^{13}C_{A_i}$ for a given pair of atoms of an $ELCO_b$ often reveals a type of homogeneous response to the effects induced by $\mathfrak{E}$. However, the distribution obtained for $ELCO_b$ IV (Fig. 5a) shows a secondary behavior related to the particular responses of atom C_{A_1}. Indeed, two distinct zones of occurrence greater than 10 constitute this distribution: the first zone, centred around the centroid of the cluster, contains 95% of the points in the area covering 17% of the range of variation and characterizes the type of response most frequently observed for this $ELCO_b$; the second, much smaller zone (1.5% of the points in 1.3% of the overall range

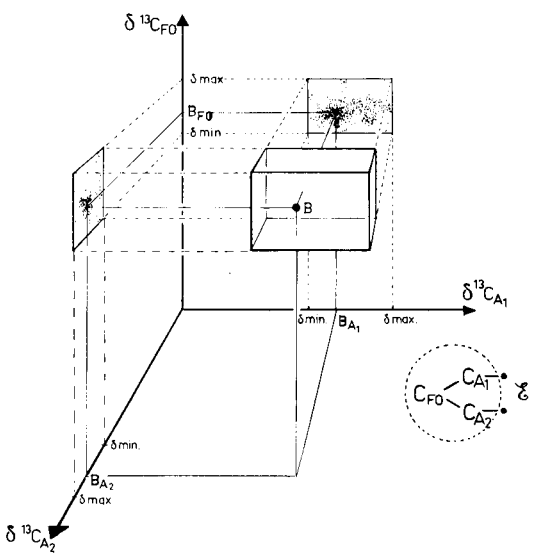

Fig. 6. Schematic projection onto a subspace ($\delta^{13}C_{FO} \times \delta^{13}C_{A_1} \times \delta^{13}C_{A_2}$) of the statistical distribution of the $\delta^{13}C$ values associated with $ELCO_b$ IV in SS/I space. The variation ranges of the chemical shifts observed for the pairs $\delta^{13}C_{FO} \times \delta^{13}C_{A_1}$ and $\delta^{13}C_{FO} \times \delta^{13}C_{A_2}$ are marked on each axis by δ_{min} and δ_{max} (cf. values shown in Fig. 5). These range limits, together with the centroid B, are characteristic of $ELCO_b$ IV in SS/I space.

of variation), indicates the particular response of atom C_{A_1} when it is bonded to an oxygen atom (Fig. 5b).

This result illustrates the importance of the interaction between the degree of selectivity of the elementary substructures and the statistical description of the associated chemical shifts. It confirms the interest that lies in placing the different substructures (ELCO) organized into concentric and ordered layers around the same central focus. The hierarchies established between ELCO's of increasing selectivity (from layer A to layer C) constitute a flexible and efficient means for grasping the determining role that the molecular environment of a carbon atom plays in its chemical shift. It makes it possible to extend a substructure by specifying its description and, in the present case, simultaneously to improve the structure/δ^{13}C relation.

IDENTIFYING SUBSTRUCTURES WITH AN $ELCO_C$ LIBRARY AND SS/I SPACE

Structural interpretation of a ^{13}C-n.m.r. spectrum

The $ELCO_C/\delta^{13}C$ library and SS/I space are two different aspects of the same reference population, i.e., the DARC-PLURIDATA ^{13}C-n.m.r. bank. In the $ELCO_C/\delta^{13}C$ library, each substructure is associated with the chemical shift variation range of its ^{13}C focus only, whereas in SS/I space each $ELCO_b$ is characterized by the chemical shift variation ranges of all its constituent carbon atoms (C_{FO} and C_{A_i}). Thus the $ELCO_C/\delta^{13}C$ library constitutes a more restricted representation of available data than the SS/I space. The noise related to structural interpretations of ^{13}C-spectra and corresponding to the selection of irrelevant structural moieties is one of the major obstacles to the elaboration of computerized structure-elucidation procedures. The number of $ELCO_C$ substructures from the $ELCO_C/\delta^{13}C$ library compatible with a chemical shift and its peak multiplicity depends mainly on the size of the reference population used. Most of the time, these selection criteria by themselves are not enough for a priori elimination of irrelevant candidate substructures. $ELCO_C$'s from Table 1 and those corresponding to γ-substructures in Table 2 reflect the diversity and number of structural environments compatible with a triplet at 28.1 ppm/TMS. However, the noise accompanying a structural interpretation from an $ELCO_C/\delta^{13}C$ library is not the only drawback to use of this library. In the case of the EPIOS system, where all substructures used to generate candidate structures stem exclusively from the interpretation of a spectrum, silence (i.e., the non-selection of a fragment required in the target structure) can impede elucidation. The probability of encountering such silence during interpretation certainly depends on the available reference population, but it also depends on the selectivity of the substructure/δ^{13}C relations used to retrieve the information contained in this population. The interpretation of serine [47] illustrates the inherent risk in the systematic use of substructures defined as precisely as the $ELCO_C$'s. Although serine is in the reference population, one of its constituent $ELCO_C$'s cannot be identified from the query spectrum δ^{13}C value of 63.9 ppm (Table 3).

TABLE 3

Identification of $ELCO_C$ and $ELCO_b$ constituents of serine. $ELCO_C$ III cannot possibly be identified from $\delta^{13}C_3$ and the variation range characterizing it in the library. The corresponding $ELCO_b$ ($ELCO_b$ VII), characterized in a more exhaustive manner, is identified from $\delta^{13}C_{FO} = \delta^{13}C_3$ (63.9 ppm) and $\delta^{13}C_{A_1} = \delta^{13}C_2$ (57.5 ppm)

	$ELCO_C$	$\delta^{13}C$ Min—max	$N(N')$[a]	Ref.		$ELCO_b$	$\delta^{13}C$			Centroid		$N(N')$[a]
							C_{FO}	C_{A_1}	C_{A_2}	B_{FO}	B_{A_i}	
I	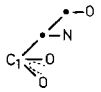	172.6—183.7	9(2)	48 49	V		170—185	40—80		178.2	60.9	39(11)
II		57.2—59.1	2(1)	49	VI		50—65	160—185	35—75	56.9	175.0 56.9	18(22)
III	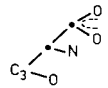	61.0—63.0	2(1)	49	VII		55—80	30—85		64.2	57.8	58(54)

[a] N is the number of $\delta^{13}C$ associated with the atoms studied. N' is the number of structures containing an ELCO. Spectrum of serine (ppm/TMS): $\delta^{13}C_1 = 178.9$, $\delta^{13}C_2 = 57.5$, $\delta^{13}C_3 = 63.9$.

The three $ELCO_C$'s centred on the carbon atoms of serine (Table 3) are associated with the variation ranges of the chemical shift of these atoms. The limits of these ranges are determined by the $\delta^{13}C$ values for the reference population structures containing these three $ELCO_C$'s. Two reference structures contain $ELCO_C$ I: serine itself [48, 49] and phosphoserine [48]. The values recorded for this latter compound make it possible to associate the C_1 carbon atom with a wider shift range (172.6—183.7 ppm) than that observed for serine (173.1—175.1 ppm). They thereby justify the selection of $ELCO_C$ I for $\delta^{13}C_1$ = 178.9 ppm in the query spectrum [47]. $ELCO_C$ II and $ELCO_C$ III are characterized by the ranges determined by the values of $\delta^{13}C$ for two spectra associated with serine in the reference population. Thus $ELCO_C$ II is selected because 57.5 ppm is actually in the $\delta^{13}C_2$ variation range (57.2—59.1 ppm), but $ELCO_C$ III is eliminated because 63.9 ppm is beyond its $\delta^{13}C_3$ variation range (61.0—63.0 ppm).

Although serine is in the reference population, its $ELCO_C$ III constituent cannot be identified from a new spectrum unless the value of the chemical shifts of this spectrum are approximated.

Medium effects on $\delta^{13}C$ chemical shifts

The example of serine illustrates that the presence of a particular substructure in a reference population is not enough to guarantee its identification from the chemical shift of a new spectrum. Experimental conditions (pH, concentration or solvent effects) are a frequent source of differences in the spectra of the same compound. In the case of phosphoserine ($HOOC—C_\alpha HNH_2—C_\beta H—O—PO_3H_2$) studied by Pogliani et al. [48], the chemical shift variations of 11.1, 3.4 and 4.1 ppm for atoms C—O, C_α and C_β, respectively, are dependent on the pH of the solutions considered (pH 1.1—13.0). A systematic analysis of solvent effects on the chemical shift of the carbon atoms of acetone conducted by Tiffon and Dubois [50] in the gas phase or in different concentrations in 19 different solvents detected a variation amplitude reaching 18.9 ppm for the carbonyl carbon and 8.5 ppm for the methyl carbon. The differences in the sensitivity to these variations in experimental conditions displayed by the carbon atoms studied (C_{sp^2} or C_{sp^3}) reveals the complexity of their behavior. Under these conditions, i.e., where intramolecular effects can be affected by outside actions, characterizing highly-defined substructures (up to position γ or δ) by only a narrow chemical shift range (0—3.8 ppm) [2, 6] associated with a single central atom sometimes turns out to be unsuitable. Interpreting the spectrum of an unknown compound from a library constituted in this fashion supposes not only a great similarity between this compound and the reference population, but it also supposes an exact equivalence between the experimental conditions used to measure the query and reference spectra. The difficulty involved in interpreting the spectrum of serine when recorded under different conditions than the reference spectra [48, 49] illustrates the importance of medium effects.

The $ELCO_b$/multichemical shift relations established from a wide variety of structural environments subjected to various medium effects indicate the responses of connected pairs of $ELCO_b$ carbon atoms to these situations. This set of responses, when weighted statistically, describes the behavior of $ELCO_b$. The statistical distribution of $\delta^{13}C_{FO}$ and $\delta^{13}C_{A_i}$ chemical shift pairs thereby reveals the standard behavior for each $ELCO_b$ which is expressed by high occurrences around a centroid, and other more specific behaviors defining the distribution range. The size of the statistical sample used to establish this distribution therefore considerably affects not only the quality, but also the general character of the description of the behavior of an $ELCO_b$.

Thus, in the example of serine, $ELCO_b$ **VII** is contained in 54 reference compounds, making it possible to characterize each one of its carbon atoms by 58 $\delta^{13}C$ values instead of by only two $\delta^{13}C$ values for the central atom of the corresponding $ELCO_C$ **III**. The variation ranges of its two carbon atoms thereby justify the selection of $ELCO_b$ **VII**: the coordinates of the centroid (64.2 and 57.8 ppm) are in good agreement with the values accepted, respectively, by C_{FO} and C_{A_1} (63.9 and 57.5 ppm) (Table 3).

The interest of using $ELCO_b$ substructures and SS/I space in the EPIOS elucidation system is not restricted to an initial substructural selection phase. Assigning chemical shifts to each carbon atom of an $ELCO_b$ substructure, together with the easy EPIOS treatment of these small structural entities, makes it possible to approach the generation of structures matching a query spectrum without having to face an excessively difficult combinatorial problem. Thus, after an initial selection, the EPIOS system conducts a rapid comparison of $ELCO_b$ candidates and selects only those actually able to coexist in a structure. The so-recognized coexistences between the selected $ELCO_b$'s thus guides the generation of structures matching a query spectrum.

CONCLUSION

Using the topological parameter λ_R to examine the effects of alkyl environments R on the carbon atoms of the $ELCO_b$ elementary substructures allows the behavior of these atoms to be isolated. A relation within $ELCO_b$ is defined by correlating the responses of the bonded atoms therein to the perturbations induced by external environment R.

Going from the separate relations ($\delta^{13}C_{FO}/\lambda_R$ and $\delta^{13}C_{A_i}/\lambda_R$), expressing the response of each atom as dependent on the topology of R, to this internal relation ($\delta^{13}C_{FO}/\delta^{13}C_{A_i}$) describes the behavior of a substructure with satisfactory accuracy, independently of an assessment of external effects. In the case of $ELCO_b$ substructures and of alkyl environments, this relation leads to accurate descriptions of the behavior of $ELCO_b$ (straight lines or networks of straight lines from correlations) specifically determined by their topology.

For very diversified environments, the relation $\delta^{13}C_{FO}/\delta^{13}C_{A_i}$ is used. By generalizing it to all the data in the DARC-PLURIDATA ^{13}C-n.m.r. bank,

each substructure can be characterized by N statistical distributions associated with the N pairs of C_{FO}—C_{A_i} constituting the substructure. These distributions correspond to a certain loss of accuracy of the correlations obtained for the alkyl environments. However, on the whole, their coherence is good and they can be used to characterize and correlate the effects of structural environments on $\delta^{13}C$ chemical shifts. These observations led to the choice of $ELCO_b$, among the various more or less extensively layered substructures in Fig. 1, as the reference substructure.

The data concerning several bonded atoms (here, C_{FO} and its neighbors C_{A_i}) can express the behavior of this scaled-down substructure. This behavior can thus be placed and located in the SS/I space (Fig. 6) which constitutes an heuristic organization of raw structure/^{13}C-n.m.r. spectrum data.

The flexibility of the concentric description of substructures makes it possible to adjust the degree of definition of a substructure ($ELCO_B$ or $ELCO_C$) while at the same time specifying the description of its behavior. This optimized use of reference data increases the discriminating ability of the SS/I space. For certain complex elucidations, experience should be the guide in seeking to improve this optimization. In other words, when distant effects are known, they can be taken into consideration in describing the behavior of an $ELCO_b$, but the use of more selective $ELCO_n$ substructures with more layers is also conceivable. This means that the use of $ELCO_b$ allows very different areas of chemistry to be scanned rapidly, but that for particular areas which are very rich in information, the organization of the SS/I space can remain unchanged when $ELCO_b$ is associated with more extensively layered substructures.

At this stage of our work, the choice of $ELCO_b$ as reference substructure is sufficient to create a search SS/I space with satisfactory accuracy, and allows the elucidation of unknown structures which are not akin to the reference population. In the absence of explicit structure/$\delta^{13}C$ relations, this type of space makes it possible to use observations which have not yet been theoretically interpreted. The EPIOS elucidation system for the generation of full and partial structures from their ^{13}C-n.m.r. spectrum is based on these internal semi-empirical relations and will be dealt with in a forthcoming paper.

The authors thank the referees for their useful comments and constructive suggestions, particularly about medium effects.

REFERENCES

1 H. L. Surprenant and C. N. Reilley, Anal. Chem., 49 (1977) 1134.
2 N. A. B. Gray, C. W. Crandell, J. G. Nourse, D. H. Smith, M. L. Dageforde and C. Djerassi, J. Org. Chem., 46 (1981) 703.
3 R. E. Carhart, D. H. Smith, H. Brown and C. Djerassi, J. Am. Chem. Soc., 97 (1975) 5755.
4 W. Bremser, M. Klier and E. Meyer, Org. Magn. Reson., 7 (1975) 97.

5 W. Bremser, Z. Anal. Chem., 1 (1977) 286.
6 W. Bremser, Anal. Chim. Acta, 103 (1978) 355.
7 J. Zupan, S. R. Heller, G. W. A. Milne and J. A. Miller, Anal. Chim. Acta, 103 (1978) 141.
8 C. A. Shelley, H. B. Woodruff, C. R. Snelling and M. E. Munk, ACS Symp. Ser., 54 (1977) 92.
9 J. E. Dubois, M. Carabedian and B. Ancian, C.R. Acad. Sci., Ser. C., 290 (1980) 369, 383.
10 J. E. Dubois and J. C. Bonnet, Anal. Chim. Acta, 112 (1979) 245.
11 J. E. Dubois, D. Laurent and H. Viellard, C.R. Acad. Sci., Ser. C, 263 (1966) 764; J. E. Dubois, Isr. J. Chem., 14 (1975) 17; J. E. Dubois, in A. T. Balaban (Ed.), The Chemical Applications of Graph Theory, Academic Press, New York, NY, 1976, p. 336.
12 R. A. Friedel and H. L. Retcofsky, J. Am. Chem. Soc., 85 (1963) 1300.
13 G. B. Savitsky and K. Namikawa, J. Phys. Chem., 68 (1964) 1956.
14 D. M. Grant and E. G. Paul, J. Am. Chem. Soc., 86 (1964) 2984.
15 D. K. Dalling and D. M. Grant, J. Am. Chem. Soc., 96 (1974) 1827.
16 L. P. Lindeman and J. Q. Adams, Anal. Chem., 43 (1971) 1245.
17 J. D. Roberts, F. J. Weigert, J. I. Kroschwitz and H. J. Reich, J. Am. Chem. Soc., 92 (1970) 1338.
18 H. Eggert and C. Djerassi, J. Am. Chem. Soc., 95 (1973) 3710.
19 H. Brouwer and J. B. Stothers, Can. J. Chem., 50 (1972) 1361.
20 D. E. Dorman, M. Jautelat and J. D. Roberts, J. Org. Chem., 36 (1971) 2757.
21 D. R. Paulson, F. Y. N. Tang, G. F. Moran, A. S. Murray, B. P. Pelka and E. M. Vasquez, J. Org. Chem., 40 (1975) 184.
22 H. Eggert, C. L. Van Antwerp, N. S. Bhacca and C. Djerassi, J. Org. Chem., 41 (1976) 71.
23 J. E. Dubois and J. P. Doucet, Org. Magn. Reson., 2 (1978) 87.
24 R. E. Carhart and C. Djerassi, J. Chem. Soc., Perkin Trans., 2 (1973) 1753.
25 D. H. Smith and P. C. Jurs, J. Am. Chem. Soc., 100 (1978) 3316.
26 T. Yamasaki, H. Abe, Y. Kudo and S. Sasaki, ACS Symp. Ser., 54 (1977) 108.
27 G. M. Schwenzer and T. M. Mitchell, ACS Symp. Ser., 54 (1977) 58.
28 J. T. Clerc and H. Sommerauer, Anal. Chim. Acta, 95 (1977) 33.
29 J. Zupan, Anal. Chim. Acta, 103 (1978) 273.
30 T. M. Mitchell and G. M. Schwenzer, Org. Magn. Reson., 11 (1978) 378.
31 C. W. Crandell, N. A. B. Gray and D. H. Smith, J. Chem. Inf. Comput. Sci., 22 (1982) 48.
32 E. Lippmaa, T. Pehk, K. Anderson and C. Rappe, Org. Magn. Reson., 2 (1970) 109.
33 S. G. Davies and G. H. Whitham, J. Chem. Soc. Perkin Trans., 2 (1975) 861.
34 G. Stork and T. Takahashi, J. Am. Chem. Soc., 99 (1977) 1275.
35 E. B. Whipple and M. Ruta, J. Org. Chem., 39 (1974) 1666.
36 G. A. Olah and P. W. Westerman, J. Org. Chem., 38 (1973) 1986.
37 U. Edlund, C. Holloway and G. C. Levy, J. Am. Chem. Soc., 98 (1976) 5069.
38 J. W. Blunt and J. B. Stothers, Org. Magn. Reson., 9 (1977) 439.
39 J. E. Dubois, D. Laurent and A. Aranda, J. Chim. Phys., 70 (1973) 1608.
40 S. A. Knight, Org. Magn. Reson., 6 (1974) 603.
41 S. W. Pelletier and N. Y. Mody, J. Am. Chem. Soc., 99 (1977) 284.
42 F. A. L. Anet and I. Yavari, J. Am. Chem. Soc., 99 (1977) 7640.
43 D. K. Dalling, D. M. Grant and E. G. Paul, J. Am. Chem. Soc., 95 (1973) 3718.
44 J. E. Dubois and M. Carabedian, Org. Magn. Reson., 14 (1980) 264.
45 D. E. Dorman, D. Bauer and J. D. Roberts, J. Org. Chem., 40 (1975) 3729.
46 D. M. Grant and B. V. Cheney, J. Am. Chem. Soc., 89 (1967) 5319.
47 D. Schipper, J. L. Van der Baan and F. Bickelhaupt, J. Chem. Soc. Perkin Trans. 1, 8 (1979) 2017.
48 L. Pogliani, C. Kruger and D. Ziessow, Org. Magn. Reson., 9 (1977) 504.
49 S. Harada, T. Kishi and E. Mizuta, J. Am. Chem. Soc., 100 (1978) 4895.
50 B. Tiffon and J. E. Dubois, Org. Magn. Reson., 11 (1978) 295.

Analytica Chimica Acta, 158 (1984) 235—246
Elsevier Science Publishers B.V., Amsterdam — Printed in The Netherlands

CLUSTER ION FORMATION IN LASER MASS SPECTROMETRY OF SUBSTITUTED PYRIDINES

TUAN A. DANG, ROBERT J. DAY[a] and DAVID M. HERCULES*
Department of Chemistry, University of Pittsburgh, Pittsburgh, PA 15260 (U.S.A.)
(Received 19th August 1983)

SUMMARY

Emission of cluster ions occurs during laser irradiation of substituted pyridines even at threshold laser power densities. The clusters generated include dimers and trimers, and appear in both positive-ion and negative-ion laser mass spectra. Fragments of cluster ions are observed and can be rationalized as losses of neutral molecules from $(nM \pm H)^{\pm}$. Dissociation of clusters occurs primarily from substituents on the pyridine ring. Laser mass spectrometry of pyridoxine hydrochloride and pyridoxamine-dihydrochloride resulted in the emission of clusters analogous to those observed for nicotinic acid. In contrast to these results, secondary-ion and field-desorption mass spectra of salts contain the ions $C_nA_{n-1}^+$ and $C_nA_{n+1}^-$, that were not detected in the laser mass spectra.

The use of laser radiation to volatilize and ionize samples for mass spectrometry has led to development of ionization methods applicable to involatile and thermally labile compounds [1—12] and to the application of laser microprobe techniques to complex samples [9, 11, 12]. Applications of laser mass spectrometry (l.m.s.) include generation of cationized molecules for high-molecular-weight saccharides and glycosides [1, 9]. Generation of both protonated and cationized molecules has been reported for nucleosides [1].

Positive-ion l.m.s. is characterized by abundant cationized and protonated molecules and in some cases, cationized fragments [1], while negative-ion spectra routinely contain $(M - H)^-$ as the major peak. Laser mass spectra of many inorganic compounds contain cluster ions, for example, Cu_3S^+, $Cu_4S_2^+$, and $Cu_5S_2^+$ and $Cu_2S_3^-$, $Cu_3S_2^-$ and $Cu_3S_3^-$ in the spectra of Cu_2S [9]. Similarly, emission of carbon clusters was observed for laser irradiation of graphite foil [13] while M_n^+, $M_nO_m^+$ and $M_nS_m^+$ species were detected in the l.m.s. of metals, metal oxides, and metal sulfides, respectively [14]. Although some evidence for cluster ion emission from organic samples has been observed for sodium acetate [1] and nicotinic acid [9], detailed investigation of these processes has not been reported.

---

[a]Present address. IBM Corporation, General Technology Division, Endicott, NY 13760, U.S.A.

0003-2670/84/$03.00 © 1984 Elsevier Science Publishers B.V.

This paper describes the generation of cluster ions in the laser mass spectra of nitrogen-containing organic compounds. Detailed study of cluster ions is important for interpretation of mass spectra derived from techniques like l.m.s. These ions represent a complication in the use of l.m.s. for structural purposes.

EXPERIMENTAL

Spectra were obtained using both Leybold-Heraeus LAMMA-500 and LAMMA-1000 laser microprobe mass spectrometers. The laser beam strikes samples on the same side as ion extraction in the LAMMA-1000, while it must penetrate the sample in the LAMMA-500. Both instruments are equipped with a *Q*-switched frequency quadrupled Nd-YAG laser (λ = 265 nm) having a pulse width of approximately 15 ns. Power densities ranged from $\approx 10^8$ W cm^{-2} at threshold to $\approx 2 \times 10^9$ W cm^{-2}. Ions are accelerated into a time-of-flight mass spectrometer with a 1.8-m drift tube. An ion reflector is used to compensate for the initial spread in ion energies. Mass resolution in the range 800—1000 m Δm^{-1} is attainable. Accumulated mass spectra are processed with a Hewlett-Packard series 10E computer. Samples were obtained commercially and were deposited as powders onto metal foils (LAMMA-1000) or from solution onto copper grids coated with a thin film layer of formvar (LAMMA-500).

RESULTS AND DISCUSSION

Cluster formation in organic compounds

Table 1 gives a summary of l.m.s. results for a series of substituted pyridines. They all show emission of cluster ions in both positive-ion and negative-ion l.m.s. Typical cluster ion formation is illustrated in Fig. 1, which shows the positive and negative l.m. spectra of nicotinic acid. These spectra were obtained at threshold power density (2×10^8 W cm^{-2}) using the LAMMA-1000. As shown in Fig. 1(a), in addition to the protonated molecular ion, m/z = 124, ions of higher mass were also detected in the positive-ion l.m. spectra. These cluster ions can be explained as fragments of $(2M + H)^+$. For example, the ion at m/z 203 corresponds to loss of CO_2 from $(2M + H)^+$. Consecutive loss of CO_2 and formic acid results in the peak at m/z 157. The small peak at m/z 201 corresponds to $(2M + H - HCOOH)^+$. The intensity of the ion at m/z 203 is comparable to that of the protonated molecular ion $(M + H)^+$. Thus, emission of cluster ions is significant even at the threshold laser power density (2×10^8 W cm^{-2}). In the negative-ion l.m. spectra of nicotinic acid, the deprotonated dimer, $(2M - H)^-$, and its fragment ions account for the peaks observed above the quasimolecular ion $(M - H)^-$, m/z 122. Ions at m/z 245, 199 and 155 correspond to $(2M - H)^-$, $(2M - H - HCOOH)^-$ and $(2M - H - HCOOH - CO_2)^-$, respectively, as shown in Fig. 1(b). It is noteworthy that cluster formation was not reported in a secondary-ion mass spectrometry (s.i.m.s.) study of nicotinic acid [15].

TABLE 1

Summary of l.m.s. results of substituted pyridines

Compound	Structure	Size of the largest cluster observed		Compound	Structure	Size of the largest cluster observed	
		Positive	Negative			Positive	Negative
Nicotinic acid	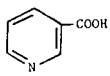	3	2	Nicotinamide	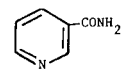	2	3
Isonicotinic acid		3	2	Isonicotinamide		2	3
2,6-Pyridine dicarboxylic acid	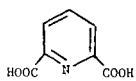	2	2	Picolinamide	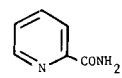	2	3
Nicotinic acid *N*-oxide	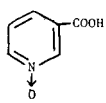	2	2	6-Chloronicotinamide	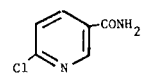	3	3
Isonicotinic acid *N*-oxide	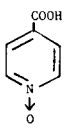	2	2	Pyridoxine-HCl	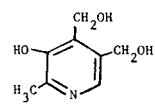	3	2
Picolinic acid *N*-oxide	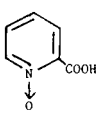	2	2	Pyridoxamine-2HCl	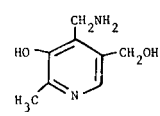	2	3

Comparison of l.m.s. results for nicotinic acid using both the LAMMA-500 and the LAMMA-1000 along with different types of sample preparation (powder or deposition from solution onto a thin film) showed that emission of cluster ions is independent of the instrument and the sample preparation methods used.

The neutral loss assignments for cluster ions from nicotinic acid were confirmed by comparing l.m.s. results for nicotinic acid and nicotinic acid having the COOH group labeled with deuterium. For the positive-ion l.m.s., peaks corresponding to $(2M + D - CO_2)^+$, *m/z* 206 and $(2M + D - HCOOD)^+$, *m/z* 203 are seen in Fig. 2(a). In addition, ions corresponding to $(M + D)^+$ and $(M + D - CO_2)^+$ account for peaks at *m/z* 126 and 82, respectively. All of these ions correspond exactly to the proton-derived peaks in Fig. 1(a). Clusters analogous to $(2M - H)^-$ and $(2M - H - COOH)^-$ are $(2M - D)^-$ and $(2M - H - HCOOD)^-$, which account for peaks at *m/z* 246 and *m/z* 249, respectively, in Fig. 2(b). Thus, both the positive-ion and negative-ion l.m. spectra correspond exactly for the protonated and deprotonated derivatives.

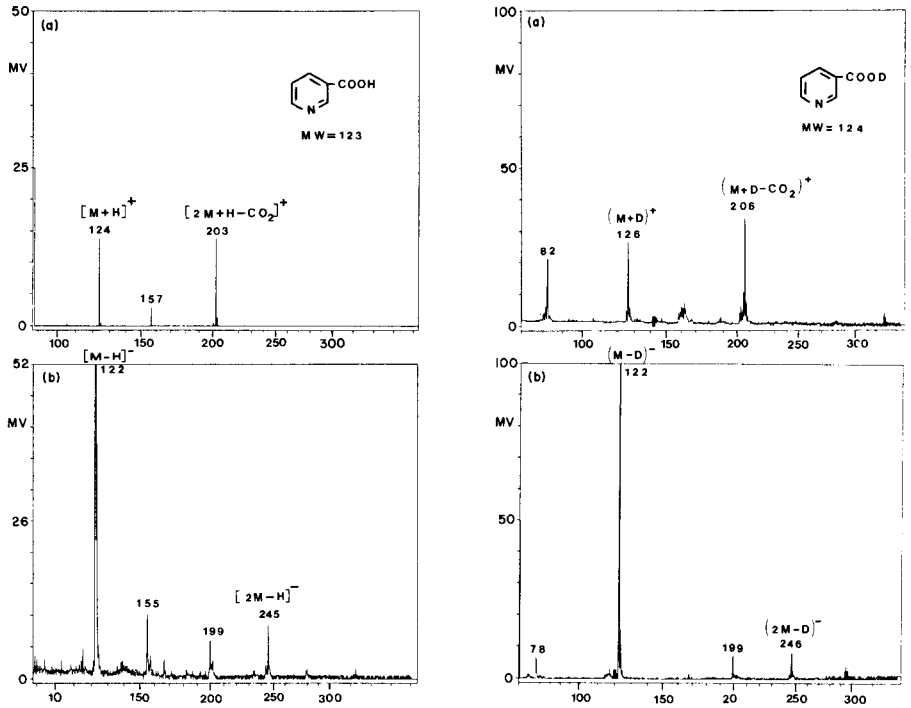

Fig. 1. Laser mass spectra of nicotinic acid (LAMMA-1000): (a) positive (2.0×10^8 W cm^{-2}); (b) negative (3.7×10^8 W cm^{-2}).

Fig. 2. Laser mass spectra of deuterium-exchanged (RCOOD) nicotinic acid (LAMMA-1000): (a) positive (6.1×10^8 W cm^{-2}); (b) negative (4.0×10^8 W cm^{-2}).

Similar cluster ions were observed in the l.m.s. of nicotinic acid *N*-oxide as shown in Table 2. The ion at *m/z* 261 corresponds to loss of H_2O from $(2M + H)^+$. Consecutive losses of $(H_2O + O)$, $(H_2O + O + CO_2)$, or $(H_2O + O + 2CO_2)$ from $(2M + H)^+$ correspond to peaks at *m/z* 245, 201 and 157, respectively. The decarboxylation process observed in nicotinic acid is not seen for nicotinic acid *N*-oxide. However, loss of formic acid (HCOOH) from $(2M + H)^+$ corresponds to a peak at *m/z* 233 in the positive l.m.s. of nicotinic acid *N*-oxide.

Fragmentation of the ion at *m/z* 233 can account for peaks at *m/z* 217, $(2M + H - HCOOH - O)^+$; *m/z* 189, $(2M + H - HCOOH - CO_2)^+$; and *m/z* 173, $(2M + H - HCOOH - O - CO_2)^+$. The base peak in the spectrum corresponds to $(M + H)^+$, *m/z* 140. Loss of O, CO and CO_2 from $(M + H)^+$ results in peaks at *m/z* 124, 112 and 96, respectively.

A peak corresponding to $(2M - H)^-$, was not detected in the negative-ion l.m. spectra of nicotinic acid *N*-oxide, but its fragments account for peaks observed at *m/z* 231, $(2M - H - HCOOH)^-$ and *m/z* 187 $(2M - H - HCOOH - CO_2)^-$. Both $(2M - H - HCOOH)^-$ and $(2M - H - HCOOH -$

TABLE 2

Cluster ions generated by l.m.s. of pyridine carboxylic acid *N*-oxides

Pyridine carboxylic acid *N*-oxides		Nicotinic acid *N*-oxide[a]	Isonicotinic acid *N*-oxide[b]	Picolinic acid *N*-oxide[c]	Deuterium-exchanged (RCOOD) nicotinic acid *N*-oxide[d]	
m/z	Assignments				*m/z*	Assignments
Positive					*Positive*	
261	$(2M + H - H_2O)^+$	X	X		262	$(2M + D - D_2O)^+$
245	$(2M + H - H_2O - O)^+$	X	X		246	$(2M + D - D_2O - O)^+$
233	$(2M + H - HCOOH)^+$	X	X	X	235	$(2M + D - HCOOD)^+$
217	$(2M + H - HCOOH - O)^+$	X	X		219	$(2M + D - HCOOD - O)^+$
201	$(2M + H - H_2O - O - CO_2)^+$	X	X		202	$(2M + D - D_2O - O - CO_2)^+$
189	$(2M + H - HCOOH - CO_2)^+$	X	X		191	$(2M + D - HCOOD - CO_2)^+$
173	$(2M + H - HCOOH - O - CO_2)^+$	X	X	X	175	$(2M + D - HCOOD - O - CO_2)^+$
157	$(2M + H - H_2O - O - 2CO_2)^+$	X	X	X	158	$(2M + D - D_2O - O - 2CO)^+$
140	$(M + H)^+$	X	X		142	$(M + D)^+$
130	$(2M + H - H_2O - O - CO_2 - HCN)^+$			X		
124	$(M + H - O)^+$	X	X		126	$(M + D - O)^+$
96	$(M + H - CO_2)^+$	X	X	X		
Negative					*Negative*	
231	$(2M - H - HCOOH)^-$	X	X	X	231	$(2M - D - HCOOD)^-$
187	$(2M - H - HCOOH - CO_2)^-$	X	X	X	187	$(2M - D - HCOOD - CO_2)^-$
154	$(M + O - H)^-$	X	X	X	155	$(M + O - H)^-$
138	$(M - H)^-$	X	X	X	138	$(M - D)^-$
122	$(M - H - O)^-$	X	X	X		
94	$(M - H - CO_2)^-$	X	X	X		

[a]LAMMA-1000. Positive l.m.s. = 6.1×10^8 W cm^{-2}. Negative l.m.s. = 5.6×10^8 W cm^{-2}. [b]LAMMA-1000. Positive l.m.s. = 8.0×10^8 W cm^{-2}. Negative l.m.s. = 5.3×10^8 W cm^{-2}. [c]LAMMA-1000. Positive l.m.s. = 4.0×10^8 W cm^{-2}. Negative l.m.s. = 3.5×10^8 W cm^{-2}. [d]LAMMA-1000. Positive l.m.s. = 8.0×10^8 W cm^{-2}. Negative l.m.s. = 4.0×10^8 W cm^{-2}.

$CO_2)^-$ were observed in the negative-ion l.m. spectra of nicotinic acid (Fig. 1b). The quasimolecular ion $(M-H)^-$ is responsible for the base peak at *m/z* 138 in the spectrum of nicotinic acid *N*-oxide. Loss of O, CO and CO_2 from $(M-H)^-$ results in peaks at *m/z* 122, 110, and 94, respectively.

The ion at *m/z* 154 probably is not a fragment from a cluster ion. Instead, it can be explained as $(M+O-H)^-$ resulting from nucleophilic substitution of an oxygen atom into the pyridine ring. This type of ion-molecule reaction has been reported in chemical-ionization mass spectrometry [16].

The formation of $(M+15)^-$ is confirmed by l.m.s. results for deuterium-exchanged nicotinic acid *N*-oxide (RCOOD), as shown in Table 2. The position of the peak corresponding to $(M+O-H)^-$ is shifted one mass unit higher because of the presence of deuterium in the compound. This is consistent with loss of a ring hydrogen in the substitution reaction.

Assignments for other fragment ions observed for nicotinic acid *N*-oxide are verified by comparison of the l.m. spectra of nicotinic acid *N*-oxide and the deuterium-exchanged isomer (RCOOD). It is readily seen from Table 2 that cluster ions from nicotinic acid *N*-oxide have corresponding peaks one or two mass units higher in the deuterium-substituted isomer. For example, clusters analogous to $(2M+H-H_2O)^+$ and $(2M+H-HCOOH)^+$ are $(2M+D-D_2O)^+$ and $(2M+D-HCOOD)^+$, respectively. The peak corresponding to $(2M+H-HCOOH)^+$ in the *D*-oxide corresponds to $(2M+D-HCOOD)^+$. This indicates that loss of formic acid from the cluster involves abstraction of a ring hydrogen.

It is interesting to compare l.m.s. results for nicotinic acid *N*-oxide with those of its two other isomers, isonicotinic and picolinic acid *N*-oxides. Table 2 shows that, at comparable laser powers, the same major clusters are observed for both nicotinic and isonicotinic acid *N*-oxides in both the positive-ion and negative-ion spectra. In contrast, although no distinction can be found between the negative-ion l.m. spectra of picolinic *N*-oxide and the other two isomers, the positive-ion l.m. spectra of picolinic *N*-oxide shows only three of the cluster ions that are observed for the other two isomers: $(2M+H-HCOOH)^+$, *m/z* 233, $(2M+H-HCOOH-O-CO_2)^+$, *m/z* 173 and $(2M+H-H_2O-O-2CO_2)$ *m/z* 157. These results are summarized in Table 2. The ion *m/z* 130 for picolinic acid *N*-oxide can be explained as $(2M+H-H_2O-O-2CO_2-HCN)^+$. The quasimolecular ion $(M+H)^+$, *m/z* 140, which was detected in both isonicotinic and nicotinic acid *N*-oxides, was not seen in picolinic acid *N*-oxide.

Emission of cluster ions was also observed in the l.m. spectra of amides such as nicotinamide, isonicotinamide, picolinamide and 6-chloronicotinamide; both dimeric and trimeric cluster ions were detected. In contrast to the acid *N*-oxides, where there is some difference between the positive-ion l.m. spectra of picolinic acid *N*-oxide and its other two isomers, both the positive-ion and negative-ion l.m. spectra of picolinamide were found to be almost identical with those of nicotinamide and isonicotinamide. One exception is that the peak at *m/z* 130, $(2M+H-HCOHN_2$

$-HNCO-HCN)^+$, was seen in the positive-ion spectrum of picolinamide. These results are summarized in Table 3. It is worth mentioning that the s.i.m. spectrum of nicotinamide does not show any of the clusters reported here [17].

Figure 3 shows the positive-ion and negative-ion l.m. spectra of 6-chloronicotinamide. Detailed assignments are given in Table 4. In general, peak assignments are readily confirmed by the chlorine isotope patterns. Ions from *m/z* 159 to *m/z* 279 in Fig. 3(a) correspond to positive dimeric cluster ions (Table 4) whereas trimeric clusters, $(3M + H - HCl - 2Cl)^+$ and $(3M + H - 2HCl)^+$, are responsible for the peaks at *m/z* 363, 365 and

TABLE 3

Cluster ions generated by l.m.s. of nicotinamide, isonicotinamide and picolinamide

m/z	Assignment	Nicotinamide[a]	Iso-nicotinamide[b]	Pico-linamide[c]
Positive				
243	$(2M + H - H_2)^+$	X	X	X
200	$(2M + H - HCONH_2)^+$	X	X	X
157	$(2M + H - HCONH_2 - HNCO)^+$	X	X	X
130	$(2M + H - HCONH_2 - HNCO - HCN)^+$			X
123	$(M + H)^+$	X	X	X
106	$(M + H - NH_3)^+$	X	X	X
Negative				
363	$(3M - H - H_2)^-$	X	X	X
320	$(3M - H - HCONH_2)^-$	X	X	X
241	$(2M - H - H_2)^-$	X	X	X
226	$(2M - H - NH_3)^-$	X	X	X
198	$(2M - H - HCOH_2)^-$	X	X	X
121	$(M - H)^-$	X	X	X

[a]LAMMA-1000. Positive l.m.s. = 5.7×10^8 W cm^{-2}. Negative l.m.s. = 1.4×10^9 W cm^{-2}.
[b]LAMMA-1000. Positive l.m.s. = 8.0×10^8 W cm^{-2}. Negative l.m.s. = 1.3×10^9 W cm^{-2}.
[c]LAMMA-1000. Positive l.m.s. 6.9×10^8 W cm^{-2}. Negative l.m.s. = 1.2×10^9 W cm^{-2}.

TABLE 4

Cluster ions generated by l.m.s. of 6-chloronicotinamide[a]

m/z	Assignment	*m/z*	Assignment
Positive l.m.s.[a]		*Negative l.m.s.*	
397,399	$(3M + H - 2HCl)^+$	395,397	$(3M - H - 2HCl)^-$
363	$(2M + H - HCl - 2Cl)^+$	309,311	$(3M - H - 2HCl - 2HNCO)^-$
277,279	$(2M + H - HCl)^+$	275,277	$(2M - H - HCl)^-$
157,159	$(M + H)^+$	155,157	$(M - H)^-$
140,142	$(M + H - NH_3)^+$		

[a]LAMMA 1000: 6×10^8 W cm^{-2}.

397, 399, respectively. In the case of negative-ion mass spectra, in addition to the three cluster ions corresponding to $(3M - H - 2HCl)^-$ with *m/z* 395, 397, $(3M - H - 2HCl - 2HNCO)^-$ with *m/z* 309, 311, and $(2M - H - HCl)^-$ with *m/z* 275, 277, ions at *m/z* 169, 171, 173 and 175 which correspond to $ZnCl_3^-$ were also detected. These ions arise when the laser beam impinges on both the sample (containing chlorine) and the zinc foil supporting the sample.

Cluster formation in hydrochloride salts

Clusters similar to those detected in the l.m. spectra of nicotinic acid were observed for the hydrochloride salts of pyridoxamine and pyridoxine. The spectra of pyridoxamine-2HCl are shown in Fig. 4. Cationic clusters ranging from *m/z* 305 to *m/z* 335 and anionic clusters ranging from *m/z* 285 to *m/z* 469 are observed. The highest mass cation, *m/z* 335, corresponds to $(2M + H - H_2)^+$. Cations at *m/z* 320 and *m/z* 305 can be rationalized as loss of NH_3 and CH_3OH, respectively, from $(2M + H)^+$. The variety of substituent

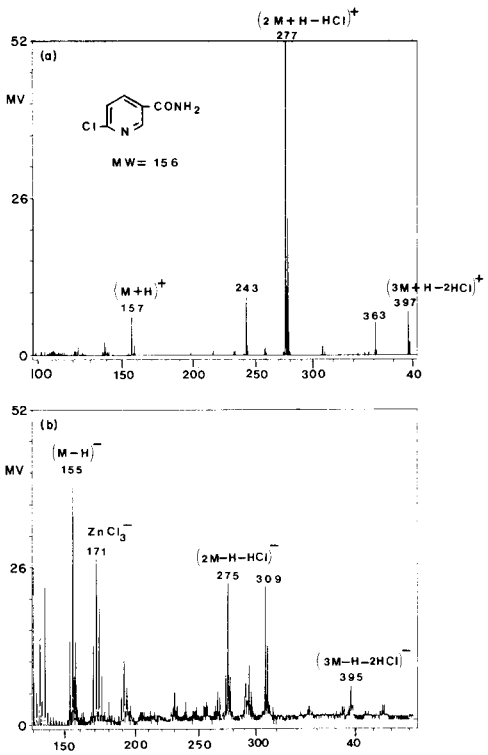

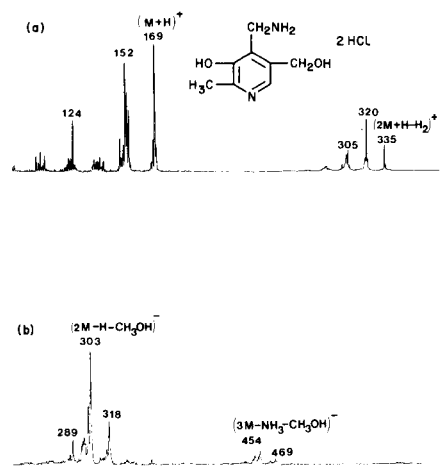

Fig. 3. Laser mass spectra of 6-chloronicotinamide (LAMMA-1000): (a) positive (5.6×10^8 W cm^{-2}); (b) negative (6.0×10^8 W cm^{-2}).

Fig. 4. Laser mass spectra of pyridoxamine 2HCl (LAMMA-500): (a) positive; (b) negative.

groups in pyridoxamine makes definition of unique sets of neutral losses for a particular cluster difficult. Exact mass measurements would be required to distinguish between the possible fragmentation modes in some cases. For example, one could assign *m/z* 305 either to $(2M + H - CH_3OH)^+$ or to $(2M + H - 2CH_4)^+$. The base peak in the positive spectrum corresponds to $(M + H)^+$, *m/z* 169. Loss of NH_3 from this quasimolecular ion results in a peak at *m/z* 152 while consecutive loss of NH_3 and CH_2NH gives rise to the peak at *m/z* 124.

Both dimeric and trimeric anions are observed in the spectra of pyridoxamine dihydrochloride. Although $(2M - H)^-$ was not detected, fragments were seen at *m/z* 469 $(3M - H - CH_4 - H_2O)^-$ and *m/z* 454 $(3M - H - NH_3 - CH_3OH)^-$. Dimeric anions detected included $(2M - H - NH_3)^-$, *m/z* 318; $(2M - H - CH_3OH)^-$, *m/z* 303; $(2M - H - CH_4 - H_2O)^-$, *m/z* 301; and $(2M - H - CH_2NH - NH_3)^-$, *m/z* 289. It is noteworthy that even though the hydrochloride salt of pyridoxamine was studied, ions of the form $C_2A_x^+$ and CA_2^- (C = cation, A = anion) which might be expected on the basis of field-desorption mass spectrometry [22] were not observed.

Pyridoxine hydrochloride differs from pyridoxamine dihydrochloride in that the substituent para to the pyridine nitrogen is CH_2OH instead of CH_2NH_2. Cluster emission was again observed. As seen in Table 5, positive clusters can be explained as dissociation from both $(3M + H)^+$ and $(2M + H)^+$ while negative clusters can be rationalized as fragments of $(2M - H)^-$.

Effect of laser power

Although cluster ion emission is not affected by sample preparation or the direction of laser radiation, it was found to depend somewhat on the laser power density. In general, increasing the laser power increased the size of the clusters observed. For example, only dimeric cluster ions of nicotinic acid were observed at threshold laser power (2×10^8 W cm^{-2}) (Fig. 1a). At higher laser power (1.2×10^9 W cm^{-2}), ions corresponding to the trimeric

TABLE 5

Cluster ions generated by l.m.s. of pyridoxine-HCl[a]

m/z	Assignment	*m/z*	Assignment
Positive l.m.s.		*Negative l.m.s.*	
472	$(3M + H - 2H_2O)^+$	335	$(2M - H - H_2)^-$
456	$(3M + H - 2H_2O - CH_4)^+$	319	$(2M - H - H_2O)^-$
337	$(2M + H - H_2)^+$	303	$(2M - H - CH_3OH)^-$
321	$(2M + H - H_2O)^+$	301	$(2M - H - H_2O - CH_4)^-$
305	$(2M + H - H_2O - CH_4)^+$	168	$(M - H)^-$
287	$(2M + H - 2H_2O - CH_4)^+$		
170	$(M + H)^+$		

[a]LAMMA-1000:7 $\times 10^8$ W cm^{-2}

clusters $(3M + H - HCOOH - 2CO_2)^+$, *m/z* 236, and $(3M + H - HCOOH - CO_2)^+$, *m/z* 280, were detected in addition to the dimeric clusters. Additional fragments from both $(2M + H)^+$ and $(M + H)^+$ were also generated at high laser power (1.2×10^9 W cm^{-2}). Further increase of laser power (1.8×10^9 W cm^{-2}) caused even more fragmentation as well as increasing the intensities of the cluster ions.

A similar effect of laser power was found for negative cluster ions. Results for isonicotinamide are shown in Fig. 5 as an example. As can be seen, clusters containing two isonicotinamide molecules were seen even at threshold laser power (7.0×10^8 W cm^{-2}). The ion at *m/z* 241 corresponds to $(2M + H - H_2)^-$. Loss of NH_3, $HCONH_2$ and both $HCONH_2$ and HNCO from $(2M - H)^-$ resulted in peaks at *m/z* 226, 198 and 171, respectively. Larger clusters [$(3M + H - H_2)^-$, *m/z* 363, and $(3M + H - HCONH_2)^-$, *m/z* 320] were observed when higher laser power was used (1.3×10^9 W cm^{-2})

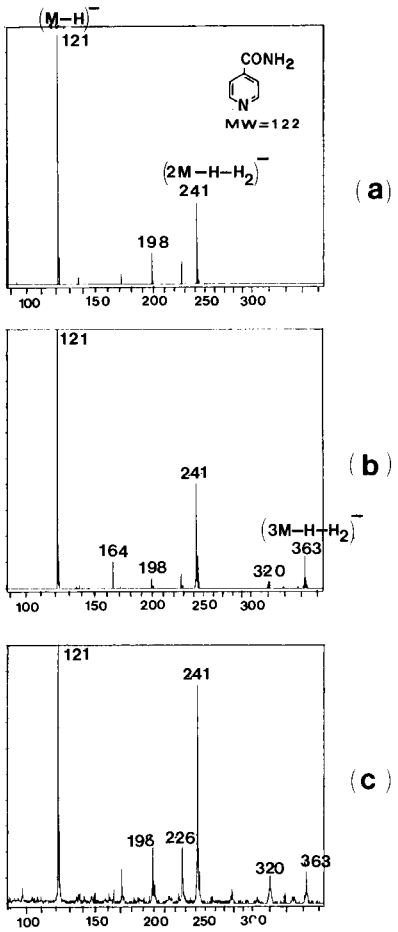

Fig. 5. Negative l.m. spectra of isonicotinamide at different laser powers: (a) 7.0×10^8 W cm^{-2}; (b) 1.3×10^9 W cm^{-2}; (c) 1.6×10^9 W cm^{-2}.

(Fig. 5b). The intensities of these cluster peaks increased with increasing laser power (1.6×10^9 W cm^{-2}) (Fig. 5c).

Comparison with other mass spectral techniques

It is of interest to compare clusters formed in l.m.s. with those observed using other ionization methods. Emission of ions $C_nA_{n-1}^+$ (C = cation, A = anion) is characteristic of field-desorption mass spectra of organic and inorganic salts [18—20]. For example, clusters up to $C_4A_3^+$ were observed in field desorption of dibutyldimethylammonium iodide [19]. Similar species have been generated by secondary ion bombardment of amine salts [21]. For instance, the chloride-bound dimer, $[N(CH_3)_3H]_2Cl^+$ was seen in the s.i.m. spectrum of trimethylamine hydrochloride. These salt clusters are combinations of salt cations and anions, and are distinct from the molecular clusters generated in the l.m.s. of substituted pyridines and their hydrochloride salts. Clusters having somewhat greater similarity to those reported in l.m.s. were observed in the s.i.m. spectra of frozen benzene [22]. Species up to C_{32} ($C_{32}H_8$) were rationalized as fragments of products from ion molecule reactions of $C_6H_6^+$ with vaporized benzene molecules in the near surface or selvage region. In the case of ^{252}Cf plasma desorption, although the cationized cluster $(2M + 4Na - 3H)^+$ was seen for an oligonucleotide, the protonated dimer as well as negative clusters were not detected [23]. In contrast, both $(2M + Na)^+$ and $(2M + H)^+$ were reported in field-desorption analysis of acids [24] (tartaric, maleic acid, etc.). Protonated and deprotonated clusters which retain their molecular character were also generated in chemical ionization spectra [25—28]. For example, ions of composition $(2M + H)^+$ were observed in chemical ionization mass spectra of amino acids [25], alcohols [26], and esters [27]. Similarly, anionic dimers have been formed by negative chemical ionization (n.c.i.) of benzonitrile and several other aromatic nitriles [28]. It is interesting that both aromatic nitriles and arylacetonitriles showed $(M - H)^-$ as the dominant quasimolecular ion, while they differ in the dimeric species formed. The former gave $(2M - H)^-$ ions, but for the latter, dimeric species were radical ions of composition $(2M - 4)^{\cdot-}$ and $(2M - 29)^{\cdot-}$ which were rationalized as $(2M - 2H_2)^{\cdot-}$ and $(2M - H_2 - HCN)^{\cdot-}$. Other peaks detected above $(M - H)^-$ were attributed to radical ions arising by further loss of neutral molecules from $(2M - 4)^{\cdot-}$ and $(2M - 29)^{\cdot-}$ [28]. In addition, chloride associated dimers, $(2M + Cl)^-$, have been observed in n.c.i. mass spectra of aromatic chlorinated pesticides [29].

Comparison of these results with those obtained by l.m.s. indicates that the l.m.s. clusters are comparable to those observed by chemical ionization or field desorption of acids in that they retain their molecular character. However, the l.m.s. clusters are even electron ions, compared to the odd electron clusters formed by negative chemical ionization.

It is not certain how a cluster ion is formed in l.m.s. It could possibly be ejected directly from the sample surface or could be a fragment of a larger cluster which has been desorbed from the surface. Yet it could also be a

product of an ion molecule reaction in a region of high relative pressure generated by laser beam. Since the dense 'cloud' (high pressure region) is only generated at high laser power and the l.m.s. cluster emission was seen even at threshold laser power density, direct ejection seems to be the more likely mechanism. Direct ejection of a cluster from the solid vs. fragmentation of a larger cluster cannot be decided on the basis of the present experiments.

This work was supported by the National Science Foundation under Grant No. CHE8108495. We thank H. Heinen and H. Vogt for their assistance in the work.

REFERENCES

1 M. A. Posthumus, P. G. Kistemaker, H. L. C. Meuzelaar and M. C. Ten Noever deBrauw, Anal. Chem., 50 (1978) 985.
2 K. Balasanmuga, T. A. Dang, R. J. Day and D. M. Hercules, Anal. Chem., 53 (1981) 2296.
3 D. M. Hercules, R. J. Day, K. Balasanmugam, T. A. Dang and C. P. Li, Anal. Chem., 54 (1982) 280A.
4 R. O. Mumma and F. J. Vastola, Org. Mass Spectrom., 6 (1972) 1373.
5 F. J. Vastola, R. O. Mumma and A. J. Pirone, Org. Mass. Spectrom., 3 (1970) 101.
6 R. J. Cotter, Anal. Chem., 52 (1980) 1767.
7 B. Schueler and F. R. Krueger, Org. Mass Spectrom., 15 (1980) 295.
8 F. R. Krueger and K. Wien, Adv. Mass Spectrom., 7 (1978) 1429.
9 H. J. Heinen, S. Meier, A. Vogt and R. Wechsung, Adv. Mass Spectrom., Part A, 8 (1980) 942.
10 J. A. Gardella, Jr., D. M. Hercules and H. H. Heinen, Spectrosc. Lett., 13 (1980) 347.
11 R. Kaufmann, F. Hillenkamp and R. Wechsung, Med. Prog. Technol. 6 (1979) 109.
12 U. Seydel and H. J. Heinen, 6th Int. Symp. Mass Spectrom. Biochem. Med., Venice, 1979.
13 N. Furstenau, F. Hillenkamp and R. Nitsche, Int. J. Mass Spectrom. Ion Phys., 31 (1979) 85.
14 V. S. Ban and B. E. Knox, Int. J. Mass Spectrom. Ion Phys., 3 (1969) 131.
15 A. Benninghoven, Proc. 9th Mat. Res. Symp., April, 1978, NBS, MD.
16 W. J. Bouma and K. R. Jennings, Org. Mass Spectrom., 16 (1981) 331.
17 S. E. Unger, R. J. Day and R. G. Cooks, Int. J. Mass Spectrom. Ion Phys., 39 (1981) 231.
18 H.-R. Schulten and F. W. Röllgen, Angew. Chem. Int. Ed. Engl., 14 (1975) 561.
19 H. J. Veith, Org. Mass Spectrom., 11 (1976) 629.
20 H.-R. Schulten and F. W. Röllgen, Org. Mass Spectrom., 10 (1975) 649.
21 R. J. Day, Ph.D. Thesis, Purdue University, 1980.
22 G. M. Lancaster, F. Honda, Y. Fukuda and J. W. Rabalais, J. Am. Chem. Soc., 101 (1979) 1951.
23 C. J. McNeal and R. D. McFarlane, J. Am. Chem. Soc., 103 (1981) 1609.
24 H. J. Heinen, U. Giessmann and F. W. Röllgen, Org. Mass Spectrom., 12 (1977) 710.
25 P. A. Leclercq and D. M. Desiderio, Org. Mass Spectrom., 7 (1973) 515.
26 F. H. Field, J. Am. Chem. Soc., 92 (1970) 2672.
27 F. H. Field and D. P. Weeks, J. Am. Chem. Soc., 92 (1970) 5621.
28 K. L. Busch, C. E. Parker, D. J. Harvan, M. M. Bursey and J. R. Hass, Appl. Spectrosc., 35 (1981) 85.
29 R. C. Dougherty, J. D. Roberts and F. J. Biros, Anal. Chem., 47 (1975) 54.

Analytica Chimica Acta, 158 (1984) 247—256
Elsevier Science Publishers B.V., Amsterdam — Printed in The Netherlands

X-RAY DIFFRACTOMETRIC DETERMINATION OF SUB-MILLIGRAM AMOUNTS OF HEMATITE BY A SUSPENSION-FILTRATION METHOD WITH SILICON AS INTERNAL STANDARD

TSUTOMU FUKASAWA*, MASAAKI IWATSUKI and LAKSHMAN RAJAPAKSE

Department of Applied Chemistry, Faculty of Engineering, Yamanashi University, Takeda-4, Kofu-shi 400 (Japan)

(Received 25th July 1983)

SUMMARY

Silicon powders of four particle-size ranges were prepared from reagent-grade silicon by the Andreasen pipet method and elutriation. Thin-layer specimens were prepared by a suspension-filtration method using membrane filters. Silicon powder of 1.0—2.5 μm diameter is recommended as internal standard from the study of particle-size effects. Stable suspensions of silicon and hematite were prepared with a 0.05% dextrin solution. Relative standard deviation for determinations by the internal-standard method were <9% for 100 μg of hematite in a mixed powder sample of 600 μg and <5% for 400 μg of hematite in mixed samples of 900—1400 μg. Absorption effects in mixed powders are discussed.

Powder samples such as airborne particulates, iron factory dust and soils contain hematite, magnetite and other crystalline compounds, which have to be measured quantitatively. In previous studies of the characterization of airborne particulates, it has been suggested that small amounts of these compounds may be determined successfully by x-ray diffraction (x.r.d.) examination of thin-layer specimens, after separation and concentration with heavy liquids [1] and by other means [2]. In this paper, a silicon internal standard method is discussed for the determination of sub-mg hematite particles in a simple sample such as that concentrated by heavy liquid separation and other techniques, as a basic study for x.r.d. determination of trace crystalline substances in various powder samples.

Metallic silicon has accurately measured lattice parameters. It does not normally exist in airborne particulates, iron factory dust and many other powder samples. Its powder provides a simple x.r.d. pattern with a limited number of sharp peaks. For these reasons, silicon powder is a convenient external or internal standard for measurements of accurate diffraction angles or lattice parameters of crystalline substances by the powder method [3]. Also it has occasionally been used as an internal standard for the correction of matrix effects in the quantitative x.r.d. analysis of bulk powder samples [4, 5].

No detailed work has been published about the effect of particle size of the powdered silicon in any thin-layer specimen. This paper therefore

0003-2670/84/$03.00 © 1984 Elsevier Science Publishers B.V.

describes the preparation of refined silicon powders with given size ranges, of standard silicon and sample suspensions, and of thin-layer specimens by a suspension-filtration method. It also describes the recoveries of silicon and iron oxides when preparing thin-layer specimens, the particle-size effect of silicon in the thin-layer specimen, the most suitable particle size of silicon for use as the internal standard, and the determination of sub-mg hematite particles in mixed powder samples by the suspension-filtration method with silicon as internal standard. The mixed powder samples used in the investigation (hematite, magnetite, quartz and rutile) were taken as simulated samples of airborne particulates or soils.

EXPERIMENTAL

Pure samples, membrane filters and apparatus

The silicon powder used was of 99.9% purity and 100-mesh (Wako Pure Chemical Industries). Iron oxides, silicon dioxide and titanium dioxide of reagent grade were used as pure samples of hematite and magnetite, quartz and rutile, respectively, after assessment of their purity by x.r.d. The particle sizes (diameters) of the iron oxides, rutile and quartz were <1 μm, 1 μm and 3—5 μm, respectively. An aqueous dextrin solution (0.05%) was prepared.

A MF-Millipore membrane filter GS (0.22-μm pore size, 25-mm diameter; Millipore Corp.) was used in the preparation of the thin-layer specimen, where a detachable glass filter (16 mm i.d.) was used to support the filter.

A Toshiba MX-460G electric mixer and a Shimadarika 100-W ultrasonic bath (3 l) were used for dispersing powder samples in water or the dextrin solution. A Cahn 26 electrobalance and a Yanaco LTA-2S oxygen plasma asher were used for weighing of samples and incineration of the specimens, respectively.

A Rigaku x-ray diffractometer was used together with a standard rotating sample holder. A thin-layer specimen was placed between a standard aluminium holder (50 × 35 × 1.5 mm) with a square aperture (20 × 16 mm) and an aluminium plate (35 × 30 × 0.2 mm) with a round aperture (23-mm diameter), and fixed with scotch tape to keep its surface flat. This assembly was mounted on the rotating sample holder so that x-rays irradiated the specimen through the round aperture, where two 0.15-mm spacers equivalent to the specimen thickness were used to adjust the position of the irradiated surface. The conditions are shown in Table 1. Intensities were recorded on a chart recorder. The intensity of the (101) plane of quartz in a porcelain plate was often measured as a standard for the correction of variation of the intensity of the Cu $K\alpha$ radiation used.

Preparation of standards and specimens

Preparation of refined silicon powders with given size ranges. Silicon powders with particle size ranges of 10—20, 3—5, 1.0—2.5 and 0.4—0.8 μm were prepared as follows. Four powder suspensions with particle diameters

TABLE 1

Conditions for x-ray diffraction

X-ray tube	Cu	Receiving slit	0.3 mm
Voltage	35 kV	Divergence and antiscatter slits	1°
Current	14 mA	Time constant	2 s
Filter	Ni	Scan speed	0.25° min^{-1}
Chart speed	40 mm min^{-1}		

of <20, <5, <2.5 and <0.8 μm were prepared. Silicon powder (3 g, 100 mesh) was ground in a boron carbide mortar until most of the particles were <20 μm. The ground powder was transferred to the electric mixer and agitated in about 150 ml of water for 5 min at 7500 rpm. The resulting suspension was transferred to a 275-ml Andreasen pipet, and water was added up to the top mark. After shaking, the suspension was allowed to stand. Four portions of 10 ml each were successively pipetted into four 100-ml graduated cylinders after the elapse of the times (t) calculated for the particles of 20, 5, 2.5 and 0.8 μm from the Stokes' equation

$$t = 18\eta h/d^2 g(\rho - \rho_0) \quad (1)$$

where t is the time required for the particles of size d and density ρ to travel down a distance h in a liquid of density ρ_0 and viscosity η under gravitational acceleration g. The times were 5.3 min, 82 min, 5.2 h and 48 h for particles of 20, 5, 2.5 and 0.8 μm, respectively. The cylinders contained particles of <20, <5, <2.5 and <0.8 μm, respectively.

Next, smaller particles outside the required range were removed from each of the above suspensions. After addition of 40 ml of water, each cylinder was shaken well and allowed to stand. At the elapsed time calculated from Eqn. 1 for the minimum particle size in each range to be obtained, the upper suspension was pipetted out without disturbing the lower suspension and sediment, and discarded. The times were 16 min, 3.0 h, 27 h and 6.9 days for 10, 3, 1.0 and 0.4 μm, respectively. This process was repeated until the lower suspension was confirmed to be free from particles smaller than the minimum size by microscopic observation, to give a refined suspension with the required particle size range.

The three coarser refined suspensions in the cylinders were transferred to three weighing bottles, and allowed to settle to get refined sediments of the required particle ranges. The supernatant liquid in each bottle was pipetted out and discarded. The refined suspension of the 0.4—0.8 μm particles was centrifuged in a 15-ml centrifuge tube for 30 min at 2000 rpm, and the supernatant liquid was pipetted out and discarded, leaving the refined sediment. The four classes of sediments were dried at 110°C to prepare silicon powders with the required sizes.

Preparation of standard and multicomponent suspensions. A standard suspension of silicon (100 μg ml^{-1}) with a given particle-size range was prepared

by dispersing 25.0 mg of the corresponding refined silicon powder in 0.05% dextrin solution in a 250-ml measuring flask by ultrasonic irradiation for 5 min with occasional shaking by hand. Four kinds of standard silicon suspensions of 100 μg ml^{-1} each were prepared, corresponding to the particle sizes of the refined silicon powders for the study of particle-size effect. Standard hematite and magnetite suspensions (100 μg ml^{-1}) were also prepared by the same procedure. Multicomponent suspensions with different compositions were prepared by use of 0.05% dextrin solution, appropriate aliquots of the standard suspensions, and weighed amounts of coexisting substances. All the suspensions were necessarily subjected to the dispersing procedure just before use.

Preparation of thin-layer specimens. The thin-layer specimen of silicon was prepared by filtering a 10.0-ml aliquot of the silicon suspension through a membrane filter on the detachable glass filter. Many 25-mm diameter specimens with a 16-mm diameter thin layer of silicon were prepared for the studies of recovery and particle-size effects.

A 25-mm diameter specimen with a 16-mm diameter thin layer of multicomponents was prepared by filtering the multicomponent suspension, where the 1.0—2.5-μm silicon was used as the internal standard. Specimens of different compositions were prepared and used for basic studies of the recoveries of silicon and iron oxides in thin-layer specimens, and the effects of x-ray absorption and coexisting substances.

Correction of absorption effect

The observed x.r.d. intensities (I) from hematite in the multicomponent thin-layer specimens were corrected by the well-known equation in the discussion of absorption effects

$$I_c = 2\mu x \operatorname{cosec}\theta I/[1 - \exp(-2\,\mu x \operatorname{cosec}\theta)] \qquad (2)$$

where I_c is the corrected intensity of the hematite at angle 2θ measured for a specimen of thickness x and linear absorption coefficient μ.

Recommended procedure for the determination of hematite in powder samples

A sample obtained by the heavy-liquid separation technique, or other means, is transferred to a 20-ml test tube with the aid of some solvent. A small amount of powder sample (0.1—6 mg) is weighed on the ultramicro balance and transferred to a 20-ml test tube. After adding 10 ml of the standard silicon suspension (1.0—2.5 μm, 100 μg ml^{-1}), it is dispersed by ultrasonic irradiation and shaking, and filtered onto a 25-mm diameter membrane filter to give a 16-mm diameter thin layer. The intensities of the (104) line of hematite and the (111) or (220) line of silicon are measured for the determination of hematite by the internal standard method. The quantity of hematite is found from the average of duplicate measurements by using a calibration graph prepared from standard hematite samples.

RESULTS AND DISCUSSION

Recoveries of silicon and iron oxides in thin-layer specimens

Silicon in silicon specimens. A dried thin-layer specimen of silicon was placed in a small glass pan, and treated in the plasma asher for 1.5 h to incinerate the membrane filter. The residue of silicon was weighed. Other samples of silicon powder weighed accurately were treated in the plasma asher with and without the membrane filter, to test for oxidation of the silicon.

The results for silicon with or without the filter (Table 2) show that silicon powder was not oxidized during the treatment in the oxygen plasma, regardless of the presence of the filter. The results for silicon specimens show good recovery and reproducibility of silicon in the preparation of the thin-layer specimen, irrespective of the particle size. The results also show that homogeneous silicon suspensions were obtained by the ultrasonic agitation, and shaking by hand just before use, irrespective of particle size, and that the prepared silicon thin-layer specimens are applicable to the study of particle-size effects.

Iron oxides and silicon in multicomponent specimens. For iron oxides, a specimen was decomposed in hot (1 + 1) hydrochloric acid and diluted with water. The solution was filtered through a Toyo filter paper no. 7. The residue was used for the determination of silicon as described below. Iron in the filtrate was determined spectrophotometrically with 1,10-phenanthroline. For silicon, the filter paper with the residue obtained by the above procedure was burnt over a Bunsen flame in a platinum crucible and then fused with 100 mg each of sodium and potassium carbonates. The cooled melt was dissolved in 50 ml of water and 3 ml of (1 + 4) hydrochloric acid. Silicon was determined spectrophotometrically as molybdosilicate.

Table 3 shows that the recoveries of silicon and iron oxides were satisfactory for use in the x.r.d. studies. The results also show that silicon and iron

TABLE 2

Results for oxygen-plasma treatment and recovery of silicon

Sample	Particle size (μm)	Si taken (mg)	Mass after treatment (mg)	Mean recovery (%)
Si specimen	3—5	1.00[a]	1.01	101
		1.00[a]	1.01	
	0.4—0.8	1.00[a]	1.01	101
		1.00[a]	1.01	
Si	3—5	1.02	1.01	100
		1.01	1.02	
Si with filter	3—5	1.02	1.03	100
		1.01	1.01	

[a]10.0 ml of standard silicon suspension.

TABLE 3

Recoveries of silicon and iron oxides in preparation of multicomponent specimens

Specimen	Amounts taken (mg)			Other substances added (mg)		Amount found (mg)		Recovery (%)	
	Silicon	Hematite	Magnetite	Quartz	Rutile	Si	Fe	Si	Iron oxides
10	1.00	0.60	0.00	0.0	0.0	0.98	0.40 (0.57)[a]	98	96
11	1.00	0.60	0.20	0.0	0.0	1.02	0.55 (0.78)[a]	102	97
12	1.00	0.40	0.40	3.1	2.2	—	0.56 (0.78)[a]	—	98
13	1.00	0.40	0.40	2.0	0.9	—	0.56 (0.78)[a]	—	98

[a]Numbers in parentheses are the results as iron oxides.

oxides were homogeneously suspended in their standard suspensions by the ultrasonic agitation and shaking.

Effect of particle size of silicon on its line intensities and width

The line intensities and widths for the (111) and (220) planes of silicon were measured under rotating or stationary conditions for seven thin-layer specimens of silicon for each particle size. The integral intensity was calculated from peak intensity multiplied by the peak width at half maximum.

Figure 1 shows the relationships between average peak intensity, integral intensity and peak width at half maximum intensity vs. particle size of silicon for the rotating specimens (the intensities and widths were the same for rotating or stationary specimens, except for their standard deviations, as

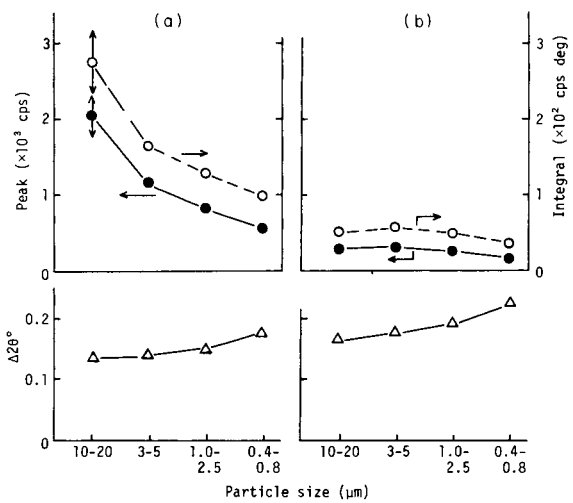

Fig. 1. Relations between average peak and integral intensities or width at half maximum (Δ $2\theta°$) and particle size of silicon in rotating specimens. (a) (111) plane; (b) (220) plane. (•) Peak intensities; (○) integral intensities; (Δ) width at half maximum.

shown later). For the (111) plane, the peak and integral intensities decreased greatly as the particle size decreased. For the (220) plane, the intensities were weak and their decreases were significant only in the finest powder. The widths at half maxima of both planes increased with decreasing particle size, especially for the finest powders. The increase in line width shows that the larger decrease of intensities with the finer powders is due to increased disorder in the crystals or an increase in the number of sub-μm particles caused by grinding, or both, which is unavoidable.

Figure 2 shows the relations between the relative standard deviation (r.s.d.) of the intensity or width at half maximum intensity vs. particle size for both stationary and rotating specimens. The r.s.d. values for the peak and integral intensities for the (111) and (220) planes were almost the same for each particle size. Those for the coarsest powder, which were decreased somewhat by specimen rotation during measurements, were especially large (>10%). This shows the sensitivity of the intensities to the particle-size effect and the preferred orientation of the crystallites. The r.s.d. values for <5-μm silicon were less than 6% for both planes, and the effect of specimen rotation on intensity was not significant. The r.s.d. values for peak and integral intensities for 1.0—2.5-μm particles were less than 3%, irrespective of the rotation of the specimen and the identity of the diffracting planes. This suggests that there is little or no particle-size effect. The r.s.d. of the peak width measurements is also shown in the figure, because the width was used for the calculation of the integral intensities.

Silicon powder of 1.0—2.5-μm particle size is recommended for use as the internal standard, because of the small r.s.d. of intensity measurements and the moderate intensity.

Though either peak or integral intensities can be used for accurate determinations, measurements of the former are easier than those of the latter.

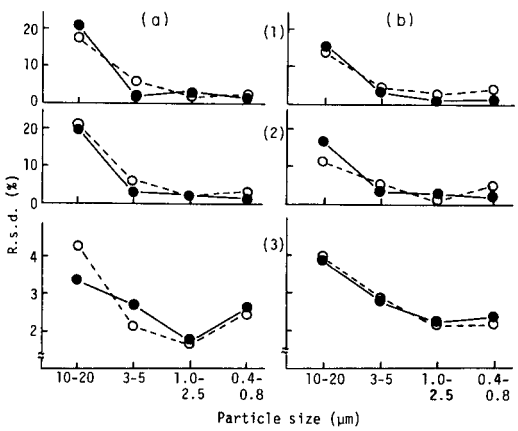

Fig. 2. Relations between particle size of silicon and r.s.d. of: (1) peak intensity; (2) integral intensity; (3) width at half maximum; (•) (111) plane; (○) (220) plane. Conditions: (a) stationary; (b) rotating.

Either the (111) or (220) line should be used, depending on the lines of the substance to be determined and the matrix components.

Effects of x-ray absorption and coexisting substances

Figure 3A shows the relationship between the average peak intensity for the (104) plane and the quantity of hematite in thin-layer specimens of different compositions, prepared using the standard and multicomponent suspensions. Figure 3B shows the relation between the quantity of hematite and the intensity, corrected for the absorption effect, for the same data. The different slopes of the lines in Fig. 3A show that the peak intensity of hematite was changed markedly by the presence of other substances. However, correction of the absorption effect considerably decreased the differences, and the plots were converted into a single line, as shown in Fig. 3B. The r.s.d. for the values shown for 400 μg of hematite was 6.8%. These results show that the major cause of the difference between the slopes in Fig. 3A is absorption, and that this effect should be considered carefully even for quantitative x.r.d. of thin-layer specimens.

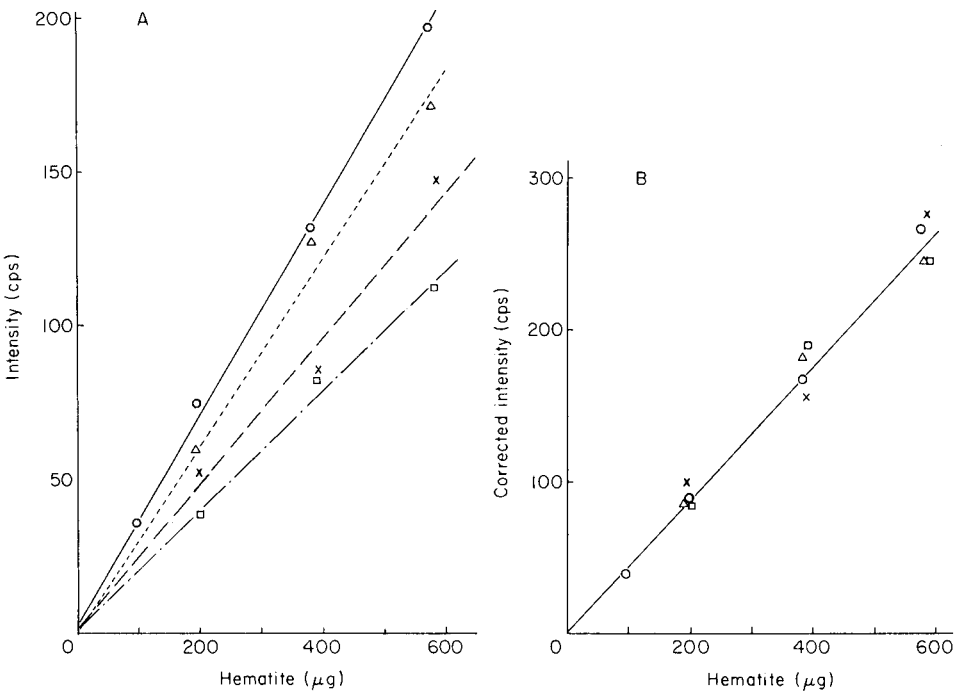

Fig. 3. Relations between (104) peak intensity and quantity of hematite with the following additives: (○) none; (△) 0.2—0.6 mg of magnetite; (×) 0.2—0.6 mg of magnetite, 2 mg of quartz and 1 mg of rutile; (□) 0.2—0.6 mg of magnetite, 3 mg of quartz and 2 mg of rutile. All specimens contained 1.00 mg of silicon; each point is the mean of 2 results. (A) Without correction; (B) with correction for the absorption effect. The least-squares line equation is $y = 0.443x + 1$, with $\sigma_x \bar{x} = 6.8\%$.

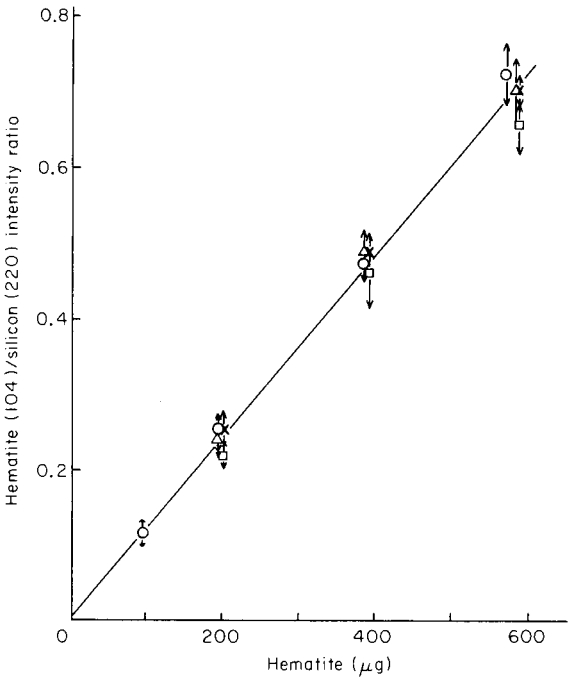

Fig. 4. Relation between hematite (104)/silicon (220) peak intensity ratio and quantity of hematite. For symbols, see Fig. 3. Least squares line: $y = 0.00120x - 0.01$; $\sigma_x/\bar{x} = 4.8\%$; arrows show the range of duplicate measurements.

Figure 4 shows the relationship between the hematite (104)/silicon (220) peak intensity ratio and the quantity of hematite in thin-layer specimens of different compositions. In this case also, the average of duplicate measurements was used. The absorption effect was eliminated by use of the silicon internal standard. The relative standard deviation was 4.8% for 400 μg of hematite, which was better than the standard deviation obtained above from the corrected absolute intensity.

TABLE 4

Compositions of mixed powder samples

Sample	Compounds taken (mg)				
	Hematite	Magnetite	Quartz	Rutile	Total
1	0.101	0.10	0.30	0.10	0.60
2	0.403	0.10	0.30	0.10	0.90
3	0.401	0.20	0.60	0.20	1.40
4	0.403	0.20	0.60	0.0	1.20

TABLE 5

Determination of hematite in mixed samples by intensity ratio measurements [hematite (104)/silicon(111) or (220)]

Sample	Si (111)			Si (220)		
	Hematite found (mg)		Error (%)	Hematite found (mg)		Error (%)
	Mean	Range		Mean	Range	
Peak ratios						
1	0.109	0.002	8	0.110	0.001	9
2	0.410	0.010	2	0.406	0.002	1
3	0.416	0.017	4	0.402	0.045	0
4	0.410	0.010	2	0.398	0.002	−1
Integral ratios						
1	0.104	0.000	3	0.110	0.005	9
2	0.396	0.017	−2	0.406	0.008	1
3	0.399	0.008	−1	0.404	0.041	1
4	0.420	0.015	4	0.410	0.010	2

Determination of sub-mg amounts of hematite in prepared samples

Several powder samples were prepared by mixing weighed amounts of powdered hematite, magnetite, quartz and rutile, and were analyzed by the recommended procedure. Table 4 shows the compositions of the mixed powder samples. Table 5 shows the results for duplicate measurements on each specimen. The errors were independent of whether peak or integral intensity was measured and which plane was used; they were $<9\%$ for 100 μg of hematite and $<5\%$ ($\leqslant 2.4\%$ mean) for 400 μg.

This work was supported by a Grant-in-Aid for Scientific Research from the Ministry of Education, Japan.

REFERENCES

1 T. Fukasawa, M. Iwatsuki, S. Kawakubo and K. Miyazaki, Anal. Chem., 52 (1980) 1784.
2 T. Fukasawa, in Special Project Research on Detection and Control of Environmental Pollution, Steering Group of the Special Project Research Supported by the Ministry of Education, Japan, Vol. 1, 1979, p. 38.
3 G. D. Rieck and K. Lonsdale, in C. H. MacGillavry and G. D. Rieck (Eds.), International Tables for X-ray Crystallography, Vol. 3, Kynoch Press, Birmingham, 1968, p. 122.
4 H. J. Thomas, A. G. Alvarez and E. Pereira, Verres Refract., 25 (1971) 18.
5 A. A. Tabikh and R. J. Weht, Cem. Concr. Res., 1 (1971) 317; Cem. Concr. Res., 2 (1972) 159.

Analytica Chimica Acta, 158 (1984) 257—265
Elsevier Science Publishers B.V., Amsterdam — Printed in The Netherlands

EVALUATION AND CHARACTERIZATION OF A COMMERCIAL ZEEMAN-MODULATED TUNGSTEN-STRIP ELECTROTHERMAL ATOMIC ABSORPTION SPECTROMETER

D. C. GREGOIRE* and G. E. M. HALL
Geological Survey of Canada, 601 Booth Street, Ottawa, Ontario K1A OE8 (Canada)
(Received 1st August 1983)

SUMMARY

The operating parameters and the quantitative characteristics of an AAZ-2 Zeeman-modulated tungsten-strip atomic absorption spectrometer are reported. The figures of merit for Ag, Au, Cd, Co, Cu, Fe, Mn, Ni, Pb, Tl, and Zn are reported. Detection limits obtained with the AAZ-2 were comparable to those obtained with other metal atomizers reported in the literature. A maximum heating rate of 12 K ms^{-1} was measured for the tungsten-strip atomizer.

Since their introduction, electrothermal atom sources in atomic absorption spectrometry have enjoyed great popularity and widespread application in trace metal determinations. Hundreds of papers have appeared on all aspects (theoretical and practical) of electrothermal atomization with various forms of graphite as substrate material. A much smaller, but still impressive body of literature exists on the use of metal atomization surfaces. All-metal atomizers in the form of filaments, ribbons, tubes, etc., have been reported; substrate materials used for these atomizers include metals such as Pt [1], W [2, 3], Mo [4—6] and Ta [6—8]. Significant improvements in performance over graphite atomizers have been reported for the determination of lead [2]. Aggett and Sprott [7] found an improvement in sensitivity for many metals including Al, Cr, Cu, Au, Pb, and Ag, by using a tantalum rather than a graphite atomization surface.

An alternative to atomizers made entirely of metal has been the use of metal collars or linings placed inside the graphite tube. Renshaw [9] used a tantalum foil lining and reported a 20-fold increase in sensitivity for barium compared to that obtained on a graphite surface. This technique was successfully applied to the determination of barium in gunshot residues [10]. A tungsten collar inserted inside an HGA-70 graphite atomizer increased sensitivity in 10 of 16 metals studied by Wall [11]. L'vov and Pelieva [12] described the use of a tantalum foil-lined HGA-76B graphite atomizer; enhancement factors of up to 10 were reported for Ag, Al, Ba, Cu, Mn, Ni, Sn, Sr, Ti, and Zr. The sensitivities for yttrium and some rare earth elements were increased by factors up to 100.

0003-2670/84/$03.00 © 1984 Elsevier Science Publishers B.V.

Among the advantages attributable to metal atomizers are simplicity of design, interchangeability of atomizers made from different metals to suit specific applications, no cooling water requirement (depending on design), low power requirement, very high heating rates, low chemical reactivity of substrate material, and low background emission (compared to graphite) during atomization in the 250—350-nm spectral range. Some serious disadvantages include the possibility of formation of involatile intermetallic compounds between the analyte and the substrate and a low mechanical resistance of the atomizer after repeated firings.

Despite the impressive results obtained on laboratory instrumentation, the commercial development of metal atomizers has proceeded slowly. It is possible that the popular demand for these atomizers has been dampened by reports of serious interference effects [6, 7, 13] or the lack of information available concerning the fundamental processes leading to atom formation that predominate in metal atomizers.

Until recently, the mechanism of atom formation in metal atomizers had been considered by only a few authors [4, 5, 7]. Renewed interest in metal atomization surfaces has led to studies such as the one by Wahab and Chakrabarti [14] on the mechanism of atom formation of yttrium on tantalum and tungsten surfaces. Gregoire and Chakrabarti [15] determined the mechanism of atom formation of U, V, Ni, Mn, Cu, and Mg in a graphite atomizer lined with tantalum foil. With the exception of copper, free metal vapour was produced by the dissociation of metal oxides in the gas phase. These results support the conclusions reached by Aggett and Sprott [7]. In their study, Suzuki and Ohta [4] concluded that analyte reduction by the substrate (Mo) was instrumental in producing free atoms of Cu, Se, Te, Sn, and Sb. Cobalt, Mn and Pb were produced by the thermal dissociation of metal oxide.

The development of a tungsten tube atomizer by Sychra and co-workers [3, 16, 17] has led to the commercial production of the WETA tungsten tube atomizer (Kovo, Prague, Czechoslovakia). The work of Vyskocilova et al. [16] established that, in this atomizer, free-metal vapour for Al, Ba, Co, Pb, Ni, and V was mainly produced by the thermal dissociation of metal oxide (or hydroxide) when atomization took place in an argon atmosphere.

Another instrument now available is the Scintrex AAZ-2 Zeeman-modulated atomic absorption spectrometer (Scintrex, Concord, Ontario, Canada). Originally introduced as a field-portable instrument to be used in geochemical exploration applications, the AAZ-2 is also a valuable laboratory tool. This paper reports on the operating characteristics and the quantitative performance of the AAZ-2 for a series of eleven elements important in geochemical exploration.

EXPERIMENTAL

Apparatus

A Scintrex AAZ-2 Zeeman-modulated atomic absorption spectrometer interfaced with an Apple II+ computer was used for all measurements. The single-beam instrument consists of: (1) a tungsten strip atomizer located between two poles of an electromagnet used to provide the Zeeman modulation field (14 kgauss), (2) double convex optics, (3) an off-axis Ebert-type monochromator, with a grating ruled at 2360 grooves mm^{-1} (blaze wavelength of 280 nm) and with a reciprocal linear dispersion of 4.3 nm mm^{-1}, and (4) a Hamamatsu R106 photomultiplier tube. The selection of wavelength in the range 180—400 nm was accomplished by using a calibrated micrometer mounted on the side of the monochromator housing. The slit was fixed at 2.2 nm.

A detailed view of the atomizer workhead and tungsten strip is shown in Fig. 1. The tungsten atomizers were made from high-purity tungsten strip, 6 mm in width and 0.085 mm in thickness.

The only modification made to the instrument comprised placing a 1-mm diameter aperture on either side of the atomizer workhead. This was done to prevent resonance radiation that had not passed through the sample zone from reaching the detector.

Reagents

All chemicals were of reagent-grade purity. Stock solutions (1000 mg l^{-1}) for each metal studied were obtained from Fisher Scientific with the exception of the silver solution (J. T. Baker). The gold stock solution was prepared by dissolving gold chloride (J. T. Baker) in 0.1 M hydrochloric acid. Stock thallium solution was prepared by dissolving thallium sulfate (Fisher Scientific) in distilled water. All other solutions were in the nitrate form with the exception of iron which was prepared as the chloride. High-purity argon used as a sheath gas was passed through a Model 6406 (Matheson Co.) gas purifier to remove traces of water and oxygen. The presence of water and oxygen in the argon gas accelerates the deterioration of the tungsten atomizer. Unless otherwise stated, an argon flow rate of 600 ml min^{-1} was maintained.

Solutions were delivered to the atomizer by means of a 10-μl Eppendorf pipette fitted with disposable plastic tips.

Fig. 1. Atomizer workhead and tungsten strip.

Procedures

Temperature measurement. Equilibrium surface temperatures in the range up to 1300°C were measured with a Keithley Model 871 digital thermometer equipped with a NiCr/NiAl thermocouple. Temperatures in the range 1300—2500°C were estimated using the melting points of pure metals (as powders). The ashing control of the AAZ-2 was calibrated in this way as well as the maximum atomization temperatures by increasing the instrument setting until the metal powder contained in the atomizer became fused.

Estimation of heating rates. The heating rate of the atomizer could not be measured directly by the use of an optical pyrometer because the emissivity of the tungsten surface changes significantly as its temperature is increased. The physical and chemical state of the tungsten surface is uncertain, thus making the calibration of an optical pyrometer or other optical device difficult.

The appearance temperatures of certain elements atomized on metal surfaces can be used as a probe for the estimation of the heating rate provided that an accurate measurement of the appearance time can be made. For this study, the appearance temperatures for cadmium and zinc [7] atomized on a tantalum surface were used to determine the heating rate of the atomizer. Aggett and Sprott [7] found the appearance temperatures of cadmium and zinc to be 300°C and 820°C, respectively. Studies [7, 18] have shown that the mechanism of atom formation for these elements proceeds via the thermal decomposition of the oxide or the chloride in the gas phase. Tungsten and tantalum have also been shown to behave similarly as atomization surfaces for many elements [8, 14] and thus it is reasonable to conclude that both systems would give the same appearance temperatures for cadmium and zinc.

The appearance time was measured by determining the time, after the start of the atomization cycle, that a perceptible signal could be measured above the baseline noise. The appearance times of both cadmium and zinc were determined at the same instrument setting and the difference (ms) was divided into the difference in appearance temperatures for the two metals to give the heating rate.

RESULTS AND DISCUSSION

Effects of heating rates

The effects of atomizer heating rates on analyte absorbance pulses are well recognized [19, 20]. The heating rate is the controlling factor for analyte atom production as well as many processes responsible for the removal of atoms from the sample volume [17]. Factors which affect the dependency of peak absorbance on the heating rate include the volatility of the analyte and/or analyte atom precursors, the design of the atomizer, and the time constant of the electronic measurement system. The AAZ-2 time constant

is limited by the half-cycle of the modulation frequency of the Zeeman magnet (10 ms).

Because, in most atomizer systems, the peak absorbance marks the point of balance between the rate of production and loss of free atoms, the heating rate will affect both the peak absorbance and the shape of the absorption pulse.

The transient absorption pulses for a series of elements of varying volatilities over a wide range of heating rates were studied. The atomization times (τ_1) are presented in Table 1 and residence times (τ_2) are presented in Table 2 for five elements.

Before the pulse characterization times obtained on the AAZ-2 and the tungsten tube atomizer [17] are compared, a brief comparison of the two atomizers should be given. The tungsten tube atomizer [17] is made from two profiled tungsten strips which form a cylindrical tube 10 mm in length with an internal diameter of 3.5 mm. In contrast, the AAZ-2 atomizer is open above the atomization surface and is 6 mm in width. It would be reasonable to expect that the partly enclosed AAZ-2 would give experimental residence times that are much shorter than those reported for the tube atomizer [17].

A comparison of the results obtained for cadmium in both atomizers showed that the atomization times are shorter and the residence times

TABLE 1

Experimental atomization time

Heating rate (K ms^{-1})	τ_1 (ms)				
	Mn	Ni	Cu	Zn	Cd
2.2	—	—	—	240	130
3.3	—	380	330	120	95
4.8	—	230	210	90	75
6.8	470	190	175	80	60
9.1	270	150	145	75	45
12	215	140	130	55	40

TABLE 2

Experimental residence time

Heating rate (K ms^{-1})	τ_2 (ms)				
	Mn	Ni	Cu	Zn	Cd
2.2	—	—	—	150	100
3.3	—	—	250	85	75
4.8	—	265	135	70	55
6.2	430	215	95	60	45
9.1	180	175	85	50	40
12	125	125	65	40	30

are greater for the AAZ-2 than for the tube atomizer. These unexpected results can be explained as follows. Because the peak of the absorption pulse is the point of balance between the rate of atom formation and those processes (diffusion, convection, etc.) responsible for atom loss, any changes in these processes will change the relative position of the pulse peak. For the AAZ-2, the partly open nature of the atomizer and the relatively narrow width of the tungsten strip should cause the residence time to be less than that observed in a fully enclosed atomizer of greater width. However, in the AAZ-2, it is possible that atomization of the analyte continues beyond the pulse peak or that analyte vaporized at the beginning of the atomization cycle is deposited on colder zones of the atomizer and vaporized again as these zones reach the appearance temperature of the analyte. These two factors would cause the atomization time to be less and the residence time to be greater than their actual theoretical values.

Figure 2 is a plot of the peak absorbance as a function of the heating rate. As the heating rate of the atomizer is increased, there is a rapid rise followed by a levelling off at higher heating rates. For the more volatile elements, the point at which the peak absorbance remains constant with increasing heating

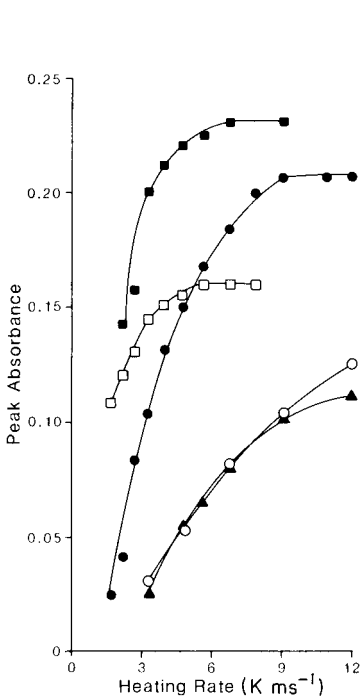

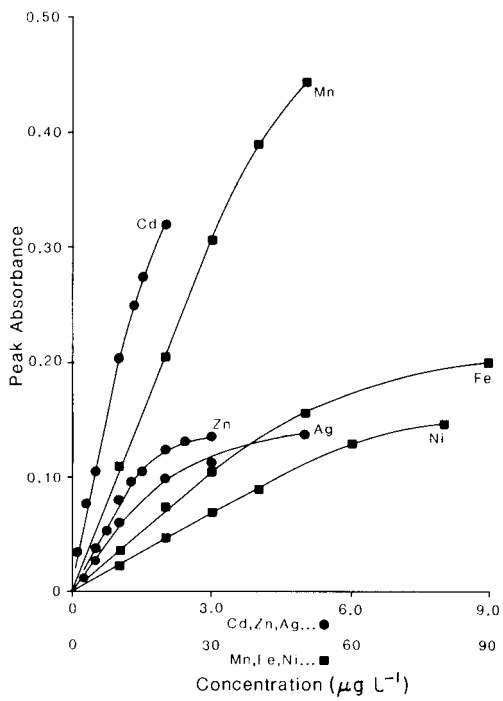

Fig. 2. Effect of heating rate on peak absorbance: (○) Ni; (▲) Co; (■) Cd; (●) Cu; (□) Zn.

Fig. 3. Typical calibration curves obtained on AAZ-2: (●) upper abscissa; (■) lower abscissa.

rate occurs at lower heating rates than for less volatile elements. For example, for cadmium and zinc, this point occurs at a heating rate of about 6 K ms^{-1}, whereas for copper, peak absorbance levels off at a heating rate of 9 K ms^{-1}. The apparent reduction in slope of the curves in Fig. 2 has been attributed to an increase in the diffusional loss of atoms from the analytical volume as the heating rate is increased [18]. It is probable that at even higher heating rates these curves would eventually bend downward toward the abscissa. This loss in sensitivity, however, could greatly be outweighed by a decrease or even elimination of interference effects at these high rates of heating [19].

Quantitative performance

Table 3 lists the figures of merit for eleven elements atomized under optimum experimental conditions. The AAZ-2 atomizer reached a maximum temperature of 2700 K when a heating rate of 12 K ms^{-1} was selected. The maximum temperature of the atomizer was limited by the maximum input power to the atomizer (250 W).

The detection limits (3 s.d.) were calculated for a 10-μl sample injection volume. Up to 50 μl can be accommodated by the atomizer and thus even lower detection limits (concentration) should be attainable. Detection limits obtained on the AAZ-2 were generally about an order of magnitude better than those obtained on the tungsten ribbon atomizer of Hwang et al. [21] and inferior by the same degree to those obtained by Suzuki and Ohta [4] in a molybdenum microtube atomizer. The quantitation of molybdenum was attempted but the sensitivity obtained was very low because of interaction of molybdenum with tungsten metal to form an intermetallic com-

TABLE 3

Figures of merit for some metals atomized under optimum conditions

Element	Wavelength (nm)	Atomization temp. (K)	Heating rate (K ms^{-1})	Detection limit[a] ($\mu g\ l^{-1}$)	Characteristic concentration (pg/1% absorption)
Ag	328.1	2700	12	0.08	1.0
Au	242.8	2600	11	0.15	2.2
Cd	228.8	2050	5.7	0.05	0.2
Co	240.7	2700	12	0.50	9.8
Cu	324.8	2450	9.1	1.0	2.0
Fe	248.3	2700	12	4.0	9.2
Mn	279.5	2700	12	0.20	1.8
Ni	232.0	2700	12	6.0	20
Pb	283.3	2050	5.7	0.70	8.8
Tl	276.8	2700	12	0.90	11.7
Zn	213.9	1650	3.3	0.20	0.6

[a] 10-μl sample volume.

pound or refractory alloy. Interestingly, nickel was easily quantified at a tungsten surface, but severely depressed when atomized at a tantalum surface [15].

Figure 3 presents typical calibration curves for six elements. The linear ranges for these elements are fairly typical for electrothermal atomization devices.

Performance of tungsten atomizer

The useful lifetime of the tungsten strip atomizer varies significantly with the heating program used. For relatively low atomizer temperatures, the useful lifetime is about 200 firings. For an element such as nickel, for which high atomization temperatures are required, atomizers can be used for about 100 firings. Tungsten strips for the AAZ-2 are easily replaced and are available for about one tenth the cost of graphite tubes. No memory effects were observed for any of the eleven metals studied when the atomization time (i.e., duration of atomization cycle) was $\geqslant 3$ s. Solutions containing 100 mg l^{-1} metal were run without any carry-over to subsequent firings.

The lifetime of the tungsten strip can be seriously affected by several factors. The quality of the purge gas is very important. The removal of oxygen and water from the argon gas reduced the amount of tungsten oxide formed on the poles of the Zeeman magnet opposite the surface of the tungsten strip. However, the accumulation of a smaller amount of oxide persisted even when a gas scrubber or when argon containing 10% hydrogen was used.

The loss of metal opposite the magnet poles on the surface of the atomizer (about 5 mm above the sampling surface on both sides) causes an eventual thinning of the material. The result is that electrothermal heating of the thinned areas occurs in preference to the area where the sample is located. Hence, the response sensitivity can decrease by 50% over 100 firings. Frequent recalibration of the instrument is necessary to compensate for the gradual decrease in sensitivity. Periodic cleaning of the magnet poles as well as the use of a gas purifier are effective in controlling this problem.

REFERENCES

1 M. P. Bratzel, Jr., R. M. Dagnall and J. D. Winefordner, Anal. Chim. Acta, 48 (1969) 197.
2 J. E. Cantle and T. S. West, Talanta, 20 (1973) 459.
3 V. Sychra, D. Kolihova, O. Vyskocilova and R. Hlavac, Anal. Chim. Acta, 105 (1979) 263.
4 M. Suzuki and K. Ohta, Prog. Anal. At. Spectrosc., 6 (1983) 49.
5 T. Hasegawa, M. Yanagisawa and T. Takeuchi, Anal. Chim. Acta, 89 (1977) 217.
6 N. S. McIntyre, M. G. Cook and D. G. Boase, Anal. Chem., 46 (1974) 1983.
7 J. Aggett and A. J. Sprott, Anal. Chim. Acta, 72 (1974) 49.
8 T. Takeuchi, M. Yanagisawa and M. Suzuki, Talanta, 19 (1972) 465.
9 G. D. Renshaw, At. Absorpt. Newsl., 12 (1973) 158.

10 J. H. Sherfinski, At. Absorpt. Newsl., 14 (1975) 26.
11 C. D. Wall, Talanta, 24 (1977) 755.
12 B. V. L'vov and L. A. Pelieva, Can. J. Spectrosc., 23 (1978) 1.
13 M. P. Newton and D. G. Davis, Anal. Chem., 47 (1975) 2003.
14 H. S. Wahab and C. L. Chakrabarti, Spectrochim. Acta, Part B, 36 (1981) 475.
15 D. C. Gregoire and C. L. Chakrabarti, Spectrochim. Acta, Part B, 37 (1982) 611.
16 O. Vyskocilova, V. Sychra, D. Kolihova and P. Puschel, Anal. Chim. Acta, 105 (1979) 271.
17 P. Puschel, Z. Formanek, R. Hlavak, D. Kolihova and V. Sychra, Anal. Chim. Acta, 127 (1981) 109.
18 D. C. Gregoire, C. L. Chakrabarti and P. C. Bertels, Anal. Chem., 50 (1978) 1730.
19 C. Riandey, R. Gavinelli and M. Pinta, Spectrochim. Acta, Part B, 35 (1980) 765.
20 R. E. Sturgeon, C. L. Chakrabarti and C. H. Langford, Anal. Chem., 48 (1976) 1792.
21 J. Y. Hwang, C. J. Kokeler and D. A. Ullucci, Anal. Chem., 44 (1972) 2018.

Analytica Chimica Acta, 158 (1984) 267—276
Elsevier Science Publishers B.V., Amsterdam — Printed in The Netherlands

AN ECONOMICAL, LOW-POWER, INDUCTIVELY-COUPLED PLASMA DISCHARGE SYSTEM FOR RESEARCH AND INSTRUCTIONAL APPLICATIONS

G. MARK ALLEN and DAVID M. COLEMAN*

Department of Chemistry, Wayne State University, Detroit, MI 48202 (U.S.A.)

(Received 8th August 1983)

SUMMARY

Design and construction of an economical radio-frequency generator and impedance matching network for inductively-coupled plasma emission spectrometry are described. The generator was made from radio-kit assemblies and the impedance-matching network from conventional electronic components. Comparisons with commercially available instrumentation are discussed with respect to performance, cost, and operation. Characteristics of the system include (discontinuous) burst operating conditions, low power, and low argon consumption.

Inductively-coupled plasma emission spectrometry (i.c.p.e.s.) has become increasingly important as an effective technique for simultaneous quantitation of multiple elements [1]. Because of the widespread acceptance of this method, much emphasis has been directed toward development of methodology and applications [2]. In contrast, there is less published information on advances in instrumental design. Most of such papers have focussed on modifications to the impedance-matching network and to the discharge apparatus. The generator itself has received surprisingly little attention since the development and marketing of a popular high-power, crystal-controlled, air-cooled unit several years ago. Universal acceptance of the conventional i.c.p. has been hindered by excessive energy requirements and by high argon consumption. In addition, spectroscopists interested in establishing i.c.p. technology are often limited by the required initial expense.

The efforts reported here stem directly from research which requires the availability of multiple i.c.p. generator units. This research includes investigation of several approaches to segregated sampling/excitation spectrometry [3]. The cost of such instrumentation, in commercial form, prompted this work.

This paper describes the design and fabrication of an inexpensive generator and impedance-matching network which are used in conjunction with a low-power torch assembly with low argon consumption recently reported by Rezaaiyaan et al. [4]. These new torches are easily ignited and support low-power (250—500 W) discharges. The system reported here can be fabricated

0003-2670/84/$03.00 © 1984 Elsevier Science Publishers B.V.

from components for approximately 10—20% of the cost of commercially available systems. Many chemists are not skilled in the fabrication of generator and impedance matching circuitry. Accordingly, the design criteria included the utilization of easily assembled radio-generator and power-amplifier kits wherever possible. A detailed description of the resulting instrumentation is provided. A new operational method called burst mode, as well as design compromises are discussed. Preliminary data are presented in an effort to assess quantitative potential. Finally, operation and performance are compared to commercial instrumentation under identical conditions.

INSTRUMENTATION

An i.c.p. system is comprised of several discrete subassemblies including a radiofrequency generator, impedance-matching network, discharge apparatus, feed optics, monochromator, and detection electronics. This arrangement is shown schematically in Fig. 1A. The first three assemblies are the focus of this investigation and are discussed in detail.

Radiofrequency generator

The radiofrequency generator was assembled with modular components, integrated in a manner similar to commercial generators. These modules include the exciter/driver and amplifier stages.

The exciter/driver stage is a Heath (Division of Veritechnology Electronic Crop., P.O. Box 167, St. Joseph, MI 49085) radiotransmitter (Model HX-1681) and power supply (Model PS-23). Both are available in kit form. Specifications are summarized in Table 1. The variable-frequency oscillator (v.f.o.) includes a field-effect transistor used in a Hartley [5] configuration. Output from the v.f.o. is coupled to the heterodyne frequency oscillator circuit (h.f.o.) through a series of buffer stages and low-pass filters with a resultant frequency range of 5.0—5.5 MHz. The h.f.o. circuit uses piezoelectric crystals in a Colpitts configuration [5]. Each normal frequency range is derived from an individual crystal corresponding to the appropriate band. The v.f.o. and h.f.o. signals are combined in a double-balanced mixer

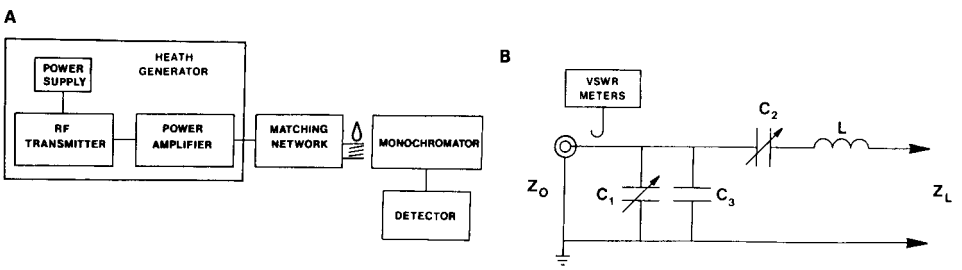

Fig. 1. Block diagrams of (A) basic i.c.p. instrumentation; (B) modified Heath impedance-matching network.

TABLE 1

Transmitter (exciter) specifications.(Heath Electronics, Model HX1681)

RF power output	100 W (80—15 m), 75 W (10 m)
Output impedance	50 ohm
Frequency coverage	3.5—4.0, 7.0—7.5, 14.0—14.5, 21.0—21.5, (28.0—28.5) MHz (27.0—27.5 MHz as modified)
Mode of operation	CW (keying)
Power requirements (PS23 power supply)	120 VAC 50/60 Hz, 350 W

and the difference frequency is coupled to the driver circuit. This circuit amplifies the signal, through a tunable output tank, to a level suitable to drive the amplification stage. The final stage is a parallel amplifier tube arrangement functioning as a class AB amplifier with a tunable output tank.

Transmitter circuitry was modified to produce an output frequency of 27.12 MHz in accordance with Industrial Scientific and Medical (ISM) standards established by FCC regulations. This modification included replacement of the standard 33.5-MHz crystal with a 32.5-MHz crystal in the 10-m band of the h.f.o. circuit. The resultant output, combined with the v.f.o. signal, permitted operation at the desired frequency. Properly tuned, the transmitter was capable of 75-W forward power at 27.12 MHz.

The power-amplifier stage of the generator is a Heath linear amplifier (Model SB-200). This unit is also available in kit form. Specifications are summarized in Table 2. The grounded grid, dual amplifier tubes are configured for parallel class B operation [5]. The driven cathodes require an exciter level of approximately 100 W for maximum output (1 kW). Linear amplifier output is coupled to the matching network by a tunable pi output tank circuit.

Impedance-matching network

Impedance-matching circuitry is essential in order to facilitate efficient transfer of power from the generator to the i.c.p. discharge coil. Several approaches to this problem have been described [6]. Because load-coil impedance varies before and after plasma ignition, it is necessary to transform this impedance to the 50-Ω output impedance of the linear amplifier

TABLE 2

Linear power amplifier specifications (Heath Electronics, Model SB200)

Band coverage	80, 40, 20, and 10 m (10-m band used)
Power drive requirements	100 W
Duty cycle	SSB: continuous modulation CW: 50% (key down not to exceed 5 m)
Output impedance	50 ohm
Power requirements	120 VAC, 16 A

during all phases of starting and operation. In these studies, a modified L-network [6] was used because of its wide tuning range and design simplicity. This circuit is shown schematically in Fig. 1B with corresponding components detailed in Table 3. The shunt or load capacitors (C1 and C3) are variable air-dielectric and ceramic transmitting capacitors, respectively. The series or phase capacitor (C2) is a variable vacuum capacitor. The significance of this component is discussed later in this paper. Both of these capacitors are manually adjusted to achieve the desired impedance match. Output from the phase capacitor is coupled to the load coil through a short (and straight) length of copper banding. The impedance-matching network is of hybrid design and incorporates many components from a Heath (Model SA—2060) radio-antenna impedance-matching assembly.

Discharge apparatus

The discharge apparatus includes the torch, spray chamber, nebulizer, load coil, tesla ignition transformer, and associated argon gas controls. This apparatus will not function with conventional i.c.p. torches. Its successful operation is dependent upon utilization of low-power torches similar to those described earlier [4]. Modification of this torch design is shown in Fig. 2. The critical parameters which distinguish this torch from conventional units are a reduction of the clearance between the coolant and auxiliary tubes and a constricted aerosol orifice. These quartz torches were readily fabricated in our glass shop. The pyrex spray chamber and concentric glass nebulizer are conventional components. Power is delivered to the torch assembly through a three-turn (diameter 22 mm) water-cooled copper load coil. Other system specifications and operational conditions are summarized in Table 4.

RESULTS AND DISCUSSION

The i.c.p. instrumentation described here is operated differently than conventional high-power units. These differences are a direct result of formation

TABLE 3

Impedance-matching network specifications (see Fig. 1B)

C1	Variable air capacitor (capacitor C1 from Heath SA-2060 tuner)	0—250 pF
C2	Variable vacuum capacitor (Jennings Radio UCS300, glass housing, vacuum bellows-driven. Part of assembly ERAA XD61942. Acquired surplus)	0—300 pF
C3	Ceramic "doorknob" transmitting capacitor (Centralab 859S-150Z)	150 pF (15 kV)
L	Stray inductance	
Z_O	Generator output impedance	50 ohm
Z_L	Load-coil impedance	variable

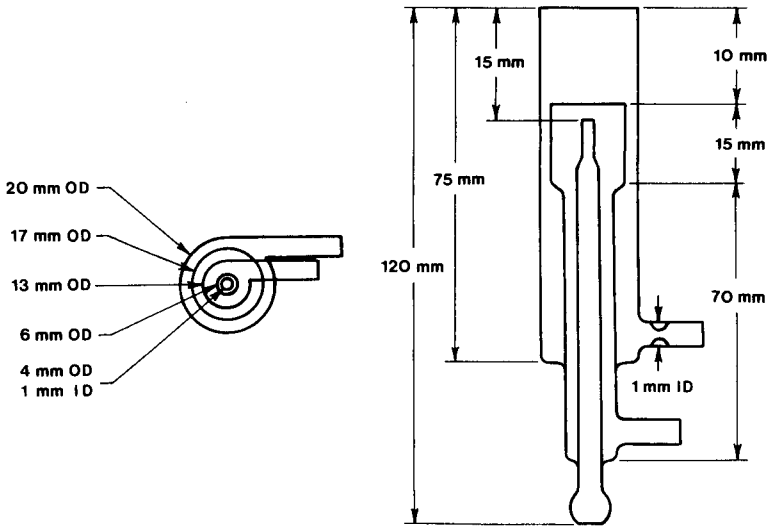

Fig. 2. Low-power, low-flow quartz torch.

TABLE 4

Experimental conditions

Generator	
Forward power	500 W
Reflected power	<10 W
Frequency	27.12 MHz
Discharge apparatus	
Load coil	3 turns (22 mm diam.), water-cooled
Gas flows (l min^{-1})	
coolant	5
auxiliary	0.2
aerosol	0.2
Discharge parameters (mm)	
height	15
diameter	15
observation height	10 (above coil)
Sample aspiration	
peristaltic pump	2.5 ml min^{-1}
Optical instrumentation	
Monochromator	Model 310 SMP, Minuteman Laboratories, Acton, MA.
Focal length	1 m
Configuration	Asymmetric Czerny-Turner
Grating	2400 g mm^{-1} ruled. First-order dispersion 4.2 A mm^{-1}.
Optical speed	*f*/9.9
Slits	100 μm
Collection optics	25-cm *f*1. quartz lens adjusted for 1:2 source demagnification
Photomultiplier	1P28 operated at 700 V
Wide-band preamplifier	10×

and stabilization of a discharge at reduced radiofrequency power, reduced argon flow rates, and duty cycle limitations of the generator.

System operation

Proper tuning of the integrated exciter and amplifier stages is critical. The Heath transmitter is first aligned and tuned in the 10-m band with the output directed to an oil-filled 50-Ω resistive dummy load (Heath Model HN-31). A maximum output of 75 W was achieved at 27.12 MHz. Without changing any settings, the tuned transmitter was then used to drive the linear amplifier. The linear amplifier output, which was next terminated into the 50-Ω dummy load, was then optimized for maximum forward and minimum reflected power using the internal VSWR (voltage standing wave ratio) meters. Initial adjustment of the impedance-matching network load and phase capacitors is by trial and error at reduced power levels. This procedure can be simplified by locating a radiofrequency dip meter about 40 mm from the load coil; this provides visual feedback of coupling efficiency. Once established, these settings allow routine ignition of the plasma at 500 W. After ignition, the phase capacitor is again adjusted for minimum reflected power with resultant formation of a stable discharge and matched plasma operation. The resultant forward-power output range (75—750) W is controlled by the linear power amplifier stage.

Radio operators are restricted from continuous-wave broadcasting for long durations by FCC regulations. Consequently, transmission components are normally designed for discontinuous operation, with limited duty cycle capability, and with little allowance for dissipation of excessive heat. This is true in the case of Heath components, a situation which dictates discontinuous or burst-mode i.c.p. operation to avoid thermal damage to electrical components. To re-emphasize, the transmitter and linear amplifier components used here exceed technical requirements for the radio transmissions for which they were designed. The present adaptation is indeed nonstandard in terms of Heath design criteria. Nonetheless, a functional instrument, with specific characteristics and with resultant operational compromises, is achieved.

Data acquisition occurs as a rapid, stepwise, and sequential process which includes: (1) analyte introduction, (2) discharge initiation, (3) impedance-matching network optimization, (4) warmup, (5) spectrometric data measurement, and (6) discharge termination. Burst-mode operation, while clearly a design compromise, is simple to undertake and yields nearly equivalent results. Steps (2—6) normally take about 2 min to complete. A 50% duty cycle, with maximum continuous operation of 5 min, is allowable. An emission intensity/time profile for a single determination is shown in Fig. 3. The decay of emission intensity observed may be the result of excessive heat production in the amplifier output tubes. Data acquisition can be done reproducibly during a 15—20-s interval after instrument warm-up and stabilization. An attempt to enhance heat dissipation with an auxiliary cooling fan was unsuccessful.

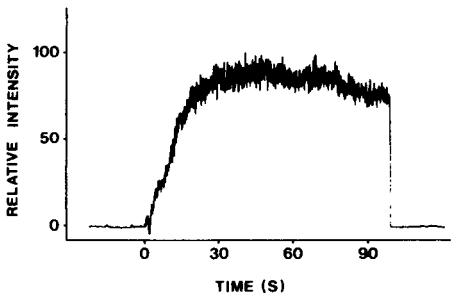

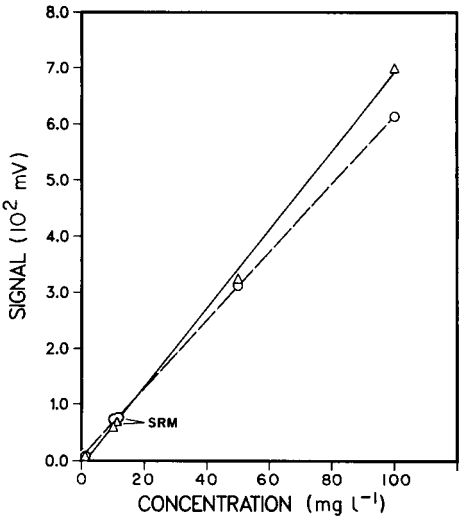

Fig. 3. Emission intensity vs. time profiles.

Fig. 4. Performance of the Plasma-Therm and Heath systems in low-power operation. Experimental conditions as in Table 5: Fe 259.9-nm line. (△) Plasma-Therm; (○) system described herein.

The resultant plasma discharge differs from that obtained under conventional conditions (1500 W, 15 l min^{-1} argon) in its physical dimensions and in the spatial distribution of plasma zones. The entire discharge extends approximately 15 mm from the preheating to the measurement zone. The latter is broader (i.e., less pinched) than its conventional counterpart. Because of this deformation, in addition to the low incident power and aspiration characteristics, a peristaltic pump is suggested to supplement aspiration of analyte into the discharge in order to enhance emission intensity.

Performance and compromises

The merits of this instrumental system and operational mode were compared with commercially available instrumentation. A Plasma-Therm Model HFP 2500D radiofrequency generator was operated under identical conditions for comparison. This unit is equipped with APCS-1 automatic power control and AMNS automatic impedance-matching network systems. The automatic power control system can maintain forward power within 1% of a preset value via a closed feedback loop. The automatic matching network system is equipped with a servo motor-controlled phase capacitor. This network continuously maintains minimum reflected power levels. Relative to the commercial instrumentation, advantages include compactness, simplicity of assembly, and lower cost. It is interesting to note that the modular components assembled from radiotransmitter kits closely resemble those which comprise the commercial generator (see Fig. 1A): an exciter stage

consisting of a crystal oscillator and multiplier isolated from the amplifier stage by a buffer. Both amplifier stages are air-cooled. However, the commercial instrument has a ceramic power amplifier tube, with an air-cooled anode, which is configured for class C operation. It has a much more elaborate forced-air cooling system. In general, it is more robust in design to permit continuous operation. Performance characteristics of power amplifier design (classes A, B, AB, and C) are varied in terms of amplification efficiency, distortion, and impedances best matched. Distortion tends to be more significant for class C than for class A; whereas amplification efficiency is better in class C designs. This approach also often requires a more elaborate tunable tank to compensate for high output impedance (1000—2000 Ω). For i.c.p. generators capable of very high output power, and where losses may be less critical, class C operation is chosen as in the case of Plasma-Therm operation. Low power operation can be accommodated with class A configurations such as provided by the Heath linear amplifiers. For i.c.p. application, distortion is at acceptable levels with all four classifications.

The initial intention was to also implement a Heath antenna impedance-matching network which utilized pi-network matching circuitry. This device could not be made to function for two reasons: (1) the effective load impedance of the discharge could not be matched; (2) significant power losses occurred within components. Consequently, the more suitable L-network was used with a vacuum capacitor in the series leg and a ceramic capacitor in the shunt leg to minimize power absorption. Losses were sufficiently high when variable air-dielectric capacitors were used that plasma ignition was not possible. In Fig. 1B, C1 serves as a trimming capacitor for the 150 pF ceramic unit, C3. The capacitance of C3 will be determined by the i.c.p. coil configuration and by the physical layout of the impedance-matching network. Capacitor C3 should be chosen so that C1 is only slightly meshed under matched conditions. The network is built in an aluminum Faraday cage further to reduce power losses and to minimize radiofrequency interference. The assembly of these components into a compact unit allows the possibility of benchtop operation, a topic considered by previous investigators [7]. Photographs showing component layouts are available upon request.

The major advantage of the system is expense; the system described here can be fabricated from components valued at about 10—20% of the cost of commercially available systems. This cost would increase somewhat if one had to purchase new vacuum capacitors, but these capacitors are often readily available at modest cost from a variety of electronic surplus outlets. The units described were fabricated, assembled, and tested in approximately one man-month by a student who had limited electronics experience.

This economic advantage is not without compromise. The disadvantages of the new system concern quantitative utility and ease of operation. These are attributable to the constraints imposed by discontinuous operation and the elimination of automatic power control and matching. These difficulties

have been minimized by the development of a burst-mode operation. This approach avoids excessive heat production and minimizes power instability. Manual impedance matching is done before and immediately after plasma ignition. Because data acquisition proceeds stepwise, this process must occur rapidly and methodically. Single-point, discrete-wavelength data collection is more practical than attempting lengthy wavelength scans. This instrument may be directly applicable to experiments which utilize discontinuous sample introduction (e.g., electrothermal vaporization).

The system is intended to be used in a graduate level, instructional instrumental laboratory to illustrate i.c.p. principles and operation. However, it is important to remember that the combination of voltages and frequencies used can be lethal and unpredictable. Safe operation with good grounds and interlocks is crucial. A series of such instructional experiments is being developed and copies will be provided upon request.

Results

A preliminary characterization of instrument performance is summarized in Table 5 and Fig. 4. This experiment involves the determination of trace quantities of iron in a National Bureau of Standards SRM brass sample. A calibration graph was prepared to assess linearity and detection limits. The resulting data are representative of system capability under conditions of low power and low argon consumption. These determinations were also done with the Plasma-Therm system under identical power and gas flow conditions. The Plasma-Therm unit was, however, operated with the automatic matching network and power control systems activated. It is apparent that while burst-mode operation may provide a viable alternative, there are difficulties. Detection limits observed with conventional high power and flow

TABLE 5

Quantitative results obtained with two systems with measurements at the Fe I 259.9-nm line[a]

Concentration ($mg\ l^{-1}$)	Heath systems		Plasma-Therm system	
	Signal (mV)	Std. dev. (mV)	Signal (mV)	Std. dev. (mV)
1.0[b]	7.0	1.6	9.0	2.1
10.0[b]	74.0	5.1	60.0	12.9
11.51[c]	77.0	10.1[d]	70.0[e]	8.4
50.0[b]	312.0	26.8	325.0	46.0
100.0[b]	614.0	73.9	700.0	79.7

[a]Data reported are the averages of five measurements obtained over a 2-h interval. [b]Standards prepared from Spex Industries 1000 mg l^{-1} solution 2% (v/v) nitric acid. [c]NBS SRM 1101 cartridge brass B, Fe 370 mg kg^{-1}. Sample: 1.59 g 50 ml^{-1}, dissolved in concentrated nitric acid and diluted to 2% (v/v) nitric acid. [d]The result found is 362 mg kg^{-1} iron. [e]The result is 350 mg kg^{-1} iron.

Analytica Chimica Acta, 158 (1984) 277—285
Elsevier Science Publishers B.V., Amsterdam — Printed in The Netherlands

A MICROPROCESSOR-CONTROLLED, MULTICHANNEL FLUORIMETER FOR ANALYSIS OF SEA WATER

P. B. OLDHAM, G. PATONAY and I. M. WARNER*
Department of Chemistry, Emory University, Atlanta, GA 30322 (U.S.A.)
(Received 9th September 1983)

SUMMARY

The multichannel fluorimeter described provides good sensitivity and rapid data acquisition. The advantages of multichannel fluorescence detection are discussed with special reference to the continuous monitoring of in vivo chlorophyll fluorescence in sea waters. Experiments on chlorophyll *a* determinations indicate a detection limit of 5×10^{-12} M with a linear range over at least three orders of magnitudes of concentration.

Fluorescence spectrometric techniques are characterized by low detection limits and good selectivity. The detection limit of fluorescence is typically three to four orders of magnitude below that of absorbance. This advantage arises from the direct detection of photons using fluorescence in contrast to the measurement of a small difference in two large photon signals in absorbance. The many parameters of fluorescence spectrometry which can be exploited provide the advantage of excellent selectivity. Emission intensity is dependent on both the wavelengths of excitation and emission. Many fluorophores can be spectrally separated based on these two parameters alone. However, by incorporating other parameters such as fluorescence lifetimes, phosphorescence spectra and lifetimes, and polarization, even greater selectivity can be obtained. Recent studies have cited the multiparametric advantage of luminescence spectrometry and have utilized it with multicomponent samples [1, 2].

Advances in instrument design have been crucial to the development of methods which capitalize on the favorable detection limits and selectivity of fluorescence. Early instruments used simple bandpass filters to restrict the wavelengths of excitation and emission. Later, more sophisticated spectrofluorimeters incorporated scanning monochromators for excitation and emission resolution. Recent advances in instrumentation have been facilitated by improvements in computer technology and optoelectronic detection devices [3]. Improved computer technology allows the acquisition and subsequent evaluation of large data sets while reducing operator time. The development of imaging devices such as vidicons, charge-coupled devices, and linear photodiode arrays has provided simultaneous multiwavelength detec-

0003-2670/84/$03.00 © 1984 Elsevier Science Publishers B.V.

tion. The linear photodiode arrays and intensified arrays are the newest of the multichannel detectors and offer several advantages over the older vidicons. These arrays are usually constructed as one-dimensional detectors in contrast to the two-dimensional vidicons. However, their good sensitivity, minimal lag, and minimal blooming provide superior performance for many applications [4, 5].

Lorenzen [6] demonstrated that fluorescence is a sensitive method for the measurement of in vivo chlorophyll *a* in the ocean. He was able to detect as little as 10^{-11} M chlorophyll *a* by using a simple Turner model III fluorimeter equipped with a red-sensitive photomultiplier tube (PMT). This approach to chlorophyll monitoring has become increasingly popular [7, 8] because of capabilities for continuous data acquisition. The previous methods involved discrete sampling, filtering, extraction, and subsequent measurement by either the trichromatic method of light absorbance [9] or fluorescence [10]. These techniques are time-consuming and offer little topographical information.

This paper presents the design of a portable, multichannel fluorimeter for use on board ship for measurements of fluorescent species in the ocean. Preliminary laboratory evaluation and experimental results will be discussed with regard to applications in the marine environment. The potential for shipboard operation in the continuous monitoring of the excitation and emission spectra of in vivo chlorophyll *a* will be described along with the apparent detection limits.

EXPERIMENTAL

Samples

Standard chlorophyll *a* was obtained from Sigma Chemical Company and the *Chlamydomonas reinhardi* from Carolina Biological Supply. The extracted chlorophyll *a* samples were collected on the November, 1982 cruise of the R.V. Gyre in the Gulf of Mexico. Sample collection required filtering approximately 500 ml of sea water through a Whatman GF/C filter. The filters were frozen for transport and storage. A tissue grinder facilitated extraction of chlorophyll *a* into 90% acetone, as described by Yentsch and Menzel [10].

Instrumentation

Six characteristics had to be incorporated into the design of the multichannel fluorimeter: portability, low detection limits, rapid data acquisition, multidimensional detection, automation capabilities, and rugged construction. Portability is required because many fluorescent species, especially in biological systems, must be investigated in their natural environment; the instrument must be easily transportable and capable of operation in a nonlaboratory environment. A low detection limit is crucial because concentrations of chlorophyll *a* in the ocean are typically 10^{-8}—10^{-11} M. Rapid data

acquisition and multidimensional detection are needed to provide the spectral information with sufficient time resolution to allow topographical mapping. It is also desirable to incorporate capabilities for automation into the design of the instrument because it will often be operating continuously. Finally, the construction of the fluorimeter must be sufficiently rugged to withstand transport and rough weather conditions at sea.

These characteristics were obtained by using an intensified 512-element photodiode-array detector. When coupled to a flat field spectrograph, this array can simultaneously detect the spatially dispersed emission spectrum over a 600-nm window. The detection system used was a Tracor Northern (Middleton, WI) IDARSS system which consists of an intensified array, spectrograph, and multichannel analyzer.

Multidimensional detection is possible by the rapid acquisition of emission spectra at several different excitation wavelengths. A circular variable filter wheel (Optical Coating Laboratory, Santa Rosa, CA) provided the excitation resolution. This filter wheel is an interference filter constructed so that the transmitted wavelengths vary linearly with the angular position of the wheel. The wavelength range is 400—700 nm with the transmittance ranging from 20% at 400 nm to 46% at 700 nm. A 200-step stepping motor (Superior Electric, Bristol, CT) drove the filter wheel.

Both the diode array and the stepping motor driven filter wheel were interfaced to an Apple II+ with 64 kbyte (8 bit/byte) of RAM, two floppy disk drives, and a CRT monitor. An Apple Super Serial interface (Apple Computer, Cupertino, CA) provides the RS-232c serial communication link between the Apple II+ and the TN-1710 multichannel analyzer which controls the diode array. The stepping motor is accessed by a Cybernetic (San Gregorio, CA) CY512 stepping motor controller via a SSM (San Jose, CA) parallel interface. Software control of the stepping motor is provided through the CY512 by ASCII commands from the Apple II+.

Custom-built, foam-insulated cases with an ABS plastic outer shell protect the instrument in shipment and from environmental conditions during operation. These cases were modified to accommodate electrical and water connections and to reduce stray light. A diagram of the completed fluorimeter is given in Fig. 1.

RESULTS AND DISCUSSION

Sensitivity

A comparative evaluation was made of the portable instrumentation, a video fluorimeter [3], and a Perkin-Elmer LS-5. The different modes of detection and signal readout used by the three instruments make a completely equal comparison difficult. However, Talmi [11] compared the detection sensitivity of a photomultiplier tube, a SIT vidicon, a diode array, and an intensified array by the calculation of signal-to-noise ratios (S/N) at peak maxima, approximately equating the total exposure times. This method

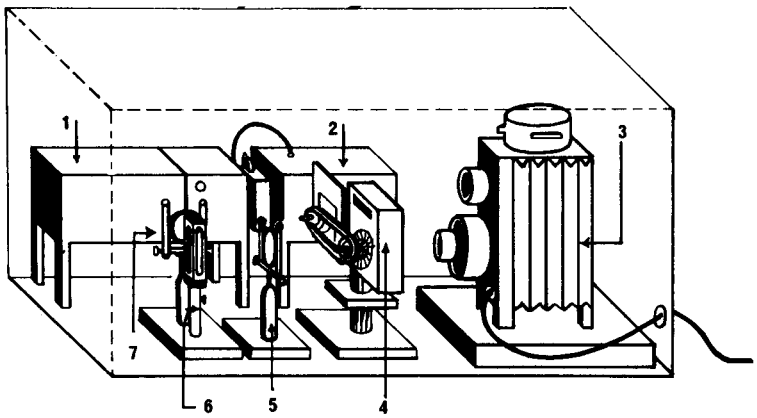

Fig. 1. Diagram of the portable multichannel fluorimeter. (1) Spectrograph; (2) diode array; (3) lamp; (4) filter wheel and stepping motor; (5, 7) lenses; (6) sample cuvet. The surrounding casing is about 8 cm thick.

seemed to be the most satisfactory and informative comparison for the present purpose and was, therefore, used in this study.

In order to obtain the S/N values, 100 replicate standard chlorophyll *a* (10^{-8} M) spectra were acquired. The mean value of the emission maxima was calculated as the signal. The noise at the peak was characterized by the standard deviation of the peak maxima. By calculating the S/N at the peak in this manner, both photon flicker and dark-current contributions were accounted for. The experimental conditions and the S/N values obtained here for the three fluorimeters are given in Table 1. Exposure times were selected so that a fair comparison could be obtained under relatively normal conditions. As expected from Talmi's results [11], the proposed instrumentation with its intensified array is significantly more sensitive than either the

TABLE 1

Comparison of detection for chlorophyll *a* between the portable fluorimeter, video fluorimeter and the Perkin-Elmer LS-5[a]

	Integration time	Average signal at peak (Counts)	Average noise at peak (Counts)	S/N at peak
Portable fluorimeter	30 scans; 0.205 s/scan ET = 6.15 s	98 006	1120	87
LS-5	50 nm/scan; 8 nm s^{-1} ET = 6.25 s	88	1	73
Video fluorimeter	11 scans; 0.573 s/scan ET = 6.31 s	2 114	79	27

[a]Measurements were made at λ_{ex} = 430 nm, λ_{em} = 667 nm.

LS-5 or the video fluorimeter. In addition, the exposure time for the LS-5 was for a 50-nm scan whereas the portable instrument covered 600 nm and the video fluorimeter covered over 200 nm in both excitation and emission dimensions. Therefore, both the multichannel and the video fluorimeter are relatively more versatile than is apparent from Table 1 because of the multiplex advantage [12].

Detection limit and linearity

The calibration graph for standard chlorophyll *a* given by the equation $y = 5.67x - 5.49$, where x is the signal (in counts) and y is the concentration ($\times 10^{-10}$ M), shows linear response over three orders of magnitude in concentration with a correlation coefficient of 0.9997. The standard deviation of the slope (s_m) was 0.006 and the standard deviation of the intercept (s_i) was 0.73. The standard error of estimate, relative signal range, and number of points were 13.4, 234.1, and 7, respectively. These data were acquired with an exposure time of 0.205 s per scan. A detection limit of 5×10^{-12} M chlorophyll *a* was calculated for S/N = 2 by accumulating 30 scans with an exposure of 1 s per scan. However, this detection limit is somewhat arbitrary because of the dependence of signal on integration time. By using longer integration times, a reduction in detection limit proportional to the square root of the integration time is expected. Therefore, the limit of detection falls well below that necessary for studies of chlorophyll *a* in the ocean.

Computer control and data acquisition

The multichannel fluorimeter is controlled by using Applesoft BASIC software with some simple task-specific 6502 machine-language subroutines. Communication between the Apple II+ and the fluorimeter is accomplished through the interfaces described previously. A simple flowchart of a sample control program is given in Fig. 2. Programs are easily modified to accommodate specific applications.

Data are acquired by sequentially gathering the emission spectrum at different excitation wavelengths. The TN-1710 multichannel analyzer contains 8 kbyte (16 bits/byte) of RAM and can store up to 16 emission spectra at a time. After the data have been acquired by the TN-1710, they are transferred to the Apple II+ and stored on floppy disks as one-dimensional arrays. A list of the data acquisition and storage capabilities of the portable instrument is given in Table 2.

After the emission spectra have been stored, they can be recalled individually or accumulated into a more extended matrix similar to that achieved by the video fluorimeter. Figure 3 is such a spectrum acquired by the multichannel fluorimeter. This capability provides the investigator with significant versatility. A complete spectrum can be rapidly generated when desired. However, for many applications, only a few excitation wavelengths are needed, thus increasing the time resolution between spectra and reducing the data storage space required.

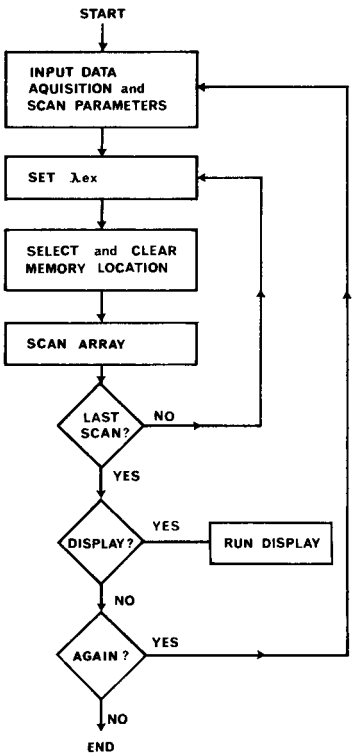

Fig. 2. Sample BASIC program flow chart for data acquisition and control of the multichannel fluorimeter.

Preliminary experiments

A total luminescence spectrum of standard chlorophyll *a* was acquired on the video fluorimeter (Fig. 4). There are four excitation bands and one major emission band. The most intense excitation band at 430 nm is the Soret band, which is usually monitored during in vivo chlorophyll *a* determinations; thus the following data will focus on this excitation band.

Characteristic spectra were acquired of the in vivo fluorescence of *Chlamydomonas reinhardi*, which is a member of the *Chlorophyta* (green algae)

TABLE 2

Data acquisition and storage capabilities

No. of emission spectra	16
Data acquisition time (min)	1—4
Data storage time (min)	3
Total time (min)	4—7
Storage capacity (spectra/disk)	98

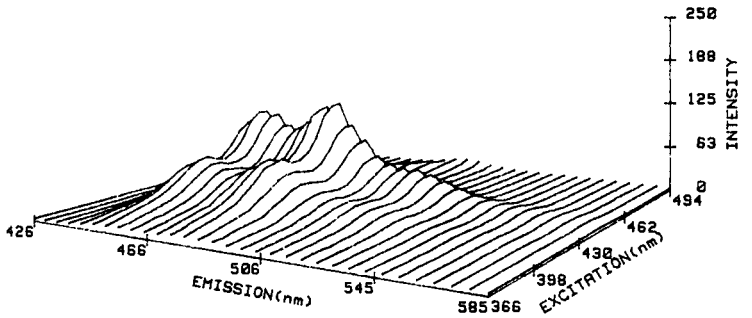

Fig. 3. Fluorescence spectrum of perylene (10^{-6} M) acquired by the method described.

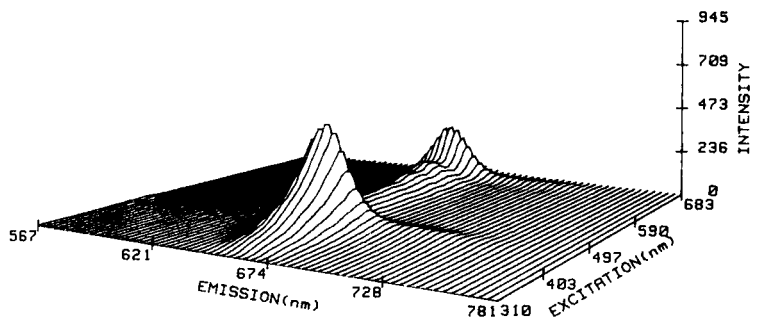

Fig. 4. Fluorescence spectrum of chlorophyll *a* (10^{-6} M) acquired by the video fluorimeter.

phylum. Spectra were also acquired for extracted chlorophyll *a* from seawater samples. All of these spectra were obtained with the multichannel fluorimeter for comparison with standard chlorophyll *a* spectra (Fig. 5). Both of the extracted chlorophyll *a* spectra were similar to the standard spectra. However, the excitation band for the extracted sample is slightly broadened. This is likely due to the secondary pigments present in the phytoplankton.

There is a significant difference between the excitation spectrum of the in vivo sample and the other two. This difference is accounted for by the transfer of excitation energy from the secondary pigments to chlorophyll *a* [13]. A 15—20-nm red shift of the emission profile is also characteristic of in vivo fluorescence [14].

These preliminary data confirm previously reported results [15] which indicate the excitation spectrum as a useful fingerprint of phytoplankton cultures. Further investigation is required to determine adequately the extent of spectral differentiation between phytoplankton cultures. The described portable multichannel fluorimeter provides the mechanism whereby the characterization of phytoplankton populations can be easily explored. It enables the continuous acquisition of "total luminescence" spectra useful not only for fingerprinting populations but also for detecting the spectral distribution of fluorescent species in relation to topography.

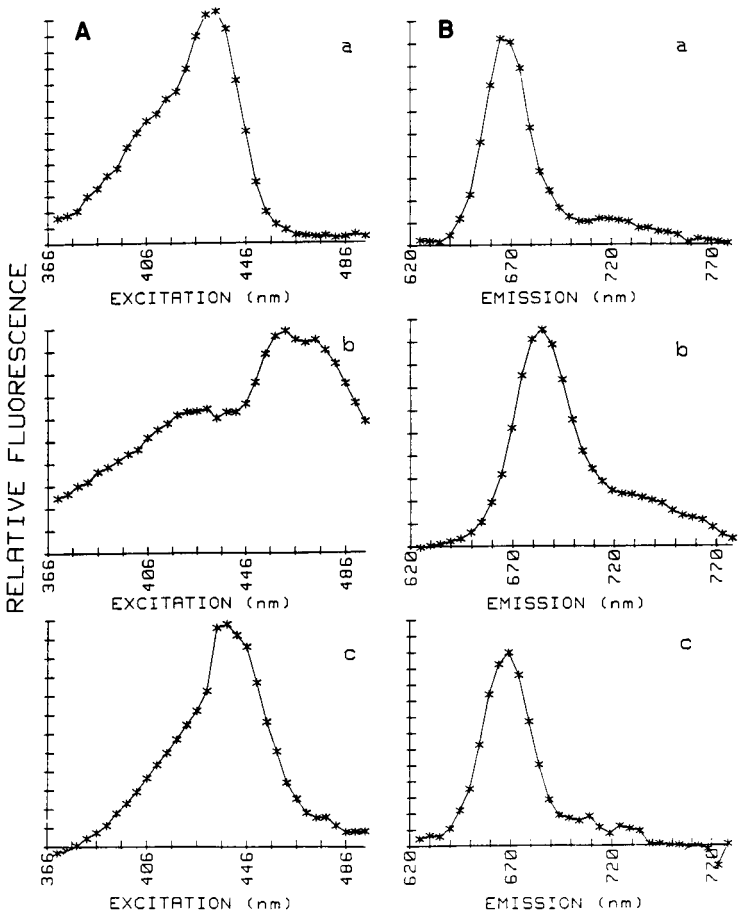

Fig. 5. (A) Excitation spectra and (B) emission spectra: (a) standard chlorophyll *a*, (b) in vivo *Chlamydomonas reinhardi*, (c) extracted sea-water sample. Excitation spectra measured with emission wavelength at 670 nm except for (b) for which λ_{em} - 685 nm. Emission spectra measured with λ_{ex} = 430 nm.

The authors are grateful to Dr. D. R. Schink, S. T. Sweet and P. J. Setser, all of the Department of Oceanography, Texas A & M University, for their assistance in acquiring ship time and for useful discussions concerning chemical oceanography. This work was supported by the Office of Naval Research grant N00014-83-K-0026.

REFERENCES

1 C. N. Ho and I. M. Warner, Anal. Chem., 54 (1982) 2486.
2 M. P. Fogarty and I. M. Warner, Appl. Spectrosc., 36(4) (1982) 460.
3 I. M. Warner, M. P. Fogarty and D. C. Shelly, Anal. Chim. Acta, 109 (1979) 361.
4 R. E. Dessey and C. A. Nunn, J. Chromatogr. Sci., 14 (1976) 195.

5 J. D. Ingle, Jr. and M. A. Ryan, in E. L. Wehry (Ed.), Modern Fluorescence Spectroscopy, Vol. 4, Plenum, New York, NY, 1981, p. 95.
6 C. J. Lorenzen, Deep-Sea Res., 13 (1966) 223.
7 S. I. Heaney, Freshwater Biol., 8 (1978) 115.
8 R. E. Slovacek and J. J. Hannan, Limnol. Oceanogr., 22(5) (1977) 919.
9 F. A. Richards and T. G. Thompson, J. Mar. Res., 11 (1952) 156.
10 C. S. Yentsch and D. W. Menzel, Deep-Sea Res., 10 (1963) 221.
11 Y. Talmi, Appl. Spectrosc., 36(1) (1982) 1.
12 K. W. Busch and B. Malloy, in Y. Talmi (Ed.), Multichannel Image Detectors, American Chemical Society, Washington, DC, 1979, p. 31.
13 S. Udenfriend, Molecular Biology: Fluorescence Assay in Biology and Medicine, Vol. 3, Academic Press, New York, NY, 1962, p. 376.
14 Govindjee, G. Papageorgiou and E. Rabinowitch, in G. G. Guilbault (Ed.), Practical Fluorescence, M. Dekker, New York, NY, p. 569.
15 C. S. Yentsch and C. M. Yentsch, J. Mar. Res., 37(3) (1979) 471.

Analytica Chimica Acta, 158 (1984) 287—296
Elsevier Science Publishers B.V., Amsterdam — Printed in The Netherlands

SPECTROFLUORIMETRIC DETERMINATION OF TITANIUM, ZIRCONIUM AND HAFNIUM AND THEIR BINARY MIXTURES WITH BIACETYLMONOXIME NICOTINYLHYDRAZONE

M. A. CEJAS, A. GOMEZ-HENS and M. VALCÁRCEL*
Department of Analytical Chemistry, Faculty of Sciences, University of Cordoba (Spain)
(Received 26th July 1983)

SUMMARY

The synthesis, characteristics and analytical applications of biacetylmonoxime nicotinylhydrazone are described. This compound forms fluorescent complexes with titanium(IV) (λ_{ex} = 430, λ_{em} = 540 nm), zirconium (λ_{ex} = 415 nm, λ_{em} = 505 nm) and hafnium (λ_{ex} = 400, λ_{em} = 500 nm) in an acidic medium. Titanium forms a 1:2 metal:ligand complex, whereas zirconium and hafnium form 1:2:1 metal:ligand:sulphate ternary complexes. Highly selective spectrofluorimetric methods for titanium (20—100 ng ml^{-1}), zirconium and hafnium (5—100 ng ml^{-1}) are proposed, and procedures for the analysis of binary mixtures of these ions are described.

Biacetylmonoxime has been used in many clinical [1] and inorganic [2—5] analyses. Some hydrazone derivatives of this compound have been described as reagents for the spectrophotometric determination of inorganic ions [6—8] but no derivative has been used in inorganic fluorimetry. Several hydroxyflavones (flavonol, morin, quercitin, datiscetin) [9] have been used as fluorimetric reagents for zirconium and hafnium. Reagents such as 8-quinolol [10], calcein blue [11—13] and 3-hydroxychromone [14] have been proposed for the fluorimetric determination of zirconium. Few fluorimetric methods for the determination of titanium(IV) have been described [15, 16].

No reagent has previously been proposed for the determination of all three elements. Biacetylmonoxime nicotinylhydrazone (BMNH; **I**) is described here as a new fluorimetric reagent for the determination of titanium(IV), zirconium and hafnium. The methods proposed permit the analysis of binary mixtures of these species.

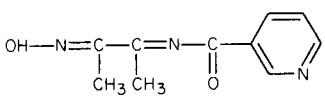

(I)

EXPERIMENTAL

Apparatus and reagents

The fluorescence measurements were made with a Perkin-Elmer MPF-43 spectrofluorimeter with a 1-cm quartz cell and xenon arc source. A set of

0003-2670/84/$03.00 © 1984 Elsevier Science Publishers B.V.

polymeric fluorescence standards was used daily to calibrate the spectrofluorimeter response to compensate for changes in source intensity. Slit-widths were adjusted to give a 6-nm bandpass, in both the excitation and emission monochromators. A Perkin-Elmer model 599 spectrometer with a temperature-programmed cell was used for the infrared studies.

Biacetylmonoxime nicotinylhydrazone was used as a 2.3×10^{-3} M solution in ethanol. A standard titanium(IV) solution (1.000 g l^{-1}) was prepared by dissolving titanium metal at 110°C in 100 ml of 6 M hydrochloric acid and making up to 1 l with distilled water. Further dilutions were made daily as required. A standard zirconium solution (0.985 g l^{-1}) was prepared by dissolving zirconyl chloride (hafnium-free) in 1.4 M hydrochloric acid. It was standardized gravimetrically by precipitation with ammonia and ignition to ZrO_2 [17]. Working solutions were prepared daily by suitable dilution with water. A standard hafnium solution (0.966 g l^{-1}) was prepared by dissolving hafnium chloride (containing 2.1% $ZrCl_4$) in 1.4 M hydrochloric acid. It was standardized and diluted in a similar way to zirconium. Potassium hydrogenphthalate buffer solution was adjusted to pH 2.6 with hydrochloric acid. All solvents and reagents were of analytical-reagent grade.

Synthesis of biacetylmonoxime nicotinylhydrazone. Dissolve biacetylmonoxime (1 g) in 20 ml of ethanol and add it to a solution containing 1.354 g of nicotinic acid hydrazide in 20 ml of distilled water. Adjust to pH 3 with hydrochloric acid. Stir for 2 h, cool to 0°C and recrystallize the white product from hot (1 + 1) ethanol—water. (Calculated for $C_{10}H_{12}O_2N_4$, 54.5% C, 5.4% H, 25.4% N; found 54.8% C, 5.5% H, 25.4% N.)

Procedures

Determination of titanium. To a 25-ml volumetric flask add a sample solution containing 0.5—2.5 μg of titanium, 2 ml of 2.3×10^{-3} M BMNH solution, 5 ml of 0.1 M phthalate buffer (pH 2.6), 3 ml of 1 M potassium chloride solution and dilute to the mark with distilled water. Measure the fluorescence intensity (λ_{ex} = 430 nm, λ_{em} = 540 nm) after 30 min at 25 ± 0.1°C. The calibration graph is prepared from the results obtained by using standard solutions of titanium(IV) treated in the same way. Instrumental conditions are: sensitivity 1, both slits 6.

Determination of zirconium. To a 25-ml volumetric flask containing a sample with 0.12—2.50 μg of zirconium, add 3 ml of 2.3×10^{-3} M BMNH solution, the necessary volume of 1 M sulphuric acid to adjust the final pH to 1.5 ± 0.1 and dilute to the mark with distilled water. Measure the fluorescence intensity (λ_{ex} = 415 nm, λ_{em} = 505 nm) at 25 ± 0.1°C. (For the analysis of mixtures and to avoid some interferences, the pH must be adjusted to 0.5 with sulphuric acid; see below.) The calibration graph is prepared from the results obtained by using standard solutions of zirconium treated in the same way. The instrumental conditions are given in Fig. 2.

Determination of hafnium (0.12—2.5 μg). Use the same procedure for preparing the solution for spectrofluorimetry as for zirconium. Measure the

fluorescence intensity (λ_{ex} = 400 nm, λ_{em} = 500 nm) at 25 ± 0.1°C. (For the analysis of mixtures and to avoid some interferences, the pH must be adjusted to 0.4 with sulphuric acid; see below.) The calibration graph is prepared from the results obtained by using standard solutions of hafnium treated in the same way. The instrumental conditions are given in Fig. 2.

RESULTS AND DISCUSSION

Analytical properties of the reagent

The solubility of BMNH was measured in various solvents. It is soluble in isoamyl alcohol (11.5 g l^{-1}), benzyl alcohol (10.7 g l^{-1}), acetone (5.9 g l^{-1}), dimethylformamide (4.1 g l^{-1}), ethanol (1.8 g l^{-1}) and methanol (1.1 g l^{-1}), but is hardly soluble in water or benzene.

The i.r. spectrum of BMNH in a potassium bromide disk was obtained at 20°C. The bands were assigned to N—H stretch (3190—3180 cm^{-1}), ring C—H (3040 cm^{-1}), C=O (1670 cm^{-1}), ring C=C and N=C (1600 cm^{-1}), aliphatic OH (1370 cm^{-1}) and C=N (1300 cm^{-1}).

A 4.5 × 10^{-5} M BMNH solution in 4% ethanol shows an absorbance maximum at 280 nm (pH 5.0). In a more acidic medium, the absorbance is decreased and there is a hypsochromic shift; in an alkaline medium there is also an absorbance decrease but the maximum remains at 280 nm. The absorption spectrum at pH 5.0 is stable for at least 2 days. The reagent solution does not fluoresce at any pH.

A simultaneous potentiometric and spectrophotometric method was used to determine the ionization constant in 4% ethanol; the average pK_a value found was 9.5 ± 0.1. This value was determined by the Stenstrom and Goldsmith procedure [18] and probably corresponds to the hydroxyl group.

The reagent spectrum did not show important changes when oxidizing reagents such as peroxodisulphate, iodate, hydrogen peroxide or bromate were added in acid and alkaline media, but metaperiodate caused a bathochromic shift and decreased absorbance.

The reactions of the reagent with 47 inorganic ions at various pH values were systematically investigated. Only the reactions with copper(II) and cobalt(II) at pH 5.0 and nickel(II) at pH 10.5 have any spectrophotometric interest. The reactions with titanium(IV), zirconium, hafnium, tin(II) and tin(IV) in an acidic medium produce fluorimetric species.

Spectrofluorimetric study of the reactions of BMNH with titanium(IV), zirconium and hafnium

Titanium(IV) system. Titanium(IV) forms a yellow complex with BMNH which has an intense green fluorescence in an acidic medium. The excitation spectrum shows two bands with maxima at 300 and 420 nm (λ_{em} = 540 nm) and the emission spectrum one band with maximum intensity at 540 nm (λ_{ex} = 420 nm) (Fig. 1). After 30-min for reaction, the fluorescence intensity does not change for at least 5 h.

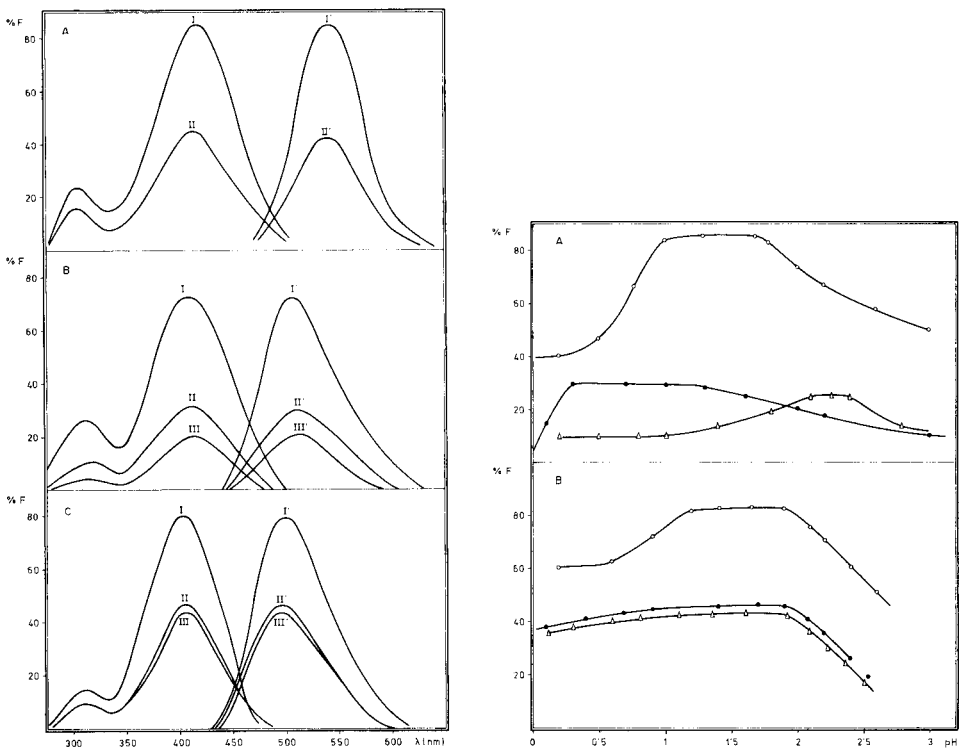

Fig. 1. Excitation and emission spectra. (A) Ti—BMNH system: (I) HCl or phthalate buffer; (II) H_2SO_4 or monochloroacetate buffer. (B) Zr—BMNH system: (I) H_2SO_4; (II) $HClO_4$; (III) HCl. (C) Hf—BMNH system: (I) H_2SO_4; (II) $HClO_4$; (III) HCl.

Fig. 2. Effect of the pH on the complexes with: (A) Zr; (B) Hf. The pH was adjusted with (○) H_2SO_4: (•) $HClO_4$; (△) HCl. Instrumental conditions: (A) sensitivity 3, slit-widths both 8; (B) sensitivity 1, slit-widths both 6.

The pH range for maximum fluorescence is 1.5—3.0. There is no fluorescence at pH <1.0. When the pH is adjusted with hydrochloric acid or with phthalate buffer, the intensity is about twice that obtained with sulphuric acid or monochloroacetate. Variations in phthalate concentration do not affect the fluorescence.

Several salts (KCl, KNO_3, $NaClO_4$) were tested at different concentrations in order to study the effect of ionic strength and the presence of various anions on the fluorescence intensity. None of these salts affects the system, but in order to work at constant ionic strength, solutions are best made 0.12 M in potassium chloride.

As the BMNH is dissolved in ethanol, the effect of this solvent on the system was studied. When the 8—12% (v/v) ethanol is present, the fluorescence intensity does not change, but it decreases when the concentration is higher. Increase in temperature decreases the intensity by 0.62%/°C. Varia-

tions in the order of addition of reagents do not affect the intensity, nor does the BMNH concentration when this is 0.58—1.8 × 10^{-3} M. Higher concentrations cause decreased fluorescence by inner filter effects.

The stoichiometry of the titanium(IV)—BMNH complex was found to be 1:1 by the mole ratio and continuous variations methods.

Zirconium system. The excitation and emission spectra of the zirconium—BMNH system in an acidic medium are also shown in Fig. 1. Maxima in the excitation spectrum occur at 315 and 415 nm (λ_{em} = 505 nm) and in the emission spectrum at 505 nm (λ_{ex} = 415 nm). The intensities change according to the acid used to adjust the pH. With sulphuric acid, the intensity is twice that obtained with perchloric or hydrochloric acid (Fig. 1).

Figure 2 shows the variation of the fluorescence intensity with pH when different acids are used. For sulphuric acid, the optimum pH range is 1.0—1.8. At pH 1.5 the fluorescence of the complex is stable for at least 4 h. The system also fluoresces when the pH is more acidic, but the intensity is lower.

To examine the effect of sulphate, several samples were prepared by adjusting the pH to 1.5 with hydrochloric acid and adding different amounts of sodium sulphate, to give 0.4—4 × 10^{-2} M sulphate solutions. In all cases the results were the same as those obtained when the pH was adjusted with sulphuric acid. This effect may be due to the formation of a ternary complex with sulphate.

The ionic strength and modest variations in ethanol concentration do not affect the fluorescence intensity, nor does the order of addition of reagents. The intensity decreases by 0.82%/°C. The optimum concentration range for BMNH is 0.8—4.5 × 10^{-4} M. Decreases in intensity were observed at higher and lower reagent concentrations.

The stoichiometry of the zirconium—BMNH—sulphate complex was evaluated by the continuous variations and the mole ratio methods. Both methods were applied to determine the zirconium: BMNH ratio with a constant excess of sulphate ions. This was found to be 1:2 in each instance. The Zr:sulphate and BMNH:sulphate ratios were evaluated by the mole ratio method, with a constant excess of BMNH and zirconium, respectively. The former ratio found was 1:1 and the latter 2:1. Figure 3 shows the experimental results. Thus, the stoichiometry for the Zr—BMNH—sulphate complex in solution is 1:2:1.

Hafnium system. Hafnium reacts with BMNH in an acidic medium to give a green fluorescence similar to that of the zirconium complex, but with greater intensity. The excitation spectrum shows two bands with maximum intensity at 315 and 400 nm (λ_{em} = 500 nm) and the emission spectrum has one band centred at 500 nm (λ_{ex} = 400 nm). When sulphuric acid is used to adjust the pH, the fluorescence intensity is greater than when perchloric or hydrochloric acid is used (Fig. 1).

The variation of the fluorescence intensity with the pH was tested with different acids. When sulphuric acid is used, the optimum pH is 1.1—1.9.

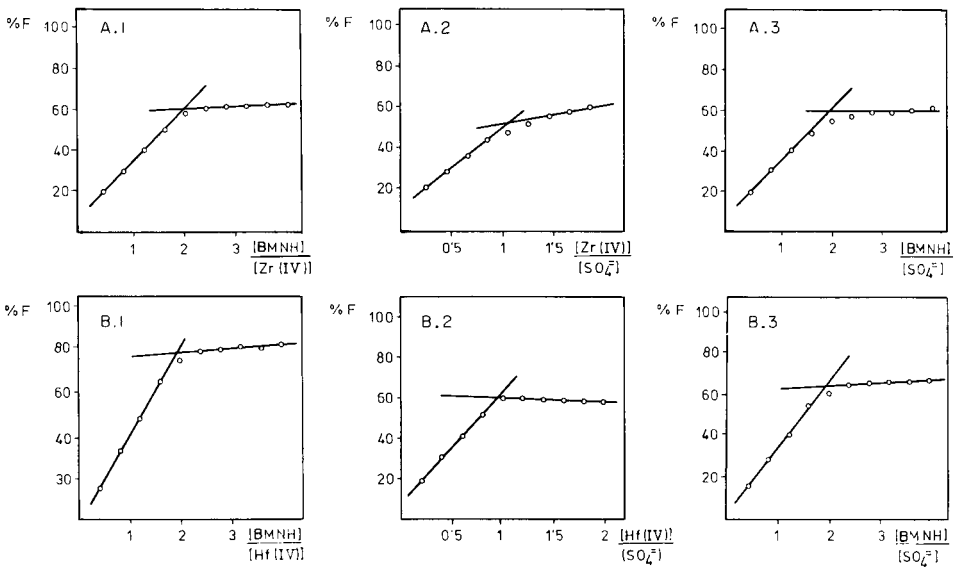

Fig. 3. Results of mole ratio experiments for complexes of BMNH with: (A) Zr; (B) Hf. (1) Excess of sulphate; (2) excess of Zr or Hf; (3) excess of BMNH.

This interval is larger if perchloric or hydrochloric acid is used, but the intensity is less at all pH values tested. The stability of the complex was studied at pH 1.5 and 0.4, for all the three acids. In each case, the complex is stable for at least 2 h.

The fluorescence intensity of the complex is the same whether the pH is adjusted with sulphuric acid or with hydrochloric acid and different concentrations of sodium sulphate. Other anions such as nitrate and acetate were also tested, but only sulphate increases the intensity, as for the zirconium complex.

The ionic strength, the ethanol concentration and the order of addition of reagents do not affect complex formation. The fluorescence intensity decreases by 0.78%/°C. The optimum concentration range of BMNH is 0.9—4.5×10^{-4} M.

The stoichiometry of the Hf(IV)—BMNH—sulphate complex was evaluated in a similar way to that of the zirconium complex. The hafnium:BMNH ratio was 1:2 and the hafnium:sulphate ratio was 1:1 (Fig. 3). To find the BMNH:sulphate ratio, the mole ratio method was used with a constant excess of hafnium. The ratio found was 2:1 (Fig. 3). Thus, the Hf—BMNH—sulphate complex in solution is 1:2:1.

Spectrofluorimetric determination of titanium, zirconium and hafnium

There is a linear relation between the fluorescence intensity and the titanium(IV) concentration between 20 and 100 ng Ti ml^{-1} in the final solution. When the recommended procedure was applied to a series of 10 solutions (60 ng Ti ml^{-1}), the 95% confidence limit of the mean was found to be ±0.9%.

Linear calibration graphs were established for two ranges of zirconium concentration at pH 1.5, covering a total range of 5—100 ng Zr ml^{-1}. For two series of 10 measurements on 60 and 15 ng Zr ml^{-1}, the 95% confidence limits of the means were ±1.3 and ±2.8%, respectively. To avoid the interference of several foreign ions, another calibration graph, for 20—100 ng Zr ml^{-1} at pH 0.5, was established. In this case the 95% confidence limit of the mean for 60 ng Zr ml^{-1} was ±1.4% (10 measurements).

The calibration graphs for hafnium were linear over the range 5—100 ng Hf ml^{-1} at pH 1.5. The standard errors for 60 and 15 ng Hf ml^{-1} were 1.2 and 4.6%, respectively (10 measurements, $P = 0.05$). Another calibration graph was established for 20—100 ng Hf ml^{-1}, at pH 0.4 to increase the tolerance to foreign ions. The 95% confidence interval of the mean was ±1.6% (10 measurements at 60 ng Hf ml^{-1}).

Interference studies

The effect of 58 ions on the three proposed methods was studied. For each ionic species, the concentration of titanium, zirconium or hafnium was kept constant at 60 ng ml^{-1}. There are 43 ions that do not interfere in any of the methods, at least when the foreign ion/analyte ion ratio is 170:1. These are Na, K, Li, Be, Mg, Ca, Sr, La, Cr(III), Mn(II), Co(II), Ni, Pt(IV), Cu(II), Au(III), Zn, Cd, Hg(II), Al, Tl(I), As(III), Bi(III), Se(IV), Th, W(VI), Ce(IV), Br^-, I^-, IO_4^-, SCN^-, SiO_3^{2-}, $S_2O_3^{2-}$, NO_3^-, ClO_4^-, CO_3^{2-}, PO_4^{3-}, $P_2O_7^{4-}$, $S_2O_8^{2-}$, $B_4O_7^{2-}$, CH_3COO^-, $C_2O_4^{2-}$, tartrate and citrate. For W(VI) and $C_2O_4^{2-}$, it is necessary to prepare the zirconium and hafnium samples at pH 0.5 and 0.4, respectively.

Figure 4 shows the tolerance limits of the ions that at higher concentrations cause interference in one or more of the three proposed methods. The method for the determination of titanium is less selective than the methods for zirconium and hafnium because the pH is higher. The most serious interferences are from tin(II) and tin(IV), which interfere at equal concentrations to zirconium. They are tolerated in equal amounts to titanium and at 2.5 times the amount of hafnium.

Iron(II), iron(III), indium, osmium(VIII) and EDTA are tolerated at equal amounts to titanium in its determination. Osmium(VIII) does not interfere in the determination of zirconium or hafnium, and the other species above do not interfere in these determinations when pH values of 0.5 and 0.4, respectively, are used.

Titanium(IV) does not interfere in the determination of zirconium or hafnium when the methods are applied at pH 0.5 and 0.4, respectively. Zirconium interferes in the determination of titanium but not in the deter-

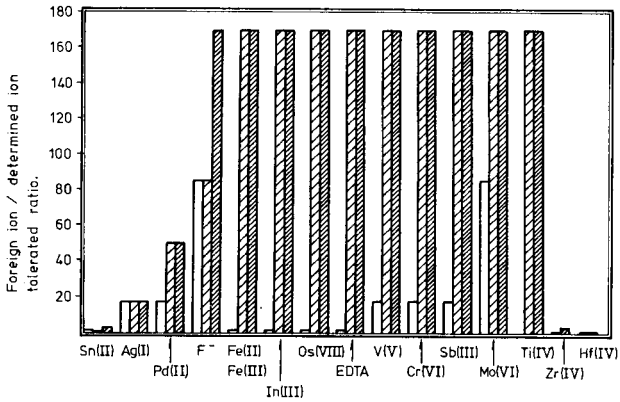

Fig. 4. Tolerance limit ratios (w/w); the determination of Ti(IV) (unshaded blocks), Zr (lightly shaded blocks) and Hf (heavily shaded blocks).

mination of hafnium at pH 0.4 when the hafnium concentration is 2.5 times that of zirconium. Hafnium interferes in the determination of titanium and zirconium.

Spectrofluorimetric analysis of binary mixtures

Titanium and zirconium. The procedure described for the determination of zirconium, with the pH adjusted to 0.5 with sulphuric acid, gives the

TABLE 1

Spectrofluorimetric determination of Ti(IV), Zr(IV) and Hf(IV) in binary mixtures

Mixture taken (ng ml^{-1})			Concentration found[a] (ng ml^{-1})		
Ti	Zr	Hf	Ti	Zr	Hf
70.0	30.0		69.0	28.5	
60.0	40.0		59.0	40.5	
50.0	50.0		48.5	49.0	
40.0	60.0		40.0	60.0	
30.0	70.0		31.5	68.5	
70.0		30.0	68.5		32.5
60.0		40.0	60.5		41.0
50.0		50.0	48.5		50.0
40.0		60.0	41.0		59.0
30.0		70.0	30.0		70.5
	70.0	30.0		71.5	30.5
	60.0	40.0		60.0	40.5
	50.0	50.0		50.5	51.0
	40.0	60.0		40.0	60.0
	30.0	70.0		31.5	71.5

[a]Mean of 3 determinations.

concentration of zirconium in the mixture. Another sample is treated by the procedure for the determination of titanium. The contribution of zirconium to the intensity is evaluated from a calibration graph for zirconium obtained under these conditions, and the concentration of titanium is obtained by difference. The instrumental conditions are those recommended for titanium. The results for several mixtures are shown in Table 1.

Titanium and hafnium. A similar procedure to that for titanium and zirconium is used. The hafnium is determined after the pH has been adjusted to 0.4 with sulphuric acid. Table 1 shows the results obtained for some mixtures.

Zirconium and hafnium. The procedure described for the determination of hafnium at pH 0.4 is unaffected by the presence of up to 2.5 times the weight of zirconium. The use of the procedure for zirconium at pH 1.5 allows the total concentration of both ions to be obtained by preparing separate calibration graphs for zirconium and hafnium. Zirconium is determined by subtraction.

Conclusions

Biacetylmonoxime nicotinylhydrazone is a new fluorimetric reagent for the determination of titanium(IV), zirconium and hafnium. The methods described are very sensitive, and it is the first time that the same reagent has permitted the direct determination of all three ions. The methods are also very selective with only tin causing very troublesome interference. The selectivity of the zirconium and hafnium methods increases as the pH is decreased and, though the sensitivity also decreases slightly, this permits the analysis of binary mixtures of these ions. This includes mixtures of hafnium and zirconium, the analysis of which is always problematical [19], although the discrimination is not as great as that achieved with quercetin [19, 20].

REFERENCES

1 N. W. Tietz, Fundamentals of Clinical Chemistry, Saunders, Philadelphia, PA, 1976.
2 P. K. Paria and S. K. Majumdar, Z. Anal. Chem., 275 (1975) 205.
3 A. Narayanan and P. Subbaraman, Indian J. Chem., 5 (1967) 436.
4 C. Calzolari and A. Donda, Ann. Chim. (Roma), 44 (1954) 280.
5 V. M. Peshkova, Yu. A. Barbalat, T. V. Polenova and N. A. Plekhanov, Zh. Anal. Khim., 28 (1973) 902.
6 M. Kenigsberg and I. Stone, Anal. Chem., 27 (1955) 1339.
7 I. Hofman, Analyst (London), 87 (1962) 650.
8 P. K. Paria and S. K. Majumdar, Indian J. Chem., 14 (1976) 916.
9 F. D. Snell, Photometric and Fluorimetric Methods of Analysis, (Metals), Part II, Wiley-Interscience, New York, NY, 1978.
10 H. O. Schneider and M. E. Roselli, Analyst (London), 96 (1971) 330.
11 R. V. Hems, G. F. Kirkbright and T. S. West, Anal. Chem., 42 (1974) 784.
12 L. T. Har and T. S. West, Anal. Chem., 43 (1971) 136.
13 L. H. Tan and T. S. West, Analyst (London), 96 (1971) 281.
14 T. Ito and A. Murata, Jpn. Anal., 23 (1974) 274.

15 M. D. Luque de Castro and M. Valcarcel, Talanta, 27 (1980) 645.
16 Yu. B. Titkov, U.S.S.R. Pat., 256 (1969) 332.
17 L. Erdey, Gravimetric Analysis, Part II, Pergamon Press, Oxford, 1966, p. 476.
18 W. Stenstrom and N. Goldsmith, J. Phys. Chem., 30 (1926) 1683.
19 A. Brookes and A. Townshend, Analyst (London), 95 (1970) 529, 781.
20 T. Kouimtzis and A. Townshend, Analyst (London), 98 (1973) 40.

Analytica Chimica Acta, 158 (1984) 297—303
Elsevier Science Publishers B.V., Amsterdam — Printed in The Netherlands

SCREENING FOR VANADIUM IN URINE AND BLOOD SERUM BY ELECTROTHERMAL ATOMIC ABSORPTION SPECTROMETRY AND D.C. PLASMA ATOMIC EMISSION SPECTROMETRY

LAURI PYY* and ERKKI HAKALA

Oulu Regional Institute of Occupational Health, P.O. Box 451, SF-90101 Oulu 10 (Finland)

LAURI H. J. LAJUNEN

Department of Chemistry, University of Oulu, SF-90570, Oulu 57 (Finland)

(Received 31st October 1983)

SUMMARY

Practical detection limits were 2 and 10 $\mu g\ l^{-1}$ vanadium for pyrolyte graphite-furnace a.a.s. and d.c.p.-a.e.s., respectively, which allowed screening for urinary vanadium ($\geqslant 10\ \mu g\ l^{-1}$) in exposed subjects, by direct measurements. Extraction of vanadium with ammonium 1-pyrrolidinecarbodithioate into 4-methylpentan-2-one gave detection limits of 0.5 and 2.5 $\mu g\ l^{-1}$ vanadium, respectively, for the two techniques.

Occupational exposure to vanadium can be determined by means of workplace air measurements [1] and biological monitoring [2]. In biological monitoring, the vanadium content of the urine of the workers is measured. The Institute of Occupational Health in Finland has used vanadium levels of 0.1 $\mu mol\ l^{-1}$ and 0.6 $\mu mol\ l^{-1}$ (1 μmol = 50.94 μg) as the reference value for unexposed subjects and the biological threshold limit value, respectively. The latter concentration indicates excessive exposure to vanadium [2].

There are several reports on the determination of vanadium in biological samples, by atomic absorption spectrometry (a.a.s.). The methods are based on graphite-furnace a.a.s. because the sensitivity of flame a.a.s. is inadequate for such samples. For example, vanadium has been determined in tissue [3, 4] and selected foods [5] after pretreatment by wet ashing. For the vanadium content of serum, concentrations of 2.2—3.9 $\mu g\ l^{-1}$ have been found by analysing diluted samples directly [4]. Methods involving liquid-liquid extraction have been reported for biological samples in marine research [6] and for urine samples [7, 8]. For unexposed subjects, urinary vanadium values of 0.3—0.7 $\mu g\ l^{-1}$ have been reported [7]. Neutron activation analysis gave values of about 10 $\mu g\ l^{-1}$ for urinary vanadium and 1 $\mu g\ l^{-1}$ for blood vanadium for workers in a ferroalloy plant [9]. The normal vanadium values in blood and serum analysed by neutron activation have been reported to be in the range 0.02—11 $\mu g\ l^{-1}$ [10].

0003-2670/84/$03.00 © 1984 Elsevier Science Publishers B.V.

Atomic emission spectrometry (a.e.s.) utilizing a plasma has not been reported for biological monitoring of vanadium. The determination of vanadium with an inductively-coupled plasma [11—13] and a d.c. plasma [14] in conjunction with a.e.s. in other types of matrices has been reported.

The aim of the present study was to investigate graphite-furnace a.a.s. and d.c.p.-a.e.s. methods for the determination of excessive vanadium in urine and serum. There was especial interest in testing the suitability of d.c.p.-a.e.s. for the analysis of concentrated solutions because the a.a.s. method suffered from serious interferences.

EXPERIMENTAL

Equipment and reagents

Instrumentation. A Perkin-Elmer model 603 atomic absorption spectrometer equipped with a deuterium background corrector, a HGA-74 graphite furnace, an AS-1 autosampler, a model 56 chart recorder, and a digital PRS-10 printer were used. The 318.4-nm vanadium resonance line was used. Samples (20 μl) were dried for 20 s at 120°C, ashed for 20 s at 2300°C, and atomized for 30 s at 2700°C. Standard graphite and pyrolytic graphite tubes were employed. The flow of argon purge gas was interrupted during atomization.

A Spectrometric SpectraSpan III single-channel spectrometer, consisting of a d.c. plasma source, an echelle monochromator and a dynamic background compensator, was used for the emission measurements. A Hewlett-Packard 85A processor was used for data output. The analyte lines at 437.924 and 309.311 nm were used. The slit openings, as recommended by the manufacturer were: entrance 50 × 300 μm, exit 100 × 300 μm. The photomultiplier voltage was 800 mV; 5-s integrations were used with 3 integrations per sample.

Reagents. All reagents used were reagent grade quality. A 1000 mg l^{-1} vanadium stock solution (Merck Titrisol) was used to prepare all the working standards. Ammonium 1-pyrrolidinecarbodithioate (APDC; Fluka) and 4-methyl-pentan-2-one (MIBK; Merck) were used as received.

Procedures

Samples and sample preparation. Samples were taken from workers processing vanadium pentoxide and from persons unexposed to vanadium. The sampling procedures were as discussed earlier in studies of occupational exposure [15]. The urine samples were collected in acid-washed polyethylene bottles by 24-h sampling or as spot samples. The serum samples were collected in heparinized glass tubes. Special emphasis was placed on the avoidance of contamination by following recommended procedures [16]. The samples were stored at −21°C.

Liquid-liquid extraction method. The sample (usually 20 ml) was digested with a mixture of 10 ml of 65% nitric acid and 2 ml of 70% perchloric acid.

The dry residue was dissolved in water and diluted to 150 ml. A 5-ml portion of 10% (w/v) potassium hydrogenphthalate solution was added, the pH was adjusted to 3.6 ± 0.1 with 6 M ammonia solution and 5 ml of aqueous 2% (w/v) APDC was added. The complex was extracted with 10 ml of MIBK. After the layers had separated, the MIBK phase was transferred to a 50-ml beaker and evaporated to dryness. The residue was wet-ashed with 5 ml of 65% nitric acid, and dissolved in and diluted to 5 ml with 1.2 M hydrochloric acid or 0.1 M sodium hydroxide. Because the possibility of contamination could not be excluded, two water samples were treated as blanks in each run throughout the whole sampling and measurement procedure.

The extracts were analyzed for vanadium by graphite-furnace a.a.s. and d.c.p.-a.e.s. under the conditions given above.

RESULTS AND DISCUSSION

Graphite-furnace a.a.s.

The characteristic concentrations (the concentration which gives 1% absorption) for vanadium, as given by the slopes of the calibration graphs (Table 1), were 30 $\mu g\ l^{-1}$ and 5 $\mu g\ l^{-1}$ for standard and pyrolytic graphite tubes, respectively. These values correspond to the biological threshold limit value of urinary vanadium and to the reference value for unexposed subjects. The direct analysis of biological fluids was evaluated by spiking two urine and two serum samples with 0, 5, 10, 25, 50 $\mu g\ l^{-1}$ vanadium (Table 1). linear calibration graphs were obtained with pyrolytic tubes. The practical detection limits (2 × background noise) for urine and serum were 10 and 2 $\mu g\ l^{-1}$ for standard and pyrolytic graphite tubes, respectively.

TABLE 1

Characteristics of calibration graphs for the direct determination of vanadium by graphite-furnace a.a.s. (absorbance vs. concentration)

Method	Matrix	Slope[a]	Standard error of slope[b]	Intercept	Standard error of intercept[b]
Standard graphite tube	Water	0.114	0.003	−0.005	0.011
	0.1 M NaOH	0.128	0.001	0.006	0.001
	1.2 M HCl	0.105	0.001	0.000	0.003
Pyrolytic graphite tube	Water	0.829	0.015	0.007	0.006
	0.1 M NaOH	0.828	0.022	0.014	0.009
	1.2 M HCl	0.653	0.026	0.009	0.011
Pyrolytic graphite tube	Urine 1[c]	0.841	0.028	0.003	0.000
	Urine 2[c]	0.840	0.022	0.002	0.000
	Serum 1[c]	1.058	0.017	0.002	0.000
	Serum 2[c]	0.975	0.032	0.002	0.000

[a]Concentration in mg l^{-1}; six calibration points. [b]Ref. 17. [c]Standard addition method with sample made 0.8 M in HNO_3.

With a view to improving the detection limits, a wet ashing procedure followed by evaporation to concentrate the vanadium was investigated. However, it was unsatisfactory because of interferences arising from the matrix. The wet-ashing method was then modified so that vanadium was separated by APDC-MIBK extraction [6, 7]. Instability problems [7] with the complex were avoided by evaporating the MIBK phase, destroying the complex with nitric acid and dissolving the vanadium in hydrochloric acid or sodium hydroxide solution. The advantage of sodium hydroxide is that sodium acts as an ionization buffer and improves the sensitivity. Five aqueous standards and 5 urine samples (pooled samples of unexposed subjects) spiked with 0, 5, 10, 20 and 50 $\mu g\ l^{-1}$ vanadium were extracted and injected. Peak height signals were compared with the 1.2 M hydrochloric acid standards. In all three cases, the calibration graphs were essentially identical and the recovery was 100% (Table 2). Similar samples in 0.1 M sodium hydroxide solutions were also analysed. The slopes (Table 2) show that the sensitivity was improved by ca. 30%. A sample concentration of 5 $\mu g\ l^{-1}$ determined by extraction and the use of a pyrolytic tube gave an absorbance of 0.020. The sample blanks gave absorbances of 0.000—0.002; 0.002 corresponds to the detection limit, which is 0.5 $\mu g\ l^{-1}$. The detection limit with a standard tube was 2.5 $\mu g\ l^{-1}$.

Within-run precision was evaluated by analysing 9 aliquots of urine samples from two exposed workers. A relative standard deviation (r.s.d.) of 6.7% was obtained for a mean of 26.8 $\mu g\ l^{-1}$, and 9.8% for 15.3 $\mu g\ l^{-1}$. Between-run precision was determined by analysing the same pooled sample 7 times during one year; the r.s.d. of the mean (13.9 $\mu g\ l^{-1}$) was 10.6%. This concentration level is typical for exposed workers.

The suitability of the procedure for serum was also investigated. A pooled sample of serum from unexposed subjects spiked with 0, 5 and 10 $\mu g\ l^{-1}$

TABLE 2

Characteristics of calibration graphs for vanadium by the extraction/a.a.s. method (peak height (mm) vs. concentration ($\mu g\ l^{-1}$))

Sample	Matrix	Slope[a]	Standard error of slope	Intercept	Standard error of intercept
Standards	1.2 M HCl	2.24	0.05	2.88	1.42
Extracted standards		2.34	0.03	2.40	0.98
Spiked urine		2.24	0.11	1.26	2.86
Standards	0.1 M NaOH	3.06	0.03	1.14	0.90
Extracted standards		3.01	0.02	1.73	0.67
Spiked urine		2.99	0.02	6.30	0.59

[a]6 calibration points.

vanadium gave complete vanadium recovery. The absorbance for unspiked serum was equal to the blank value, 0.5 $\mu g\ l^{-1}$. Serum from 5 exposed workers had a mean of 10 $\mu g\ l^{-1}$ (range 2—18). These values are higher than, for example, in the study of Gylseth et al. [9].

Direct-current plasma a.e.s.

The instrumental detection limits for vanadium obtained by d.c.p.-a.e.s. were 6 and 3 $\mu g\ l^{-1}$ at 437.924 and 309.311 nm, respectively [1], for the present instrumentation. The practical detection limit at both lines was ca. 10 $\mu g\ l^{-1}$. However, it was not possible to determine vanadium directly in biological fluids by using the emission line at 309.311 nm because of spectral interference by magnesium at 309.299 nm (Fig. 1). No spectral interference was noted at 437.924 nm (Fig. 1). However, the detection limit was again too large for direct analysis.

As before, samples were concentrated 4-fold after acid digestion. The high matrix concentrations, however, caused serious interferences. Two examples are shown in Fig. 2. Potassium chloride and sodium chloride strongly enhanced the vanadium signal, at the concentrations expected in the treated urine samples. The situation became more complicated when the solution contained many species. Figure 3 shows the effect of phosphate and potassium together, at various concentrations. The effect of the addition of sodium to a solution containing potassium and phosphate is also shown. Thus, phosphate seems to exert a small chemical interference effect on the vanadium signal. The presence of potassium and phosphate in about the same

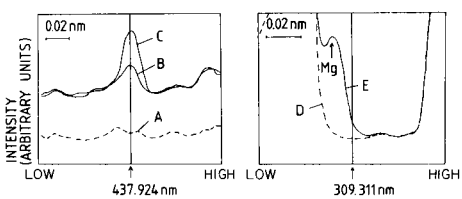

Fig. 1. Spectral profiles of vanadium emission lines at: (A—C) 437.924 nm; (D, E) 309.311 nm: (A, D) distilled water; (B, E) urine; (C) 20 $\mu g\ l^{-1}$ V spiked urine.

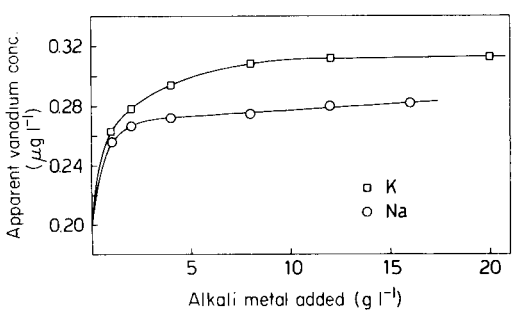

Fig. 2. Effect on vanadium emission intensity at 437.924 nm of: (□) K^+; (○) Na (as chlorides).

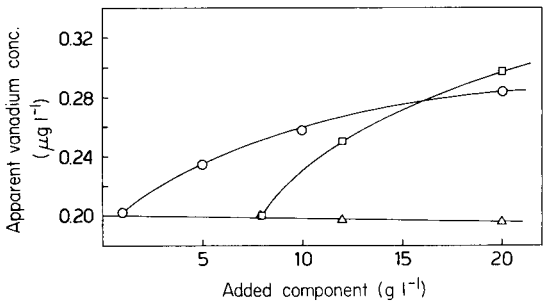

Fig. 3. Effect of added compounds on vanadium emission intensity at 437.924 nm: (△) K^+ and phosphate; (○) Na^+, in the presence of 10 g l^{-1} K^+ and 10 g l^{-1} phosphate; (□) K^+ in the presence of 8 g l^{-1} phosphate.

concentrations allows the determination of vanadium without interference. When the potassium concentration is higher than that of phosphate, there is interference from the excess of potassium ions. The interaction of sodium with phosphate is not so significant as that between potassium and phosphate. Thus the interference in a solution containing sodium, potassium and phosphate ions is caused mainly by sodium ions.

Since inorganic species in urine samples may vary considerably [18], the suspected interference mechanisms discussed above require the determination of interfering ions and a combined inter-element correction. Thus, the acid digestion method is not suitable for determination of vanadium by d.c.p.-a.e.s., and the liquid-liquid extraction procedure had to be applied.

A sample analysed by graphite-furnace a.a.s. with the extraction method was also analysed by d.c.p.-a.e.s. after extraction. The pooled sample had a mean of 15.2 μg l^{-1} and a r.s.d. of 3.5% (5 results). The a.a.s. mean was 13.9 μg l^{-1}, in reasonable agreement with d.c.p.-a.e.s. Both emission lines may be used but 437.924 nm is recommended, because of the better detection limit, 2.5 μg l^{-1} vanadium.

Conclusions

Urine can be analysed directly for vanadium levels $\geqslant$10 μg l^{-1} if the method of standard additions is used; this is adequate as a screening method for exposed workers. Both graphite-furnace a.a.s. and d.c.p.-a.e.s. can be applied. The extraction procedure, in conjunction with a.a.s. in pyrolytic graphite-coated tubes, gave the best detection limit (0.5 μg V l^{-1}). Even this, however, is insufficient for analysing specimens from unexposed subjects.

We express our thanks to the Rautaruukki Company for providing the opportunity to obtain the sample material, and to Mrs Helvi Pirkola and Ms Irma Taipaleenmäki for their skilful technical assistance.

REFERENCES

1 L. Pyy, L. H. J. Lajunen and E. Hakala, Am. Ind. Hyg. Assoc. J., 44 (1983) 609.
2 R. D. Soule, in G. D. Clayton and F. E. Clayton (Eds.), Patty's Industrial Hygiene and Toxicology, Vol. 1, Wiley, New York, NY, 1978, p. 762.
3 S. S. Krishnan, S. Quittkat and D. R. Crapper, Can. J. Spectrosc., 21 (1976) 25.
4 S. D. Stroop, G. Helinek and H. L. Greene, Clin. Chem., 28 (1982) 79.
5 D. R. Myron, S. H. Givand and F. H. Nielsen, J. Agric. Food Chem., 25 (1977) 297.
6 D. A. Segar and J. L. Gilio, Int. J. Environ. Anal. Chem., 2 (1973) 291.
7 J. P. Buchet, E. Knepper and R. Lauwerys, Anal. Chim. Acta, 136 (1982) 243.
8 M. Ishizaki and S. Ueno, Talanta, 26 (1979) 523.
9 B. Gylseth, H. L. Leira, E. Steinnes and Y. Thomassen, Scand. J. Work. Environ. Health, 5 (1979) 188.
10 J. Versieck and R. Cornelis, Anal. Chim. Acta, 116 (1980) 217.
11 K. Akatsuka and I. Atsuya, Bunseki Kagaku, 29 (1980) 714.
12 A. Gomez Coedo, M. T. Dorado Lopez and J. L. Jimenez Seco, Rev. Metal., 15 (1979) 97.
13 R. A. Nadkarni, Anal. Chem., 52 (1980) 929.
14 R. Sara, S-G. Hulden and L. Harju, Kemia-Kemi, 8 (1981) 774.
15 M. Kiviluoto, L. Pyy and A. Pakarinen, Scand. J. Work. Environ. Health, 5 (1979) 362; Int. Arch. Occup. Environ. Health, 48 (1981) 251.
16 Quality Control in the Occupational Toxicology Laboratory, WHO Regional Office for Europe, Copenhagen, 1981, p. 5.
17 R. K. Mackie, T. M. Shepherd and C. A. Vincent, Mathematical Methods for Chemists, The English Universities Press, Glasgow, 1972, p. 102.
18 Clinical Laboratory, Medico-Chemical Investigation Methods, 11th edn., E. Merck, Darmstad, 1974, p. 545.

Analytica Chimica Acta, 158 (1984) 305—322
Elsevier Science Publishers B.V., Amsterdam — Printed in The Netherlands

THE APPLICABILITY OF THE SUPERPOSITION PRINCIPLE IN DIFFERENTIAL PULSE POLAROGRAPHY

ROLF DANIELSSON* and PER BAECKLUND

Department of Analytical Chemistry, Institute of Chemistry, University of Uppsala, P.O. Box 531, S-751 21 Uppsala (Sweden)

ANDERS KÄLLSTRÖM

Institute of Mathematics, University of Uppsala, Thunbergsv.3, S-752 38 Uppsala (Sweden)

(Received 30th September 1983)

SUMMARY

It is shown theoretically that the superposition principle is applicable to pulse voltammetry if the electrochemical system can be separated into a potential-dependent non-linear part and a linear part. For systems not complicated by adsorption or electrode kinetics, the applicability of the principle depends on diffusion coefficients, electrode and cell geometry. For plane semi-infinite diffusion, applicability is expected; this is generally not the case for spherical electrodes or bounded regions (film electrode or thin-layer cell). The implications of the theory on differential pulse polarography are discussed and an experimental study on the applicability for iron(III), cadmium(II) and lead(II) is presented.

In several theoretical treatments of pulse voltammetry, the current response to a composite potential waveform has been expressed as the sum of current responses to single potential steps. In some cases, this was the result of rigorous derivations; in other cases, it was the starting point for the calculations. The basis for the method has been referred to as the superposition principle, for example, by Bard and Faulkner [1]. The origin of the principle, for voltammetry, seems to be a paper by Kambara [2].

The superposition principle, although not explicitly mentioned, was utilized by Osteryoung and co-workers [3, 4] in the first derivation of the equation for a differential pulse polarogram. Another striking example is the treatment of pulse voltammetry at stationary electrodes by Rifkin and Evans [5]. The application of this principle was questioned by Heijne and van der Linden [6], who attempted to obtain a more rigorous solution of the diffusion equations for differential pulse polarography. The result, slightly differing from that of Parry and Osteryoung [3], was shown to be erroneous by Ruzic and Sluyters-Rehbach [7] and was later corrected by the authors themselves [8]. Their final treatment, however, was essentially the same as the application of the superposition principle. The reason for the failure of the first treatment has so far not been clarified fully.

0003-2670/84/$03.00 © 1984 Elsevier Science Publishers B.V.

In this paper, the general application of the superposition principle to voltammetry is discussed, mainly by using concepts from system theory. It is shown that such a principle is justified for pulse voltammetry under certain simplifying assumptions. These conditions are usually regarded as valid for many electrochemical systems. It is, however, difficult to predict the influence of deviations from the ideal model. Some non-ideal factors are discussed in detail, and experimental investigations on the relation between differential-pulse and normal-pulse polarograms for selected metal ions are presented.

THEORY

The superposition principle is frequently used to determine the output of linear systems (Fig. 1A). For a linear system, the Laplace transforms, denoted by bars, of the input signal $x(t)$ and the output signal $y(t)$ are related via the system transfer function $G(s)$

$$\overline{y(t)} = G(s)\,\overline{x(t)} \tag{1}$$

Such a system is referred to as a causal system, where the output value at a given point of time depends on the present and the previous values of the input. Unless $G(s)$ is a constant (i.e., independent of s), the previous values have influence, and memory effects are inherent in the system. It follows from the linear properties of the Laplace transformation, that if $y_1(t)$ and $y_2(t)$ are the responses to input signals $x_1(t)$ and $x_2(t)$, respectively, then the input signal $x_1(t) + x_2(t)$ gives the response $y_1(t) + y_2(t)$. In this way, a complex problem may be reduced to a number of simpler problems.

A superposition principle for pulse voltammetry

In voltammetry, the input of the electrochemical system (Fig. 1B) is the potential $E(t)$ and the response is the cell current $i(t)$. The relation between input and output is determined by a number of different processes, where the potential influences the exponent in rate expressions for the reaction.

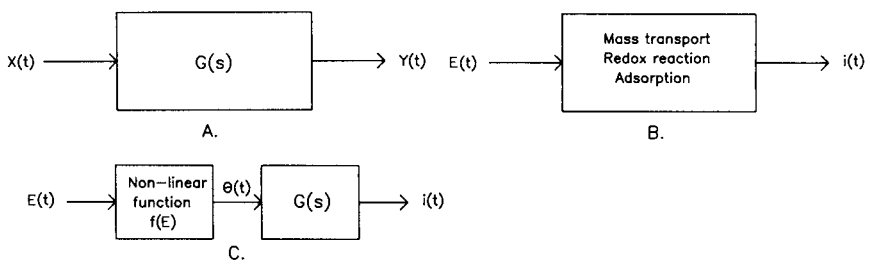

Fig. 1. Block diagram notation for a linear system (A), and for an electrochemical system in its original (B) and separated (C) form.

Therefore, the system is linear only for small variations in potential, and the direct application of the superposition principle should be restricted to small-perturbation methods (e.g., a.c. methods). A similar principle, however, can be formulated for pulse techniques, where the potential is changed by stepping between discrete values. The response to a complex input with a series of steps is then obtained as the sum of single-step responses. Because each single step is related to only one of the steps in the original input signal and is independent of all other values, the procedure can be referred to as a superposition principle. It will be shown that this procedure is justified if the electrochemical system can be separated into a non-linear function and a linear system (Fig. 1C). The output of the non-linear block is a function of the instantaneous input value only, i.e., $\theta(t) = f[E(t)]$. This auxiliary signal is the input to the linear subsystem with transfer function $G(s)$ $\overline{i(t)} = G(s)\,\overline{\theta(t)}$.

The essential feature of the separation of the system is that the non-linearities and the memory effects are separated. The non-linear functions should depend only on the instantaneous value of the potential, while the operations including the previous values should be linear. For convenience, it is assumed that the input potential is referred to the equilibrium potential, so that $E(t) = 0$ gives $\theta(t) = 0$ and hence $i(t) = 0$. It is also assumed that the solution is initially homogeneous, i.e., the concentration is constant throughout the volume.

Relation to single-step responses

In pulse voltammetry, the signal $E(t)$ can be written as a sequence of constant values E_k valid during the time interval $t_{k-1} < t < t_k$

$$E(t) = \Sigma E_k [H(t - t_{k-1}) - H(t - t_k)] \tag{2}$$

The time window is expressed by the use of the Heaviside function $H(t - t_k)$, which has zero value for $t < t_k$ and unit value for $t > t_k$. Because $f(0) = 0$, the auxiliary variable can be expressed as the sum

$$\theta(t) = \Sigma f(E_k)[H(t - t_{k-1}) - H(t - t_k)] \tag{3}$$

This expression can be written as

$$\theta(t) = \Sigma\theta_k H(t - t_{k-1}) - \Sigma\theta_k H(t - t_k) \tag{4}$$

where $\theta_k = f(E_k)$.

According to the superposition principle, which can be applied to the linear system $G(s)$, the response $i(t)$ to $\theta(t)$ is the difference between two sums

$$i(t) = \Sigma i_{1k} - \Sigma i_{2k} \tag{5}$$

In view of Eqn. 4, the term i_{1k} is the response to $\theta_k H(t - t_{k-1})$, which is also the response to a single potential step applied at $t = t_{k-1}$, with $E(t) = 0$ for $t < t_{k-1}$ and $E(t) = E_k$ for $t > t_{k-1}$. Similarly, i_{2k} is the response to an

identical step applied at $t = t_k$. It should be noted that two single-step responses are assigned to each step in the input potential: one is to remove the further effect of the previous input value, and the other is to account for the new value. Because both single steps proceed from the equilibrium potential for a homogeneous solution, the problem is significantly simplified.

The separation of the system, as shown in Fig. 1C, validates the treatments by Osteryoung and co-workers [3, 4], by Rifkin and Evans [5] and by Bard and Faulkner [1]. The question remains, however, under what conditions the separation itself is valid.

Separation of the electrochemical system

A model of the electrochemical process for a redox couple, $O + ne \underset{k_b}{\overset{k_f}{\rightleftharpoons}} R$, including mass transport and adsorption is shown in Fig. 2. The difference between bulk (C^b) and surface (C') concentrations is introduced as the auxiliary variables $C^*_O(t)$ and $C^*_R(t)$. The potential variable $E(t)$ is not regarded as a direct input to the system. Instead, its influence on the model parameters is indicated by dashed lines. The redox process is assumed to follow the Butler—Volmer equation

$$i(t) = I_0 \{\theta_O [E(t)] \cdot C'_O(t) - \theta_R [E(t)] \cdot C'_R(t)\} \tag{6}$$

where the potential dependency for the rate constants are expressed as

$$\theta_O [E(t)] = \exp\{-\alpha nf [E(t) - E^0]\} \tag{7}$$

$$\text{and } \theta_R [E(t)] = \exp\{(1-\alpha) nf [E(t) - E^0]\} \tag{8}$$

The exchange current is denoted by I_0, the transfer coefficient by α and the standard equilibrium potential by E^0, and $f = F/RT$.

The mass transport processes for the species O and R are described by linear differential equations. As a consequence, the flux at the electrode surface $J^*(t)$ depends on the surface concentration according to

$$\overline{J^*(t)} = B(s) \cdot \overline{C^*(t)} \tag{9}$$

The explicit expression for $B(s)$ depends on the transport mechanisms, the cell geometry, etc. In the Appendix, the expressions for $B(s)$ are derived for some cases commonly applied in voltammetry.

If the species are adsorbed, the adsorbed amount, $\Gamma(t)$, is related to the surface concentrations via an isotherm including a possibly potential-dependent parameter. The rate of change (transfer function s) of the adsorbed amount contributes to the current.

As shown in Fig. 2 there are three ways to arrive at an expression for $i(t)$ from $C^*(t)$. In order to reduce the system to the desired form, two ways are regarded as feedback paths. Thereby, the auxiliary inputs $C^*_O(t)$ and $C^*_R(t)$ are determined by the potential-dependent parameters. Considerations on the simplified system in Fig. 3A will show the necessary conditions for the proposed separation. The influence of the potential-dependent

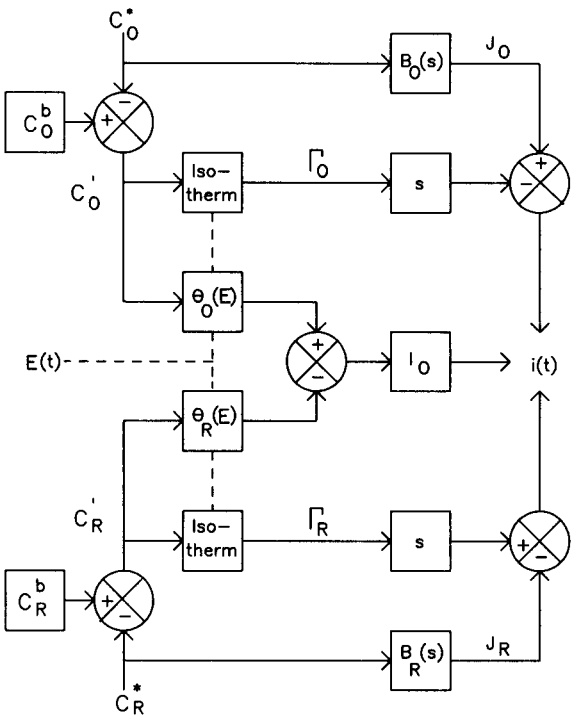

Fig. 2. Model of the electrochemical system including mass transport, electrode reaction and adsorption of species O and R. C^* is the difference between bulk concentration C^b and surface concentration C'. I_O is the exchange current, Γ indicates the amount adsorbed, and $B(s)$ is the transfer function for mass transport. Dashed lines indicate influence of the input potential $E(t)$.

factor $\theta[E(t)]$ on the feedback signal $y(t)$ is given by multiplication with the signal $x(t)$ (Fig. 3B). Then an additional time dependence on $C^*(t)$, other than that which originates from $E(t)$, can be introduced through $y(t)$, thus making the separation impracticable. The transfer function related to this dependence is given by the ratio $B(s)/A(s)$. This ratio must be constant (i.e., not a function of s) to make the proposed separation possible. The separated form of the system is shown in Fig. 4A. The non-linear function $f(x)$ is found by rearranging the equation for $C^*(t)$

$$C^*(t) = C^b - x(t) \cdot k \cdot C^*(t) \tag{10}$$

where k is the constant ratio $B(s)/A(s)$, into

$$C^*(t) = C^b/[(1+k)x(t)] = f[x(t)] \tag{11}$$

The result is shown in Fig. 4B. A more rigorous way of stating the separation condition is to use the inverse $g(t)$ of $B(s)/A(s)$ given by $\overline{g(t)} = B(s)/A(s)$, and the convolution integral for the feedback signal

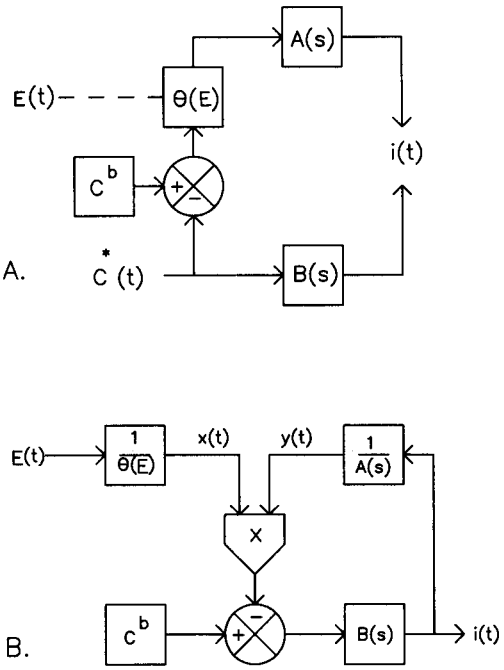

Fig. 3. Simplified two-path system with $C^*(t)$ as input to two-path system (A), transformed into a feedback system with potential input (B).

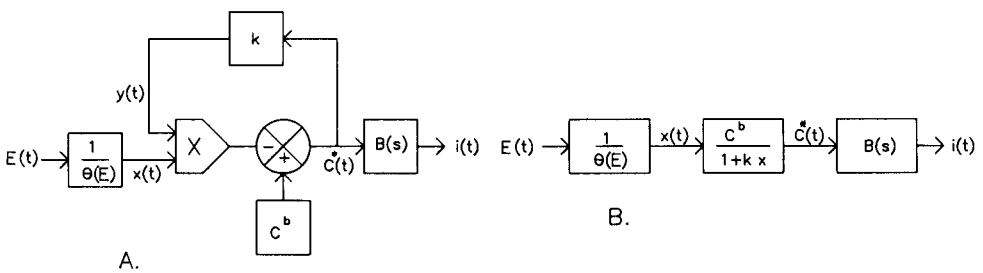

Fig. 4. Separation of simplified feed-back system (cf. Fig. 3) with $B(s)/A(s) = k$; (A) with and (B) without feed-back path.

$$y(t) = g(t) * C^*(t) = \int_0^t g(t-\tau) \cdot C^*(\tau)\, d\tau$$

The equivalent of Eqn. 10 is then the integral equation

$$C^*(t) = C^b - x(t) \cdot [g(t) * C^*(t)]$$

Clearly the condition for exclusion of memory effects is that the convolution integral is independent of the previous values of $C^*(t)$. Then $g(t)$ must be a delta function $k\,\delta(t)$, which has a constant inverse function $B(s)/A(s) = k$.

The separation procedure is now applied to the original system (Fig. 2).

The difference between this system and the reduced system (Fig. 3A) is mainly the number of parallel paths. Such paths can be combined to a single path under certain conditions. If there are two parallel paths, each in the separated form with potential-dependent non-linear functions f_1 and f_2, and linear transfer functions G_1 and G_2, respectively, then if $x(t)$ is the input signal, the output is given by

$$\overline{y(t)} = G_1(s) \cdot \overline{f_1[x(t); E(t)]} + G_2(s) \cdot \overline{f_2[x(t); E(t)]}$$

To arrive at the desired form

$$\overline{y(t)} = G(s) \cdot \overline{f[x(t); E(t)]}$$

either one path must be negligible, or both paths must have identical linear systems or non-linear functions. For example, if $G_1(s) = G_2(s) = G(s)$ then

$$\overline{y(t)} = G(s) \cdot \overline{\{f_1[x(t); E(t)] + f_2[x(t); E(t)]\}}$$

First, the parallel adsorption and mass transport processes are considered. Because mass transfer is linear in surface concentration and not potential-dependent, only linear adsorption with a potential-independent adsorption coefficient is permitted. Then the combined process can be expressed by a single potential-independent function $B(s)$ by adding the transfer functions of the parallel paths. The resulting model is shown in Fig. 5. In the feed-back loop, two parallel paths must be considered, one derived from diffusion of the component O and the other from the kinetics of the redox process. It can be seen that although both paths are of the desired form (no potential-dependent memory effects), the combination is not separable. Thus only one

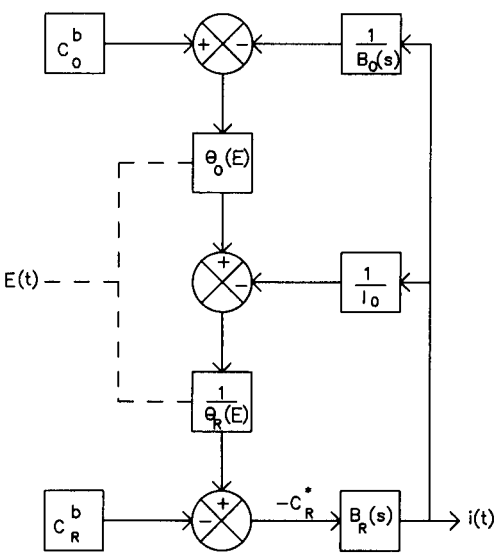

Fig. 5. Feed-back version of electrochemical system with linear potential-independent adsorption.

path is allowed, i.e., either a totally irreversible or a reversible reaction. For an irreversible reaction, the scheme is immediately reduced to that in Fig. 3B with $A(s) = I_0$. The separation condition as discussed before is then that $B_R(s)/I_0$ is a constant. This corresponds to a reaction controlled only by kinetics, where the current is determined by the instantaneous potential value (i.e., no memory effects), and the application of the superposition principle is trivial. Hence only reversible reactions, i.e., negligible $1/I_O$, should be considered.

The final transformations are illustrated in Fig. 6, and the conditions for the application of the superposition principle can be summarized. First, the electrode reaction should be reversible and with only linear potential-independent adsorption. Secondly, the mass transport, including changes in the amount adsorbed, of the two species should be identical in the sense that the ratio $B_R(s)/B_O(s)$ does not depend on s. When diffusion of both species is taken into account Eqn. 10 is extended to

$$C_R^*(t) = C_R^b - \{\theta_O[E(t)]/\theta_R[E(t)]\} \cdot [C_O^b + k \cdot C_R^*(t)] \tag{12}$$

With Eqns. 7 and 8 inserted, the result is

$$C_R^*(t) = \{C_R^b - \theta[E(t)] \cdot C_O^b\}/\{1 + \theta[E(t)] \cdot k\} \tag{13}$$

where $\theta[E(t)] = \theta_O[E(t)]/\theta_R[E(t)] = \exp\{-nf[E(t) - E^0]\}$ and $k = B_R(s)/B_O(s)$.

It should be noted that the conditions necessary for the separation are stated as necessary for the application of the superposition principle. Such a principle implies that the current is the output of a linear system, the input of which must be independent of the previous course of the process. Only then can the response to a series of potential steps be related to single-step responses without solving the original problem.

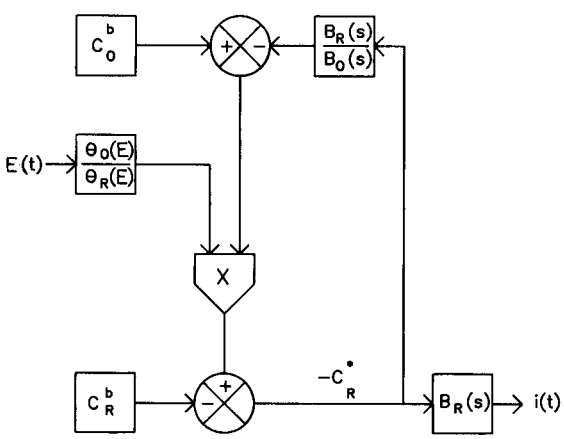

Fig. 6. Reduced system for reversible reaction, separable if $B_R(s)/B_O(s)$ is constant (cf. Figs. 4A and 1C).

THE SUPERPOSITION PRINCIPLE APPLIED TO DIFFERENTIAL PULSE POLAROGRAPHY

In differential pulse (d.p.) polarography, the drop is held at the potential E until the time t_p, when the potential is stepped to $E + \Delta E$. It is assumed that the pre-step potential E is constant during the growth of the drop, which holds to a good approximation for slow sweep rates. If the superposition principle can be applied, the current may be decomposed into three terms (cf. Eqn. 5)

$$i(t) = i_1(t) + i_2(t) + i_3(t) \tag{14}$$

where $i_1(t)$ is the response to a constant potential E, $i_2(t)$ is the effect of returning the potential from E to the equilibrium potential at $t = t_p$, and $i_3(t)$ is the response to a step at $t = t_p$ from the equilibrium potential to $E + \Delta E$. Clearly these components can be identified as the instantaneous currents obtained with direct current (d.c.) polarography at E, normal pulse (n.p.) polarography at E (although with reversed sign), and n.p. polarography at $E + \Delta E$, respectively.

Conventionally, the current is sampled twice in d.p. polarography, at t_p (or actually just before) and at $t_p + \Delta t$. In view of Eqn. 14, the difference is given by

$$i(t_p + \Delta t) - i(t_p) = i_1(t_p + \Delta t) - i_1(t_p) - i_2(t_p + \Delta t) + i_3(t_p + \Delta t) \tag{15}$$

This difference is the point $I_{d.p.}(E)$ on the d.p. polarogram. The first two right-hand terms can be regarded as the difference between points on two d.c. polarograms sampled at $t_p + \Delta t$ and t_p, respectively, which usually is termed the d.c. contribution $\Delta_t I_{d.c.}(E)$. The last two terms can be identified as points on the n.p. polarogram, $I_{n.p.}(E)$ and $I_{n.p.}(E + \Delta E)$, respectively. Then the relation can be written as

$$I_{d.p.}(E) = I_{n.p.}(E + \Delta E) - I_{n.p.}(E) + \Delta_t I_{d.c.}(E) \tag{16}$$

which is equivalent to the result of Osteryoung and co-workers [3, 4]. The "rigorous" treatment by Heijne and van der Linden [7] gave a larger d.c. contribution, which did not correspond to the time difference of the d.c. currents for $\Delta E = 0$. The reason for the failure was an oversimplification of the concentration profile prior to the pulse. Only a linear profile was retained, resulting in a constant partial solution to the diffusion equation. The time dependence of the corresponding current is then $t^{2/3}$, because of the surface expansion, rather than $t^{1/6}$, as given by the Ilkovič equation. Consequently, the calculated d.c. contribution was about four times larger than that predicted by Eqn. 16.

Testing the superposition principle

It is possible to eliminate the d.c. contribution by a measurement technique similar to the alternate-drop d.p. method [9]. The current is sampled

at $t = t_p + \Delta t$ for two drops, the first with and the second without the pulse ΔE. In the first case, all three terms of Eqn. 14 must be considered, while only the first term is non-zero in the second case. If the difference is taken, the first terms will cancel, and only the true pulse contribution $I_{p.c.}(E)$ arising from ΔE will remain

$$I_{p.c.}(E) = I_{n.p.}(E + \Delta E) - I_{n.p.}(E) \tag{17}$$

The right-hand difference in Eqn. 17 can be measured with the n.p. technique. It is also called the pseudo-differential pulse current [10] and will be denoted by $I_{p.d.p.}(E)$. The equivalence of the true pulse contribution and the pseudo-differential pulse result provides a means of testing the applicability of the superposition principle.

Mass transfer by diffusion

As stated before, the superposition principle is strictly applicable only under certain assumptions. Not only should the reaction be uncomplicated (e.g., not influenced by kinetics or adsorption) but there are also restrictions for the mass transport in that the ratio $B_R(s)/B_O(s)$ should be independent of s. Unless the transport mechanisms and the geometry are identical for the two forms O and R, this ratio has to be examined. Usually only diffusion is taken into account, and the mass transport expressions may differ because of unequal diffusion coefficients or diffusion in separate regions (in the solution and in the electrode).

In the Appendix, three cases, commonly adopted in electrochemical theory, are treated, namely (i) plane diffusion, (ii) spherical diffusion and (iii) diffusion towards an expanding plane. All cases may be transformed into the same form, and a general expression relating the concentration and the flow at the surface is given. More elaborate models like (iii) with spherical correction or (ii) with spherical expansion cannot easily be incorporated. No adsorption is included in the model. It should be noted that for the expanding plane model (iii), the true current is obtained by multiplying the flow by the expanding area. Moreover, the factor $t^{2/3}$ in the expression for the physical gradient (see Appendix) should be incorporated. However, these factors will cancel when the loop transfer function is evaluated, and again the ratio $B_R(s)/B_O(s)$ has to be considered. From the results (Eqn. A8 and the following special cases), it is seen that there are two complicating factors; the sphericity expressed by the electrode radius (r_0) and the boundary other than the electrode surface (z_1). For plane diffusion and unbounded region (semi-infinite diffusion), the ratio $B_R(s)/B_O(s)$ is always a constant. Such a model is often applied to pulse polarography and is useful to predict the short-time behaviour, where the thickness of the diffusion layer is small compared to other measures (electrode radius, film or cell thickness). It follows that as long as the potential is constant, the surface concentration is also constant, which was the main assumption made by Kambara [2].

For spherical diffusion or bounded regions, the values of the diffusion coefficients are critical. For diffusion in the same region, they must be equal to assure a constant ratio $B_R(s)/B_O(s)$. This assumption is sometimes made "for mathematical convenience" when spherical diffusion is treated, but as shown it has a more fundamental significance. Metal ions forming amalgams when reduced will diffuse into the electrode, and the regions will then be unequal. For plane diffusion within bounded regions (film electrodes, thin-layer cells) a constant ratio may be obtained by matching the dimensions to the diffusion coefficients. For spherical diffusion, however, a constant ratio can never be obtained. In conclusion, it can be stated that ideally both forms should be transported in the solution and have the same diffusion coefficient. However, there are few reactions without amalgam formation that proceed fast enough to be regarded as reversible in pulse polarography and uninfluenced by adsorption.

Other deviations from theory

In polarography, the processes taking place at each mercury drop are treated as a system with initially constant concentration profiles. However, the depletion of reactant resulting from previous drops is only partially removed by the convection caused by the mercury drop dislodgement. A "first-drop" technique must be utilized to obtain homogeneity. One method of doing this is to hold the electrode at the initial potential for several drops.

Some instrumental influences should also be recognized. The uncompensated resistance R_u, partly from the capillary and partly from the solution, causes the actual potential to depart from the imposed potential by the amount $i(t)R_u$. This effect may be modelled by an additional feedback path from the output to the input in the reduced scheme (i.e., Fig. 6) resulting in a non-separable system. The influence on the current is not easily predicted. Numerical calculations for a single potential step showed that the current is initially lowered, and then gives an over-shoot with asymptotic approachment to the ideal case. For values of R_u below some hundreds of ohms and sample concentrations in the millimolar range, the effect has declined after 10 ms and is negligible for times when the current normally is sampled. These findings were confirmed by measurements with external resistors in series with the mercury electrode. Furthermore, the current-measuring device usually contains a low-pass filter and a clipping circuit. This combination cannot be expressed by a linear transfer function and may affect the applicability of the superposition principle on the recorded current.

Overall, there are several factors causing deviations from the separable situation. It is difficult, however, to predict their influence on the proposed test experiment, i.e., the comparison of the true pulse current contribution and the pseudo-differential pulse current. The effects may cancel to some extent, or have the same influence on both currents. Recently, Lovrić et al. [11] compared results obtained by simulation for quasi-reversible reactions

and found deviations between $I_{p.c.}(E)$ and $I_{p.d.p.}(E)$. Few experimental results suitable for comparison have been reported, and to test the applicability of the superposition principle, some test systems commonly used in polarography were investigated.

EXPERIMENTAL

Chemicals and instrumentation

All chemicals were of analytical-reagent grade. Distilled water was further purified in a Millipore Milli-Q filtration system. Twice-distilled mercury was further purified by treating it with 10% (w/v) sodium hydroxide solution for several hours, then with (1 + 9) nitric acid and finally with pure water.

Solutions were degassed with nitrogen for at least 15 min before measurement. The reference electrode was a saturated Ag/AgCl electrode, separated from the solution under test by a salt bridge containing the supporting electrolyte. The auxiliary electrode was a platinum wire. The working electrode was a DME with a drawn-out capillary tip [12]. Mercury flow rates were measured in the supporting electrolyte used and with the working electrode disconnected from the potentiostat.

The voltammetric instrument was based on a microcomputer system (Intel SYS-80/10A) and a personal computer (Luxor Scandia Metric ABC80). The Intel computer was interfaced to a potentiostat and an I/E converter via a 16-bit D/A and a 12-bit A/D converter. The Intel computer handles the real-time operations while the ABC80 is used to set up experiments and for calculation of results. The instrument has been described [13]. The measurement and control program for this experiment was an extension of a program for pulse voltammetry [14]. Instrument performance was checked against published data and with experiments on dummy cells, etc.

Procedures

The polarograms to be compared, $I_{p.c.}(E)$ and $I_{p.d.p.}(E)$, were obtained in the following way. The potential range was scanned by stepwise changes of E. For each value of E, the current measurements were done on four drops, each one preceded by three drops at the initial potential. The potentials during the four "active" drops (Fig. 7) were controlled in accordance with the following polarographic techniques: (i) d.c. at E, (ii) d.p. at E with pulse ΔE, (iii) n.p. at E, and (iv) n.p. at $E + \Delta E$. The current was sampled during three 20-ms intervals for each "active" drop, and for each interval the mean value was stored. The centre of the intervals corresponded to 20, 50 and 125 ms after the time of pulse application, which occurred 135 ms before drop dislodgement. In this way, the measurements necessary to calculate $I_{p.c.}(E) = I_{d.p.}(E) - I_{d.c.}(E)$ and $I_{p.d.p.}(E) = I_{n.p.}(E + \Delta E) - I_{n.p.}(E)$ were obtained sequentially to avoid error from long-term drift, and results for three values of Δt were obtained simultaneously.

In all evaluations, background curves, measured in the supporting elec-

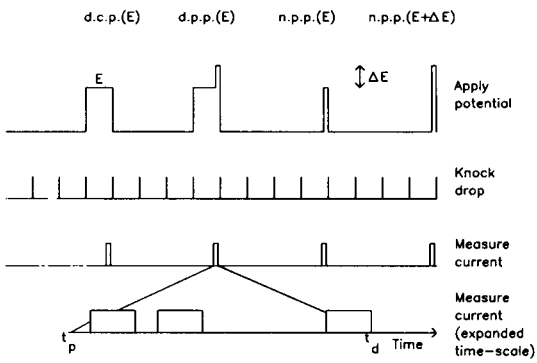

Fig. 7. The potential program used in this study, shown for a single point on the sweep.

trolyte, were subtracted from the test solution curves. Peak heights (I_p) and positions (E_p) were evaluated by fitting a second-degree polynomial to the top of the peak. The maximum point of the polynomial then gave the desired quantities. On both flanks of the peak, straight lines were fitted and the half-peak potentials were determined. The half-peak width ($w_{1/2}$) was then obtained as the difference between these potentials. The errors in the determination of E_p and $w_{1/2}$ are estimated to be within 0.5 mV, and the relative error in peak current is estimated to be less than 1%.

RESULTS

Four electrochemical systems were used as test systems; iron(III) in 1 M potassium oxalate, cadmium(II) in 0.1 M potassium chloride or 0.1 M sodium nitrate, and lead(II) in acidified 1 M sodium nitrate. The iron reduction has been shown to proceed reversibly [15] at mercury electrodes; furthermore, diffusion of both reactant and product takes place in the solution. This choice therefore seems ideal for testing the superposition principle. The other two, also reversible, systems are commonly used to test polarographic theory. Because these ions form amalgams, the effects of diffusion in different regions may be distinguished. Ligand-induced adsorption of cadmium is believed [16] to occur in chloride media, therefore nitrate was also used as supporting electrolyte. The results are presented as peak heights I_p, peak positions E_p, and half-peak widths $w_{1/2}$ in Table 1. In Fig. 8, typical polarograms for the three metal ions are shown. The results presented here were obtained with an ordinary DME. Results obtained with the PARC 303 static mercury drop electrode showed essentially the same features.

DISCUSSION

Iron(III)

Figure 8 shows the p.c. and p.d.p. polarograms for the reduction of Fe(III) in 1 M potassium oxalate. The curves, obtained from the first samplings,

TABLE 1

Characterization of peaks for iron(III), cadmium(II) and lead(II)[a]

Sampling time (ms)	Pulse contribution (p.c.)			Pseudo-differential pulse (p.d.p.)		
	E_p (mV)	I_p (μA)	$w_{1/2}$ (mV)	E_p (mV)	I_p (μA)	$w_{1/2}$ (mV)
1.20 mM Fe(III) in 1 M potassium oxalate[b]						
20	−164.5	2.39	101.4	−161.8	2.43	94.9
50	−163.5	1.85	100.1	−165.1	1.92	101.7
125	−163.3	1.66	98.8	−163.6	1.74	99.9
0.770 mM Cd(II) in 0.1 M KCl[b]						
20	−587.0	5.64	64.7	−586.5	5.60	63.8
50	−586.9	4.10	64.4	−586.1	4.07	63.6
125	−586.8	3.45	64.4	−586.2	3.47	63.1
0.622 mM Pb(II) in 1 M sodium nitrate/0.01 M nitric acid[c]						
20	−323.1	3.39	63.3	−323.2	3.42	63.7
50	−322.7	2.32	63.6	−323.2	2.37	63.6
125	−322.4	1.87	63.3	−322.3	1.98	62.3

[a]In all cases, no surfactant was added and the pulse height was 50 mV. [b]Drop time 0.35 s, M = 1.1 mg s^{-1}. [c]Drop time 0.30 s, M = 0.99 mg s^{-1}.

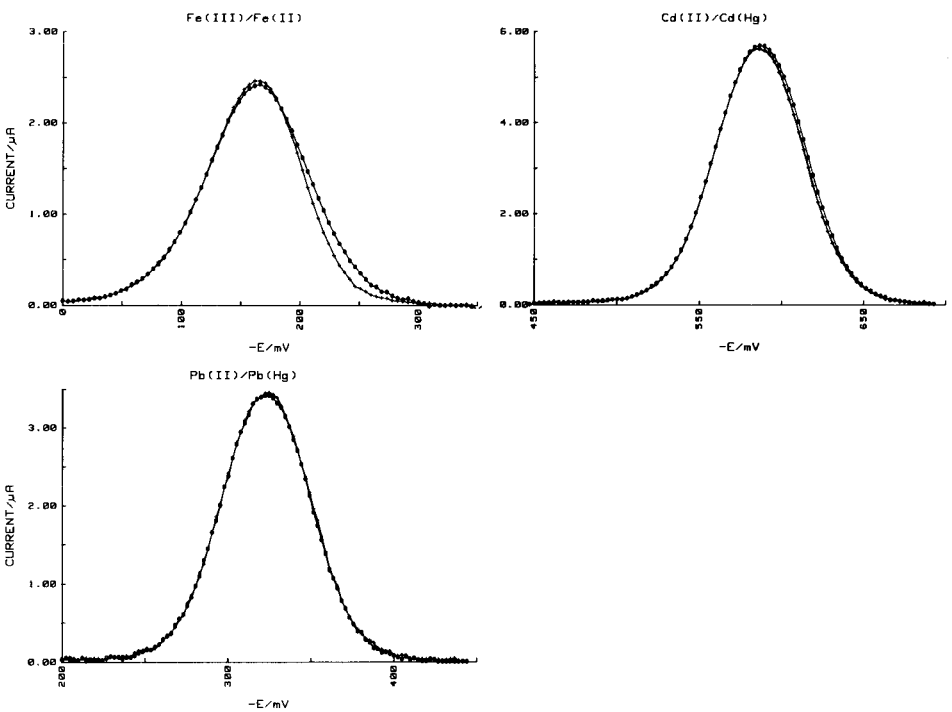

Fig. 8. Polarograms of the reduction of Fe(III), Cd(II) and Pb(II). Modes: (+) p.d.p.; (○) p.c. Sampling time 20 ms; other parameters as in Table 1.

show a marked difference. The p.d.p. peak is narrower than the p.c. peak. The half-peak width expected for the reversible uncomplicated wave (ΔE = −50 mV, n = 1) is 99.1 mV as calculated from the theoretical curve [3]. For the second and third samplings, the half-peak width is about 1 mV larger in the p.d.p. case than the p.c. case, the latter being in good agreement with the theoretical value. The ratio between two peak currents recorded for adjacent samplings should be about 1.5 if the transient decays according to theory at a spherical electrode. The ratio of the first two samplings is 1.3 and the ratio between the second and third sampling is 1.2. This indicates that the current is not solely controlled by diffusion.

Adsorption of the electroactive species would increase the normalized peak current, I_p/C, more at low than high concentrations of iron(III) [17]. The I_p/C values in Fig. 9 follow this trend; further a small hump could be seen on the n.p. polarograms. It is thus likely that adsorption causes the observed deviations.

Cadmium(II)

The p.c. and p.d.p. polarograms for 0.603 mM cadmium(II) in 0.1 M KCl (Fig. 8) agree in peak height to within 1%. However, the p.c. curve has a half-peak width of about 1 mV larger than the p.d.p. curve (Table 1). Because cadmium in the solution and in the mercury have diffusion coefficients differing by a factor of 2, and they are transported in unequal regions, the superposition principle cannot be expected to be strictly valid. The observed difference may also be due to other types of non-ideal behaviour. If adsorption induced by the ligand causes the difference in $w_{1/2}$, it should be affected by a change of ligand. However, no significant change in $w_{1/2}$ was noted (Table 2) when chloride was replaced by nitrate. Streaming of the first kind

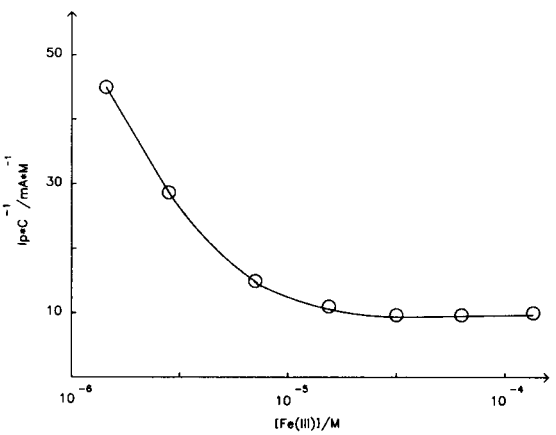

Fig. 9. Normalized peak current as function of Fe(III) concentration in 1 M potassium oxalate. Conditions: PARC 303 static electrode, drop size "large", drop time 0.3 s, sampling time 20 ms, ordinary d.p. polarography.

TABLE 2

Peak halfwidths and normalized peak currents for 0.603 mM Cd(II) in 0.1 M KNO_3 and 0.770 mM Cd(II) in 0.1 M KCl[a]

Triton added (mg l^{-1})	$w_{1/2}$ (mV)				Normalized peak current (mA M^{-1})			
	KNO_3		KCl		KNO_3		KCl	
	P.d.p	P.c.	P.d.p.	P.c.	P.d.p.	P.c.	P.d.p.	P.c.
0[b]	63.0	64.1	62.8	64.1	7.11	7.25	7.31	7.40
5	62.7	63.4	62.7	63.4	6.87	6.87	7.01	7.05
50	62.8	62.4	62.8	61.9	6.48	6.34	6.54	6.46

[a]Drop time 0.350 s, sampling time 20 ms. For a two-electron reduction with ΔE = −50 mV, $w_{1/2}$ is expected to be 61.7 mV. [b]Nitrate media irradiated with u.v. radiation before measurement.

has been observed for cadmium(II) [18]. If streaming is present, the p.c. and p.d.p. polarograms could be influenced by convection to a different degree. With 5 mg l^{-1} Triton X-100 present, the p.c. and p.d.p. peak heights and halfwidths agree better. A further increase in concentration of the surfactant causes the p.d.p. curve to become higher and narrower than the p.c. curve. The heterogeneous rate constant for cadmium at the DME is very dependent on the amount of surfactant present [19]. This could explain the deviations at higher concentrations of Triton X-100. It has been shown that p.d.p. curves become higher than the p.c. curves when charge-transfer kinetics must be considered [11]. This supports the proposed kinetic effect of Triton X-100. More work is needed to clarify the difference between the p.c. and p.d.p. polarograms for cadmium.

Lead(II)

The peak currents obtained for 0.622 mM lead(II) in 1 M sodium nitrate are higher in the p.d.p. than the p.c. mode (Table 1). The ratios between two adjacent current samplings are 1.5 and 1.2. The former is in good agreement with the theoretical value but the latter ratio is lower than expected. One possible explanation for this is that streaming is present. Upon addition of Triton X-100, the agreement between curves was better on the flanks of the peak, but a difference of about 2% in peak height persisted. This seems to point in the same direction as the cadmium case, and it may be a kinetic effect.

Conclusions

The applicability of the superposition principle to the iron-oxalate system is likely to be limited by adsorption. For the cadmium and lead systems, streaming is possibly a limiting factor. Because of the non-ideal conditions present in the practical polarographic situation, it is unlikely that a closer agreement between the test polarograms can be obtained.

This work was supported by a grant from the Swedish National Science Research Council, which is gratefully acknowledged.

APPENDIX

The transfer functions $B(s)$ are derived for the three cases: (i) plane diffusion, (ii) spherical diffusion and (iii) diffusion towards an expanding plane. In order to give a unified treatment, new variables (Table A1) are introduced. The new concentration variable C^* is the deviation from the bulk concentration C^b, and r_0 is the radius of the spherical electrode. A further assumption is that the initial concentration is such that $C^* = 0$ in all parts of the solution at $t = 0$. In terms of these variables, the physical gradient of the concentration in the three cases will be $-\delta C^*/\delta z$, $[1/(z + r_0)][(C^*/(z + r_0)) - (\delta C^*/\delta z)]$ and $-t^{2/3}\delta C^*/\delta z$, respectively.

Laplace transformation with respect to the time variable y of the diffusion equation in the three cases will lead to the same equation $D(\delta^2\overline{C^*}/\delta z^2) = s\overline{C^*}$, where the bar $\overline{C^*}$ denotes the Laplace transform; D is the diffusion coefficient and s the transform variable. The general solution of this equation is

$$\overline{C^*}(z, s) = A_1(s)\exp(-\alpha z) + A_2(s)\exp(\alpha z) \tag{A1}$$

where $\alpha = (s/D)^{1/2}$, from which it follows that

$$\delta\overline{C^*}/\delta z = -\alpha[A_1(s)\exp(-\alpha z) - A_2(s)\exp(\alpha z)] \tag{A2}$$

The functions $A_1(s)$ and $A_2(s)$ can be obtained from the values of $\overline{C^*}$ and $\delta\overline{C^*}/\delta z$ at the electrode surface (i.e., $z = 0$)

$$[\overline{C^*}]_{z=0} = A_1 + A_2 \tag{A3}$$

$$[\delta\overline{C^*}/\delta z]_{z=0} = -\alpha(A_1 - A_2) \tag{A4}$$

A boundary condition is now introduced at a free boundary $z = z_1$ (z_1 is to be specified later and will essentially correspond to "where the solution ends"). The boundary condition is $[\text{grad } C]_{z=z_1} = 0$. For the case of a spherical electrode, this gives

$$[1/(z_1 + r_0)][A_1\exp(-\alpha z_1) + A_2\exp(\alpha z_1)] + \alpha[A_1\exp(-\alpha z_1) - A_2\exp(\alpha z_1)] = 0$$

implying that $\{\alpha + [1/(z_1 + r_0)]\}\exp(-\alpha z_1)A_1 - \{\alpha - [1/(z_1 + r_0)]\}\exp(\alpha z_1)A_2 = 0$.

Introducing the notation $z_A A_1$ for the first term of the last equation and $z_B A_2$ for the second term yields $z_A A_1 - z_B A_2 = 0$. From this, it follows easily that $A_1 + A_2 = A_2(z_B + z_A)/z_A$ and $A_1 - A_2 = A_2(z_B - z_A)/z_A$. Consequently, from Eqns. A3 and A4,

$$(\delta\overline{C^*}/\delta z)_{z=0} = -\alpha z(\alpha)[\overline{C^*}]_{z=0} \tag{A5}$$

$$\text{where } z(\alpha) = (z_B - z_A)/(z_B + z_A) \tag{A6}$$

The function $z(\alpha)$ reflects the influence of the free boundary $z = z_1$ and can be evaluated for some special cases.

(a) Plane diffusion ($r_0 \to \infty$). For the bounded region, $z(\alpha) = \tanh(\alpha z_1)$ and for semi-infinite diffusion ($z_1 \to \pm\infty$), $z(\alpha) \to \pm 1$.

TABLE A1

Variable substitutions for a unified treatment of diffusion towards a plane, spherical, and expanding plane electrode

	Plane	Spherical	Exp. plane
Concn. variable	$C^* = C^b - C$	$C^* = r(C^b - C)$	$C^* = C^b - C$
Space variable	$z = x$	$z = r - r_0$	$z = x t^{2/3}$
Time variable	$y = t$	$y = t$	$y = (3/7)\, t^{7/3}$

(b) Spherical diffusion. For diffusion inside the electrode (i.e., amalgam formation) and with the free boundary at $z_1 = -r_0$ (the centre of the drop), $z(\alpha) = -\coth(\alpha r_0)$. For diffusion outside the electrode (i.e., a solution-soluble product), and with the free boundary at $z_1 \to +\infty$, $z(\alpha) = +1$.

The connection between the flow J towards the electrode and the surface concentration is calculated next. The general equation is $J = -D[\text{grad } C]_{z=0}$. For the expanding plane electrode, the flow is divided by $t^{2/3}$, i.e., $[\text{grad } C]/(t^{2/3}) = -(\delta C^*/\delta z)$ is taken. So that the flow is always towards the electrode ($z = 0$), the equation is modified to $J = -\text{sgn}(z_1)D[\text{grad } C]_{z=0}$, where $\text{sgn}(z_1)$ is equal to $+1$ if z_1 is >0 and -1 if z_1 is <0.

For the spherical case, this gives

$$J = -\text{sgn}(z_1)D\{([C^*]_{z=0}/r_0^2) - (1/r_0)(\delta C^*/\delta z)_{z=0}\}$$

Taking the Laplace transform of this and inserting Eqn. A5 gives

$$\overline{J} = -\text{sgn}(z_1)D\{(1/r_0) + \alpha z(\alpha)\}[\overline{C^*}]_{z=0}/r_0$$

which implies

$$\overline{J} = -\text{sgn}(z_1)D\{(1/r_0) + \alpha z(\alpha)\}[\overline{C^b - C}]_{z=0} \tag{A7}$$

The function $B(s)$ is defined as

$$B(s) = \text{sgn}(z_1)D\{(1/r_0) + \alpha z(\alpha)\} = \text{sgn}(z_1)\{(D/r_0) + (sD)^{1/2}z[(s/D)^{1/2}]\} \tag{A8}$$

This is the transfer function in the general case, valid for all the cases. For a plane electrode, $r_0 \to \infty$, and with expansion the result must be multiplied by $t^{2/3}$. The function $z(\alpha)$ is inserted for some special cases.

(a) Plane diffusion. $B(s) = (sD)^{1/2}\tanh[(s/D)^{1/2}|z_1|]$

Here $z_1 \to \pm\infty$ implies $B(s) \to (sD)^{1/2}$

(b) Spherical diffusion. For diffusion of the product into the electrode ($z_1 = -r_0$)

$$B(s) = (sD)^{1/2}\coth[r_0(s/D)^{1/2}] - D/r_0$$

For semi-infinite diffusion of product into the solution

$$B(s) = D/r_0 + (sD)^{1/2}$$

REFERENCES

1 A. J. Bard and L. R. Faulkner, Electrochemical Methods, Wiley, New York, NY, 1980.
2 T. Kambara, Bull. Chem. Soc. Jpn., 27 (1954) 523.
3 E. P. Parry and R. A. Osteryoung, Anal. Chem., 37 (1965) 1634.
4 J. H. Christie and R. A. Osteryoung, J. Electroanal. Chem., 49 (1974) 301.
5 S. C. Rifkin and D. H. Evans, Anal. Chem., 48 (1976) 1616.
6 G. J. M. Heijne and W. E. van der Linden, Anal. Chim. Acta, 82 (1976) 231.
7 I. Ruzic and M. Sluyters-Rehbach, Anal. Chim. Acta, 99 (1978) 177.
8 G. J. M. Heijne and W. E. van der Linden, Anal. Chim. Acta, 99 (1978) 183.
9 J. H. Christie, L. L. Jackson and R. A. Osteryoung, Anal. Chem., 48 (1976) 242.
10 J. E. Anderson and A. M. Bond, Anal. Chem., 53 (1981) 504.
11 M. Lovrić, J. J. O'Dea and J. Osteryoung, Anal. Chem. 55 (1983) 704.
12 L. Meites, Polarographic Techniques, Wiley, New York, NY, 1965, p. 76.
13 P. Baecklund and R. Danielsson, Anal. Chim. Acta, 154 (1983) 61.
14 P. Baecklund and G. Wikmark, Publication UUIC A82/03, Institute of Chemistry, University of Uppsala, 1982.
15 T. E. Cummings, M. A. Jensen and P. J. Elving, Electrochim. Acta, 23 (1978) 1173.
16 J. B. Flanagan, K. Takahashi and F. C. Anson, J. Electroanal. Chem., 81 (1977) 261.
17 F. C. Anson, J. B. Flanagan, K. Takahashi and A. Yamada, J. Electroanal. Chem., 67 (1976) 253.
18 H. H. Bauer, in A. J. Bard (Ed.), Electroanalytical Chemistry, Vol. 8, M. Dekker, New York, NY, 1975, pp. 169—279.
19 J. E. B. Randles and K. W. Somerton, Trans. Faraday Soc., 48 (1952) 951.

Analytica Chimica Acta, 158 (1984) 323—333
Elsevier Science Publishers B.V., Amsterdam — Printed in The Netherlands

DIFFUSION-LIMITED MASS TRANSFER IN THIN-LAYER (FLOW-THROUGH) ELECTROCHEMICAL DETECTORS WITH SINGLE AND DUAL ELECTRODES

E. M. M. ROOSENDAAL and H. POPPE*

Laboratory for Analytical Chemistry, University of Amsterdam, Nieuwe Achtergracht 166, 1018 WV Amsterdam (The Netherlands)

(Received 19th October 1983)

SUMMARY

This paper describes in detail a theoretical approach to calculate the variables in a flat thin-layer flow-through electrode, in which Poiseuille flow is assumed. A new approximation to the electrode current is derived, reproducing some older results and completing them. Attention is also given to the system with dual electrodes in series, which consists of two electrodes separated by a gap, with the potentials of the electrodes not necessarily equal. The current of the second electrode is given as a function of the gap and electrode lengths.

Electrochemical detection systems in which a thin layer of liquid flows along a flat electrode, embedded in (or forming one wall of) a thin cell duct, are widely used, especially in combination with high-performance liquid chromatography for anodically active species, such as phenols, amides, uric and ascorbic acids and especially catecholamines [1—5].

Although various expressions for the electrochemical diffusion-limited current, as a function of operating conditions and concentrations, have been used in order to speculate about the optimization of such designs [6, 7], close examination reveals that these expressions are often either not applicable or are used outside the range for which they can properly be derived. This in itself provides a reason for reconsideration of the problem. A stronger impetus to re-assessment of the problem has been given by recently reported experiments [8, 9] on the use of interacting, dual-electrode systems in thin-layer cells. In such systems, compounds electrochemically generated at the first electrode can be measured at the second electrode, often under more favourable conditions than direct measurement would allow. In function and operation, the systems are analogous to the ring-disk rotating electrode system [10].

In the dual-electrode systems, the first electrode can be used to induce periodic variations in concentration by modulating its potential. These variations can then be detected at the second electrode kept at a constant potential at which the analyte is converted. In this way the solute-switching

0003-2670/84/$03.00 © 1984 Elsevier Science Publishers B.V.

principle [11], useful for suppressing low-frequency noise and drift, can be applied in electrochemical flow-through detection, as was discussed by MacCrehan and Durst [8] and van Rooijen [12]. Further, it may be possible to enhance selectivity by shielding the second electrode [9].

In order to be able to predict the performance of such systems, quantitative insight into the mass-transfer phenomena is needed. Such insight would also allow some prediction of the performance of miniaturized systems with extremely small cell volumes such as are needed to develop faster systems for liquid chromatography [13] and flow injection analysis [14, 15].

Definition of the problem

As indicated above, the cell considered is that of the thin-layer type. The main alternative, the "confined wall jet" [16, 17] will be dealt with in future work. Further, the present discussion is limited to those cases in which the parabolic flow profile has been developed fully at the position of the electrode. This choice can be justified in the following way. In liquids, and considering solutes of reasonable molecular weight (<1000), the Schmidt number (*Sc*) is approximately 1000; the Schmidt number is the ratio of the kinematic viscosity, ν, of the liquid and the diffusion coefficient, D, of the solute in that liquid. Therefore the development of the flow profile (considered as a function of the length coordinate, in the direction of the flow) is much faster than the development of the concentration diffusion layer. Moreover, in all thin-layer cells known to the authors, the electrode surface is either so large, or so far removed from the liquid centre, that the parabolic flow profile is the best approximation of the real situation.

Many authors have used the equation originally given by Levich [18], which applies to the case where flow and concentration profiles develop simultaneously along the length coordinate. This equation states that the mass transfer for short electrodes is proportional to the product $Re^{1/2}\ Sc^{1/3}$ where *Re* is the Reynolds number. However, the assumption made by Levich is that at the front edge of the electrode the flow is uniform, and it is hard to see how this condition is to be met, even approximately, in the thin-layer cells of interest. It seems better therefore to assume a parabolic flow profile. The result is that *Re* and *Sc* occur in the same power in all equations, i.e., the viscosity of the liquid (with a given average flow) plays no role.

When larger liquid volumes and small electrodes are used, the mass transfer can be well described by equations which have been constructed by several workers, and which are based on work by Levêque [19]. The principle of the treatment has been described very clearly by Newman [20]. These equations apply to flat as well as annular electrodes in thin layers and tubes respectively. When the depletion of the liquid at the end of the electrode is small, and consequently the thickness of the diffusion layer is small compared to the channel width or diameter, it is accurate to describe the velocity

profile by a proportionality between velocity and distance to the electrode. A similarity transformation [20] then makes it possible to derive that the mass transfer is proportional to $(ReSc)^{1/3}$. Unfortunately, the basic assumption of that treatment, i.e., the small depletion of the liquid, is not well fulfilled in present designs. Conversions are a few percent in most cases [5]; simple enlargement of the electrode area leads to semi-coulometric operation [2]. Also the present trend towards miniaturization and lower flow rates will make the assumption less and less accurate.

Electrode kinetics are not considered in this paper. It is assumed throughout that the electrode is either at a potential such that the concentration of the electroactive species vanishes at the surface, or at a potential such that no conversion takes place at all and the flux perpendicular to the surface is zero.

MATHEMATICAL APPROACH

It is assumed that the system depicted in Fig. 1 is infinitely long and uniform in the axial direction. The differential mass-balance equation is then

$$\partial c/\partial t = D\,[(\partial^2 c/\partial x^2) + (\partial^2 c/\partial z^2)] - v\,(\partial c/\partial z) \tag{1}$$

$$\text{with } v = 6\bar{v}\,[(x/d) - (x/d)^2] \tag{2}$$

where c is the concentration of the electroactive species considered, t is the time, and D the diffusion coefficient of the species; x is the coordinate perpendicular to the flow vector and the electrode surface, z the length coordinate, v the local velocity, $\bar{v}$ the average velocity, and d the channel height (layer thickness).

Boundary conditions are $\partial c/\partial x = 0$ at $x = d$ and $c = 0$ at $x = 0$ $(0 < z < z_1)$ and $(z_2 < z < z_3)$, or $\partial c/\partial x = 0$ at $x = d$ and $\partial c/\partial x = 0$ at $x = 0$ $(z_1 < z < z_2)$, and $c = c_0$ at $z = 0$, $0 < x < d$.

Without loss of generality, it is possible to write $c_0 \equiv 1$ and to introduce the dimensionless variables $\rho = x/d$ and $\chi = 2D/\bar{v}d^2$. Likewise, the coordinates of the electrode edges z_1, z_2 and z_3 are converted to χ_1, χ_2 and χ_3. The lengths z_1, $z_2 - z_1$ and $z_3 - z_2$ of the first electrode, gap, and the second electrode are indicated in the dimensionless system as ξ_1, ξ_2 and ξ_3 respectively. Thus, e.g., $\xi_2 = (z_2 - z_1)\,D/\bar{v}d^2$. Considering that for stationary situations the left-hand side is zero, the differential Eqn. 1 becomes

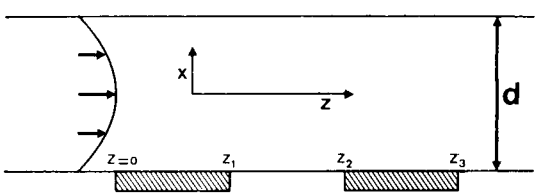

Fig. 1. Scheme of the cell geometry.

$$(\partial^2 c/\partial\rho^2) - 6(\rho - \rho^2)(\partial c/\partial\chi) + (D^2/\bar{v}^2 d^2)(\partial^2 c/\partial\chi^2) = 0 \tag{3}$$

At this point, it is assumed that the third term is small compared to the other two, and can therefore be neglected without seriously affecting the solution. In other words, longitudinal diffusion is neglected. This enables variables to be separated by putting $c = R(\rho)X(\chi)$, which yields $R''(\rho)/6(\rho - \rho^2)R(\rho) = \beta = X'(\chi)/X(\chi)$, β being a constant. As β should be negative, it is replaced by $\beta = -\lambda^2$. The right-hand side of the equation easily yields $X(\chi) = \exp(-\lambda^2\chi)$. The left-hand side of the equation cannot, however, be solved in terms of elementary functions. This differential equation

$$Y'' + 6\lambda^2(\rho - \rho^2)Y = 0 \tag{4}$$

together with boundary conditions constitutes a Sturm—Liouville problem. For several values of λ (the eigenvalues), the boundary conditions are satisfied, and solutions emerge, which are called eigenfunctions. These functions are orthogonal with respect to the weight function $6(\rho - \rho^2)$, i.e., when Y_m and Y_n are both solutions then

$$\int_0^1 6(\rho - \rho^2)\, Y_m\, Y_n\, d\rho = 0 \tag{5}$$

provided $m \neq n$. Solving the differential equation by putting

$$Y = \sum_{n=0}^{\infty} c_n \rho^n \tag{6}$$

and evaluating the coefficients c_n, yields two distinct, complete sets of eigenfunctions. The first one has polynomials P_k with eigenvalues λ_k and norms $L_k^{1/2}$ (the norm of P_k being equal to $[\int_0^1 P_k^2\, 6(\rho - \rho^2)d\rho]^{1/2}$) and is applicable for $0 < \chi < \chi_1$ and $\chi_2 < \chi < \chi_3$. The second one applies to the interval $\chi_1 < \chi < \chi_2$ and has functions Q_k, eigenvalues μ_k and norms $M_k^{1/2}$. The first five eigenfunctions of each set are shown in Fig. 2.

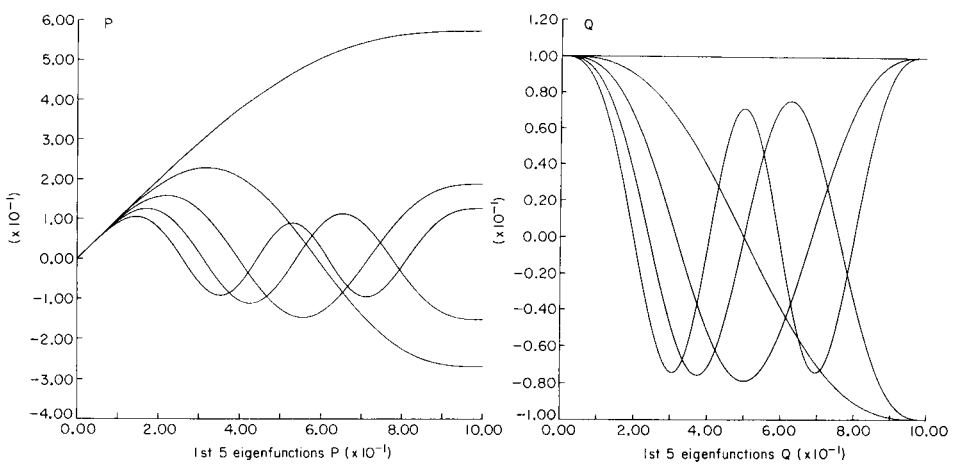

Fig. 2. The first five eigenfunctions of the P and Q sets.

For $\chi < \chi_1$, the concentration can then be expressed directly in a type of Fourier transform, as

$$c(\rho,\chi) = R(\rho)\, X(\chi) = \sum_{k=0}^{\infty} (a_k/L_k)\, p_k \exp(-\lambda_k^2 \chi) \tag{7}$$

with

$$a_k = \int_0^1 6(\rho - \rho^2)\, 1\, P_k \mathrm{d}\rho = 1/\lambda_k^2 \tag{8}$$

the boundary condition at $z = 0$, $c(\rho, 0) = 1$, is satisfied. A similar approach was described by Brown [21] and Prins et al. [22] for the one-electrode case.

The current through the first electrode is, of course, proportional to the converted fraction of the analyte, F, which can be obtained from the mass balance

$$F = 1 - \int_0^1 c(\rho, \xi_1)\, 6(\rho - \rho^2)\, \mathrm{d}\rho \tag{9}$$

or, with Eqn. 8,

$$F = 1 - \int_0^1 6(\rho - \rho^2) \sum_{k=0}^{\infty} (a_k/L_k)\, P_k \exp(-\lambda_k^2 \xi_1)\, \mathrm{d}\rho = 1 - \sum_{k=1}^{\infty} [\exp(-\lambda_k^2 \xi_1)/\lambda_k^4 L_k] \tag{10}$$

It can be seen that for the calculation of the converted fraction, it suffices to know the norms and eigenvalues; the eigenfunctions themselves are not needed to obtain these results.

When $\chi > \chi_1$, the boundary conditions differ from the previous ones, and the profile has to be expressed by the second set of polynomials. With $c(\rho,\chi) = \sum_{m=0}^{\infty} (b_m/M_m)\, Q_m \exp[-\mu_m^2(\chi - \chi_1)]$, b_m can be calculated as

$$b_m = \sum_{k=1}^{\infty} \int_0^1 6(\rho - \rho^2)\, P_k Q_m \, \mathrm{d}\rho \exp(-\lambda_k^2 \xi_1)/(\lambda_k^2 L_k) \tag{11}$$

By elementary calculus it follows that

$$\int_0^1 6(\rho - \rho^2) P_k Q_m \, \mathrm{d}\rho = 1/(\lambda_k^2 - \mu_m^2) \tag{12}$$

whereby one directly obtains

$$b_m = \sum_{k=1}^{\infty} [1/(\lambda_k^2 - \mu_m^2)] \exp(-\lambda_k^2 \xi_1)/\lambda_k^2 L_k \tag{13}$$

By the same methods one can return to the first set of polynomials at $\chi = \chi_2$, and for $\chi > \chi_2$ the concentration can be written as

$$c(\rho,\chi)=\sum_{n=1}^{\infty}\left\{\sum_{m=1}^{\infty}\left[\sum_{k=1}^{\infty}\frac{\exp(-\lambda_k^2\xi_1)}{\lambda_k^2 L_k(\lambda_k^2-\mu_m^2)}\right]\frac{\exp(-\mu_m^2\xi_2)}{M_m(\lambda_n^2-\mu_m^2)}\right\}\frac{P_n\exp[-\lambda_n^2(\chi-\chi_2)]}{L_n} \tag{14}$$

and the converted fraction reads

$$F=\sum_{n=1}^{\infty}\left\{\sum_{m=1}^{\infty}\left[\sum_{k=1}^{\infty}\frac{\exp(-\lambda_k^2\xi_1)}{\lambda_k^2 L_k(\lambda_k^2-\mu_m^2)}\right]\frac{\exp(-\mu_m^2\xi_2)}{M_m(\lambda_n^2-\mu_m^2)}\right\}\frac{1-\exp(-\lambda_n^2\xi_3)}{\lambda_n^2 L_n} \tag{15}$$

With the aid of this formula, it is easy to calculate the effect of varying either ξ_1, ξ_2, or ξ_3 on F.

Reversing the reaction at the second electrode

If the potential at the second electrode ($\chi_2 < \chi < \chi_3$) is properly chosen and the electrode reaction is reversible, the product formed at the first electrode will be reconverted into its original state [9]. Assuming that the original analyte and the product have identical diffusion constants, it is easily seen that $c_{\text{product}}(\rho,\chi) = 1 - c_{\text{original}}(\rho,\chi)$, i.e., both concentrations are complementary to each other. Reconverted fractions can therefore be calculated in a straightforward way. Combination of some of the formulae above yields

$$F_R = 1-\sum_{k=1}^{\infty}\frac{\exp(-\lambda_k^2\xi_3)+\exp(-\lambda_k^2\xi_1)}{\lambda_k^4 L_k}+\sum_{n=1}^{\infty}\left\{\sum_{m=1}^{\infty}\left[\sum_{k=1}^{\infty}\frac{\exp(-\lambda_k^2\xi_1)}{\lambda_k^2 L_k(\lambda_k^2-\mu_m^2)}\right]\frac{\exp(-\mu_m^2\xi_2)}{M_m(\lambda_n^2-\mu_m^2)}\right\}\frac{\exp(-\lambda_n^2\xi_3)}{\lambda_n^2 L_n} \tag{16}$$

where F_R is the amount of material reconverted into its original state at the second electrode, divided by the total amount of analyte.

RESULTS AND DISCUSSION

The eigenfunctions were calculated by evaluating the power series. In order to avoid heavy numerical errors, occurring in these alternating sign series, a modified series was used, to be constructed for every small interval Δ, taking $X(0)$ and $X'(0)$ as calculated from the previous interval.

The eigenvalues were determined by calculating the eigenfunctions and finding all values at which $X'(1) = 0$ by a bisectional method. Two hundred eigenvalues and norms were calculated in both sets and used in all further work.

One electrode

The plot of $\log(F)$ versus $\log(\xi_1)$ is shown in Fig. 3. At low values of ξ_1, the result is in excellent agreement with one obtained by the Levêque approach [19, 20], which states that

$$F = [(3/2)^{2/3}/\Gamma(4/3)]\ \xi_1^{2/3} = 1.467\ \xi_1^{2/3} \tag{17}$$

Both the absolute values and the slope of Levêque's and the present results are nearly identical for values of ξ_1 between 10^{-5} and 10^{-2}.

An expression for $\xi_1 > 0.1$ was arrived at by totally different means (and, in fact, for a different purpose) by Lankelma and Poppe [2] who gave

$$F = 1 - \exp(-2.43\ \xi_1) \tag{18}$$

as an approximation. This is in fact just a one-term representation of Eqn. 10. As it was found that $\lambda_1^2 = 2.4305$ and $a_1 = 0.896$, the validity of this approximation is immediately appreciated. To calculate F in the interval $0.01 < \xi_1 < 0.1$, the use of a third approximation consisting of the first three terms of the series is recommended. Then F becomes

$$F = \sum_{i=1}^{3} a_i \exp(-\lambda_i^2\ \xi_i) \tag{19}$$

with $a_i = \lambda_i^{-4} L_i^{-1}$. The values of a_i and λ_i are given in Table 1. By using this approximation and the former two, it is possible to obtain a value of F with a maximum error of ±3% with respect to the real curve over the entire range of ξ_1 by simple means. The relative errors of the respective approximations are shown in Fig. 4.

Two series electrodes

When the second electrode is at the same potential as the first, a shielding effect occurs. This effect is of course of greatest magnitude when the two electrodes are adjacent; on increasing the gap between the electrodes, the

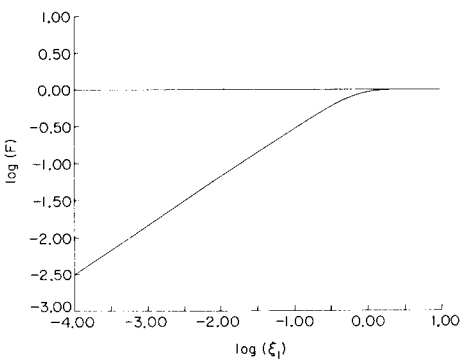

Fig. 3. Converted fraction F at the (first) electrode as a function of ξ_1.

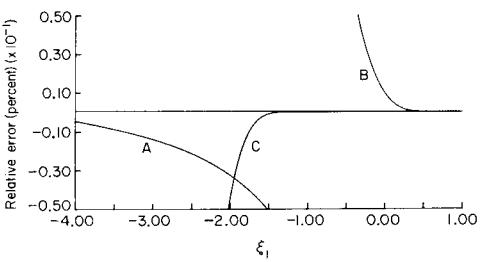

Fig. 4. Accuracy of three approximating expressions for the converted fraction F at one electrode as a function of the electrode length. Curves: (A) Eqn. 17; (B) Eqn. 18; (C) Eqn. 19.

TABLE 1

Constants to be used in Eqn. 19 for the calculation of F in the range $0.01 < \xi_1 < 0.1$

i	a_i	λ_i
1	0.896	1.559
2	0.061	4.857
3	0.018	8.134

shielding effect decreases [23, 24]. However, it does not approach zero, as the average depletion of the layer will still be monitored by the second electrode.

It is useful to define a shielding factor α_S as

α_S = 1 — (current observed when first electrode is active/current observed without operation of first electrode)

As explained, the shielding factor for given electrode lengths ξ_1 and ξ_3 is maximal when ξ_2 is zero, and it approaches a value of $(1 - F_1)$ when ξ_2 is large; F_1 is the conversion factor F for the first electrode.

When the potential and conditions are such that reconversion of the product formed at the first electrode occurs, it is likewise useful to define an effectiveness factor α_E as

α_E = (current observed at second electrode/current observed at first electrode)

which in fact is the fraction of converted molecules produced at the first electrode which reacts at the second one. The effectiveness factor is likewise maximal when ξ_2 is zero; it approaches F for the second electrode, F_2, when ξ_2 is large, because then the second electrode is in contact with a homogeneous solution of the product.

The factors α_S and α_E are both functions of ξ_1, ξ_2 and ξ_3. It is possible to eliminate some redundancy in the presentation of the following results, by considering again that the total concentration (analyte + product) is constant and uniform in the system (provided that the diffusion coefficients are the same). From this, it can be derived that

$$\alpha_S = \alpha_E \, F_1/F_2 \tag{20}$$

However, for the sake of clarity, results for both α_S and α_E are given. Furthermore, it can be noted that the normalized mass flux towards the second electrode in the reconversion experiment, $\alpha_E \, F_1$, is a symmetrical function of ξ_1 and ξ_3 and this leads to another redundancy in the next results.

Figures 5 and 6 show, as an illustration, the concentration profiles calculated for the series electrode system with $\xi_1 = \xi_2 = \xi_3 = 0.01$. Lengths corresponding to these curves are indicated in the legend. It is clearly observable how diffusional relaxation restores the concentration in the immediate vicinity of the electrode to almost 70% of its original value.

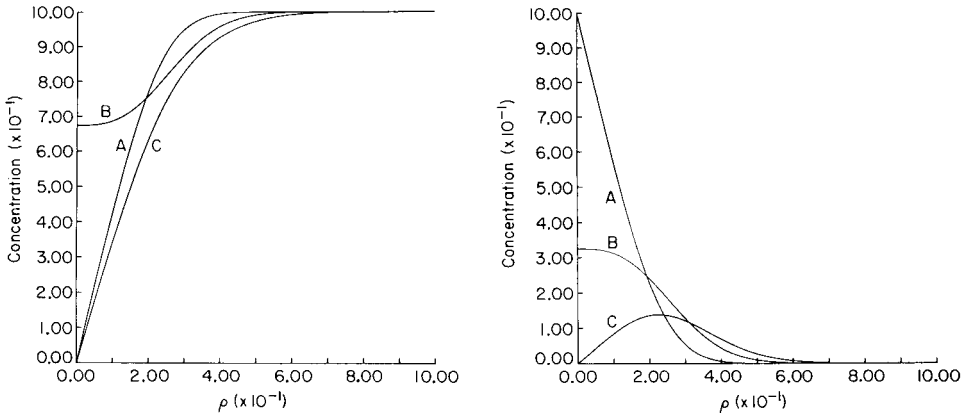

Fig. 5. Concentration profiles as calculated for the series electrode system depicted in Fig. 1. Dimensions: $\xi_1 = \xi_2 = \xi_3 = 0.01$. Curves: (A) $x = x_1$; (B) $x = x_2$; (C) $x = x_3$.

Fig. 6. Concentration profiles of the product of the reverse reaction, taking place at the second electrode, as calculated for the series electrode system. $\xi_1 = \xi_2 = \xi_3 = 0.01$. Curves: (A) $x = x_1$; (B) $x = x_2$; (C) $x = x_3$.

Figure 7 gives the mass flux at the second electrode, for the shielding case, as a function of the gap length ξ_2. In the graph, with logarithmic scale on the abscissa, the position is indicated where gap length is equal to the length of the first electrode. At that point, the shielding factor is about 0.45. The shielding factor for negligible ξ_2 and small electrode lengths, such that the Levêque treatment is applicable, can be derived in an elementary way by applying Eqn. 17 both to the first electrode and the combined first and second electrodes. In this way the limiting value ($2 - 2^{2/3} = 0.41$) for α_S can be derived [23, 24]. From the present results in Fig. 7, a value of 0.46 is obtained. The agreement can be considered to be reasonably good.

Figure 7 contains similar information for electrodes of such lengths ($\xi_1 = \xi_3 = 0.1$) that appreciable depletion (about 30%) of the whole liquid layer occurs. Naturally, the dependence of α_S on ξ_2 is less pronounced here. An important conclusion is that near 100% shielding cannot be obtained with electrodes of equal lengths unless the conversion of the first is nearly coulometric.

In order to investigate the attainable shielding factor with a relatively long first electrode and a very short second electrode, the data presented in Fig. 8 were generated. For this case, $\xi_1 = 0.2$ and $\xi_3 = 0.002$, a shielding factor of over 0.80 is observed for gap lengths smaller than the length of the second electrode. Figure 9 shows the dependence of reconversion efficiency α_E as a function of gap length ξ_2.

Conclusion

The list of eigenvalues and norms, and details of the calculations are available on request. It should be noted that a similar treatment with minor

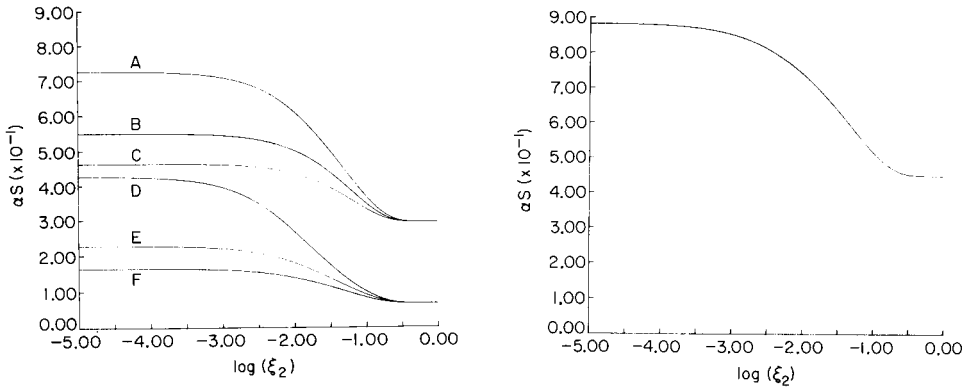

Fig. 7. Shielding factor α_S as a function of gap length ξ_2 for various electrode lengths. Curves: (A) $\xi_3 = 0.01$, $\xi_1 = 0.10$; (B) $\xi_3 = 0.05$, $\xi_1 = 0.10$; (C) $\xi_3 = 0.10$, $\xi_1 = 0.10$; (D) $\xi_3 = 0.01$, $\xi_1 = 0.01$; (E) $\xi_3 = 0.05$, $\xi_1 = 0.01$; (F) $\xi_3 = 0.10$, $\xi_1 = 0.01$.

Fig. 8. Shielding factor α_S as a function of gap length ξ_2 for $\xi_1 = 0.2$ and $\xi_3 = 0.002$.

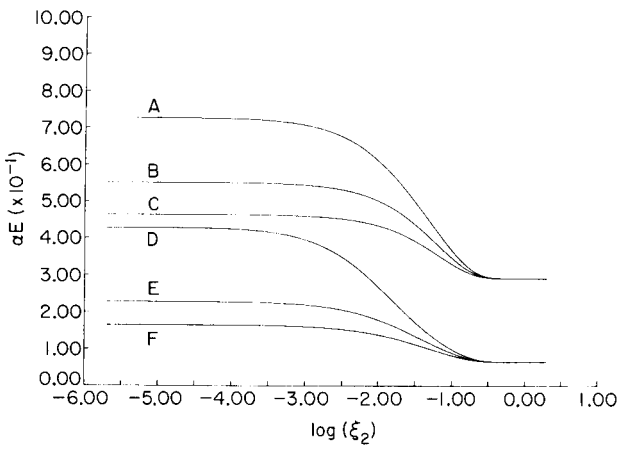

Fig. 9. Reconversion efficiency factor α_E as a function of gap length ξ_2 for various electrode lengths. Curves: (A) $\xi_1 = 0.01$, $\xi_3 = 0.10$; (B) $\xi_1 = 0.05$, $\xi_3 = 0.10$; (C) $\xi_1 = 0.10$, $\xi_3 = 0.10$; (D) $\xi_1 = 0.01$, $\xi_3 = 0.01$; (E) $\xi_1 = 0.10$, $\xi_3 = 0.01$; (F) $\xi_1 = 0.10$, $\xi_3 = 0.01$.

modifications applies to the double ring arrangement in a confined wall jet geometry [16, 17], provided that the flow profile is already parabolic at the front edge of the first electrode. The only change results from the decreasing linear flow velocity on increase of the positional (radial) coordinate. Finally this results in an expression

$$c(\rho, \xi) = \sum_k a_k P_k(\rho) \exp(-\lambda_k^2 \xi^2/2)$$

or its corollary with the Q functions. Eigenfunctions P and Q and eigenvalues λ_k^2 and μ_m^2 remain the same.

Although the present treatment is able to provide much insight into the phenomena in series electrode experiments, there is an important limitation: time-dependent phenomena cannot be handled, and therefore discussion of the maximum frequency, modulation efficiency, etc. for cases where the first electrode is modulated in potential [8, 12] is impossible. The treatment of such phenomena would appear to require the full simulation, e.g. with finite difference schemes, of the transport equations.

Mr. H. Steigstra is thanked for instructive assistance with the computational aspects in the earlier stages of this work.

REFERENCES

1 P. T. Kissinger, C. Refshauge, R. Dreihnig and R. N. Adams, Anal. Lett., 6 (1973) 465.
2 J. Lankelma and H. Poppe, J. Chromatogr., 125 (1976) 375.
3 E. Pungor, Z. Féher and M. Varadi, CRC Crit. Rev. Anal. Chem. 9 (1980) 97.
4 P. T. Kissinger, Anal. Chem., 49 (1977) 448A.
5 H. Poppe, in J. F. K. Huber (Ed.), Instrumentation for High-Performance Liquid Chromatography, Elsevier, Amsterdam, 1978.
6 H. B. Hanekamp and H. J. Nieuwkerk, Anal. Chim. Acta, 121 (1980) 13.
7 S. G. Weber and W. C. Purdy, Anal. Chim. Acta, 100 (1978) 531.
8 W. A. MacCrehan and R. A. Durst, Anal. Chem., 53 (1981) 1700.
9 D. A. Roston and P. T. Kissinger, Anal. Chem., 54 (1982) 429.
10 W. J. Alberg and M. L. Hitchman, Ring Disk Electrodes, Oxford University Press, London, 1971.
11 J. E. Lovelock, J. Chromatogr., 112 (1975) 29.
12 H. W. van Rooijen, Thesis, Amsterdam, 1982.
13 J. H. Knox and M. T. Gilbert, J. Chromatogr., 186 (1979) 405.
14 H. Poppe, Anal. Chim. Acta, 145 (1983) 17.
15 J. M. Reijn, H. Poppe and W. E. van der Linden, Anal. Chim. Acta, 145 (1983) 59.
16 B. Fleet and C. J. Little, J. Chromatogr. Sci., 12 (1974) 747.
17 K. Slais and M. Krejci, J. Chromatogr., 21 (1982) 235.
18 V. G. Levich, Physicochemical Hydrodynamics, Prentice-Hall, New York, NY, 1962.
19 M. A. Levêque, Ann. Mines, Mem., 13 (Ser. 12) (1928) 201, 305, 381.
20 J. Newman, in A. J. Bard (Ed.), Electroanalytical Chemistry, Vol. 6, M. Dekker, New York, NY, 1973, p. 187.
21 G. M. Brown, AIChE J., 6 (1960) 182.
22 J. A. Prins, J. Mulder and J. Schenk, Appl. Sci. Res., Sect. A, 2 (1951) 431.
23 R. Braun, J. Electroanal. Chem., 19 (1968) 23.
24 H. Matsuda, J. Electroanal. Chem., 16 (1968) 153.

Analytica Chimica Acta, 158 (1984) 335—341
Elsevier Science Publishers B.V., Amsterdam — Printed in The Netherlands

A SELECTIVE ELECTROLYTIC SENSOR FOR NITRITE BASED ON A MODIFIED PLATINUM ELECTRODE

JAMES A. COX* and PAWEL J. KULESZA

Department of Chemistry and Biochemistry, Southern Illinois University, Carbondale, IL 62901 (U.S.A.)

(Received 14th November 1983)

SUMMARY

The electrolytic sensor described is based on the oxidation of nitrite at a platinum electrode modified with chemisorbed iodine and coated with a thin layer of quaternized poly(4-vinylpyridine), qPVP. The sealed sensor uses an anion-exchange membrane to separate a thin-layer electrolysis cell from aqueous samples. A steady state is established between Donnan transport of nitrite across the membrane and controlled potential electrolysis at the Pt/I/qPVP indicator electrode. The sensor has a linear response to nitrite concentration in aqueous samples over the range 4×10^{-6}—2×10^{-3} M nitrite. The detection limit is 2×10^{-6} M nitrite. The sensor is free of interference by nitrate, dissolved oxygen, cations, and many neutral species. Anions that are electroactive at 0.7 V vs. Ag/AgCl would interfere, but they are uncommon in most samples. Initial tests with lake water samples suggest that this sensor is unaffected by this matrix. The system was also evaluated for monitoring nitrite levels in spiked meat extracts.

Determinations of trace levels of nitrite must frequently be done in the presence of nitrate. Several methods have been reported that are suitable for this situation. They include spectrophotometry [1—3], fluorimetry [4], differential pulse polarography [5], ion chromatography [6], and potentiometry with a nitrite reductase-based system [7]. Determination of nitrite is complicated by the fact that nitrite is unstable under a variety of conditions. Moreover, the samples of interest are often quite complicated (extracts from processed meats, for example). A direct method that minimizes chemical and physical steps and is suitable for routine field work is therefore desirable. The dip-type electrolytic sensor that is described herein is intended for such applications.

The type of electrolytic sensor used here consists of a thin-layer electrochemical cell separated from a sample solution by an ion-exchange membrane [8, 9]. By an appropriate choice of membrane, either anions or cations can be dialyzed into the cell. The steady-state current measured is developed [9] as a consequence of the relative rates of the Donnan transport and controlled-potential electrolysis of the test ion. Selectivity is achieved by properly defining the conditions for dialysis and electrolysis.

In most respects, these sensors are comparable to the widely-used oxygen

0003-2670/84/$03.00 © 1984 Elsevier Science Publishers B.V.

electrode [10] and other dissolved gas sensors; however, the membrane-transport phenomenon is different. Passive diffusion of ions through membranes is too slow to provide reasonable sensitivity. Donnan dialysis proceeds rapidly and permits ions to be transported into a cell against their concentration gradient; both factors suggest a high sensitivity for such electrolytic sensors.

The limiting factor in the design of these sensors for a particular ion is presently the difficulty of conducting reproducible controlled-potential electrolyses in sealed, thin-layer cells. To be practical, the working electrode must be a solid. Surfaces such as platinum, gold and the various forms of carbon are suited for the electrolysis of many ionic species; however, they typically require frequent conditioning (including polishing) when used in static solutions. Such steps are not compatible with the design of these sensors.

The use of surface modification can improve the long-term stability and decrease memory effects of solid electrodes. The present report describes extension of a previous study of the oxidation of nitrite at a modified platinum electrode [11]. The platinum surface was coated with a monoatomic layer of chemisorbed iodine. A protective film of an anion-exchanger, quaternized poly(4-vinylpyridine), was then deposited. The resulting surface proved to allow reproducible oxidations of nitrite in a pH 4.6 phosphate buffer in a sealed cell.

EXPERIMENTAL

Equipment and chemicals

A Princeton Applied Research Model 170 Electrochemistry System was used. In fact, any three-electrode polarograph or potentiostat could be used, because the measurements are made on a time scale of minutes under controlled-potential conditions.

All chemicals except poly(4-vinylpyridine), PVP, were ACS Reagent Grade and were used as received. The water was distilled and doubly deionized with Cole-Parmer, research-grade cartridges.

Solutions of quaternized poly(4-vinylpyridine), qPVP, were prepared by reacting PVP with benzyl chloride in methanol; 5 ml of benzyl chloride was added to 50 ml of 0.4% (w/v) PVP in methanol, and the quaternization was allowed to proceed overnight.

Preparation of the sensor

The design of the electrolytic sensor was described before [9]. The system consisted of a three-electrode thin-layer electrolysis cell which was bounded in one plane by an ion-exchange membrane. Platinum indicator, Pt counter, and Ag/AgCl reference electrodes were machined flush with the epoxy (Torr Seal, Varian Associates) plug. The volume of the resulting electrolytic chamber was about 0.1 ml. Prior to mounting the membrane, the Pt indi-

cator electrode was cleaned and modified, first with iodine, and subsequently with qPVP.

The bottom surface of the platinum was polished using sand paper of different grades and then a wet woollen cloth. It was further cleaned by polishing with 0.1-μm alumina (Fisher Gamal) on a Gamal cloth with distilled water as the lubricant. The assembly was placed in deaerated 1 M sulfuric acid and cycled at 50 mV s^{-1} between 1.4 and —0.2 V vs. SCE 50—100 times [12]. The surface was reduced at 0.4 V until the current decayed to a constant, low value [13]. That decay took 2—3 min. After this pretreatment, the electrode surface was highly reproducible and free of spurious properties. Chemical modification of the platinum surface with iodine was accomplished by exposing the assembly thus cleaned to a freshly-prepared, deaerated solution of 2 mM sodium iodide [14]. The further modification with qPVP polyelectrolyte was done on dried Pt/I surfaces prepared as described above. Adherent coatings of qPVP were obtained by dipping the system for 1 min in a 0.4% (w/v) methanol solution of the polymer. The electrode was removed, and solvent was allowed to evaporate from the surface. After coating, the assembly was washed repeatedly with methanol and air-dried. After modification of the indicator electrode, the Pt counter electrode was activated by polishing with sand paper and the Ag/AgCl reference electrode was generated.

Assembly of the electrolytic sensor was completed by filling the thin-layer electrolyte reservoir with 1 M sodium dihydrogenphosphate at pH 4.6 and attaching a P-1025 anion-exchange membrane (RAI Research Corp., Hauppauge, NY) over the open end of the plexiglas cylinder. Teflon tape and a small plastic hose clamp were used to hold the membrane in place.

Between experiments it was not necessary to remove the membrane. Because Donnan exclusion breaks down when solutions of high ionic strength are in contact with both sides of ion-exchange membranes, dipping the sensor into the 1 M phosphate solution at pH 4.6 for a few minutes regenerates the electrolyte and removes the electrolysis products. The indicator electrode is held at 0.25 V vs. Ag/AgCl during this time. Because the electrolysis product, nitrate, does not interfere, this step is necessary only occasionally.

Procedures

Previously described cells [15] were used in the experiments to characterize the Donnan dialysis of nitrite. The sample volumes were 100 ml; receiver volumes were 5 ml, and dialysis times were 30 min. The samples were magnetically stirred; the stirring rate was maintained well below the point of vortex formation. The P-1025 anion-exchange membranes were initially soaked overnight in 1 M potassium chloride. They were rinsed and stored in 1 M sodium dihydrogenphosphate. After dialysis, the content of the receiver chamber was diluted to 10 ml to correct for osmotic dilution, and the nitrite therein was quantified by linear scan voltammetry in the same

way as at the Pt/I modified electrode [11]. An enrichment factor was calculated as the ratio of the nitrite concentration in the diluted receiver after dialysis to the initial sample concentration.

Lake water samples were obtained from Campus Lake at Southern Illinois University. They were suction-filtered through Metricel membrane (0.45 μm thick, 47 mm diameter; Gelman Sciences) and used within 24 h. Because they did not contain a detectable amount of nitrite, they were spiked with known quantities just prior to the measurements.

The study of the processed meat involved a sample preparation that was based on previous reports [16—19]. A 2.5-g sample of finely chopped meat was transferred to a 250-ml volumetric flask with 150—200 ml of hot (80°C) water. The contents were heated for 2 h on a steam bath and then cooled in ice water to solidify the fat. The system was brought to room temperature, diluted to volume with water, filtered through Whatman 41 paper, and refiltered through Whatman 40 paper.

RESULTS AND DISCUSSION

The general behavior of Pt/I, a platinum electrode that is coated with a layer of chemisorbed iodine, is now well-known. The iodine layer suppresses background peaks in current-voltage curves by minimizing hydrogen and oxygen electrodeposition on the platinum [12, 14]. The overall background current is lower and more reproducible than at bare platinum. Unlike the situation at bare platinum [20, 21], the oxidation of nitrite at the Pt/I surface is reproducible and yields a well-defined peak (34-mV difference between the peak and half-peak potentials) in linear scan voltammetry [11]. The Pt/I is highly stable when only cyclic voltammetric experiments are done, but its efficacy diminishes when used for long periods in the controlled-potential electrolysis mode at pH 4.6 [11].

In order to obtain a working electrode that is stable in the controlled-potential electrolysis, the Pt/I was coated with qPVP. That polymer was selected over PVP because the latter has anion-exchange properties only in acidic solution. The former provided a porous, conductive coating that acted as an anion-exchanger even in neutral solution [22]. The resulting Pt/I qPVP working electrode gave well-defined linear scan voltammograms (Fig. 1) that were reproduced in pH 4.6 phosphate buffer for several days as long as the potential excursions were within the limits of 0.9 to —0.2 V vs. SCE. Controlled-potential electrolyses were likewise reproducible.

For successful design of the electrolytic sensor, the electrolysis conditions (pH 4.6, 1 M phosphate buffer) must be compatible with Donnan dialysis. In this regard, it is important that the rate of Donnan transport be proportional to the nitrite concentration in the sample and independent of the sample matrix, especially pH, over a wide range of conditions.

Using the above electrolyte, the enrichment factor was independent of the pH of the sample over the range of interest. With 0.5 mM sodium nitrite

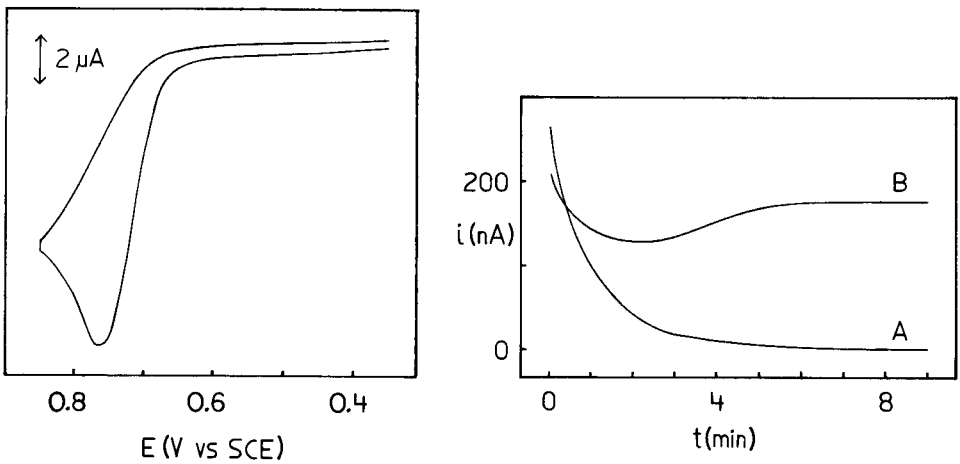

Fig. 1. Cyclic voltammetry of nitrite at a Pt/I/qPVP electrode: 1 mM nitrite in 1 M NaH_2PO_4 at pH 4.6; scan rate, 50 mV s^{-1}; electrode substrate area, 1.5 mm^2.

Fig. 2. Current-time behavior of the electrolytic sensor: (A) in a deionized water blank; (B) in 0.1 mM nitrite. Internal electrolyte and conditions as in Procedures.

samples adjusted to pH values of 3.5, 4.1, 6.0, 6.8 and 7.9 with dilute phosphoric acid or sodium hydroxide, the enrichment factors obtained were 3.8, 3.8, 4.0, 3.8 and 3.9, respectively. In addition, with the nitrite concentration varied from 0.01 to 1.0 mM in pH 4.6 samples, the relative standard deviation of the enrichment factor was only 8% (n = 8). Other studies showed that Donnan dialysis was not affected by the ionic strength of the sample (up to a value 0.01 M) or by the presence of moderate quantities of surfactants [23, 24]. It was therefore concluded that the pH 4.6 phosphate buffer was suitable as a combination of a Donnan dialysis receiver and supporting electrolyte for nitrite oxidation.

Figure 2 shows the response of the electrolytic sensor with a 0.1 mM nitrite solution when the Pt/I/qPVP electrode was held at 0.7 V vs. Ag/AgCl. A steady-state current was established in 6 min in the worst case.

The steady-state current was directly proportional to sample concentration over a wide range. Calibration graphs were prepared using the electrolysis current measured relative to the blank at a prescribed time after contact to the stirred sample. For example, with a 6-min current sampling time, linear least-squares fits of eight points over the range 4×10^{-6} M to 4×10^{-3} M nitrite yielded a slope of 4.84 ± 0.008 mA M^{-1} a y-intercept of 12 ± 12 nA, a standard error of estimate for the current of 28 nA, a standard error of estimate of concentration of 5.9×10^{-6} M and a correlation coefficient of 0.9999. The detection limit, calculated as the concentration that yields a current twice the uncertainty of the measurement on a blank solution, was 2×10^{-6} M nitrite. These data were generated by holding the Pt/I/qPVP electrode at 0.7 V vs. Ag/AgCl during the measurement.

To evaluate further the reproducibility of the electrolytic sensor, a set of five experiments was performed on a 0.1 mM nitrite sample in the following sequence. First, the current at an assembled sensor was measured. Then, the unit was dismantled several times and reassembled after a fresh preparation of the Pt/I/qPVP working electrode. The respective steady-state currents were 0.46, 0.49, 0.52, 0.44, and 0.50 μA. Generally, the repeatability of a measurement on a given sensor over several weeks was 4% at the 0.1—1 mM level and 8% below 0.1 mM.

The major interferents with this nitrite sensor are anions that are oxidized at 0.7 V vs. Ag/AgCl at the Pt/I/qPVP working electrode in pH 4.6 buffer. This group includes thiocyanate, bromide and iodide. Anions that are strong oxidizing agents were not considered because they would not be present with nitrite. Arsenic(III) did not interfere because at the pH values used, it exists primarily as arsenious acid and, hence, is not subject to Donnan dialysis. Cations were likewise excluded from the electrolysis cell. Of particular importance is the freedom of interference from nitrate and dissolved oxygen, neither of which is electroactive under the conditions used. The addition of gelatin (10 mg l^{-1}) did not change the sensitivity, which agrees with earlier studies on Donnan dialysis [23].

The sensor was tested on two types of samples. A lake water sample that did not contain a detectable level of nitrite was sequentially spiked with sodium nitrite. With six values in the range 8×10^{-6} M to 2×10^{-3} M nitrite, linear least-squares analysis yielded a slope of 4.73 ± 0.02 mA M^{-1}, a y-intercept of 10 ± 16 nA, a standard error of the current estimate of 32 nA, a standard error of the concentration estimate of 6.8×10^{-6} M, and a correlation coefficient of 0.9999. The slope is only 2% lower than that observed with laboratory standards, so that the lake water matrix significantly affected neither the rate of transport nor the electrolytic response. The detection limit was 2×10^{-6} M nitrite (0.09 mg l^{-1}) in the lake water.

The second sample was processed meat. The nitrite level in the extract was found to be 3.3×10^{-6} M by spectrophotometry [1]. The value was at the detection limit of the electrolytic sensor, so in order to evaluate the performance of the sensor in that matrix, sodium nitrite was sequentially added. The sensor was soaked in 1 M sodium dihydrogenphosphate for 5 min between measurements. For concentrations of 0.01, 0.05, 0.10, and 0.4 mM, currents of 22, 114, 233, and 922 nA were obtained. Although too few points were available for a complete statistical treatment, a linear response was apparent with a correlation coefficient of 0.9999. The slope, 2.31 mA M^{-1}, was 48% of the value obtained on laboratory standards prepared in pure water suggesting that the matrix suppressed the signal. Nevertheless, the linear response demonstrated that quantitation by standard addition was feasible. Moreover, the original response of the electrolytic sensor to laboratory standards was restored by soaking for 1 h in the 1 M phosphate solution at pH 4.6. Alternatively, the sensitivity was restored by demounting the membrane and rinsing it in methanol, soaking it in 1 M nitric acid for a few minutes, and placing it back on the sensor.

Further work is being performed to compare this nitrite sensor to the spectrophotometric procedures. The sensor may permit the use of a faster filtering step. Direct monitoring of the nitrite level during the extraction may be possible. This would permit evaluation of the loss of nitrite during the extraction.

S. Walden, Arkansas State University at Jonesboro, did some of the reported measurements. The work was supported by the National Science Foundation under grant CHE-8215371.

REFERENCES

1 Standard Methods for the Examination of Water and Wastewater, 15th edn., American Public Health Association, Washington, DC, 1981, pp. 380—383.
2 B. E. Saltzman, Anal. Chem., 26 (1954) 1949.
3 I. T. Glover and F. T. Johnson, J. Chem. Educ., 50 (1973) 426.
4 E. D. Coppla, A. F. Wickorski and J. Hanna, J. Assoc. Off. Anal. Chem., 58 (1975) 469.
5 S.-K. Chang, R. Kozeniauskas and G. W. Harrington, Anal. Chem., 49 (1977) 2272.
6 W. F. Koch, Anal. Chem., 51 (1979) 1571.
7 C. H. Kiang, S. S. Kuan and G. G. Guilbault, Anal. Chim. Acta, 80 (1975) 209; Anal. Chem., 50 (1979) 1319.
8 J. A. Cox and G. R. Litwinski, Anal. Chem., 51 (1979) 554.
9 J. A. Cox, P. J. Kulesza and M. A. Mbugwa, Anal. Chem., 54 (1982) 787.
10 I. Fatt, Polarographic Oxygen Sensors, CRC Press, Cleveland, OH, 1976, Ch. 1—3.
11 P. Kulesza and J. A. Cox, 34th Pittsburgh Conf. Exp. Anal. Chem. Appl. Spectrosc., Atlantic City, NJ, 1983, paper No. 765.
12 D. C. Johnson, J. Electrochem. Soc., 119 (1972) 331.
13 A. T. Hubbard, R. A. Osteryoung and F. C. Anson, Anal. Chem., 38 (1968) 692.
14 R. F. Lane and A. T. Hubbard, Anal. Chem., 48 (1976) 1287; J. Phys. Chem., 79 (1975) 808.
15 J. A. Cox and J. E. DiNunzio, Anal. Chem., 49 (1977) 1272.
16 W. Horwitz (Ed.), Official Methods of Analysis of the Association of Official Analytical Chemists, 12th edn., Association of Official Analytical Chemists, Washington, DC, 1975, p. 381, Sect. 24.042.
17 E. D. Coppla, A. F. Wickorski and J. Hanna, J. Assoc. Off. Anal. Chem., 59 (1976) 783.
18 K. K. Choi and K. W. Fung, Analyst (London), 105 (1980) 241.
19 R. N. Fiddler and J. B. Fox, J. Assoc. Off. Anal. Chem., 61 (1978) 1063.
20 E. Julien and M. Comtat, Rev. Chim. Miner., 6 (1969) 885.
21 J. E. Harrar, Anal. Chem., 43 (1971) 143.
22 N. Oyama, T. Shimomura, K. Shigehara and F. C. Anson, J. Electroanal. Chem., 112 (1980) 271.
23 G. L. Lundquist, G. Washinger and J. A. Cox, Anal. Chem., 47 (1975) 319.
24 J. A. Cox and Z. Twardowski, Anal. Chim. Acta, 119 (1980) 39.

Analytica Chimica Acta, 158 (1984) 343—355
Elsevier Science Publishers B.V., Amsterdam — Printed in The Netherlands

EFFECT OF SOME CHELATING LIGANDS ON THE POTENTIAL RESPONSE OF THE CHALCOCITE COPPER ION-SELECTIVE ELECTRODE

ADAM HULANICKI*, TADEUSZ KRAWCZYNSKI VEL KRAWCZYK and ANDRZEJ LEWENSTAM

Department of Chemistry, Warsaw University, Warsaw (Poland)

(Received 29th July 1983)

SUMMARY

The effects of diethylenetriamine, triethylenetetramine, tetraethylenepentamine, aminoacetic acid, iminodiacetic acid, nitrilotriacetic acid, ethylenediaminetetraacetic acid, diethylenetriaminepentaacetic acid and triethylenetetraminehexaacetic acid on the behaviour of the synthetic chalcocite (copper(I) sulphide) copper-selective electrode are described. The effects of those ligands on the electrode response at different pH values is explained on the assumption that copper(I) ions contribute to the potential indicated. Copper(I) ions originate from the membrane phase and participate in exchange and redox reactions. The effects of oxygen and temperature are reported. The electrode response can be predicted on the basis of copper(II) equilibria in solution, only if the conditions are such that there is no interference from copper(I) ions.

Investigations of the behaviour of metal ion-selective electrodes in chelating media are of importance because they may explain the potential response in complexation titrations as well as in measurements of ionic equilibrium constants. This problem has been pointed out in the literature [1—6] but no conclusions that are in agreement with all experimental facts have been offered. In this area, much work has been done with the copper-selective electrode.

This paper is concerned with the potential response of copper-selective electrodes immersed in solutions of a number of chelating agents. On the basis of their behaviour, these ligands may be divided into two groups. The first group of ligands consists of polyamines such as diethylenetriamine (dien), triethylenetetramine (trien), tetraethylenepentamine (tetren), aminoacetic acid (glycine), as well as ligands not investigated in this paper such as ammonia and citrate. In solutions of those ligands, the potential of the electrode may be at least roughly calculated on the basis of appropriate equilibrium constants. The effect of the second group of ligands cannot be fully predicted on this basis. This group comprises mainly polyaminopolycarboxylic acids such as ethylenediaminetetraacetic acid (EDTA), diethylenetriaminepentaacetic acid (DTPA) and triethylenetetraaminehexaacetic acid

(TTHA). An intermediate position is occupied by monoaminopolycarboxylic acids such as iminodiacetic acid (IDA) and nitrilotriacetic acid (NTA). Several mechanisms have been previously proposed to explain the behaviour of copper-selective electrodes but none of them seems to be fully satisfactory.

EXPERIMENTAL

Apparatus

The synthetic chalcocite (copper(I) sulphide) single-crystal electrode used was constructed in the laboratory [7] with a solid internal contact. For potential and pH measurements, Beckman (model 4500) and Orion (model 701) instruments were used. A common double-junction reference electrode was used; the electrolyte bridge was filled with 10% (w/v) potassium nitrate solution.

All measurements were done in solutions stirred with a magnetic stirrer. When thermostatted and deoxygenated conditions were needed, the solutions were placed in a Metrohm cell.

Procedures

Three types of measurements were examined. First, electrode potential vs. pH plots were prepared in the pH range 2—12 in solutions containing a 5×10^{-4} M copper complex and an excess of the same concentration of the relevant ligand. Similar tests were done with solutions containing only the ligand at the 10^{-3} M level. Such measurements were done for nine ligands, polyamines, amino(poly)carboxylic acids and polyaminopolycarboxylic acid.

Secondly, copper was titrated with trien and EDTA, and vice versa, in acetate and ammoniacal buffers at different temperatures (10, 25 and 40°C) in air-saturated solutions as well as in solutions deoxygenated with a stream of argon.

Thirdly, electrode potentials were measured as a function of a total ligand (trien, EDTA) concentration in the range 2×10^{-4}—2×10^{-2} M. These measurements were also done in acetate and ammoniacal buffers under air-saturated and deoxygenated conditions at 25°C. In some of those measurements, the electrode surface was renewed by polishing it mechanically in a 1% (w/v) ascorbic acid solution.

RESULTS

The experimental potential vs. pH curves (Fig. 1) for solutions containing various ligands in the presence and absence of added copper(II) solution were compared with those calculated on the basis of the equilibrium constants tabulated in Table 1. In the case of polyamines a relatively good fit to the expected potential values was observed for solutions containing a copper complex and excess of ligand. For aminoacetic acid, iminodiacetic acid and

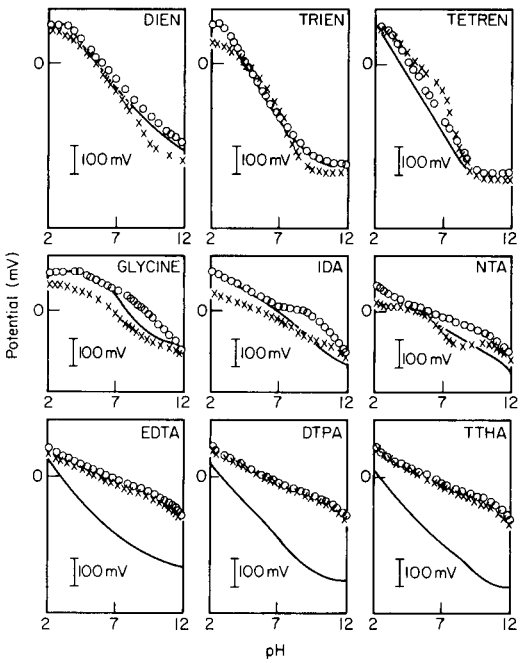

Fig. 1. Dependence of the potential of the chalcocite electrode on pH in presence of various ligands (L): (○) 5×10^{-4} M CuL + 5×10^{-4} M L; (X) 10^{-3} M L. The solid lines were calculated from the data in Table 1.

nitrilotriacetic acid, the experimental potential values were more positive at pH values above 7, above 5 and above 3, respectively, than those calculated on the basis of known solution equilibria. The measurements conducted in the presence of polyaminopolycarboxylic acids (Fig. 1) indicate that the experimentally found potential values are more positive than the calculated values over the whole investigated pH range and that the course of the relationship is practically independent of the nature of the ligand studied.

The potential vs. pH curves recorded in the absence of the copper complex differ somewhat when measured with the synthetic chalcocite electrode and with an electrode containing silver sulphide and copper sulphide as the membrane component [1]. In experiments with polyamines as ligands, the potentials are not regularly shifted in a negative direction compared to measurements conducted in the presence of the copper complex. In solutions of monoaminocarboxylic acids, significant differences were observed between the potential responses in the presence and absence of the copper complex, the largest differences being found at pH values of about 9. In the experiments with polyaminopolycarboxylic acids, the potential in presence of copper ions complexing half of the ligand added was regularly less negative; this reflects the lower free ligand concentration interacting directly with the electrode and influencing the solution equilibria.

TABLE 1

Logarithms of equilibrium constants used for calculation of potential vs. pH curves and theoretical titration curves [8] at 20°C and ionic strength (I) 0.1

Ligand	Protonation constants of ligands						Stability constants of copper(II) complexes	
	K_1	K_2	K_3	K_4	K_5	K_6	K_{CuL}	K_{CuL_2}
Dien	9.98	9.17	4.32				16.1	5.1
Trien	9.92	9.20	6.67	3.32			20.4	
Tetren	9.85	9.28	8.19	4.80	3.06		23.1	
Glycine	9.57[a]	2.36[a]					8.15[a]	6.88[a]
IDA	9.44	2.62	1.82[a]				10.63	6.05
NTA	9.71	2.48	1.8	0.8			12.96	4.47
EDTA	10.24	6.16	2.66	2.0	1.5		18.80	
DTPA	10.55	8.59	4.30	2.66	1.82		21.55	−0.4
TTHA	10.65	9.54	6.10	4.03	2.7	2.3	21.8	

Ligand	Protolytic reaction constants for copper(II) complexes					
	K^{H}_{CuHL}	$K^{H}_{CuH_2L}$	$K^{H}_{CuH_3L}$	$K^{H}_{CuH_4L}$	$K^{H}_{CuHL_2}$	K^{OH}_{CuOHL}
Dien	3.2[a]				8.2[a]	4.6
Trien	3.5					3.2
Tetren	5.2[a]	3.8[a]				
Glycine						
IDA						6.26[b]
NTA						4.39[c]
EDTA	3.0					2.5
DTPA	4.74	3.04[a]				
TTHA	8.03	4.05[a]	2.86[a]	2.04[a]		

[a] 25°C, I = 0.1. [b] 25°C, I = 0.05. [c] 25°C, I = 0.08.

The titration curves of copper ions with trien and EDTA, at 25°C in acetate and ammoniacal buffers (Fig. 2) were in good agreement with expectations before the equivalence point. After the equivalence point, when no excess of copper was present in the solution, good coincidence of the calculated and observed potential values was observed only in the case of trien. For EDTA titrations, the potential after the equivalence point was significantly more positive than expected; this is in agreement with the potential/pH curves. This discrepancy was especially large for titrations done in acetate buffers. Very similar results were obtained for the reverse titrations of ligands with the copper(II) solutions (Fig. 3).

Similar titrations were carried out at 10°C and 40°C (Fig. 4). The higher the temperature, the greater the potential jump at the equivalence point, because the titration curve corresponding to the excess of EDTA is shifted to more negative values. However, in acetate buffer this effect was small

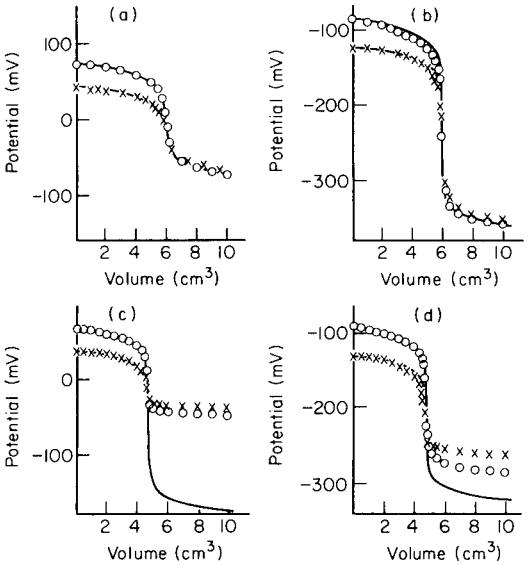

Fig. 2. Titration of copper ions with trien and EDTA: (a, b) trien as titrant; (c, d) EDTA as titrant. Buffer: (a, c) acetate; (b, d) ammonia. (○) 10^{-2} M Cu^{2+}; (X) 10^{-3} M Cu^{2+}. Solid lines were calculated from the data in Table 1.

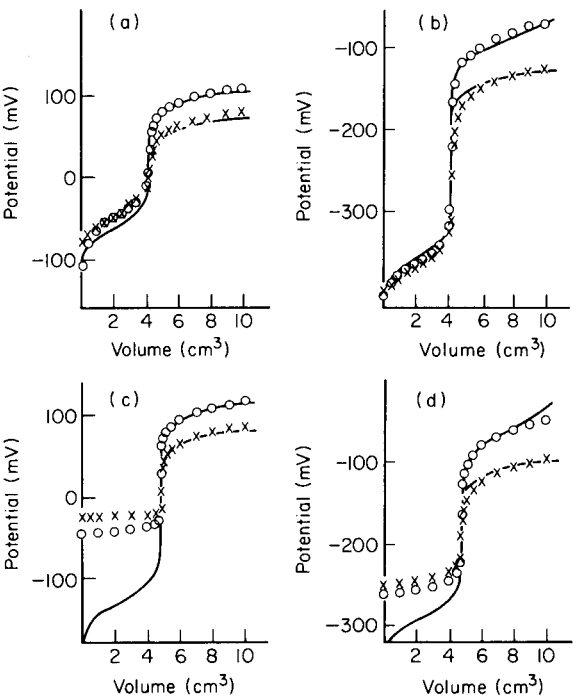

Fig. 3. Titration of trien and EDTA with copper(II) as titrant: (a, b) trien as analyte; (c, d) EDTA as analyte. Buffer: (a, c) acetate; (b, d) ammonia. (○) 10^{-2} M; (X) 10^{-3} M. Solid lines were calculated from the data in Table 1.

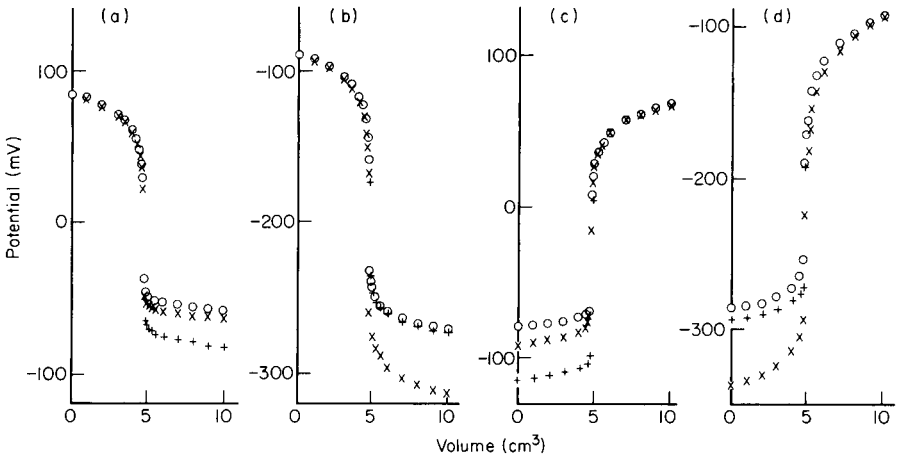

Fig. 4. Effect of temperature and oxygen removal on the titration curves: (a, b) titration of 10^{-2} M copper was EDTA; (c, d) reverse titration. (○) 10°C; (X) 40°C; (+) 10°C and oxygen removal with argon. Buffer: (a, c) acetate; (b, d) ammonia.

whereas in ammoniacal buffer at 40°C the potentials obtained were almost the same as those calculated on the basis of solution equilibria.

The effect of removing oxygen from the solutions was also studied (Fig. 4). It was found that the potential in the absence of oxygen when an excess of EDTA was present was always more negative than in air-saturated solutions. This difference was slightly greater at more elevated temperatures, and was significantly greater for acetate solutions than for ammonia solutions.

When the potential dependence on the total ligand concentration was examined, it was found that deoxygenation of the solution always decreased the electrode potential. This effect was greater when the electrodes had freshly cleaned surfaces.

DISCUSSION

The interpretation of the behaviour of the copper ion-selective electrode in complexing media involves consideration of the processes at the solution/membrane interface. Only the copper(II)—ligand equilibria in solutions were taken into account; other reactions that may occur, e.g., under the influence of light, were not considered.

Heijne and van der Linden [1] postulated a mechanism based on the fact that the copper(II) ions are strongly adsorbed on the copper sulphide precipitate [9]. Such a positively charged layer at the electrode surface would attract negatively charged copper(II) complexes as well as free ligands. This in turn causes a stronger attack on the membrane and in consequence increases the copper ion concentration. This effect is observed as a positive deviation of the potential response compared to the values calculated on the

basis of bulk concentrations. This is also the reason for the worse detection limit of the electrode under those conditions.

However, in the presence of polyamines, the ligands are neutral or positively charged as are their copper complexes, and this should prevent their attack on the membrane surface. It should be noted that strong adsorption of copper(II) ions was found under different conditions [9]. In the present case, such adsorption cannot be definitively excluded, but its role should not be overestimated. In the case of the synthetic chalcocite electrode, some increase of the potential break at the end-point of titrations at about pH 9 at elevated temperature may in fact be due to desorption of ions from the membrane surface. Nevertheless, the better agreement observed between the calculated and observed titration curves in ammoniacal buffer than in acetate cannot be fully explained on this basis.

The experiments clearly indicate that an important role is played by the presence of dissolved oxygen in the solution, which suggests the occurrence of redox processes. It is known that chalcocite may be oxidized anodically to form a series of non-stoichiometric sulphides which are also known as minerals [12]. These are djurleite, digenite, anilite, blue remaining covellite ($Cu_{1.1}S$) and finally covellite, which is a stoichiometric copper(II) sulphide. Therefore, it is necessary to consider a possible series of reactions, with the process

$$Cu_2S \rightarrow CuS + Cu^{2+} + 2e^- \quad (1)$$

being regarded as the final reaction. In parallel to the oxidation of copper(I), sulphide may also be oxidized. The E vs. pH diagram (Fig. 5) suggests that oxidation to sulphate is the most probable [13]. This diagram was plotted on the basis that the solution contains 10^{-3} M concentrations of CuEDTA and EDTA, and that the sulphate concentration formed in the oxidation is 10^{-5} M [8]. The standard potential values used in plotting Fig. 5 were taken directly or calculated from the literature data [14]. The values are as follows: $E^0_{S/S^{2-}} = -0.476$ V; $E^0_{SO_4^{2-}/S^{2-}} = -0.682$ V; $E^0_{SO_4^{2-}/S} = -0.75$ V and $E^0_{Cu^{2+}/Cu^+} = 0.159$ V.

Despite the thermodynamically probable oxidation to sulphate, there may also be some oxidation to elemental sulphur, which is one of the products of anodic oxidation of chalcocite [10]. It is not possible to decide unequivocally how far these processes go. It is well known that some sulphide electrodes, e.g., the lead ion-selective electrode containing PbS as a membrane component, are easily oxidized in the presence of aerial oxygen; the presence of sulphate ions at the surface of the electrode composed of $Ag_{1.55}Cu_{0.45}S$ has been confirmed [15]. The final oxidation may proceed according to

$$Cu_2S + 4H_2O \rightarrow 2Cu^{2+} + SO_4^{2-} + 8H^+ + 10e^- \quad (2)$$

However, even if it is accepted that formation of a certain amount of copper ion at the electrode surface is responsible for the more positive

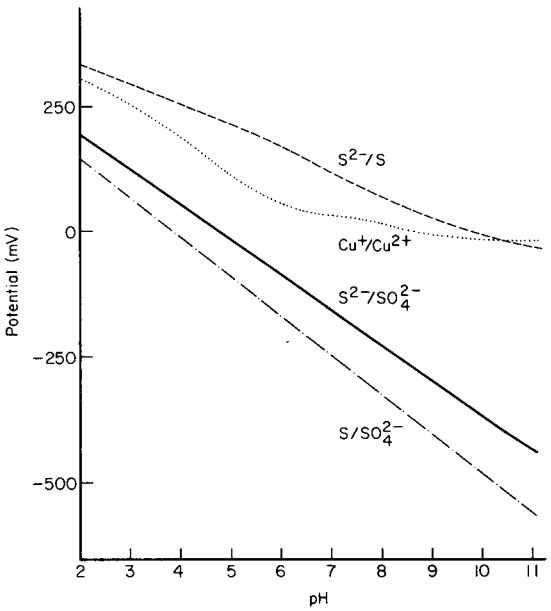

Fig. 5. Redox potential vs. pH diagram for some redox couples connected with reactions of the chalcocite electrode.

potential values, then this should occur independently of the nature of the ligand, which is not the case when polyamine ligands are considered. Further, removal of oxygen should improve the agreement between experimental and calculated titration curves, which is in fact observed. Also the temperature effect should be independent of the pH and buffer composition used in titrations.

According to the present observations, the most complete explanation of those phenomena is based on the diffusion model of the chalcocite electrode [16], which assumes an initial sensitivity to copper(I) ions. Its potential is given by

$$E = E^0 + 59.2 \log([Cu^+] + K^{pot}_{Cu^+,Cu^{2+}} [Cu^{2+}]^{1/2}) \quad (3)$$

where the potentiometric selectivity coefficient is 6.3×10^{-7} [7].

When copper(I) ions are not added to the test solution, $[Cu^+]_A = 0$, then their only source is the membrane material, by means of its solubility and the exchange reaction

$$Cu_2S + Cu^{2+} \rightleftharpoons CuS + 2Cu^+ \quad (4)$$

The equilibrium concentration of copper(I) ions was calculated on the basis of the solubility product $K_{so}(Cu_2S) = 10^{-48}$ and appropriate coefficients for the side-reactions

$$[Cu^+] = [2K_{so(Cu_2S)}\,\alpha_{S(H)}/\alpha_{Cu(I)(EDTA)}]^{1/3} \quad (5)$$

where $\alpha_{S(H)} = 1 + K_1[H^+] + K_1K_2[H^+]^2$ and $\alpha_{Cu(I)(EDTA)} = 1 + K_{Cu(I)EDTA}[EDTA] + K_{Cu(I)EDTA}K_{Cu(I)HEDTA}[H^+][EDTA]$. The protonation constants of hydrogen sulphide are $K_1 = 7.9 \times 10^{13}$ and $K_2 = 1 \times 10^7$. The stability constant of the copper(I)-EDTA complex has been given [17] as $K = 3 \times 10^8$; the value for the protonation constant may be assumed to be 10^6, similar to the constant for the silver complex. The concentration of the free ligand was calculated in the usual way, by using the constants included in Table 1.

The equilibrium concentration of copper(II) ions can be calculated from the stability constant of the complex (Table 1)

$$[Cu^{2+}] = C_{Cu^{2+}}\alpha_{EDTA(H)}/K_{CuEDTA}\,C_{EDTA} \quad (6)$$

where $C_{Cu^{2+}} = 9.5 \times 10^{-4}$ M and $C_{EDTA} = 1.05 \times 10^{-3}$ M.

These calculations indicated that the contributions of copper(I) and copper(II) ions to the electrode potential response are comparable within about one order of magnitude (Table 2). However, formation of copper(II) ions in the course of copper(I) sulphide oxidation, shifts the exchange reaction to the right, producing additional amounts of copper(I) ions at the membrane surface. This additional amount seems to be mainly responsible for the disagreement between the experimental potential values and those calculated exclusively on the basis of solution equilibria. This occurs in solutions of polyaminopolycarboxylic acids, and especially in titrations in acetate buffers.

The situation may change in the presence of ligands which complex copper(I) ions strongly, so that their contribution to the potential value becomes insignificant. Under these conditions, the electrode behaves as a copper(II) electrode and the measured potential values are in good agreement with those calculated on the basis of solution equilibria only. This is the case for polyamines, which form strong complexes with both copper(I)

TABLE 2

Contributions of copper(I) and copper(II) to the potential response (Eqn. 3) of the synthetic chalcocite electrode in 10^{-3} M CuEDTA and 10^{-3} M EDTA solution

pH	$[Cu^+]$	$[Cu^{2+}]$	$K^{pot}_{Cu^+,Cu^{2+}}[Cu^{2+}]^{1/2}$
3	1.2×10^{-11}	5.2×10^{-9}	4.5×10^{-11}
4	2.5×10^{-12}	3.6×10^{-11}	3.8×10^{-12}
5	4.8×10^{-13}	3.7×10^{-13}	3.8×10^{-13}
6	6.6×10^{-14}	5.9×10^{-15}	4.8×10^{-14}
7	8.1×10^{-15}	2.8×10^{-16}	1.1×10^{-14}
8	1.4×10^{-15}	2.5×10^{-17}	3.2×10^{-15}
9	3.0×10^{-16}	2.6×10^{-18}	1.0×10^{-15}
10	7.5×10^{-17}	3.9×10^{-19}	4.0×10^{-16}
11	2.6×10^{-17}	1.7×10^{-19}	2.6×10^{-16}

and copper(II) ions. Therefore in titrations with trien, the experimental curves coincide with the calculated curves.

In EDTA titrations, ammonia plays a similar role when an ammoniacal buffer is used; so does a substoichiometric amount of 1,10-phenanthroline. Another way to inhibit the formation of copper(I) ions and to improve the agreement between the calculated and experimental potentials is deoxygenation of the test solution. This effect is more visible when the solution does not contain species which complex copper(I) ions, which explains the larger effect of oxygen removal in titrations done in acetate than in ammoniacal buffers.

Those considerations were confirmed by a study of various treatments of the electrode surface. All measurements were obtained in 10^{-3} M copper(II) solutions at titration fraction $f = 2$ in acetate buffer (pH $\approx$ 4.3). Several sets of conditions were examined: (A) electrode surface not renewed, air-saturated solution; (B) electrode surface mechanically polished under water to prevent heating which may promote oxidation [18], air saturated solution; (C) electrode surface not renewed, oxygen removed from solution; (D) electrode surface as in (B), oxygen removed from solution; (E) electrode surface mechanically polished in ascorbic acid solution, oxygen removed from solution.

The results of those experiments (Table 3), presented as the potential decrease compared to measurements in air-saturated solutions without electrode pretreatment, indicate that electrode polishing, especially in reducing medium, and prevention of oxidation of the membrane during measurements cause a well-defined decrease of the potential. These effects are, however, not additive, which is obvious because none of those precautions corresponds to a well-defined process. Especially the polishing of the electrode is a poorly reproducible process because exact reproduction of the surface must be doubtful. The effect of 1,10-phenathroline is larger when the electrode surface is further from its ideal state (i.e., not pretreated) or is immersed in air-containing solutions. The change in the 1,10-phenanthroline concentration, always at a substoichiometric level compared to copper, has a more pronounced effect when the concentration of copper(I) is likely

TABLE 3

Lowering of the chalcocite electrode potential (mV) obtained by various methods of surface renewal, oxygen removal and 1,10-phenanthroline addition

Solution	Decrease in potential (mV) for the different conditions				
	A	B	C	D	E
Without 1,10-phen[a]	—	50	80	120	160
With 10^{-5} M 1,10-phen	60	100	110	150	170
With 10^{-4} M 1,10-phen	100	130	130	160	170

[a] 1,10-phenanthroline.

to be larger at the electrode surface. With deoxygenated solutions and a pre-reduced electrode surface, 1,10-phenanthroline has little effect.

The contribution of redox processes to the potential response of the electrode seems obvious from those experiments. The oxidant is oxygen dissolved in the solutions. Polishing of the electrode surface under reducing conditions, in an ascorbic acid solution, is practically very advantageous. The potential values obtained then almost coincided with the calculated values. Without such electrode pretreatment, nearly the same potentials were obtained, but this was possible only after many hours of continuous deoxygenation of the solution. This suggests that desorption of oxygen from the electrode surface is a very slow process [18].

All those processes are heterogeneous reactions so that their rates are poorly controlled. Therefore, it is very difficult to reproduce all conditions strictly or to record stable potential values which, for example, do not change by more than 0.1 mV min^{-1}.

The measurements of electrode potentials under the above-mentioned conditions as a function of pH (Fig. 6) confirms these suggestions. Inhibition of copper(I) ion formation by surface pretreatment and oxygen removal from solution strongly favoured decreased potentials over the whole pH range.

The influence of temperature on titration curves may be connected with desorption of copper(II) ions from the membrane surface. This becomes

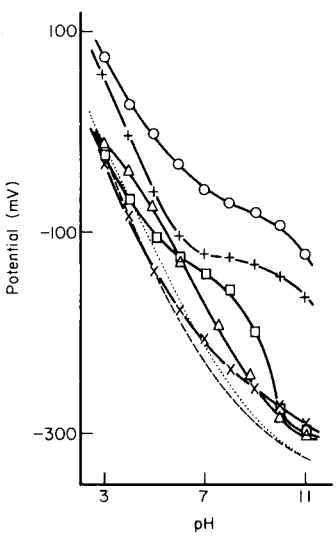

Fig. 6. Effect of various experimental parameters on the potential vs. pH curves in solutions containing 10^{-3} M CuEDTA and 10^{-3} M EDTA. (○) Electrode surface not renewed, air-saturated solution; (+) same conditions with 10^{-5} M 1,10-phenanthroline added; (□) electrode surface not renewed, air removed by argon; (X) same conditions with 10^{-5} M 1,10-phenanthroline added; (△) electrode surface polished under ascorbic acid solution, air removed by argon. (···) Curve calculated for CuEDTA + EDTA solution; (---) curve calculated for CuEDTA + EDTA solution in presence of 10^{-5} M 1,10-phenanthroline.

visible only when the copper(I) ions are removed by complexation, as in the case of titrations in ammoniacal buffer. However, it is probable that temperature rises also affect oxygen desorption.

CONCLUSIONS

It has been reconfirmed that the synthetic chalcocite electrode is primarily sensitive to copper(I) ions. The behaviour of the electrode is well described on the basis of the diffusion model, according to which the electrode potential is determined by the concentrations of both copper(I) and copper(II) ions at the electrode surface. Those concentrations depend on the composition of the solution and on the ion-exchange process in which the membrane material participates. Those concentrations also depend on the parasitic oxidation processes occurring in the presence of oxygen, when the solutions are air-saturated. In fact, the electrode potential must be considered as a mixed potential; the occurrence of several likely reaction mechanisms makes precise prediction of this potential impossible.

Adsorption of copper ions at the electrode surface may occur under the experimental conditions used, but it plays a minor role in the potential response.

The complexity of all the processes responsible for the electrode potentials and the impossibility of exact prediction of the potential values in the presence of polyaminopolycarboxylic ligands, makes it difficult to apply metal buffers reliably for electrode calibration in such media. It is probable that some other interferences have a similar origin. This also inhibits evaluation of solution equilibria with the aid of the chalcocite electrode. It does not follow directly from the experiments described in this paper, but very similar phenomena are probably responsible for the discrepancies reported between calculated and measured potentials when other types of solid-state copper-selective electrodes were used.

The authors are grateful to Dr. J. Gulens, AEC, for fruitful discussion. This paper was prepared as part of the research project MR-I-32.

REFERENCES

1 G. J. M. Heijne and W. E. van der Linden, Anal. Chim. Acta, 96 (1978) 13.
2 W. E. van der Linden and G. J. M. Heijne, Conf. Ion-Selective Electrodes, Akademiai Kiado, Budapest, 1977, p. 445.
3 G. Nakagawa, H. Wada and T. Hayakawa, Bull. Chem. Soc., Jpn., 48 (1975) 424.
4 V. K. Olson, J. D. Carr, R. D. Hargens and R. K. Forcé, Anal. Chem., 48 (1976) 1228.
5 I. Sekerka and J. F. Lechner, Anal. Lett., Part A, 11 (1978) 415.
6 M. F. El-Tarras and E. Pungor, Anal. Chim. Acta, 82 (1976) 285.
7 A. Hulanicki, M. Trojanowicz and M. Cichy, Talanta, 23 (1976) 47.
8 R. M. Smith and A. E. Martell, Critical Stability Constants, Vol. 1, Amino Acids, Vol. 2, Amines, Plenum Press, New York, NY, 1974, 1975.

9 C. C. Wu and M. H. Yang, Anal. Chim. Acta, 93 (1977) 99.
10 P. Brennet, S. Jafferali, J.-M. Vanseveren, J. Vreecken and R. Winand, Metall. Trans., 5 (1974) 127.
11 M. Lamache and D. Bauer, Anal. Chem., 51 (1979) 1320.
12 R. T. Shuey, Semiconducting Ore Minerals, Elsevier, Amsterdam, 1975, Ch. 10, p. 230, Ch. 12, p. 254.
13 M. Avrahami and R. M. Golding, J. Chem. Soc. A, (1968) 647.
14 L. G. Sillen and A. E. Martell, Stability Constants of Metal-Ion Complexes, Spec. Publ. No. 17, Chemical Society, London, 1964.
15 J. F. Coetzee, W. K. Istone and M. Carvalho, Anal. Chem., 52 (1980) 2353.
16 A. Hulanicki and A. Lewenstam, Talanta, 23 (1976) 661.
17 K. Srinivasan and R. S. Subrahmanya, J. Electroanal. Chem., 31 (1971) 257.
18 E. Peters, Trends in Electrochemistry, in J. O. M. Bockris, D. A. J. Rand and B. J. Welch (Eds.), Plenum Press, New York, NY, 1977.

Analytica Chimica Acta, 158 (1984) 357—362
Elsevier Science Publishers B.V., Amsterdam — Printed in The Netherlands

ENZYME ELECTRODE FOR THE DETERMINATION OF SALICYLATE

TEKUM FONONG and GARRY A. RECHNITZ*
Department of Chemistry, University of Delaware, Newark, DE 19711 (U.S.A.)
(Received 28th October 1983)

SUMMARY

Salicylate hydroxylase is used with a carbon dioxide sensor for the determination of salicylate in aqueous solution and pooled serum. The enzyme is physically entrapped with a dialysis membrane at the sensing tip of the carbon dioxide electrode. The enzyme catalyzes the stoichiometric formation of catechol and carbon dioxide from salicylate and reduced pyridine nucleotide in the presence of flavin adenine dinucleotide as a specific cofactor. The carbon dioxide is detected by the sensor and related to the concentration of salicylate via a calibration curve. The method compares favorably with the spectrophotometric method for assay of salicylate. Although suitable for salicylate concentrations in the range of 5—300 μg ml^{-1}, its response below 5 μg ml^{-1} is limited by the detection limit of the carbon dioxide sensor.

Acetylsalicylic acid (aspirin) is widely used as an analgesic and anti-inflammatory agent. Its common metabolites are salicylic acid, salicyluric acid, and 2,5-dihydroxybenzoic (gentisic) acid. Because formation of salicyluric acid and salicylphenolic glucuronide is capacity-limited in the therapeutic dose range [1—4], there is a disproportionate rise in plasma salicylate levels as the dose of aspirin increases. For design of safe and effective dosages for long-term therapy, it is important to be able to monitor the time course of plasma salicylate concentrations as a function of dose and frequency of aspirin administration.

Methods for the determination of salicylate include gas-liquid chromatography [5—11], thin-layer chromatography [12, 13], spectrofluorimetry [14, 15], high-performance liquid-chromatography [16—19], colorimetry [20—22], and potentiometry [23]. An enzymatic or enzyme-based method has now become attractive owing to the recent commercial introduction of the salicylate hydroxylase enzyme.

Principle of the method

The method utilizes the enzyme-catalyzed reaction in which salicylate is stoichiometrically converted to catechol and carbon dioxide

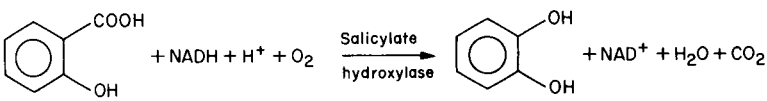

(1)

0003-2670/84/$03.00 © 1984 Elsevier Science Publishers B.V.

The carbon dioxide produced is sensed with a potentiometric pCO_2 membrane sensor.

EXPERIMENTAL

Reagents, solutions and instrumentation

Sodium salicylate, acetylsalicylic acid, salicyluric acid (*o*-hydroxyhippuric acid), sodium gentisate (sodium 2,5-dihydroxybenzoate), β-nicotinamide adenine dinucleotide, and Type S 2385 salicylate hydroxylase (E.C. 1.14.13.1) were used (Sigma Chemical Company, St. Louis, MO).

Only reagent-grade chemicals were used. Distilled-deionized water was used throughout in making solutions. Stock solutions of salicylate (6.50×10^{-3} M), gentisate (6.84×10^{-3} M), and salicyluric acid (6.84×10^{-3} M) were prepared by dissolving the appropriate amount of each compound in water. Solutions of β-NADH were made in pH 6.00 (0.10 M) phosphate/EDTA buffer. The buffer (30 mM K_2HPO_4/1 mM EDTA) was prepared by dissolving appropriate amounts of dipotassium hydrogenphosphate and disodium-EDTA in 80 ml of water, adjusting the pH to 6.00 with hydrochloric acid, and diluting to a final volume of 100 ml with water [24].

An Orion Model 95-02 carbon dioxide sensor connected to a Corning Model 12 Research pH/mV meter was used with a Heath-Schlumberger Model SR 255 B strip-chart recorder to record the potentiometric data. The chart speed was set at 0.05 cm min^{-1} at a range of 100-mV full scale. A 10-ml double-jacketed glass cell thermostated at 30.0 ± 0.1°C with a Haake Model FM constant-temperature bath was used in the measurements. Spectrophotometric data were obtained with a Hitachi Model 100-60 spectrophotometer.

Procedure

In all measurements, the initial volume of solution was 3.00 ml (0.5 ml of 0.062 M β-NADH and 2.50 ml of 0.10 M phosphate/EDTA buffer, pH 6.00). All solutions were allowed to reach thermal equilibrium (30°C) with constant stirring in the thermostated cell.

The enzyme was obtained as a lyophilized powder and was immobilized by physically entrapping 1.0 mg (4 units) at the tip of the carbon dioxide sensor with a Technicon Type C dialysis membrane. The electrode was inserted into the cell and after a steady baseline potential had been obtained (after about 20 min), the enzyme-catalyzed reaction was initiated by addition of salicylate.

RESULTS AND DISCUSSION

Effect of pH

In acidic solutions (≤pH 4.00), the activity of the enzyme decreases rapidly with time; and at ≤pH 5.50, β-NADH is almost instantly destroyed. Therefore, the choice of operating pH for the immobilized enzyme will

require a compromise between these limits and the inherent properties of the pCO_2 electrode itself. The overall pH profile obtained experimentally is shown in Fig. 1. Although the apparent pH for maximum activity is 5.50, all experiments were done at pH 6.00 to minimize the loss of β-NADH. In confirmation, the absorbance of a solution of β-NADH (1×10^{-3} M) at 340 nm was monitored at pH 6.00 for 1 h; no significant decrease was observed. Because of evidence that inhibitor can form in solutions of β-NADH without a decrease in absorbance at 340 nm [25], all solutions of β-NADH were prepared and used within 1 h.

Calibration curves and lifetime of the electrode

Calibration curves (Fig. 2) were constructed in solutions with initial volumes of 3.00 ml thermostated at 30°C, as described in the Procedure. Aliquots of stock salicylate solution (6.50×10^{-3} M) were added to initiate the enzyme-catalyzed reaction. Steady-state potentials were recorded after each addition. The response time was 8 min for the lowest salicylate concentration (1.08×10^{-5} M) and 2 min for the highest salicylate concentration (8.23×10^{-4} M).

The slope of the semilogarithmic plot was found to be 38 mV/decade for data between 7.50×10^{-5} and 7.30×10^{-4} M. Lifetime studies of the electrode were taken by constructing calibration curves daily for 15 days. After 12 days, the slope decreased.

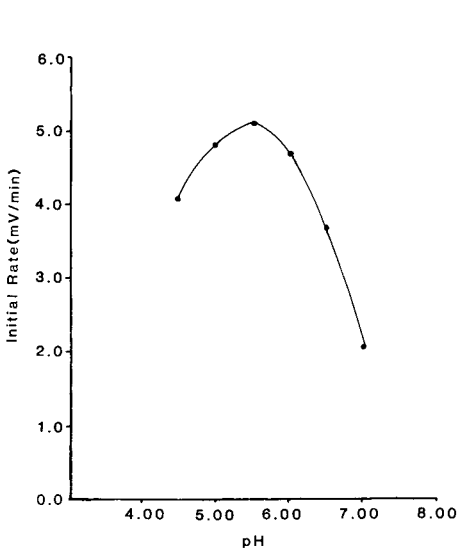

Fig. 1. pH profile of the immobilized salicylate hydroxylase electrode at 30°C.

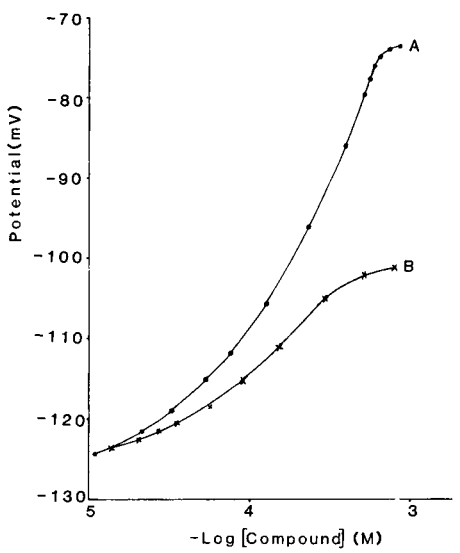

Fig. 2. (A) Typical calibration curve for salicylate with the immobilized salicylate hydroxylase electrode at 30°C and pH 6.00. (B) Response to gentisate under the same conditions.

Selectivity of the electrode

Although salicylate is the major metabolite of aspirin, minor metabolites such as gentisate and salicyluric acid are known to accumulate in the body after ingestion of large doses of aspirin. Therefore, gentisate and salicyluric acid were examined as substrates for the enzyme. It was found that only gentisate gave potential changes. The extent of interference is shown in Fig. 2. While gentisate is clearly a significant interference, the relative concentrations of salicylate and gentisate in physiological situations are such that the gentisate interference is of no practical importance in clinical samples. There was no response of the electrode to aspirin itself.

Precision studies

The precision of this determination of salicylate was tested in both aqueous solution and pooled serum. Salicylate concentrations were randomly chosen in the range of 36.0—292.5 μg ml^{-1} and quantified. Aliquots of a standard salicylate solution (6.50×10^{-3} M) were added to the aqueous or serum solution and the steady-state potential was measured for each added aliquot. The corresponding concentration obtained from the standard curve was compared to that of the sample added to the solution. Table 1 shows that the relative errors in these studies ranged from 1.2—2.4%. Within-run precision results are also given in Table 1. These values range in standard deviation from ±1.2% to ±4.1% with an average of ±2.1%.

The results of recovery studies in aqueous and pooled-serum solutions are given in Table 2. These results show an average recovery of 97% for aqueous solutions and 98% for serum solutions.

Comparison of potentiometric and spectrophotometric methods

Aqueous samples of salicylate were tested using both the electrode method and the spectrophotometric method outlined by Sigma Chemical Company. In the spectrophotometric method, the decrease in absorbance of β-NADH was monitored for each aliquot of salicylate solution added. Linear regression analysis of the two sets of results showed that the potentiometric method

TABLE 1

Precision studies and relative errors in random salicylate assays at pH 6.00 and 30°C

Salicylate concentration (μg ml^{-1})		Relative error (%)	Within-run precision[a] (%)
Taken	Found		
36.0	36.9	+2.5	±4.1
61.0	62.4	+2.3	±3.0
204.1	200.8	−1.6	±1.0
248.8	245.9	−1.2	±1.0
292.5	287.2	−1.8	±1.2

[a] RSD calculated from ten results.

TABLE 2

Recovery studies of salicylate in aqueous solutions and pooled serum

Average salicylate added (μg ml^{-1})	Recovery (%)		Average salicylate added (μg ml^{-1})	Recovery (%)	
	Aqueous solution	Pooled serum		Aqueous solution	Pooled serum
5.2	98	109	61.0	98	97
10.4	97	102	110.5	98	96
15.5	96	98	204.1	97	96
25.8	98	96	270.9	97	98
36.0	96	95	313.6	97	96

agreed well with the spectrophotometric method. For ten samples ranging from 5.2 to 200 μg ml^{-1}, a plot of the potentiometric data (y) vs. the spectrophotometric data (x), gave a straight line defined by the equation $y = (1.01 \pm 0.01)x + 2.24 \pm 0.02$ with $S_{yx} = 1.5$ and $r = 0.98$.

The results of this study show that the potentiometric method may provide an attractive alternative for the determination of salicylate. The electrode shows useful sensitivity and selectivity while requiring minimal sample pretreatment compared to other methods [26].

We are grateful to NIH (Grant GM 25308) for support of this work.

REFERENCES

1 G. Levy, J. Pharm. Sci., 54 (1965) 959.
2 G. Levy, A. W. Vogel and L. P. Amsel, J. Pharm. Sci., 58 (1969) 503.
3 T. Tsuchiya and G. Levy, J. Pharm. Sci., 61 (1972) 541.
4 T. Gibson, G. Zaphiropoulos and J. Grove, Br. J. Clin. Pharmacol., 2 (1975) 233.
5 L. J. Walter, D. F. Biggs and R. T. Coutts, J. Pharm. Sci., 63 (1974) 1754.
6 A. J. Hoffman and H. I. Mitchell, J. Pharm. Sci., 52 (1963) 305.
7 E. B. Dechene, L. H. Booth and M. J. Caughey, J. Pharm. Pharmacol., 21 (1969) 678.
8 E. R. Blakley, Anal. Biochem., 15 (1966) 350.
9 M. Rowland and S. Riegelman, Anal. Biochem., 20 (1967) 463.
10 M. Rowland and S. Riegelman, J. Pharm. Sci., 56 (1967) 717.
11 J. P. Tischio, J. Pharm. Sci., 65 (1976) 1530.
12 A. J. Cummings and M. L. King, Nature, 209 (1966) 620.
13 J. C. Morrison and J. M. Orr, J. Pharm. Sci., 55 (1966) 936.
14 G. Graham and M. Rowland, J. Pharm. Sci., 61 (1972) 1219.
15 A. Saltzman, J. Biol. Chem., 174 (1948) 339.
16 I. Bekersky, H. G. Boxenbaum, M. H. Whitson, C. V. Puglisi, R. Pocelinko and S. A. Kaplan, Anal. Lett., 10 (1977) 539.
17 G. W. Peng, M. A. F. Gadalla, V. Smith, A. Peng and W. L. Chiou, J. Pharm. Sci., 67 (1978) 710.
18 B. E. Cham, D. Johns, F. Bochner, D. M. Imhoff and M. Rowland, Clin. Chem., 25 (1979) 1420.
19 J. N. Buskin, R. A. Upton and R. L. Williams, Clin. Chem., 28 (1982) 1200.
20 D. Schachter, J. Clin. Invest., 36 (1957) 297.

21 B. B. Brodie, S. Udenfriend and A. F. Coburn, J. Pharmacol. Exp. Ther., 80 (1944) 114.
22 M. Furman and L. Firberg, J. Pediatr., 70 (1967) 287.
23 T. P. Hadjiioannou and P. C. Gritzapis, Anal. Chim. Acta, 126 (1981) 51.
24 T. Gerritsen, M. L. Fehberg and H. A. Waisman, Anal. Biochem., 11 (1965) 460.
25 C. P. Fawcett, M. M. Ciotti and N. O. Kaplan, Biochim. Biophys. Acta, 54 (1961) 210.
26 W. D. Mason and R. Gillilan, Anal. Lett., 16 (1983) 903.

Analytica Chimica Acta, 158 (1984) 363–368
Elsevier Science Publishers B.V., Amsterdam — Printed in The Netherlands

Short Communication

DISCLOSE: AN INTEGRATED SET OF MULTIVARIATE DISPLAY PROCEDURES FOR CHEMICAL AND PHARMACEUTICAL DATA

DAVID BAWDEN

Pfizer Central Research, Sandwich, Kent, CT13 9NJ (Great Britain)

(Received 7th September 1983)

Summary. An approach to providing thorough, reliable views of multivariate data is described using an integrated set of classification and display routines (DISCLOSE). The programs are mainly based on standard, published algorithms. The techniques include principal components plots, non-linear mapping, three hierarchal cluster analysis algorithms, minimum spanning tree, and nearest-neighbour representation, together with alternative methods for variable normalization. DISCLOSE, which does not require computer graphics hardware, is well suited for providing a systematic initial visualization of data-set structure, and is applicable to chemical, pharmaceutical, and biological data.

Although the importance of graphical display techniques for multivariate data has long been recognised by statisticians, it is only in recent years that they have begun to be applied to data from chemical sciences. One reason for this may be the potentially confusing array of classification and display methods available [1, 2], and of software available for computer implementation [3, 4]. The value of the application of such techniques (plotting, mapping, clustering, etc.) to chemical data was first described by Kowalski and Bender in 1973 [5], and the methods have since been widely used in chemical and pharmaceutical data analysis [6]. Applications of cluster analysis [7], principal components plots [8], and the combination of cluster analyses or minimum spanning trees with non-linear mapping [9, 10] have been reported. In virtually all of these cases no direct comparison was made between different display techniques. It is clear, however, that distinct differences exist in the displays produced by various techniques [1, 2, 11], and even between different hierarchal cluster methods [11—13], which may significantly affect interpretation of the results. Different ways of standardization of input data may have similar effects. Reliance on a single display may thus lead to erroneous conclusions about data-set structure, because of features of individual display techniques. The best way of avoiding such problems is to use a complementary set of multivariate classification and display procedures, so that the results may be readily compared and combined.

It seemed desirable to have available an integrated set of display programs which could be conveniently and rapidly applied to the data set, so as to obtain a thorough analysis, taking advantage of the different "views" of the

0003-2670/84/$03.00 © 1984 Elsevier Science Publishers B.V.

data shown by the various techniques. This would also allow in-depth evaluations of the performance of display methods, and combinations of them, with different kinds of chemical and pharmaceutical data sets. These could include sets of bioassay results, physicochemical properties, analytical or formulation data, or chemical structures.

Because no generally available statistical or pattern recognition package provided, in a convenient form, all the techniques which were required, a new suite of programs was constructed, known as DISCLOSE (DISplay and CLassificatiOn SuitE). The rationale for the choice of combination of techniques, and the means of their implementation are described here, as a guide to others who may find it worthwhile to integrate multivariate display routines in a similar fashion.

DISCLOSE Overview

DISCLOSE was designed to be run as a single system, so that a data set would be read in, and any of the available data standardization procedures and display techniques invoked in response to prompts to the user. The system is thus extremely simple to operate, to encourage its use by scientists who may not be particularly computer-orientated. It is run interactively from any VDU, and does not require any computer graphics hardware. Output is produced on a line-printer, enabling subsequent perusal at leisure, which has proved to be a very satisfactory means of digesting and analysing results of this sort. An interactive graphics capability, as an adjunct to the main system, is at present under development, and should prove particularly valuable for combinations of displays, e.g., clusters superimposed on a two-dimensional plot. It is not likely, however, that such a facility will entirely replace the proven, and highly acceptable, simpler plotting capability.

The components of DISCLOSE are: input and related procedures, data standardization, classification and display procedures, and output routines. The classification and display methods were chosen, from the large number available, to meet two criteria. First, they must have been reasonably widely used, and preferably have had some usage with chemical/pharmaceutical data, so that there would be some information available as to their characteristics, and strengths and weaknesses with particular types of data, and so that advantage could be taken of the experience of other users. Secondly, they must fit within an overall plan for the system, covering a range of complementary types of display: two-dimensional plots (including eigenvector techniques and others), clusters (with algorithms chosen for their distinct characteristics), and "checking displays" (simpler techniques, of particular value in identifying discrepancies in the other displays). Whenever possible, standard subroutines were used as the basis of implementation of the display and output procedures, again to take advantage of the experience of other users, and to ensure accuracy and reliability of the numerical procedures. The use of well-established algorithms, implemented in computer routines of proven reliability, is an important factor in enabling the user to have confidence in the results of such displays.

The overall plan of the DISCLOSE system is shown diagramatically in Fig. 1, and the individual components and the rationale for their inclusion are described below.

Components of the DISCLOSE system

Input. A data set is read into DISCLOSE in an entirely flexible manner. The present limitations on the size of problem to be evaluated are 80 objects and 80 variables. It is doubtful whether direct visual displays for larger data sets would be feasible or useful, but if required the process (with the possible exception of the principal components extraction procedure) could be scaled up.

The input data matrix may be reversed, so as to invert the meaning of "objects" and "variables". For example, given a structure/activity data set with several biological activities measured for each of a series of compounds, it would be equally convenient to classify either the compounds or the biological assays. These two-way analyses are often a valuable means of understanding data-set structure.

Standardization. It is generally accepted as necessary to standardize, or normalize, the variables used in analyses such as these, so that the results are not dominated by those variables with largest variance [2, 14]. The commonest procedures are division of each value of a variable by the range or the standard deviation for that variable. However, if the ratio of range to standard deviation is not roughly constant for all variables, distinct differences in the displays may result [15]. DISCLOSE therefore allows normalization by range or standard deviation, and allows investigation of the ratios.

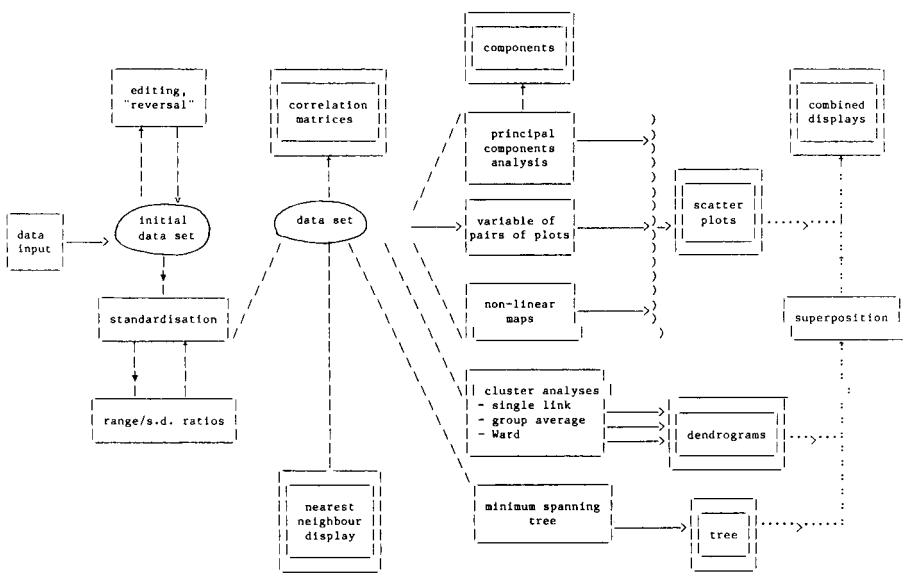

Fig. 1. DISCLOSE components: (—) automated process; (···) manual process; (=) output.

Unnormalized data may also be used in those cases where it is appropriate, e.g., in some classifications of chemical structure [12, 13].

Correlations and variable plots. Inspection of the correlation between objects and between variables, and plots of pairs of variables may often be an appropriate start to a multivariate analysis, and may also be useful in checking the results of more complex evaluation. DISCLOSE allows printing of both variable and object correlation matrices, and plotting of any pairs of variables.

Principal components plots. This technique aims to explain the variance in the original data by a smaller number of new variables, constructed as linear combinations of the original, to explain as much variance as possible; the new variables must remain uncorrelated one with another [16]. A scatter plot in the plane of the first two components will give a good representation of the structure of a data set, if the first two components explain a high proportion of the variance [1]. Additionally, examination of the structure of the components can give valuable insight into data set structure. This method is particularly useful in detecting redundant variables.

The eigenvector algorithm implementation in the DISCLOSE principal components program uses the TDIAG and LVRT subroutines, which are accurate and reliable [17].

Non-linear mapping. This is a technique for obtaining a low-dimensionality approximation to a high-dimensionality data set, such that the inter-object distances on the resulting scatter plot reflect, as much as possible, the corresponding distances in the original space. The routine implemented in DISCLOSE is that of Howarth [18], derived from an original algorithm of Sammon [19].

Cluster analysis. Various cluster analysis algorithms are available [14, 20, 21]. From these it was decided to use hierarchal, non-overlapping procedures in DISCLOSE, as being most appropriate for their role as complementary to scatter plot representations; of these, agglomerative, rather than divisive, algorithms were chosen because they have had wider usage in chemical and pharmaceutical areas [6, 7] and tend to have better performance in at least some chemical applications [13]. These algorithms give distinctly differing forms of cluster structure [12—14] and three such methods are therefore available in DISCLOSE. Single link clustering tends to give well separated but loosely-structured clusters (in some cases entirely uninformative [12, 13]); Ward's method tends to produce tightly knit clusters, whereas group average is usually somewhat intermediate. Comparison of the results of these three methods generally gives a reliable view of data-set structure.

These clustering algorithms are implemented in DISCLOSE using standard subroutines [20]. Euclidean distance is used as the measure of dissimilarity here, as in the spanning tree and nearest-neighbour procedures.

Minimum spanning tree. This method produces a tree structure linking pairs of objects of closest similarity. It is therefore closely related to single link clustering, but without any partitioning into distinct clusters [22]. Its

main use within the DISCLOSE system is for superimposition on scatter plots, to check for any inconsistencies introduced by the more complex display methods, (e.g., separation on the plot of pairs of objects which are closely similar).

The spanning tree procedure implemented in DISCLOSE is a FORTRAN version [21] of the algorithm of Gower and Ross [22].

Nearest neighbour. A display of nearest neighbours, with distances (i.e., dissimilarities) included, is a useful check on the results of more complex classifications and mappings. Examination of the pattern of nearest neighbours itself may also give additional insight into data set structure. The DISCLOSE procedure shows in a simple graphical way the relative distances between each object and its four nearest neighbours.

Output. All output, as noted earlier, is presented on a line-printer (or non-graphical VDU). Apart from straightforward tabulations, matrices, etc., the main displays from DISCLOSE are in the form of two-dimensional plots for principal components and non-linear mapping, and dendrograms (i.e. classification trees) for cluster analyses, the latter being implemented as a modification of a standard subroutine [20]. The plots are automatically varied in size according to the number of objects to minimize crowding. Nearest neighbours are represented by a linear display, indicating the relative distances of the four nearest neighbours to each object.

Superposition of clusters and spanning trees on the plots is at present done by hand, on the line-printer output. This is generally satisfactory, giving the opportunity for results to be inspected at leisure. It is, however, one of the main points to be considered in extensions to the system, applying interactive graphics.

Computer implementation

DISCLOSE is implemented as a series of subroutines, with a main program prompting the user to select options, and comprises about 3000 lines of standard FORTRAN-77. The programs are run interactively on a VAX 11/780 computer (in a heavily time-shared environment), and all processing is completed within (at most) 2—3 min of computer time.

Conclusions

Applications of the DISCLOSE system to chemical, pharmaceutical, and biological assay data have proven the usefulness of DISCLOSE in providing thorough and systematic evaluations, giving reliable insights into the structure of complex data sets. It is clear that the use of complementary display techniques, and different methods for data normalization, are necessary in avoiding misleading conclusions which may result from use of a single technique [15]. The classification and display methods included in DISCLOSE appear to be a suitable sub-set of the many such techniques available to show up complementary aspects of data sets. Their incorporation in an easily-used, integrated set of well tried algorithms aids their use as a routine tool for the

examination of complex data sets. A similar integration of such routines, chosen for their appropriateness to a particular situation, could be a worthwhile and straightforward option for other potential users of multivariate display techniques.

REFERENCES

1 B. Everitt, Graphical Techniques for Multivariate Data, Heinemann, London, 1978.
2 A. D. Gordon, Classification, Chapman and Hall, London, 1981.
3 I. Francie, Statistical Software: A Comparative Review, Elsevier, Amsterdam, 1981.
4 R. Gnanadesikan, Methods for Statistical Data Analysis of Multivariate Observations, Wiley, New York, NY, 1977.
5 B. R. Kowalski and C. F. Bender, J. Am. Chem. Soc., 95 (1973) 686.
6 P. J. Lewi, Multivariate Data Analysis in Industrial Practice, Research Studies Press, Chichester, 1982.
7 C. Hansch, S. H. Ungar and A. B. Forsythe, J. Med. Chem., 16 (1973) 1217.
8 S. R. Pattyn and F. Hebrant, Arzneim.-Forsch., 30 (1980) 2099.
9 Y. Takahashi, Y. Miyashita, H. Abe, S. Sasaki, Y. Yotsui and M. Sano, Anal. Chim. Acta, 122 (1980) 241.
10 Y. Miyashita, Y. Takahashi, Y. Yotsui, H. Abe and S. Sasaki, Anal. Chim. Acta, 133 (1981) 615.
11 B. J. T. Morgan, Statistician, 30 (1981) 205.
12 G. W. Adamson and D. Bawden, J. Chem. Inf. Comput. Sci., 21 (1981) 204.
13 P. Willett, Anal. Chim. Acta, 136 (1982) 29.
14 B. S. Everitt, Cluster Analysis, 2nd edn., Heinemann, London, 1980.
15 D. Bawden, in J. C. Dearden (Ed.), Quantitative Approaches to Drug Design, Elsevier, 1983, p. 64.
16 D. F. Morrison, Multivariate Statistical Methods, 2nd edn., McGraw-Hill, New York, NY, 1976, Ch. 8.
17 D. N. Sparks and A. D. Todd, Appl. Stat., 22 (1973) 220; Algorithm AS60, p. 260.
18 R. J. Howarth, Math. Geol., 5 (1973) 39.
19 J. W. Sammon, IEEE Trans. Comput. C-18, 5 (1969) 401.
20 M. R. Anderberg, Cluster Analysis for Applications, Academic Press, New York, NY, 1974.
21 H. Spath, Cluster Analysis Algorithms, E. Horwood, Chichester, 1980.
22 J. C. Gower and G. J. S. Ross, Appl. Stat., 18 (1969) 54; Algorithm AS15, p. 106.

Analytica Chimica Acta, 158 (1984) 369—373
Elsevier Science Publishers B.V., Amsterdam — Printed in The Netherlands

Short Communication

EFFECT OF PORE SIZE ON THE CAPACITY OF SILICA-IMMOBILIZED 8-QUINOLINOL

MONTE A. MARSHALL and HORACIO A. MOTTOLA*
Department of Chemistry, Oklahoma State University, Stillwater, OK 74078 (U.S.A.)
(Received 14th November 1983)

Summary. Optimization of the pore sizes of various silica gels used as supports in the immobilization of 8-quinolinol is described. Increased capacity is observed as pore size decreases to the optimum at about 6 nm. At smaller pore sizes, steric effects appear to predominate, and capacities decrease sharply. An explanation for these effects is proposed; it was confirmed by using molecular models.

There has been considerable interest over the past decade in the preparation and application of immobilized chelating agents capable of enhancing the selectivity of preconcentration and chromatographic systems for closely related ionic species. Many solid supports for such immobilizations have been used with varying degrees of success. Silica gel, however, seems to provide the good physical strength and swelling resistance necessary to operate under the high pressures and continuously changing solvent compositions often encountered in liquid chromatographic systems. Also, the ease of silylation of silica makes the gel an attractive choice as a support.

One of the most promising of the silica-immobilized chelating agents that have been prepared to date is 8-quinolinol (oxine). Silica-immobilized 8-quinolinol has been demonstrated to be useful for the preconcentration of metal ions [1—4] as well as for chromatographic applications such as the chelating ion-exchange separation of metal ions [5], the ion-pair separation of sulfonates [6], and the ligand exchange separation of phenols [7]. A primary disadvantage of using silica-immobilized 8-quinolinol is its relatively low capacity. Capacities range from about 15 to 260 μmol g^{-1} depending on various factors [8]; these limit the preconcentrating ability and also result in overloading problems in chromatographic applications.

Several approaches can be taken to improve capacities. The first approach is to optimize, or modify, the synthetic procedure for the preparation of the bound chelating agents. Fulcher et al. [9] optimized the conventional synthesis of these materials in a manner that resulted in improved capacities over those observed on similar silica supports. Marshall and Mottola [8] shortened the synthetic procedure itself, again obtaining improved capacities.

Another approach to improved capacities involves changing the support,

0003-2670/84/$03.00 © 1984 Elsevier Science Publishers B.V.

or optimizing and/or modifying its properties. Changing the support is an unattractive option because of the swelling and diffusional problems encountered in the use of most organic polymeric supports [10] and the ease with which the silica surface undergoes reaction. Therefore, optimization or modification of any property of the support which could result in a larger capacity is of interest. The pore size and related specific surface area of the support can have a dramatic effect on the capacity; this effect has been alluded to previously [8, 9]. However, no systematic study has previously been undertaken to optimize and evaluate the specific effect that the pore diameter of the support has on the capacity of silica-immobilized 8-quinolinol.

Experimental

Reagents. Analytical-grade reagents were used throughout. All water was distilled after being deionized by reverse osmosis. Atomic absorption standard solutions of copper (Aldrich, Milwaukee, WI) were used.

Silica supports tested included: Bead Gel spherical silica gel (Davison Chemical, Baltimore, MD), silica gel (Davison Grade 12, Supelco, Bellefonte, PA), Woelm t.l.c.-grade silica gel (ICN Pharmaceuticals, Cleveland, OH), silica gel for column chromatography (J. T. Baker, Phillipsburg, NJ), Porasil F and Porasil C (Waters Associates, Milford, MA), and four controlled-pore glasses (CPG-00075, CPG-00500, and CPG-02000 from Electro-Nucleonics, Fairfield, NJ; CPG-550 from Corning Glass, Corning, NY).

Apparatus. An atomic absorption spectrometer (Perkin-Elmer Model 290B, Norwalk, CT) was used to quantify copper.

Procedure. 8-Quinolinol was immobilized as described previously [8]. The structure of the resulting immobilized group (III) is as indicated in Table 2.

All capacities were determined by measuring the change in concentration of a standard copper(II) solution (pH 5.0) upon equilibration of an excess of Cu(II) with a given amount of the silica-immobilized material [8].

Results and discussion

Table 1 summarizes the pertinent physical characteristics (provided by the manufacturer) of the silica supports used, and the corresponding capacities obtained for the final silica-immobilized 8-quinolinol product. Although only an approximately linear relationship exists between pore diameter and specific surface area in the materials studied, high specific surface areas correspond to smaller pore sizes and low specific surface areas correspond to larger pore sizes. Controlled-pore glass is obtained by phase separation of a borosilicate glass followed by leaching of the borate groups with mineral acid; the result is essentially a silica gel that differs from the conventional gel only in its preparation.

The relationship between capacity and mean pore diameter is shown in Fig. 1. The capacity is observed to increase gradually, then rapidly, as the mean pore diameter decreases to about 5—6 nm; for smaller diameters, the

TABLE 1

Physical characteristics of silica supports and resulting capacities

Supplier or manufacturer	Type[a]	Specific surface area ($m^2\ g^{-1}$)	Pore diameter (nm)	Particle size (μm)	Capacity ($\mu mol\ g^{-1}$)
Davison	SG	800	2.2	2400	12
Supelco	SG	720—760	2.2	149—177	4
Woelm	SG	500—600	6.0	5—15	216
Baker	SG	450	6.0	74—250	185
Electro-Nucleonics	CPG	152.7	7.4	37—74	173
Waters	SG	50	20—40	75—125	79
Electro-Nucleonics	CPG	41.6	51.5	37—74	58
Corning	CPG	70	55	37—74	53
Waters	SG	1.5	150	75—125	6
Electro-Nucleonics	CPG	10.2	190	37—74	5

[a]Silica gel (SG) or controlled-pore glass (CPG).

capacity drops off sharply. This behavior is thought to be the result of two different effects. With large pore diameters, the specific surface area is relatively small which means that, for a given amount of silica gel, the number of surface silanol groups available for silylation is also small. Decrease in pore size (i.e., increased surface area) increases the number of surface silanol groups, which results in increased capacities. However, as the pore size becomes even smaller, a second effect (steric hindrance) predominates over the effect of increased surface area; i.e., the size of the immobilized functional group begins to approach the size of the pores. A similar effect has been observed for enzyme immobilizations in which enzyme activity drops off sharply below a certain cut-off pore diameter [11]. The relationship between pore size and length of the immobilized functional group has also been shown to have a marked effect on chromatographic efficiency [12].

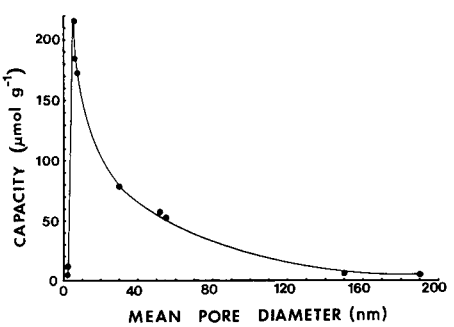

Fig. 1. Effect of mean pore diameter on capacity.

It has been proposed [9] that, once the silylation reaction or one of the subsequent reactions has been completed, the pores become even smaller and therefore may block reaction of the active functional group (i.e., 8-quinolinol) at reaction sites within the pores. Another possibility is that the functional group becomes attached, but metal ions (particularly those that are large or highly hydrated) are prevented from diffusing into the pores and therefore cannot react with the chelating agent attached within the pores [9]. Our observations seem to indicate that, in the case of silica-immobilized 8-quinolinol, the first explanation is more likely. A convenient aspect of the preparation of silica-immobilized 8-quinolinol is the red azo dye formation on coupling. The silica gels with small pore diameter appear to be easily silylated (dark blue-gray color). However, on addition of an ethanolic solution of 8-quinolinol, almost no red dye was observed whereas all the silica gels with larger pore diameter turned varying shades of red to orange, the intensity of the color decreasing with increasing pore size [8]. This seems to indicate that very little azo bond formation is taking place in the case of silica gels with very small pore diameters. This would indicate little reaction with 8-quinolinol. Some 8-quinolinol is coupled, of course,

TABLE 2

Estimated lengths of various silica-immobilized species present at different stages of the immobilization reaction

Step	Structure	Estimated length (nm)
1	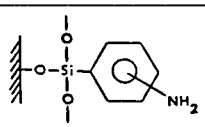 I	0.7—0.8 (*para*) 0.6—0.7 (*meta* and *ortho*)
2	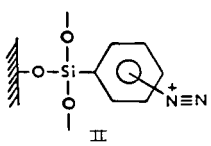 II	0.8—0.9 (*para*) 0.7—0.8 (*meta*) 0.6—0.7 (*ortho*)
3	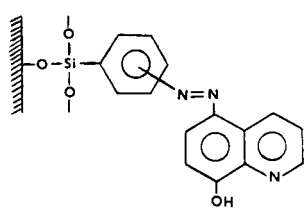 III	1.2—1.4 (*para*) 0.6—1.2 (*meta*) — (*ortho*)[a]

[a]The *ortho* isomer probably cannot form because of steric hindrance of the silica surface.

at reaction sites on the exterior surface of the silica.

In an effort to rationalize this behavior, molecular models of the silica-immobilized species were assembled and the length of the attached group was estimated for each step of the immobilization reaction. The results are shown in Table 2. It is apparent that formation of two bound 8-quinolinol moieties near the opening of a pore could block an entrance of roughly 2.4—2.8 nm. This corresponds well to the observed cut-off pore diameter. Also, a diameter of 6.0 nm, for example, should accommodate two opposing immobilized 8-quinolinol moieties (2.4—2.8 nm) and still allow for the easy passage of copper(II). This is in agreement with the high capacities observed for silica gels having pore diameters in this range. Therefore, the optimum pore diameter in terms of increased capacities appears to be in the range 4.0—6.0 nm. This optimum could be determined more accurately if silica gels with a wider variety of pore diameters and specific surface areas were available. It also should be mentioned that other factors such as pressure constraints have not been considered here and these factors must be considered when these materials are used in a system involving packed columns.

This work was partially supported by the Water Research Institute (Oklahoma State University).

REFERENCES

1 K. F. Sugawara, H. H. Weetall and G. D. Schucker, Anal. Chem., 46 (1974) 489.
2 E. D. Moorhead and P. H. Davis, Anal. Chem., 46 (1974) 1879.
3 M. M. Guedes da Mota, F. G. Römer and B. Griepink, Fresenius Z. Anal. Chem., 287 (1977) 19.
4 R. E. Sturgeon, S. S. Berman, S. N. Willie and J. A. H. Desaulniers, Anal. Chem., 53 (1981) 2337.
5 J. R. Jezorek and H. Freiser, Anal. Chem., 51 (1979) 366.
6 M.-S. Kuo and H. A. Mottola, Anal. Chim. Acta, 120 (1980) 255.
7 G. J. Shahwan and J. R. Jezorek, J. Chromatogr., 256 (1983) 39.
8 M. A. Marshall and H. A. Mottola, Anal. Chem., 55 (1983) 2089.
9 C. Fulcher, M. A. Crowell, R. Bayliss, K. B. Holland and J. R. Jezorek, Anal. Chim. Acta, 129 (1981) 29.
10 D. E. Leyden, in D. E. Leyden and W. T. Collins (Eds.), Silylated Surfaces, Gordon and Breach, New York, NY, 1980, p. 321.
11 D. L. Eaton, in D. E. Leyden and W. T. Collins (Eds.), Silylated Surfaces, Gordon and Breach, New York, NY, 1980, p. 201.
12 K. Karch, I. Sebestian and I. Halász, J. Chromatogr., 122 (1976) 3.

Analytica Chimica Acta, 158 (1984) 375—377
Elsevier Science Publishers B.V., Amsterdam — Printed in The Netherlands

Short Communication

DETERMINATION OF FUNGAL α-AMYLASE BY FLOW INJECTION ANALYSIS

PREBEN W. HANSEN

Enzyme Microbiological Laboratory, Novo Industri A/S, Novo Allé, 2880 Bagsvaerd (Denmark)

(Received 21st November 1983)

Summary. A manual iodine-starch method is adapted to analyse broths from *Aspergillus oryzae* fermentations. The method is based on degradation of starch by the enzyme, and measurement of the residual starch/iodine complex at 570 nm. Calibration graphs are linear for the range 0.01—0.1 amylase units ml^{-1}. Eighty samples per hour can be processed.

Flow injection analysis (f.i.a.) [1] has many advantages such as high sampling rates, fast response, flexibility and simple apparatus. Several manual analytical methods are laborious as well as time-consuming and could with advantage be adapted to f.i.a. In this laboratory, a manual method for determination of acid α-amylase activity in culture broth from *Aspergillus oryzae* is used daily. It is based on the degradation of starch at 37°C and pH 4.7 by the enzyme. Use is made of the colour formed when iodine is added to the starch solution. Initially it is black-blue but with progressive hydrolysis of the starch it changes to red-brown. The enzyme activity is based on the time necessary to reach a certain colour evaluated by a coloured glass standard (details are available on request). As this method suffers from the disadvantages mentioned above, it was decided to adapt it for f.i.a.

Experimental

Flow injection system. The basic units are the Bifok FIA 05 unit with a 30-μl injection valve, Bifok FIA 08 peristaltic pump, Bifok FIA 06 photometer with an 18-μl flow cell and a 570-nm filter, and an Omniscribe pen recorder (Houston Instruments). The manifold modules are of plexiglas and the tubing and coils of teflon (0.5 mm i.d.). The f.i.a. manifold is shown in Fig. 1. The coils and flow cell are thermostatted at 37°C.

Reagents. The starch solution, pH 4.7, was prepared by dissolving 0.270 g of dry starch (Merck) by gently boiling for 1 min in ca. 200 ml of acetate buffer (6.0 g of sodium acetate and 2 ml of anhydrous acetic acid per litre). After slow cooling to room temperature, acetate buffer was added to give a final volume of 400 ml. A solution of 40.0 g of potassium iodide and 4.0 g of iodine in deionized water was prepared and diluted to 1 l; it was kept

0003-2670/84/$03.00 © 1984 Elsevier Science Publishers B.V.

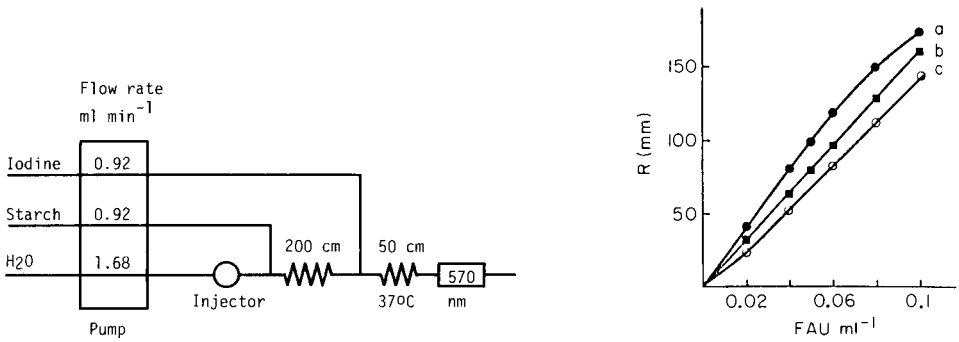

Fig. 1. Flow injection system. Coil lengths are given in cm; samples are introduced at the injector.

Fig. 2. Calibration graphs for α-amylase with 0.067% starch solution and 5 ml of iodine reagent diluted to: (a) 250 ml; (b) 180 ml; (c) 150 ml. *R* is the peak height.

in brown bottles in the dark. Before use, 5 ml of this solution was diluted to 180 ml with deionized water.

Fungamyl 800 L (Novo) with an activity of 800 FAU g^{-1} (fungal α-amylase unit; 1 FAU is the amount of enzyme which breaks down 5.26 g of starch h^{-1} using the above-mentioned manual standard method) was dissolved in deionized water to give a stock solution containing 0.2 FAU ml^{-1}. This was diluted to obtain standards in the range 0.01—0.10 FAU ml^{-1}.

Procedure. As a decrease in absorbance is measured, the photometer was calibrated in the following way. With the photometer calibration knob, the factor was adjusted to ca. 95%. While all reagents were pumped through the flow injection system, the photometer display was adjusted to 50—55 with the zero knob. This represents the highest reading that can be obtained when there is no degradation of starch, and therefore represents the baseline. Any drift in the baseline was corrected for with the zero knob only.

In the flow system, flow rates were as indicated in Fig. 1, and samples were allowed to react with starch in a 200-cm coil, before the iodine was added. The absorbance was measured at 570 nm.

Results and discussion

The reaction temperature and pH used were those normal to the manual method, 37°C and 4.7, respectively. From initial test-tube experiments, the appropriate composition of reagents was estimated, as well as the mixing proportions. It was further found that with a reaction time of about 20 s the reaction had proceeded sufficiently for a reasonable sensitivity to be achieved. Several reaction coil lengths were evaluated as were the reagent flow rates. The recommended conditions are summarized in Fig. 1.

The effect of reagent compositions (starch/iodine) on the determination of α-amylase were also investigated. With 0.09 or 0.054% starch solution, a linear calibration graph could not be obtained even with a wide variation in

TABLE 1

Comparison of results for the determination of amylase in diluted culture broth

Sample no.	α-Amylase found (FAU ml^{-1})			Difference (%)
	F.i.a. method	R.s.d.[a] (%)	Manual method	
1	0.0161	4.3	0.0158	+1.9
2	0.0697	0.0	0.0692	+0.7
3	0.0635	1.1	0.0579	+8.8
4	0.0673	0.6	0.0675	−0.3
5	0.0658	1.5	0.0647	+1.7
6	0.0731	1.0	0.0710	+2.9
7	0.0170	4.1	0.0160	+5.9
8	0.0671	0.9	0.0669	+0.3
9	0.0592	0.7	0.0556	+6.1
10	0.0671	1.0	0.0678	−1.0
11	0.0680	0.6	0.0678	+0.3
12	0.0762	0.0	0.0717	+5.9

[a] $n = 3$.

the concentration of the iodine solution. With 0.067% starch solution, the highest sensitivity and a linear calibration graph (up to 0.1 FAU ml^{-1}) were obtained when 5 ml of the iodine solution was diluted to 180 ml (Fig. 2).

The method was compared with the manual method for determination of α-amylase activity in culture broth from fermentations with *Aspergillus oryzae*. The 5-point calibration graph was prepared from standards which contained 0.010—0.10 FAU ml^{-1}. Samples were diluted with deionized water to contain amylase activity within this range. All samples and standards were injected in triplicate. The results for 12 diluted culture broth samples are compared in Table 1. There is generally good agreement between the two methods.

The f.i.a. method is well suited for the rapid, accurate and precise measurement of acid α-amylase activity in culture broths. Compared with the manual method, the f.i.a. method with a sampling rate of 80 h^{-1} allows five times more samples to be examined in a working day. This is slightly less than the recirculating procedure of Nikolelis and Mottola [2], but the procedure is much simpler and cheaper.

REFERENCES

1 J. Růzíčka and E. H. Hansen, Flow Injection Analysis, Wiley-Interscience, New York, NY, 1981.
2 D. P. Nikolelis and H. A. Mottola, Anal. Chem., 50 (1978) 1665.

Analytica Chimica Acta, 158 (1984) 379—382
Elsevier Science Publishers B.V., Amsterdam — Printed in The Netherlands

Short Communication

DYNAMIC BEHAVIOR OF POTENTIOMETRIC AMMONIA-SENSING PROBES IN SAMPLES OF HIGH OSMOLARITY

MARK A. ARNOLD*[a] and GARRY A. RECHNITZ
Department of Chemistry, University of Delaware, Newark, DE 19711 (U.S.A.)
(Received 12th October 1983)

Summary. Results are presented for potentiometric ammonia gas-sensors which show that the response times increase significantly with age of the sensor when ammonium picrate is used as internal electrolyte and the samples have greater osmolarities than the internal electrolyte solution. A build-up of ammonium picrate crystals on the inner side of the gas-permeable membrane is responsible for this increase in response time. The use of ammonium chloride as internal electrolyte provides constant response times independent of sample osmotic strength, and is recommended as a means of ensuring that optimal dynamic response characteristics are maintained.

Previous reports have noted that potentiometric gas sensors based on membranes exhibit increased potential drift when the osmolarity of the sample is significantly higher than that of the internal electrolyte solution [1—5]. It was observed here that the response of the widely used ammonia gas-sensing probe also can become drastically slowed under such conditions when ammonium salts with moderate aqueous solubility are used in the internal electrolyte. The purpose of this communication is to alert users to this possible response time problem.

Experimental

Apparatus and reagents. All potentiometric measurements were made with a Corning Model 12 pH/mV meter in conjunction with a Heath-Schlumberger SR 240 strip-chart recorder. All measurements were made in thermostated cells at 25°C using a Haake Model FS bath. Bodies, internal pH electrodes, and membranes for the Orion Model 95-10 ammonia gas-sensing probe were used for the construction of all the sensors tested.

All solutions were prepared using distilled, deionized water and analytical-grade reagents. When mentioned, the Orion 95-1002 internal filling solution was used.

Procedures. All sensors were constructed as recommended by the manufacturer, differing only in the composition of the internal electrolyte solu-

[a]Present address: Department of Chemistry, University of Iowa, Iowa City, IA 52242, U.S.A.

0003-2670/84/$03.00 © 1984 Elsevier Science Publishers B.V.

tion. Osmolarities of ammonium chloride-based internal electrolytes were adjusted with the appropriate amount of sodium chloride and 0.1 M ammonium chloride was used. The ammonium picrate-based internal electrolyte was that of Orion and had an osmolarity of 0.2 M. Each probe was stored in the respective sample solution at room temperature between measurements to reduce potential drift. Sample solutions were composed of 0.01 M sodium hydroxide with sodium chloride added to adjust the osmolarity.

Calibration graphs were obtained by making repeated additions of ammonium chloride standards to the sample solution. Stirring rates were constant throughout.

Results and discussion

Figure 1 shows the observed dynamic response of the ammonia sensor with respect to the age of the probe. Response times are shown when the sample osmolarity is 0.6 M and the osmolarities of the ammonium chloride-based internal electrolytes are 0.2, 0.6, and 1.0 M. It can be seen that the response speed remains constant over a five-day period for all situations involving the ammonium chloride-based internal electrolyte.

Because constant response times are expected when ammonium picrate-based internal electrolytes are used in conjunction with samples with osmolarities equal to or less than that of the internal electrolyte [3, 6], attention was focused mainly on situations for which the sample osmolarity was greater than the internal electrolyte osmolarity. Figure 1 shows the dynamic behavior of sensors which have ammonium picrate-based internal electrolytes. This case represents the situation when an ammonium salt with moderate aqueous solubility is used to minimize baseline drift problems [3]. In these experiments, the osmolarity of the internal electrolyte was 0.2 M while sample osmolarities of 0.6 and 1.0 were tested. The data show that a significant increase in response time is observed with increasing age under these conditions, and that the increase in dynamic response is greater when higher sample osmolarities are encountered.

Figure 2 shows the response times with respect to age of the sensor for various changes in ammonia concentrations. It can be seen that the increase in response time is more dramatic during the five-day period for lower ammonia concentrations.

Because each sensor was tested and stored in the same sample solution, increases in response times cannot be attributed to changing sample osmolarities, as in previous studies [1, 2], but to alterations in the membrane phase of the sensor. Upon disassembly of the ammonium picrate-based sensors, a thin film of yellow crystals was observed on the side of the gas-permeable membrane which was adjacent to the internal electrolyte. The gradients of osmotic pressure at the surface of these sensors are such that water vapor is removed from the thin internal electrolyte layer [1, 4, 5] which results in the crystallization of ammonium picrate onto the gas-permeable membrane. It seems likely that this salt layer decreases the rate of diffusion of

ammonia into the internal electrolyte which results in the observed increases in response times. Indeed, when the yellow salt layer was removed from the membrane surface by dissolution in water, and when the sensor was reconstructed with the same gas-permeable membrane but with ammonium chloride internal electrolyte instead of ammonium picrate, the response times remained constant over a five-day period and ranged from several seconds to 2.5 min.

Whereas drifting potentials caused by gradients of osmotic pressure can be overcome by prolonged conditioning of sensors in the high osmotic solution [1], increases in response times will result when ammonium picrate or other moderately soluble ammonium salts are used in the internal electrolyte. Storage of the sensors under iso-osmotic conditions should avoid ammonium picrate precipitation; however, considerable potential drift can be expected when sample osmolarities differ from the storage osmolarity [1—5]. In addition, manufacturers of these ammonia probes suggest that the osmolarity of the internal electrolyte be adjusted with an inert salt to correct drifting potential problems when the sample osmolarity is above 1.0 M [6]. However, significant increases in response time were found here when 0.6 M osmotic sample solutions were used with the Orion filling solution. Thus, it is suggested that the internal electrolyte be adjusted when the sample osmolarity is even slightly greater than that of the internal electrolyte, to ensure optimal response speed. An easier solution to the problem, especially when the

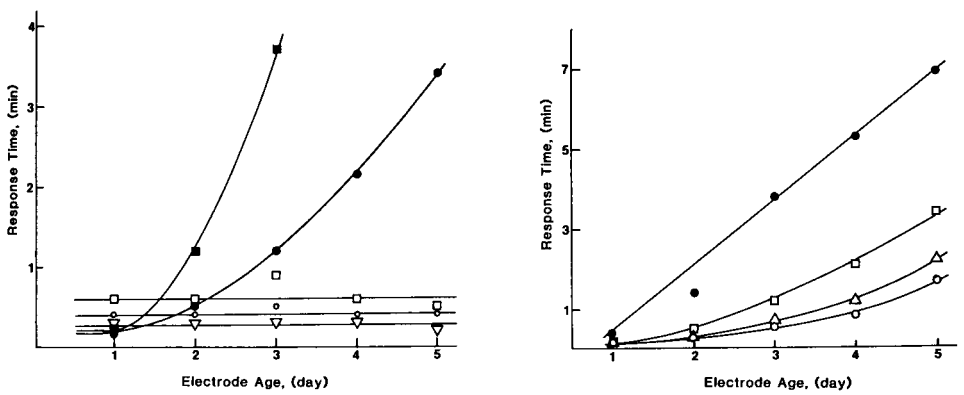

Fig. 1. Response times of ammonia sensors as a function of sensor age for different ratios of internal to external osmolarities: (○) 1.0:0.6; (□) 0.6:0.6; (▽ and ●) 0.2:0.6; (■) 0.2:1.0. Open and closed symbols represent ammonium chloride and picrate internal electrolytes, respectively. Response times are for ammonia concentration changes from 6.0×10^{-5} to 3.4×10^{-4} M.

Fig. 2. Response times at different ages of the sensor for various changes in ammonia concentration: (●) background to 6.0×10^{-5} M; (□) 6.0×10^{-5} to 3.4×10^{-4} M; (△) 3.4×10^{-5} M to 1.51×10^{-3} M; (○) 1.5×10^{-3} to 6.6×10^{-3} M, with 0.6 and 0.2 M osmolarities being used for the sample and ammonium picrate internal electrolyte solutions, respectively.

osmolarity of the sample is unknown, is to use an ammonium chloride-based internal electrolyte solution because the response time is not affected by sample osmolarity under such conditions.

We are grateful to the National Science Foundation (Grant CHE-8025625) for supporting this research.

REFERENCES

1 P. L. Bailey and M. Riley, Analyst (London), 100 (1975) 145.
2 J. W. Ross, J. H. Riseman and J. A. Krueger, Pure Appl. Chem., 36 (1973) 473.
3 J. H. Riseman, J. Krueger and M. S. Frant, U.S. Pat. 3, 830, 719, 1974.
4 P. L. Bailey, Analysis with Ion-Selective Electrodes, Heyden, Philadelphia, PA, 1980, Ch. 7.
5 M. Riley, in A. K. Covington (Ed.), Ion-Selective Electrode Methodology, Vol. 2, CRC Press, Boca Raton, FL, 1979, Ch. 1.
6 Handbook of Electrode Technology, Orion Research, Cambridge, MA, 1982, pp. A1—A3.

Analytica Chimica Acta, 158 (1984) 383–387
Elsevier Science Publishers B.V., Amsterdam — Printed in The Netherlands

Short Communication

CONSECUTIVE INDIRECT TITRATION OF PERIODATE AND IODATE WITH EDTA

I. Z. AL-ZAMIL

Chemistry Department, College of Science, King Saud University, Riyadh (Saudi Arabia)

(Received 12th July 1983)

SUMMARY

Periodate and iodate (μmol amounts) are determined successively in the same solution by their selective oxidation of iron(II) at pH 2.0 and in acetic acid, respectively. The resultant iron(III) is titrated with EDTA solution to a sulphosalicylic acid end-point. Bromate—iodate mixtures can be titrated similarly.

Several titrimetric methods have been reported for the determination of periodate and iodate when present together [1—7]. However, very few titrimetric methods are available in which both ions can be determined consecutively in the same solution. Kahane [6] selectively precipitated periodate as $Zn_5(IO_6)_2$ which was filtered off, dissolved in dilute acid and titrated iodimetrically. Iodate in the filtrate was also determined by iodimetric titration. This method is time-consuming, as the precipitate has to stand for 30 min before filtration. A more elegant method was described by Belcher and Townshend [7], who masked periodate with molybdate by formation of 6-molybdoperiodate at pH 2.9 and titrated iodate iodimetrically. On addition of oxalic acid the periodate was demasked and also titrated iodimetrically.

Many species which do not react with EDTA can be indirectly determined by reaction with a suitable metal ion followed by titration with EDTA of the excess of metal ion or, in the case of a redox reaction, of the metal ion in a different oxidation state [8, 9]. Iron(III) in the presence of iron(II) can be titrated at pH 2.0 with EDTA and salicylic acid as indicator [10]. In the present communication, periodate and iodate are determined consecutively by oxidizing iron(II) under different conditions and titrating the iron(III) produced with EDTA in each instance.

Experimental

Reagents. All chemicals used were of analytical-reagent grade. The iron(II) solution was prepared by dissolving 38.552 g of iron(II) ammonium sulphate hexahydrate in 40 ml of distilled water containing 4 ml of concentrated sulphuric acid, and diluting to 200 ml with distilled water which had been

0003-2670/84/$03.00 © 1984 Elsevier Science Publishers B.V.

deoxygenated with nitrogen for 15 min. This solution was prepared daily and kept in an amber glass bottle. The EDTA stock solution (0.1 M) was prepared from its disodium salt and standardized with calcium carbonate [8]; this was diluted to 0.02 M before use. Iodate stock solution was prepared from potassium iodate (BDH, 99.9%) previously dried at 180°C. Periodate stock solution was prepared from sodium periodate (BDH, 99.0%) and was also standardized iodimetrically [1]. The interfering anion solutions were prepared from their sodium or potassium salts. The indicator solution was prepared by dissolving 6.0 g of sulphosalicylic acid in 100 ml of distilled water.

Procedure. Transfer 5 ml of the prepared iron(II) solution to a 100-ml conical flask and neutralize to exactly pH 2 (pH meter) with 1 M sodium carbonate solution. Add 5 ml of the periodate—iodate sample solution containing 5—50 μmol of each anion. Add 1 ml of the sulphosalicylic acid solution and titrate with EDTA (0.02 M) to the disappearance of the violet colour. The colour changes, depending on the periodate concentration, to colourless or yellow. This gives the periodate concentration. To the same solution, add 5 ml of anhydrous acetic acid and heat until just boiling. Cool in tap water and titrate with EDTA to the disappearance of the violet colour. The additional titre gives the iodate concentration. Take a blank of distilled water through the whole procedure.

Results and discussion

In very dilute sulphuric acid (pH 2—3) and at room temperature, only periodate oxidized iron(II)

$$IO_4^- + 2Fe^{2+} + 2H^+ \rightarrow IO_3^- + 2Fe^{3+} + H_2O \quad (1)$$

The iron(III) formed was titrated directly with EDTA to a sulphosalicylic acid end-point (V_1). The latter indicator, which behaves similarly to salicylic acid, was used because it is more soluble in water. When concentrated acetic acid was added to the same solution, the iodate (including that formed in the above reaction) reacted with iron(II) on heating to boiling

$$IO_3^- + 6Fe^{2+} + 6H^+ \rightarrow I^- + 6Fe^{3+} + 3H_2O \quad (2)$$

The iron(III) produced was titrated as above (V_2). At both end-points, the violet colour of the iron(III) sulphosalicylate changed to the clear yellow colour of the iron(III)—EDTA complex, giving sharp end-points. The volume of EDTA that is equivalent to iodate is $V_2 - 3V_1$.

The pH of the first reaction should be $\geqslant 2$, otherwise part of the iodate reacts with iron(II) (Table 1). However, it is preferable not to increase the pH to above 3, in order to minimize the oxidation of iron(II) by atmospheric oxygen, and thus minimize the blank. The second reaction was found to be quantitative only in acetic acid. In dilute sulphuric acid (2.5 M), the reaction was not complete; when strong sulphuric acid (4.5 or 9 M) was used, the second end-point was difficult to observe because the colour changed from violet to brown.

TABLE 1

Effect of the pH for the first reaction on the consecutive titration of a mixture of 25.25 μmol of iodate and 24.75 μmol of periodate with 0.02 M EDTA

pH	Recovery (%)		Blank (ml)	
	Periodate	Iodate	V_1	V_2
0.6	118	82	0.10	0.40
1.2	112	91	0.10	0.60
1.4	100	101	0.25	0.70
2.0	99	100	0.30	0.70
2.7	101	99	0.40	0.80
3.3	102	100	0.55	0.80

It is very important that the time elapsed between pipetting the iron(II) solution and titrating the iron(III) formed in each reaction should be similar for the blank and the sample, in order to achieve reproducible and accurate results.

The precision of this method was estimated from the results obtained for 10 replicate titrations of a mixture containing 25.25 μmol of iodate and 24.75 μmol of periodate. The relative standard deviation was 1.3% for both titrations. The results of titrations of mixtures of periodate and iodate (Table 2) showed an average accuracy of 1.0% for both periodate and iodate.

The effect of some anions on the titration of periodate and iodate (25 μmol of each) was examined. The results obtained (Table 3) show that fluoride, chloride, perchlorate, borate and nitrate (500 μmol) had no significant effect on either the periodate or iodate titration. Very little effect was observed from bromide and hypochlorite. Phosphate did not interfere with the periodate determination, but in the second titration iron(III) phosphate precipitated, causing a serious negative error. Nitrite, bromate and chlorate oxidized iron(II). The reaction of iron(II) with bromate was

TABLE 2

Successive titration of mixtures of periodate and iodate

Taken (μmol)		Found (μmol)[a]	
Periodate	Iodate	Periodate	Iodate
49.50	50.50	48.83	50.00
49.50	5.05	49.97	5.11
4.95	50.50	4.89	50.26
19.80	35.35	19.97	35.09
29.70	15.15	29.34	15.37
39.60	10.10	39.15	9.98
24.75	25.25	24.52	25.20

[a]Mean of 3 experiments.

TABLE 3

Effect of some anions on the titration of a mixture containing 25 μmol each of periodate and iodate with 0.02 M EDTA

Added anion (100 μmol)	Volume of EDTA (ml)[a]		Added anion (100 μmol)	Volume of EDTA (ml)[a]	
	V_1	V_2		V_1	V_2
—	2.5	14.9	Bromide	2.8	14.6
Fluoride[b]	2.5	14.8	Bromate	32.6	15.0
Chloride	2.6	14.7	Nitrite	7.2	18.0
Hypochlorite	2.7	15.2	Nitrate[b]	2.6	14.7
Chlorate	2.7	17.6	Phosphate	2.6	12.0
Perchlorate[b]	2.6	14.8	Borate[b]	2.5	14.8

[a] After subtracting the blank.
[b] 500 μmol.

quantitative in the first titration medium (1 bromate ≡ 6 iron(II)) while that with chlorate occurred only in the acetic acid medium and was incomplete. A brief investigation showed that the consecutive titration of micromole amounts of bromate and iodate when present together is possible under the same conditions as for periodate and iodate (Table 4). The oxidation of iron(II) by bromate was slower than that by periodate. Therefore, the titration of bromate should be carried out slowly, within ca. 2 min.

In conclusion, the proposed method is simple, sensitive (particularly for iodate and bromate) and rapid. The reasonable accuracy and precision of the method could be improved by spectrophotometric detection of the end-points. This method can be modified for the consecutive titration of other anion mixtures.

The author thanks Mr. A. H. Abdel-Fattah for his technical assistance.

TABLE 4

Successive titration of mixtures of bromate and iodate

Taken (μmol)		Found (μmol)	
Bromate	Iodate	Bromate	Iodate
48.50	50.50	48.01	49.90
38.80	20.20	39.24	20.45
14.55	30.30	14.77	30.00
48.50	10.10	47.94	10.03
9.70	50.50	9.59	50.90

REFERENCES

1 I. M. Kolthoff and R. Belcher, Volumetric Analysis, Vol. 3, Interscience, New York, NY, 1957.
2 L. H. Greathouse, J. Am. Chem. Soc., 60 (1938) 2869.
3 L. Szekeres, Z. Anal. Chem., 172 (1960) 256.
4 L. Szekeres, E. Kardos and M. Rady, Z. Anal. Chem., 160 (1958) 401; 162 (1958) 430.
5 L. Malaprade, Bull. Soc. Chim. Fr., 39 (1926) 325; 43 (1928) 683.
6 E. Kahane, Bull. Soc. Chim. Fr., (1948) 70.
7 R. Belcher and A. Townshend, Anal. Chim. Acta, 41 (1968) 395.
8 F. J. Welcher, The Analytical Use of Ethylenediaminetetraacetic Acid, D. Van Nostrand, NJ, 1958.
9 A. Kellner and L. Szekeres, Chemist-Analyst, 54 (1965) 75.
10 G. Hoshikawa, Jpn. Analyst, 4 (1955) 582.

Analytica Chimica Acta, 158 (1984) 389—393
Elsevier Science Publishers B.V., Amsterdam — Printed in The Netherlands

Short Communication

A SIMPLE MONITORED THERMOMETRIC DETERMINATION OF COPPER(II) BY REACTION-RATE MEASUREMENT BASED ON THE CATALYSIS OF THE AERIAL OXIDATION OF 2,2'-DIPYRIDYLKETONE HYDRAZONE

F. GRASES*, R. FORTEZA, J. G. MARCH and V. CERDA

Department of Analytical Chemistry, Faculty of Sciences, University of Palma de Mallorca (Spain)

(Received 7th August 1983)

Summary. The initial reaction rate is measured by monitoring the rate of increase of temperature of the solution with a thermistor; 0.2—2 mg l^{-1} copper in the final solution is determined, with very few interferences.

The application of kinetic analytical techniques is sometimes restricted by complex and expensive instrumentation. In the present communication, a kinetic procedure for the determination of inorganic species is described; the increase in temperature caused by a chemical reaction is monitored. Only simple instrumentation similar to that used in thermometric titrimetry is required.

In direct injection enthalpimetry, an excess of titrant is injected into the sample solution as quickly as possible and the rise in temperature is measured. The procedure lends itself well to "inverse" reactions, in which the sample is injected into an excess of reagent. The temperature rise can be related to the reaction enthalpy, and therefore to the concentration of the species determined. The apparatus used basically consists of a Dewar flask, thermistor, Wheatstone bridge, stirrer, calibration heater and heater control. This technique has been recently applied to the determination of some inorganic species, e.g., sulphide by its catalysis of the iodine-azide reaction [1], and iodide by its catalysis of the cerium(IV)-arsenic(III) reaction [2]. There have been many other enthalpimetric-kinetic methods based on catalytic reactions [3—18], but none is based on reaction-rate measurements.

Generally, the principal advantages of methods based on initial reaction rates are their speed and accuracy. The main disadvantage of the catalytic thermometric titrations [19] is that the indicator/reagent mixture has to be added in high concentration, so that the products of the indicator reaction will be produced in high concentrations. Thus, components of the indicator system may react with substances present in the titrant, to give erroneous results. It is also necessary to add the titrant at a constant and optimal rate,

0003-2670/84/$03.00 © 1984 Elsevier Science Publishers B.V.

which is sometimes rather slow. Usually, the concentrations that can be determined are not as low as is possible by direct catalytic determinations.

To date, the use of calorimetry for the direct measurement of heat changes during chemical reactions (reaction-rate methods), has been restricted to biochemical analysis [20, 21]. The present communication offers an example of a thermometric reaction-rate technique applied to the determination of an inorganic species. Copper(II) is determined by its catalysis of the aerial oxidation of 2,2'-dipyridylketone hydrazone; this reaction has previously been utilized fluorimetrically [22].

Experimental

Reagents and solutions. 2,2'-Dipyridylketone hydrazone (DPKH) was synthesized as described previously [22]. A 1-g l^{-1} solution in water was prepared. A standard solution of copper(II) nitrate (0.9730 g Cu l^{-1}) was prepared and standardized iodimetrically. A pH 9 buffer solution was prepared according to Clark and Lubs [23].

Apparatus and measurement conditions. A thermometric titrator was built as described by Lumbiarres et al. [24]. The temperature-monitoring system consisted of a miniature thermistor with rapid response, a Wheatstone bridge and a chart recorder (Servogor RE-511). The circuit diagram is shown in Fig. 1. The thermistor was sealed in glass and had the following specifications: resistance 100 kΩ at 25°C, power dissipation <0.134 mW, effective resistance 131 kΩ at 20°C. The e.m.f. for the Wheatstone bridge was supplied from a 7.85-V stabilized source. At the sensitivity setting used, the thermistor

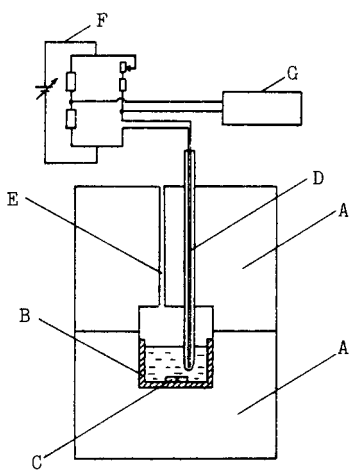

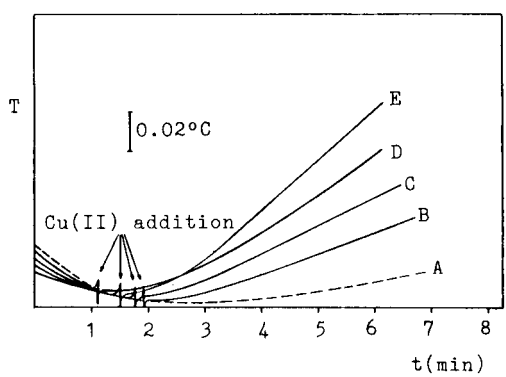

Fig. 1. Diagram of circuitry and apparatus used in reaction-rate thermometric analysis. A, Polystyrene insulator; B, plastic beaker; C, magnetic stirrer; D, thermistor; E, entrance for pipette; F, Wheatstone bridge; G, recorder.

Fig. 2. Temperature-time curves at various copper concentrations: (A) nil; (B) 0.25; (C) 0.50; (D) 1.0; (E) 2.0 mg l^{-1}. Recommended procedure was used.

bridge yielded a temperature response of 0.0165°C mV^{-1} and the full-scale deflection on the recorder was 10 mV (20 cm). An adiabatic cell (Fig. 1) was used, which incorporated a magnetic stirrer.

Procedure for determination of copper(II). A 5-ml portion of 5×10^{-3} M DPKH, 10 ml of pH 9 buffer and the volume of deionized water necessary to give a final volume of 25 ml were placed in the cell. The recorder was switched on, at a chart speed of 3 cm min^{-1}. When the temperature-time plot was horizontal, the necessary volume of cation to ensure a final concentration of copper between 0.2 and 2 mg l^{-1} was added. From the curve obtained, the rate of reaction was calculated from the initial rate (tan α). All solutions were previously thermostatted at 20°C. For calibration, appropriate concentrations of standard copper solutions were taken through the above procedure.

Results and discussion

Examples of the temperature-time curves obtained for the determination of copper are shown in Fig. 2. The slope should correspond to the temperature change (or to the amount of heat liberated) by the catalytic reaction. To obtain a stable response (horizontal temperature-time response) quickly before the addition of the cation, all solutions must be thermostatted at room temperature. A minimal background response is attained with adequate stirring. Therefore precise control of this variable is very important.

In order to find the optimal conditions for the determination of copper(II) ions, the influence of pH and the concentration of the reagent on the reaction rate were studied. The results are shown in Figs. 3 and 4. A pH of 9 and a reagent concentration of 1×10^{-3} M gave the most sensitive response. Under these conditions, there was a linear relationship between the initial rate and the copper concentration in the range 0.2—2 mg l^{-1} copper(II) in the final solution. The relative standard deviation for the determination of 1.0 mg l^{-1} was P 1.2% (n = 11, α = 0.05). The selectivity of the method was assessed by studying the effects of foreign ions on the rate of the reaction

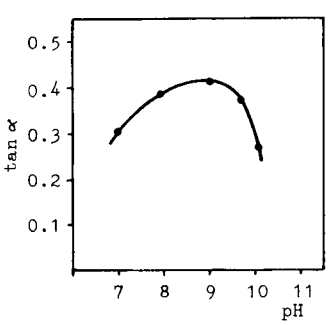

Fig. 3. Influence of pH on the initial rate (= 1×10^{-3} M DPKH, 1 mg l^{-1} Cu(II)).

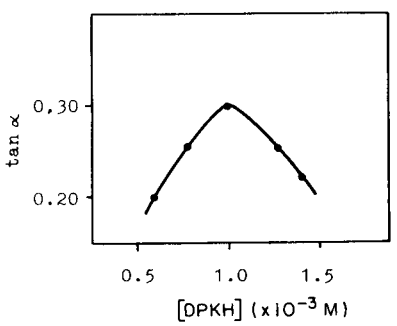

Fig. 4. Effect of DPKH concentration on the initial rate (= 1 mg l^{-1} Cu(II), pH 9).

TABLE 1

Maximum concentrations of foreign ions tolerated (error $\leq 1.2\%$) in the determination of copper (1 mg l^{-1})

Ion added	Amount tolerated (mg l^{-1})
Ca^{2+}, Ba^{2+}, Mg^{2+}, Al^{3+}, Ga^{3+}, Zn^{2+}, Cr^{3+}, Cd^{2+}, Pb^{2+}, Hg^{2+}, Mn^{2+}, UO_2^{2+}, NO_3^-, F^-, SO_4^{2-}, Cl^-	100[a]
Au^{3+}	40[b]
Ni^{2+}, Pd^{2+}	40[c]
Co^{2+}	3[b]
Fe^{3+}	3[c]

[a] Largest concentration examined. [b] Higher concentrations increased the rate. [c] Higher concentrations decreased the rate.

catalyzed by 1 mg l^{-1} copper under the recommended conditions. The results (Table 1) show that the method suffers very few interferences.

Conclusion

In principle, thermometric detection can be applied to any reaction which generates or absorbs heat. Because even very low concentrations of catalyst can greatly increase reaction rates, they can also produce relatively large amounts of heat. If the catalyst concentration is proportional to the heat produced in a fixed time or to the rate of heat production, catalyst determinations should have improved detection limits in comparison to stoichiometrically limited systems.

The measurement of a temperature (heat) change has several advantages over spectrophotometric or spectrofluorimetric procedures. There is no need for optically transparent solutions, so that the change in temperature of intensely coloured or turbid solutions can be determined. Nor is there any requirement for a component to have an accessible absorption or fluorescence band. In addition, the procedure described here retains the principal advantages of kinetic methods, i.e., speed and selectivity.

REFERENCES

1 N. Kiba, M. Nishijima and M. Furusawa, Talanta, 27 (1980) 1090.
2 J. M. Elvecrog and P. W. Carr, Anal. Chim. Acta, 121 (1980) 135.
3 G. A. Vaughan and J. J. Swithenbank, Analyst (London), 90 (1965) 594.
4 V. J. Vajgand and F. F. Gaal, Talanta, 14 (1967) 345.
5 H. Weisz, T. Kiss and D. Klockow, Z. Anal. Chem., 247 (1969) 248.
6 T. Kiss, Z. Anal. Chem., 252 (1970) 12.
7 V. J. Vajgand, F. F. Gaal and S. S. Brusin, Talanta, 17 (1970) 415.
8 H. A. Mottola, Talanta, 16 (1969) 1267.
9 H. Weisz and S. Pantel, Anal. Chim. Acta, 62 (1972) 361.
10 G. A. Vaughan, Thermometric and Enthalpimetric Titrimetry, Van Nostrand-Reinhold, London, 1973.

11 E. J. Greenhow and L. E. Spencer, Analyst (London), 99 (1974) 82.
12 R. Feys, J. Devynck and B. Trémillon, Talanta, 22 (1975) 17.
13 H. A. Mottola, CRC Crit. Rev. Anal. Chem., 4 (1975) 229.
14 H. Weisz, Angew. Chem. Int. Ed. Engl., 15 (1976) 150.
15 H. Muller and G. Werner, Z. Chem. Leipzig, 16 (1976) 304.
16 H. P. Hadjiioannou, Rev. Anal. Chem., 3 (1976) 82.
17 E. J. Greenhow and L. A. Dajer de Torrijos, Analyst (London), 104 (1979) 801.
18 V. Velich and F. Stehlik, J. Therm. Anal., 24 (1982) 299.
19 T. F. A. Kiss, Talanta, 30 (1983) 771.
20 Ch. J. Martin and M. A. Marini, CRC Crit. Rev. Anal. Chem., 8 (1979) 221.
21 B. Z. Chowdhry, A. E. Beezer and E. J. Greenhow, Talanta, 30 (1983) 209.
22 F. Grases, F. Garcia-Sanchez and M. Valcarcel, Anal. Chim. Acta, 119 (1980) 359; 125 (1981) 21.
23 W. M. Clark and H. A. Lubs, in L. Meites (Ed.), Handbook of Analytical Chemistry, McGraw-Hill, New York, NY, 1963.
24 J. Lumbiarres, C. Mongay and V. Cerdá, J. Therm. Anal., 22 (1981) 275.

ANALYTICA CHIMICA ACTA, VOL. 158 (1984)

AUTHOR INDEX

(Continued from outside back cover)

© 1984, ELSEVIER SCIENCE PUBLISHERS B.V.

0003-2670/84/$03.00

All rights reserved. No part of this publication may be reproduced, stored in a retrieval system or transmitted in any form or by any means, electronic, mechanical, photocopying, recording or otherwise, without the prior written permission of the publisher, Elsevier Science Publishers B.V., P.O. Box 330, 1000 AH Amsterdam, The Netherlands. Upon acceptance of an article by the journal, the author(s) will be asked to transfer copyright of the article to the publisher. The transfer will ensure the widest possible dissemination of information.

Submission of an article for publication entails the author(s) irrevocable and exclusive authorization of the publisher to collect any sums or considerations for copying or reproduction payable by third parties (as mentioned in article 17 paragraph 2 of the Dutch Copyright Act of 1912 and in the Royal Decree of June 20, 1974 (S. 351) pursuant to article 16b of the Dutch Copyright Act of 1912) and/or to act in or out of Court in connection therewith.

Special regulations for readers in the U.S.A. — This journal has been registered with the Copyright Clearance Center, Inc. Consent is given for copying of articles for personal or internal use, or for the personal use of specific clients. This consent is given on the condition that the copier pays through the Center the per-copy fee for copying beyond that permitted by Sections 107 or 108 of the U.S. Copyright Law. The per-copy fee is stated in the code-line at the bottom of the first page of each article. The appropriate fee, together with a copy of the first page of the article, should be forwarded to the Copyright Clearance Center, Inc., 21 Congress Street, Salem, MA 01970, U.S.A. If no code-line appears, broad consent to copy has not been given and permission to copy must be obtained directly from the author(s). All articles published prior to 1980 may be copied for a per-copy fee of US $ 2.25, also payable through the Center. This consent does not extend to other kinds of copying, such as for general distribution, resale, advertising and promotion purposes, or for creating new collective works. Special written permission must be obtained from the publisher for such copying.

Printed in The Netherlands

CONTENTS

(Abstracted, Indexed in: Anal. Abstr.; Biol. Abstr.; Chem. Abstr.; Curr. Contents Phys. Chem. Earth Sci.; Life Sci.; Index Med.; Mass Spectrom. Bull.; Sci. Citation Index; Excerpta Med.)

(Continued on inside back cover)